The emplacement and metamorphism of the blue river ultramafic body, cassiar district, British Columbia, Canada

Pinsent, R. H.

The Emplacement and Metamorphism of the Blue River Ultramafic Body, Cassiar District, British Columbia, Canada.

R.H. Pinsent, B.Sc., M.Sc.

A thesis submitted for the degree of

Doctor of Philosophy,

University of Durham.

Department of Geological Sciences.

December 1974.

ABSTRACT

The Blue River ultramafic body is one of many "alpine" peridotites intruded into the Sylvester volcanic series in northern British Columbia. The primary dunite-harzburgite assemblage consists of olivine (Fo_{89}-Fo_{95}), enstatite (En_{90}-En_{92}), and spinel. The spinel chemistry is variable, dunite spinels give a Crx100/(Cr+Al) ratio of 58 and above, and peridotite spinels are invariably below this figure. The assemblage, which was evidently intruded hot as it has formed a "hornblende hornfels" facies amphibolite aureole, is inferred to have equilibrated with volcanic magma, present in the form of bodies of gabbro.

The body has been truncated by the Cassiar batholith. Metamorphism has effected both the primary assemblage, and also an early generation of marginal serpentinite. Isograds have been established which mark the incoming of metamorphic olivine, tremolite, olivine with talc, and enstatite.

Metamorphic olivine porphyroblasts in the outer aureole of the batholith are zoned. They have an inner turbid core enriched in Fe and Mn, and a clear outer margin enriched in Mg. Ni will enter olivine only in the absence of sulphur. A maximum core to margin range of Fo_{85}-Fo_{97} was found 4,000m from the contact.

Above the olivine with talc isograd the assemblage is influenced by increased fO_2. Primary spinels in both peridotite and serpentinite are oxidized. Al substitutes in the serpentine structure to form chlorite, and the spinel absorbs Fe, Mn and Ni. The Al content in the chlorite increases towards the batholith contact. Metamorphic olivines are weakly or non zoned, and they reach a composition of Fo_{95}. Metamorphic enstatite is similarly Fe depleted, at En_{93}.

The body underwent partial alteration to antigorite during the waning stages of thermal metamorphism, and more pervasive serpentinization on cooling. Euhedral olivine porphyroblasts in a matrix of relict serpentine, retain their original outlines, and they undergo volume for volume replacement. The lizardite-chrysotile assemblage contains abundant brucite, which envelopes serpentine pseudomorphs after metamorphic olivine. This is indicative of cation mobility during serpentinization.

ACKNOWLEDGEMENTS

I would like to thank Mr. A. Saddler, President of Rio Tinto Canadian Exploration Ltd., for permission to use material collected in the course of Company work, and I would also like to acknowledge the financial contribution made by the Company, particularly in the realm of field logistics, and in the preparation of the polished thin sections. I would also like to thank Mr. H. Hall, and the Company Staff in Vancouver, for their help and assistance throughout my stay.

I would like to thank Professor G.M. Brown for his encouragement to come to Durham, and for his efforts in securing a grant, from the Natural Environment Research Council, to cover the period of research. This grant is gratefully acknowledged.

The research in Durham was supervised by Dr. D.M. Hirst, and his advice, interest and encouragement have contributed much to the end result. I would especially like to acknowledge many valuable discussions on the subject, and also his assistance in the construction of the finished manuscript.

I would like to thank Dr. A. Peckett for his instruction, and assistance, in the use of the Electron Microprobe, which has contributed so much to the study. In addition I am indebted to Dr. J.G. Holland for

assistance in whole-rock X-ray fluorescence analysis, and to Mr. R.G. Hardy, for assistance in X-ray diffraction work. Mr. R. Lambert also assisted in the wet chemical FeO determinations.

Many members of the Department of Geological Sciences, both past and present, have contributed much through active assistance and discussion. I would particularly like to mention Dr. C.H. Emeleus, Dr. J.A. Winchester, Dr. R. Powell, and Dr. K.J.A. Wills.

Data handling was much facilitated by the computer programs written by former research students, Dr. R.C.O. Gill, Dr. M.J. Reeves, and Mr. E.B. Curran. I would like to acknowledge these programs and the help of Mr. J.L. Knight, and of my other colleagues, in implementing them.

I am indebted to Mr. G. Dresser for the production of photographic plates and diagrams.

Finally, I would like to thank Mrs. C.L. Mines for typing the manuscript so expertly and efficiently.

CONTENTS

LIST OF FIGURES

CHAPTER 4:

CHAPTER 5:

CHAPTER 6:

*Figure located in the attached map pocket.

LIST OF TABLES

APPENDIX I:

APPENDIX II:

LIST OF PLATES

CHAPTER 1: INTRODUCTION

1.1 Introduction

Regional mapping, by the Geological Survey of Canada, showed that the Blue River Ultramafic body displays a number of significant features. These reflect its genesis, and its subsequent metamorphic history. The body is one of many "alpine" ultramafic intrusives in a major greenstone belt in northern British Columbia. It differs from most in having a pronounced thermal aureole. The intrusive appears to have been emplaced, while hot, into low grade spilitic volcanics. In addition, the body is itself intruded by lenses of gabbro, which are not found cutting the country rock volcanics. The gabbroic bodies appear to have a genetic association with the ultramafic rock.

The ultramafic body has been truncated by the Cassiar batholith, and serpentinized ultramafic material has been metamorphosed in the aureole of this batholith. Strain free olivine "kernels", developed in serpentinite, were attributed to thermal metamorphism. The early survey work was followed up by a more detailed study, which essentially confirmed the observed relationships, and expanded the study.

The present study is a continuation of the earlier work by Gabrielse (1955, 1963), and Wolfe (1965, 1967).

It incorporates Electron Microprobe data not available to either of the previous workers.

The chemistry of the "primary" mineral phases are considered individually, and the assemblage as a whole is considered in the light of the observed tectonic features.

The metamorphic mineralogy, and mineral chemistry, is considered in some detail, as it is possible to establish metamorphic isograds, and cryptic chemical variations, on approaching the batholith contact.

Parts of the ultramafic body have been serpentinized twice, once during normal serpentinization of the "primary" assemblage, and once after regeneration. The body thus presents natural data on the classic serpentinization-regeneration reactions, first established experimentally by Bowen and Tuttle (1949). The two olivine producing reactions that they propose have both been identified, and the chemistry of each reaction has been investigated.

Although the water-source problem has largely been resolved in favour of an external country rock source, there is still much controversy over the question of volume increase during serpentinization. Reserpentinized metamorphic olivines clearly indicate that volume for volume replacement can occur, with the accompanying migration of Si and Mg.

The widespread occurrence of serpentinite has tended

to concentrate research into problems concerning the hydrational, serpentinization process, Thayer (1966), Hostetler et al. (1966), Page (1967), Coleman (1971), Engin and Hirst (1970). The reverse process of dehydration, and olivine regeneration, has received less attention, although recent work by Trommsdorff and Evans (1972), Springer (1974), and Frost (1973), has done much to redress the imbalence. The present study is designed to discuss the regeneration process further.

Sample and outcrop data are given in Table 1.1, and mineral assemblages in sectioned samples are shown in Table 1.2. This data can be found in Appendix I.

Individual mineral analyses are referred to by table number in the text. Tables of mineral data have been assigned to Appendix II; although some tables, containing averaged values, are retained in the body of the text.

Whole rock analytical data is similarly referred to by table number in the text, although the data is located in Appendix III.

1.2 Location

The Blue River ultramafic body is situated in the McDame Map Area, at latitude 59°33', longitude 130°0', in N.T.S. block 104P/12W (Figure 1.1).

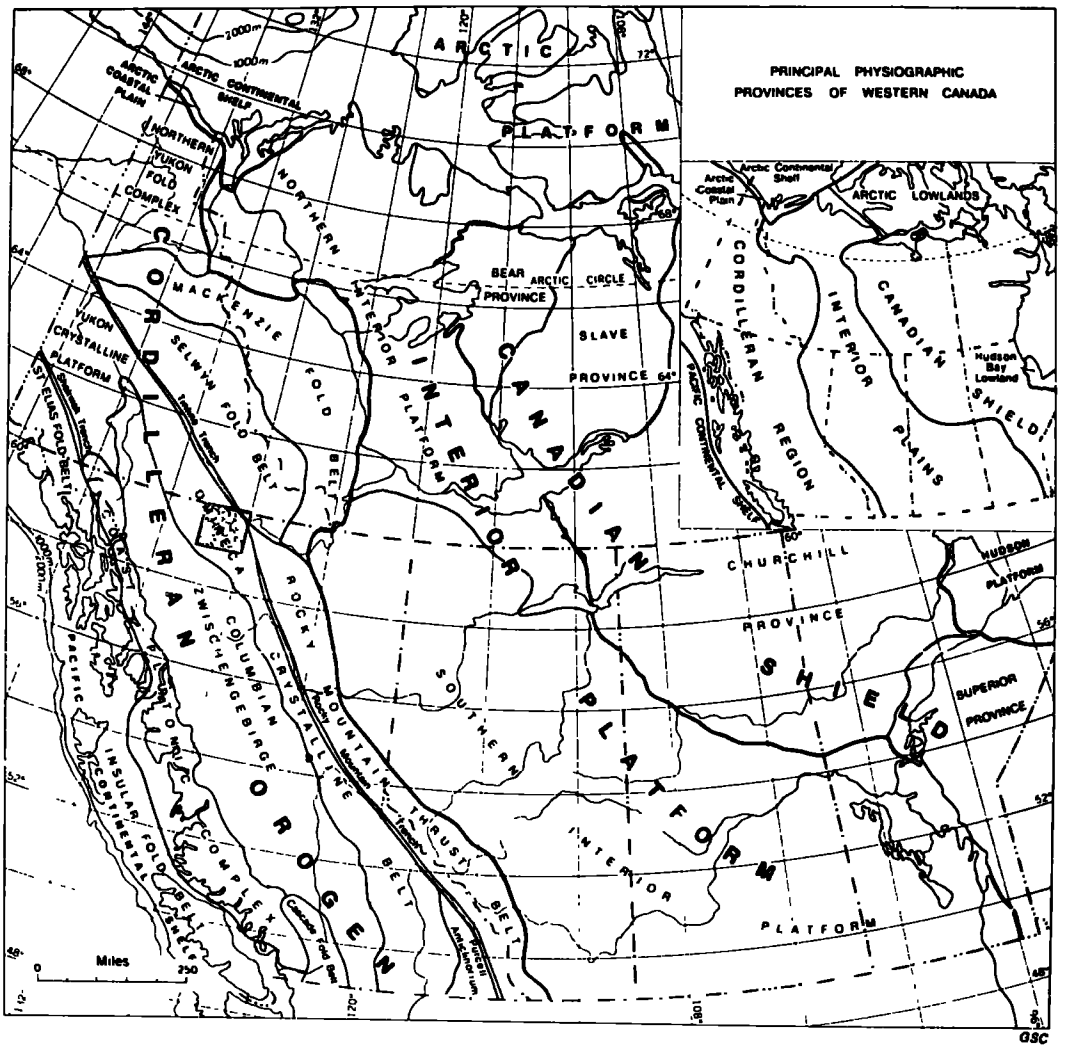

Figure 1.1 The principle structural elements of Western Canada, from Douglas et al. (1970) The McDame Map area is shown stippled.

Access to the body, which forms a twin lobed elongate lens, 6 x 3.2 km in areal extent, is to all practical purposes restricted to the helicopter service at Watson Lake, Yukon Territory.

The body is situated at the headwaters of Spudusob Creek, a tributary of the northeasterly flowing Blue River; which forms part of the Liard-Mackenzie river system. The creek is the largest of seven which drain a corrie complex elevated between 1,500 m and 2,400 m, in a hanging valley, 450 m above the level of the Blue River.

The body crops out in the Stikine Ranges, which mark the western limit of the glacial alluvium of the Liard Plain, and the onset of the more mountainous Cordilleran region.

1.3 Previous Investigations

Initial mapping by Price (1949), (in Gabrielse (1963)), and by Gabrielse, 1950-1954, led to the publication of the McDame Map Sheet, (Map 1110A, scale 1" = 4 miles), and Geological Survey of Canada Paper 1954-10.

The discovery of asbestos on Mt. McDame in 1950, and the subsequent development of the Cassiar Asbestos Corporation Orebody, which came into production in 1954, stimulated economic interest in the McDame ultramafic-greenstone belt. Gabrielse developed the field study into a doctoral dissertation at Columbia University, in which

he investigated the relationship between asbestos formation, and regional structure. In addition, he considered problems associated with serpentinization, and in part, olivine regeneration, (Gabrielse, 1955). Much of this work was later published as Geological Survey of Canada Memoir 319, "McDame Map Area, Cassiar District, B.C." (Gabrielse, 1963).

In 1962 Wolfe mapped the intrusion at a scale of 4" = 1 mile, and his map, which was published with Geological Survey of Canada Paper 64-48, has served, (with modifications), as a base map for the present study.

Wolfe developed the study of olivine regeneration as part of a doctoral dissertation at Yale University (Wolfe, 1967). His study, which is based on an optical interpretation of thin sections, and X-ray diffraction data from a suite of evenly distributed ultramafic samples, substantiates the earlier observations, and covers the associated topics of the marginal amphibolite zone, and low temperature "rodingitization".

The Blue River body has, at various times, been prospected for asbestos, chromite, and, following reports of Heazlewoodite (Ni_3S_2), by Wolfe (1965), for Nickel. It was as an exploration geologist for Rio Tinto Canadian Exploration that the author visited the body in 1970 and 1972.

1.4 Regional Tectonic Structure

Figure 1.1 shows that the McDame Map Area lies within the Omenica Crystalline Belt, which is one of the five tectonic elements which make up the Cordilleran Orogen in western Canada. The principle geological components of each element are shown in Figure 1.2.

The North American Craton, exposed as the Canadian Shield, Figure 1.1, extends westward under the Interior Platform, and it is thought to underlie the Rocky Mountain Thrust Belt.

PreCambrian and Paleozoic sediments derived from the Craton are deposited as a flatlying, westerly thickening wedge over much of the Interior Platform. Sediment also accumulated west of the Craton edge, in the Cordilleran Geosyncline. This was subsequently deformed and metamorphosed into the Omenica Crystalline Belt. Metamorphism and uplift, initiated in the Devono-Carboniferous period, culminated with locally intense deformation between the Triassic and the Cretaceous. The geosynclinal sediment underwent high grade "Barrovian" metamorphism, Figure 1.2, and a number of gneiss domes upwelled in the core of the belt. In addition, batholiths of granodiorite and granite were intruded along the length of the belt. During the Cretaceous much of the belt was emergent, and shedding sediment onto the Interior Platform. Plastic deformation

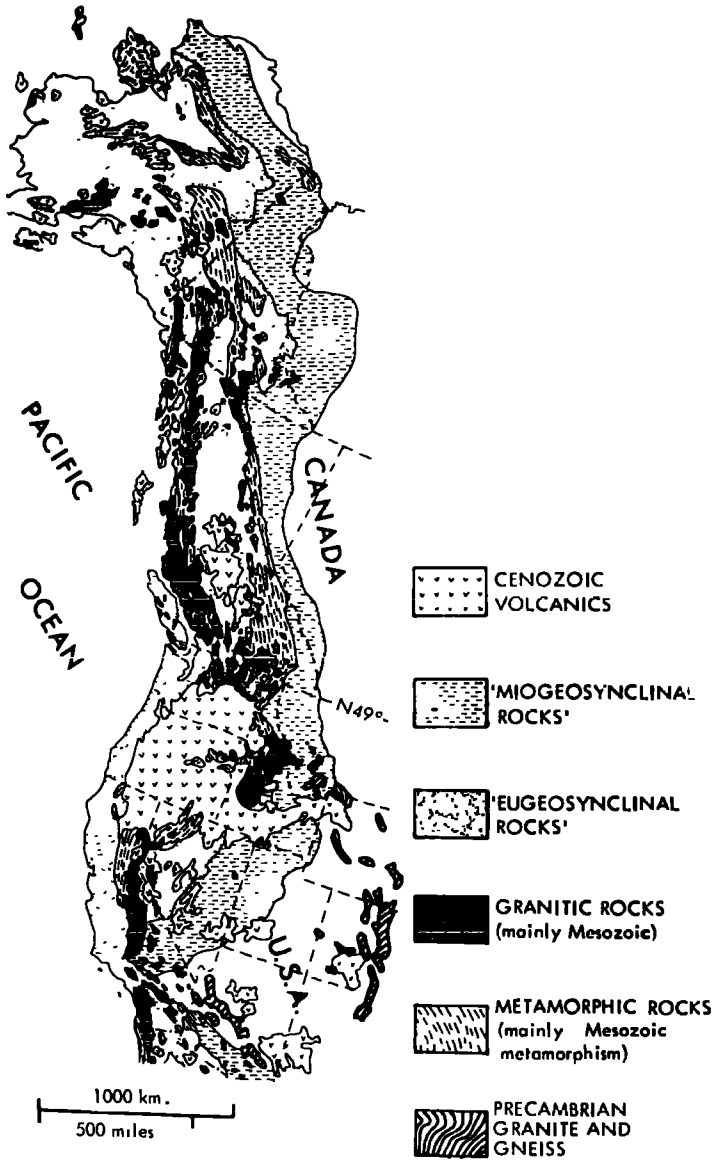

Figure 1.2 A Sketchmap of the North American Cordillera, from Monger et al. (1972). The map shows the main geological components of the structural elements given in Figure 1.1.

in the core of the unit, accompanied by isostatic uplift, caused brittle deformation of miogeosynclinal shelf sediments on the edge of the Craton. Sediments piled up in a series of north-easterly moving thrust sheets, within the Rocky Mountain Thrust Belt.

Monger et al. (1972) note that the sediment within the Omenica Crystalline Belt is clearly craton derived, and there is no evidence for rocks west of the crystalline belt prior to the Devonian-Mississipian boundary. In proposing a "plate-tectonic" model for the Cordillera, they consider the Columbian Zwischengebirge, the Coast Plutonic Complex, and Insular Fold Belt, Figure 1.1, 1.2, to be allochthonous.

The Sylvester Group, discussed in this study, is the earliest evidence for non-cratonic eugeosynclinal rock in the Canadian Cordillera. It consists of a belt of basalt, chert, and ultramafic rock, 160 km by 30 km in extent. It overlies miogeosynclinal sediments from the McDame Group with apparent conformity; although they show no sign of contamination by intruded dykes of basalt. Monger and Ross (1971) consider this problem, and they state: "it has been suggested by J. Dercourt (personal communication), that these rocks are allochthonous Ocean floor material that has been thrust eastwards over continental crust".

The Sylvester Greenstone belt evidently survived the

relatively mild orogenic activity in northern British Columbia, although it was deformed, and intruded by the Cassiar Batholith.

The Columbian Zwischengebirge is interpreted as being a similar slab of ocean floor material. It was fault bounded against the Omenica Crystalline Belt by subduction along the Pinchi-Teslin Fault system, during the Permo-Carboniferous, Monger et al. (1972). The unit represents a block-faulted eugeosynclinal plateau. Early Carboniferous volcanism was basaltic, but later Triassic volcanism was largely andesitic. Sporadic volcanism occurred in the Cretaceous, Eocene and Pleistocene periods. The original basalt slab shows no obvious sialic floor, and it is almost devoid of clastic sediment. The basalt is associated with large amounts of limestone. The Unit is cut by a number of major transcurrent faults; these are often associated with ultramafic bodies, and locally with Blue Schist facies metamorphism.

The Coast Plutonic Complex is similarly considered to be an allochthonous "Island arc", brought into juxta position with the eugeosynclinal assemblage by subduction along the Yalakom-Shakwak Fault system, during the Permo-Triassic period, Monger et al. (1972). The Coast Plutonic Complex consists of pre-Jurassic to Mid-Cretaceous plutonic rocks, intruded into a limited post Lower Mesozoic stratig-

raphy. Although intrusive activity was concentrated in this unit, some intrusions penetrated the Columbian Zwischengebirge.

The insular Fold Belt is a similar mix of eugeosynclinal volcanic material, Island arc volcanics, and younger plutonic rocks.

1.5 Regional Geology

The McDame Map area. Gabrielse (1963), can be subdivided into five geological units, which conform to the regional northwest-southeast trend. (The relevant units are shown in Figure 5.1).

1. Cassiar Batholith (Cretaceous).
2. Nizi Group Limestone (Lower Carboniferous).
3. Sylvester Group Volcanics (Devono-Mississipian(?)).
4. Good Hope Group - McDame Group (PreCambrian-Devonian).
5. Horseranch Group Metasediments (PreCambrian).

(i) Horseranch Group

A fault bounded block of regionally metamorphosed and partially granitized miogeosynclinal sediment crops out in a double plunging anticlinal structure, within the Horseranch range. Outcrop is restricted to an area of 450 km^2, and metamorphism does not extend beyond the bounds of the fault block.

(ii) Good Hope Group - McDame Group

The pattern of sedimentation established in Proterozoic time continued until Middle Devonian (Givetian) time . A thick succession of miogeosynclinal sandstones, shales, limestones and dolomites, accumulated on the Cassiar Platform, Gabrielse (1967). This was a structural high, which is now occupied by the Cassiar Batholith. An enormous thickness of sediment accumulated to the east, in a structural basin, the Kechika Trough, (Douglas et al.1970). The sediments are extremely variable in facies and in thickness, and deposition was periodically interrupted by uplift and erosion. In contrast to the early variable sedimentation, deposition of dark fetid dolomites and limestones of the McDame Group was uniform over a large area of northern Canada, Gabrielse (1967). The lower dolomites contain abundant amphipora, and the upper limestones contain stringocephalus sp. These date the unit at Givetian; Late Middle Devonian. Miogeosynclinal sediments crop out over much of the McDame map area, and underlie much of what is now the Liard Plain, an area covered by Pleistocene to recent fluvio-glacial detritus.

The McDame Group and the overlying Sylvester Group, have been deformed into a major synclinorium, the McDame Synclinorium, Gabrielse (1963).

(iii) Sylvester Group

The Sylvester Group crops out in the McDame Synclinorium, and it is restricted to a single northwest-southeast trending belt of volcanic rocks, approximately 20 km wide, in the core of this structure.

The contact between the McDame Group and the Sylvester Group is "almost invariably a fault", Gabrielse (1969), although there is a good stratigraphic correlation between the two units. Gabrielse considers that there is little or no hiatus between the two groups.

The lower part of the Sylvester succession consists of interbedded slate, silicious argillite, chert, subgreywacke, and chert pebble conglomerate. The sediments are typically eugeosynclinal, in marked contrast to the earlier strata. The sediments, which locally reach 1,000 m in thickness, are non-fossiliferous, although Gabrielse (1955) records that indistinct fossils, possibly radiolaria, were detected in one section of well bedded chert. The volcanic rocks comprise a thick succession of eugeosynclinal, submarine, lava flows, "spilites", graded tuffs, and agglomerates. These contain interbedded argillite and chert similar to that found in the basal unit, and also ultramafic intrusives, which occur at the base of the volcanic assemblage, Gabrielse (1967, 1969). Ultramafic bodies are found along the length of the synclinorium, at more or less the same stratigraphic horizon.

The Sylvester Group marks a distinct change in style of deposition. A typical eugeosynclinal assemblage occurs on the site of the Cassiar Platform, in the so-called "Sylvester Trough". The trough contains an enormous thickness of volcanic material, around 5,000 m, mainly consisting of massive structureless flows. No extensive areas of pillow formation are recorded in the succession. The synclinorium marks the eastern limit of volcanic activity in the trough.

Earlier volcanism in the miogeosynclinal assemblage was extremely limited. Remarkably little evidence of basalt magma intrusion is recorded for the Lower Palaeozoic succession, and no extensive areas of dyke and sill formation have been noted by Gabrielse. Basic volcanism also appears to have ended abruptly at the end of Sylvester time, (Gabrielse, 1967).

The overall similarity between the Sylvester Group assemblage and Oceanic Crust has been noted. The isolated nature of the volcanism supports tectonic emplacement of the eugeosynclinal assemblage on to the sinking Cassiar Platform. In view of the strong stratigraphic correlation, it may be that a sliver of oceanic crust was obducted onto the floor of the sinking Platform.

The Sylvester Group is unconformably overlain by Lower Carboniferous sandy limestones of the Nizi Group. This implies a late Devonian-Mississipian age of emplacement

for the volcanogenic assemblage. There is some evidence for tectonism at this time. Gabrielse and Wheeler (1961) note regional and local unconformaties to the west, and report differences in metamorphism. This orogenic period, the Caribooan Orogeny, uplifted the Omenica Crystalline belt, and it remained a positive tectonic element from then on.

A complicating factor to the age of the Sylvester Group is the occurrence of Permian fusulinids in limestones which cropout in the eastern corrie wall of Spudusob Creek, (Plate 1.1). Fusulinids collected by Wolfe have been identified by Ross (1969) as being Parafusulina, of Permian, Guadalupian age. The limestones appear to be conformably overlain by volcanic rocks identical to those of the Sylvester Group. This suggests that some of the Sylvester volcanics are younger than had hitherto been thought (Wolfe, 1965).

(iv) Nizi Group

The Sylvester Group and the underlying McDame Group are both unconformably overlain by well bedded sandy carbonate strata of the Nizi Group. These contain volcanic fragments (Gabrielse, 1963), and an abundant foraminiferal fauna, at their type locality on Nizi Creek, about 80 km southwest of the Blue River. The base of this unit is

Plate 1.1. Spudusob Creek Corrie, looking southeast towards the Blue River. Heazlewood Creek is in the foreground, and Spudusob Creek is in the middle distance. Note the light coloured (?)Permian limestone, (overlain by volcanic rock), which crops out in the northeast corrie wall.

Plate 2.1. White contact amphibolite foliated parallel to its interface with serpentinite. Note the rodingite veinlets cutting the amphibolite, and the sheared nature of the serpentinite. Location point 60005, on Claim Jumper Creek.

assigned a late Visean to early Namurian age (Mamet and Gabrielse, 1969). The Sylvester Group should thus have been emplaced and partially eroded by Lower Carboniferous time.

(v) Cassiar Batholith

A large elongate composite batholith has intruded along the western margin of the McDame Synclinorium. Although it crudely conforms to the regional trend, it intrudes both mio- and eugeosynclinal assemblages, and it truncates regional structures. It is essentially late to post tectonic in character, and it has imprinted a thermal aureole on low-grade regional metamorphic rocks. At the head of Spudusob Creek it truncates and metamorphoses rocks of the Blue River ultramafic body.

The batholith has been dated by K-Ar methods at 101 M.Y., where it crosses the British Columbia-Yukon border, (Gabrielse, 1967), and coexisting muscovites and biotites give ages of 123 M.Y. and 139 M.Y. respectively, at the south end of the batholith. It is thus considered to be Cretaceous in age.

CHAPTER 2: LOCAL GEOLOGY AND STRUCTURE

2.1 Local Geology

The Geology of the Blue River Ultramafic body, Figure 2.1, is taken from Wolfe (1965), with only a few minor amendments. Mapping conducted in 1970 and 1972 confirmed most of the field observations made by Wolfe; the principle exception being the identification of a distinct zone of metamorphosed marginal serpentinite, along the western contact. This unit includes the isolated pods noted by Wolfe (1965).

The recognition of a distinct western contact zone; and also the realization that late faulting and retrogressive serpentinization has influenced spatial relationships, and lithologies, enables a re-evaluation of the structural model proposed by Wolfe. The double syncline, adopted in G.S.C. Map 17-1964,(Paper 64-48), to explain the twin lobes of the body, is reinterpreted in terms of a fault controlled structural model.

The present day rock distribution, in and around the ultramafic body, is the result of a prolonged history, during which the body has undergone at least four development stages.

I. Initial Intrusion of the Ultramafic body.

II. Tectonic Emplacement of the Eugeosynclinal Assemblage Mississipian(?)

III. Thermal Metamorphism of the ultramafic rock Cretaceous .

IV. Retrogressive serpentinization and faulting. Cretaceous - recent .

Each stage has influenced the spatial distribution of mafic and ultramafic rocktypes; and differences in lithology and structure have altered the response to later events. The geology displayed in Figure 2.1 is the result of the overprinting of each of these development stages on pre-existing structural and metamorphic conditions.

The structural evolution of the body may be inferred not only from the present day spatial relationships, but also from the inherited rock textures and mineralogy.

2.1 Structural Evolution

I. Initial Emplacement

A primary ultramafic assemblage, consisting of anhydrous peridotite and dunite, was emplaced into the volcanic assemblage prior to obduction during Stage II.

The body must have been hot, as it has metamorphosed volcanic rock to amphibolite for a distance of 130 m from the contact. The amphibolite is foliated parallel to the sharp, and planar, amphibolite-peridotite interface (Plate 2.1).

The foliation, which suggests a dynamic component to the emplacement, dies out away from the contact, and the amphibolite passes into country rock volcanic material. The contact amphibolite mineralogy suggests Lower Almandine Amphibolite facies conditions (see Chapter 8), and the contact temperature is inferred to have been around 600-650°C.

The ultramafic material is thought to have equilibrated after emplacement. The peridotite-dunite assemblage is granulated and deformed, in contrast to the segregated gabbro. Following Wolfe (1967), the body is thought to have been intruded as a largely crystalline "mush", with a small percentage of basaltic magma. Mineral equilibration temperatures, estimated in Chapter 3, suggest an intrusion temperature of around 1200°C. The magma possibly segregated into pods and lenses on cooling to around 1050°C, about the temperature estimated for the final exsolution of diopside lamellae in enstatite.

The country rock volcanic material is largely unaltered "spilite". Regional metamorphism never went beyond the Greenschist facies, and they probably equilibrated at, or below "Quartz-albite-epidote-almandine" subfacies conditions. This suggests a maximum temperature of 550°C, Winkler (1967).

Pressure estimates are far more difficult, as volcanic rocks are relatively insensitive to pressure, within the greenschist facies. A pressure of 4-5 kbars is considered reasonable, although it could be appreciably higher.

The ultramafic body is one of many found close to the base of the volcanic series. This may be fortuitous, or it may mean that the major structural break lies not at the base of the Sylvester Group, but below the volcanic component of that Group. This might explain the apparent lack of hiatus between the McDame Group, and the Sylvester basal sediments. If this is the case, the ultramafics may have been intruded immediately prior to obduction. They may well have been emplaced along the same structure, that later obducted the assemblage as a whole. A schematic representation is given in Figure 2.2.

The local structure is complicated, and although amphibolite represents an original contact, minor movement on it has occurred subsequently. The original shape and size of the body is not known.

The peridotite has a well defined structural fabric, based on the layering of pyroxene in a rock composed largely of olivine. Wolfe (1965) shows that this primary banding is not related to an internal fold system, (unless it be isoclinal). No fold noses were observed, either in the field, or on plotting foliation data on a stereographic

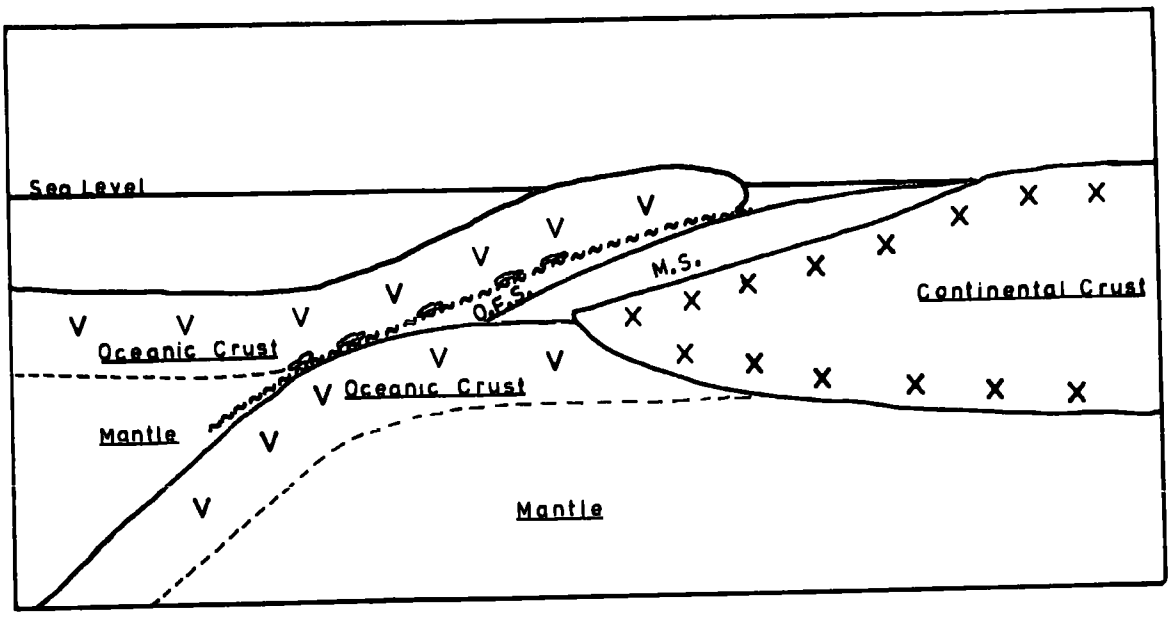

Figure 2.2 A schematic section illustrating a possible structural model for the obduction process, during Stage II. Peridotite blebs are intruded along the base of the obducted slice.
O.F.S. = Ocean Floor Sediment,
M.S. = Miogeosynclinal sediment.

projection. Wolfe shows that the foliation cuts the present day bedding at an angle of 45°. It could possibly have paralleled the amphibolite border at the time of intrusion. Bodies of gabbro are concentrated along the western contact, Figure 2.1. Although they might be expected to occur along the top of the structure, they appear to be at the tectonic base, as Sylvester sediments, and McDame limestones,lie to the west.

II. Tectonic Emplacement

The ultramafic body underwent a period of deformation and marginal serpentinization prior to the intrusion of the Cassiar Batholith. The deformational history, following emplacement during Stage I, probably started with obduction of both the ultramafic and the volcanic assemblages onto the Cassiar Platform, and ended with deformation of the area into a major synclinorium.

Breccias have formed along tectonic contacts, and primary ultramafic material has been serpentinized. In the vicinity of the batholith; where metamorphism has regenerated the marginal serpentinite, the original brecciated texture is preserved in the metamorphic assemblage. Along the western contact regenerated dunite replaces both matrix, and breccia fragments,in the vicinity of sample location point 60159, Figure 2.3. Similarly regeneration has formed

a talc-olivine assemblage from serpentinite breccia, at point 61535, in the northeast, (Plate 2.2, Figure 2.3).

Contact marginal serpentinite zones are inferred to represent active movement zones during Stage II. The amphibolite border is disrupted in the west, and water evidently got into the cold, or cooling, peridotite. The western contact was thus active during tectonic emplacement.

Figure 2.1 shows that the body consists of two lobes separated by an intervening slice of volcanic material,and amphibolite. This plunges out to the north, and the two lobes join. The slice is thought to overlie a thrust plane, the Heazlewood Thrust. This is inferred to run parallel to the creek, at the foot of the volcanic escarpment (Plate 2.3). The thrust probably extended north of Heazlewood Creek, in the manner shown in Figure 2.4. A schematic section through the body is given in Figure 2.5. This illustrates the inferred structure for the body, as it is now exposed.

Serpentinization evidently occurred between the footwall of the Heazlewood Thrust, and the fault-bounded eastern contact. This arrangement may explain the difference in width between the western and eastern marginal serpentinite. Metamorphism during Stage III is thought to have obliterated the Heazlewood Thrust north of Heazlewood Creek.

Plate 2.2. A talcose "regenerated dunite" breccia, derived from metamorphosed serpentinite. Sample location point 61535, northeast of Nickel Creek.

Plate 2.3. The southwest wall of Spudusob Creek corrie. Volcanic rock is capped by black amphibolite, and that is in juxtaposition to rusty primary peridotite. Viewed due north from Location point 60018, south of Claim Jumper Creek.

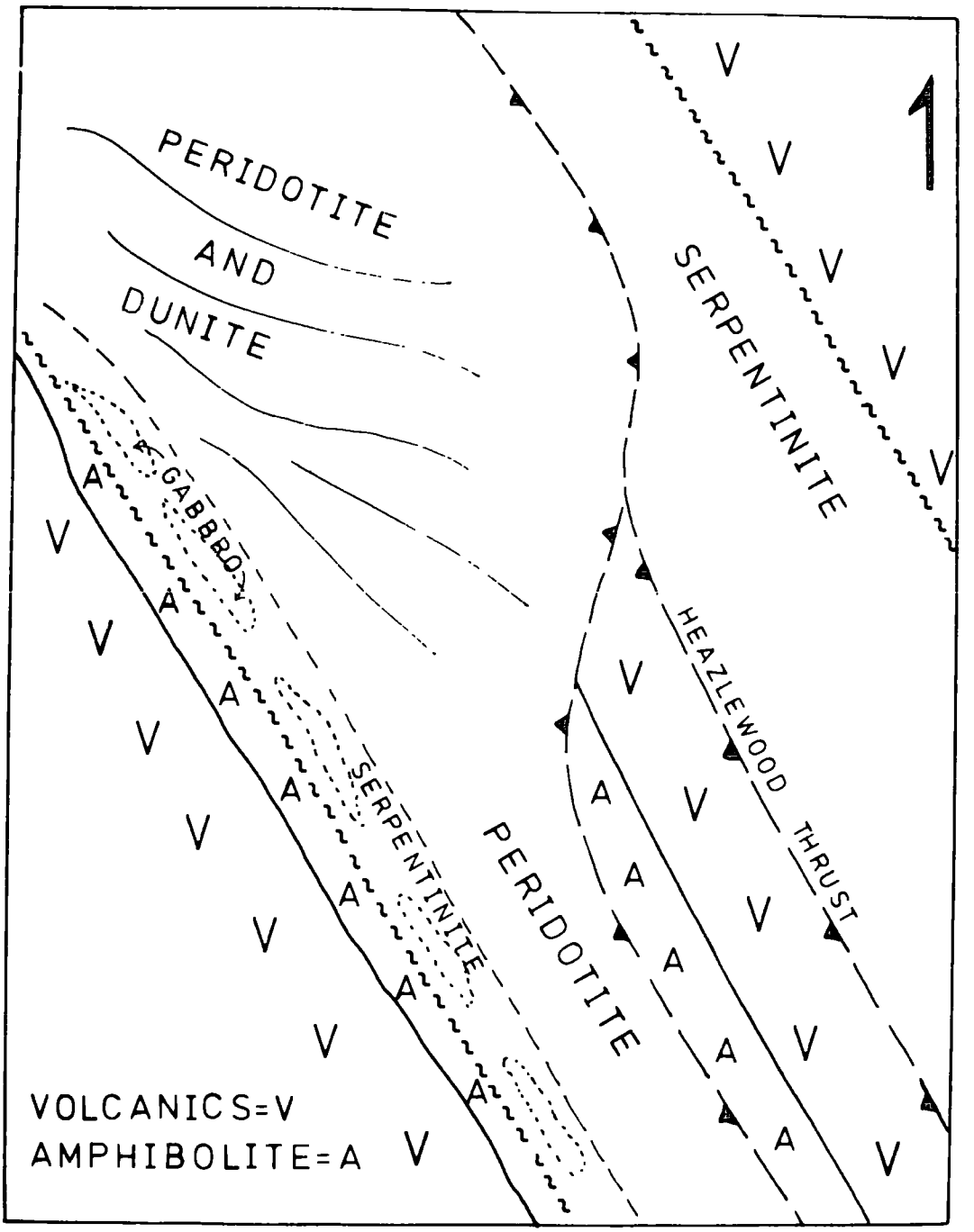

Figure 2.4 A schematic representation of the structure of the Blue River Ultramafic body prior to the intrusion of the Cassiar batholith.

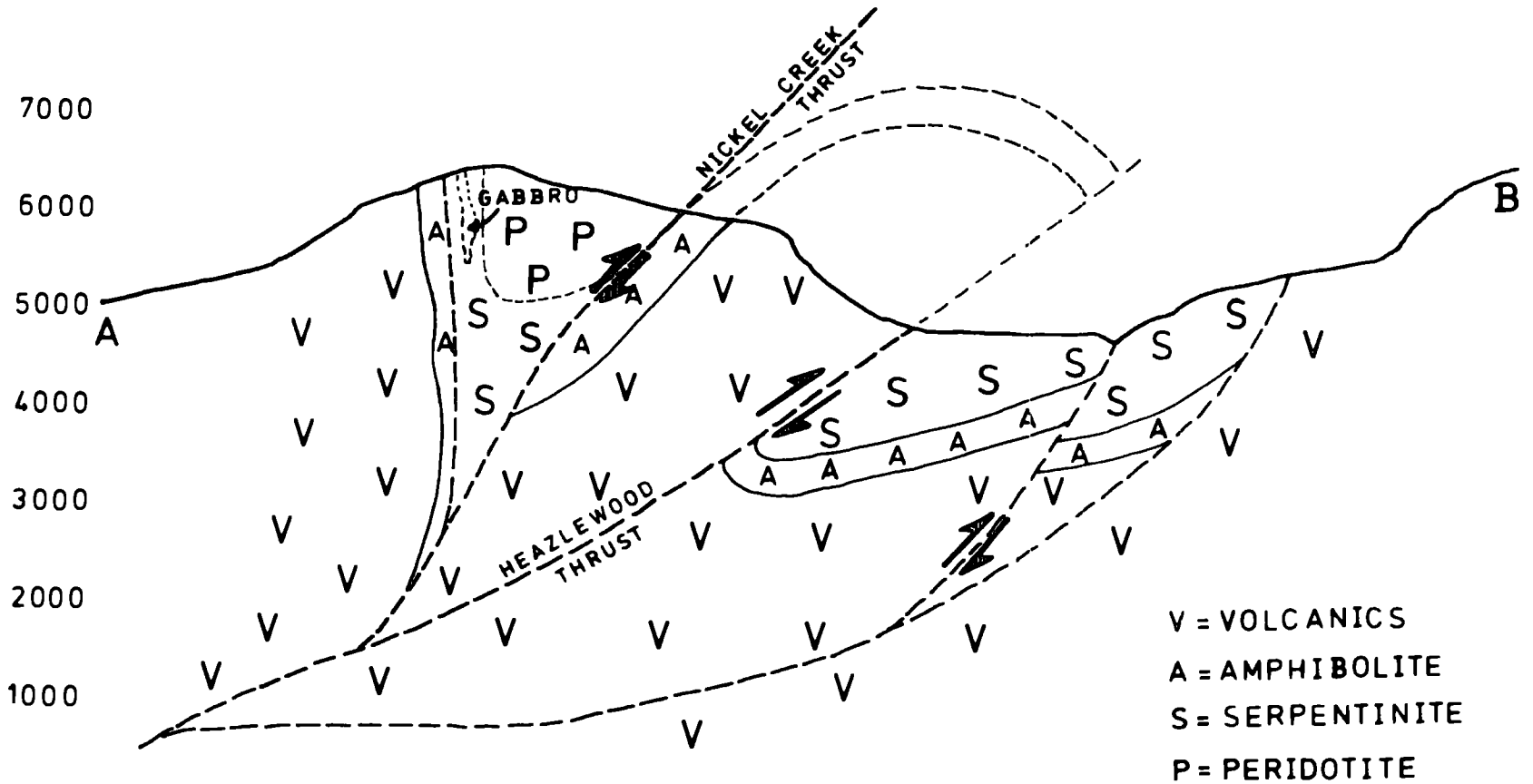

Figure 2.5 A schematic section across the Blue River Ultramafic Body. The section, A(S.W.) to B(N.E.) is shown in Figure 2.1. It represents a distance of 5200m. The vertical scale represents contours measured in feet.

Two small thrust faults have emplaced a small sliver of volcanic and amphibolite material into serpentinite, below the Heazlewood Thrust. This crops out near the junction of Heazlewood and Two Post Creeks.

III. Thermal Metamorphism

The Cassiar Batholith forms a sharp intrusive contact perpendicular to the trend of the regional structures, (Plate 2.4). It cuts both the western and eastern marginal serpentinite zones, and also the intervening "primary" core region.

Metamorphic isograds have been established, which reflect the orientation of the northeast-southwest trending batholith contact. The inferred relationships are shown in Figure 2.6.

IV. Retrogressive Serpentinization

The body underwent two periods of retrograde serpentinization. These have altered the lithology and structure of the body.

High temperature antigoritization occurred in the early waning stages of thermal metamorphism. Antigorite replaces both primary, and also secondary "regenerated" olivine; and some appears to be formed from pre-existing serpentine. Antigorite formation is associated with movement along the Nickel Creek Thrust, a fault which overlies the volcanic amphibolite slice. This fault appears to truncate the old

Plate 2.4. The contact between the Cassiar batholith and the Blue River Ultramafic body. Note the buff colouration of the dunites in the foreground, in Unit (3c); and the regenerated dunites of Unit (3b), in the far wall. Taken from location point 61553, looking northeast.

Plate 5.8. Ice Lake, and the back wall of the Spudusob Creek corrie. The Corrie beyond is underlain by the Cassiar batholith. Plate 5.9 is a continuation from Plate 2.4, looking north from location point 61553.

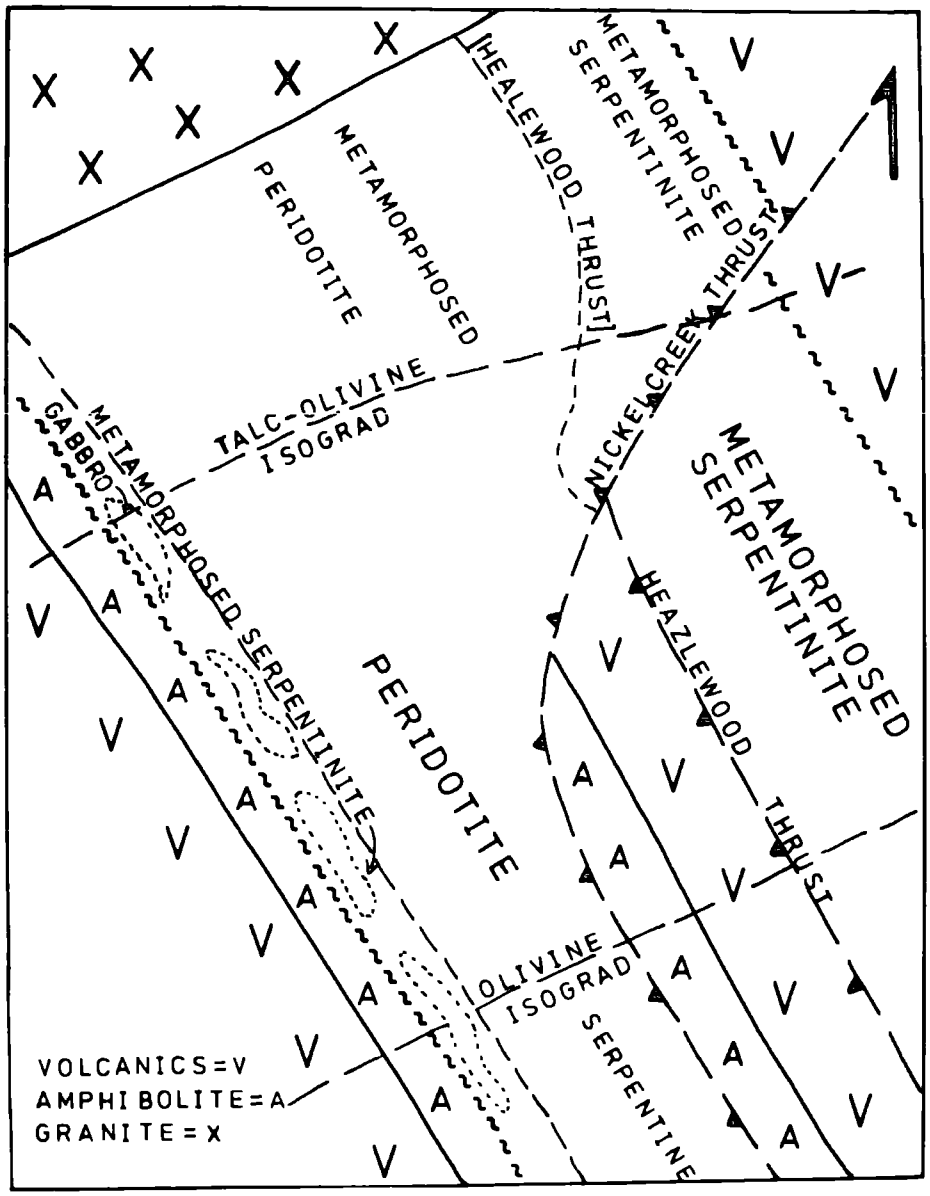

Figure 2.6 A schematic representation of the structure of the Blue River ultramafic body during Stages III and IV.

Heazlewood Thrust, north of Heazlewood Creek, and it takes up à direction subparallel to the batholith contact. Possibly the fault is controlled by a major transverse extensional joint set, which was established during deformation of the McDame Synclinorium. Movement along the fault allowed access of water to the footwall, and much of the regenerated rock has been altered. Faulting may be a response to the initial expulsion of water, and the change from ductile serpentinite to brittle dunite, during metamorphism, Raleigh and Paterson (1967). Movement along the top of the amphibolite-volcanic slice, Figure 2.6 is shown by antigorite serpentinite breccias, in the vicinity of sample location point 61627, Plates 2.5 and 2.6.

Lower temperature serpentinization to lizardite and brucite occurred away from the granite, and also along the batholith contact. In addition, chrysotile asbestos micro-veins formed in areas of both antigorite serpentinite, and of lizardite serpentinite.

Plate 2.5. Antigorite serpentinite breccia. Sheared serpentinite breccia, marking the Nickel Creek Thrust, in contact with Sylvester volcanic rocks. Location point 61627, south of Heazlewood Creek.

Plate 2.6. Antigorite serpentinite breccia. Detail from Plate 2.5, showing rounded peridotite fragments, set in a matrix of antigorite serpentinite.

CHAPTER 3: PRIMARY ULTRAMAFIC INTRUSION

3.1 Lithology and Structure

The area underlain by primary anhydrous ultramafic material is designated as Unit (1) on the accompanying map, Figure 3.1. The bulk composition of the primary intrusion is that of a "four-phase peridotite". It consists of the assemblage:

olivine, orthopyroxene, clinopyroxene, spinel.

According to Wolfe (1965), the body consists of olivine (1), 85-90%, enstatite (1), 10-15%, diopside (1), 1%, and spinel (1), 1%. The suffix (1) in this study is used to relate the mineral to the development stage during which it was formed.

The small amount of clinopyroxene means that the lherzolite component is low, and the body is comprised largely of dunite (Plate 3.1), and harzburgite (Plate 3.2). The distribution of the two rock types leads to compositional banding, which is an important internal textural feature. Harzburgite layers rich in pyroxene are separated by pyroxene free layers of dunite. The widths of each are variable: from 1.0 cm banding, to 100.0 cm banding in most instances, although some dunite zones exceed 50 m in width. Harzburgite is the predominant rock type. The layers are

Plate 3.1. Smooth weathering primary dunite in the foreground. Note the buff colouration. The Nickel Creek Thrust is exposed in the far wall. It appears to pass left of the light brown talcose regenerated dunite outcrop. Location point 61549 looking north east.

Plate 3.2. Primary peridotite outcrop. Note the colour and texture of the fresh rock, and the rough weathered surface rind. Location point 61548.

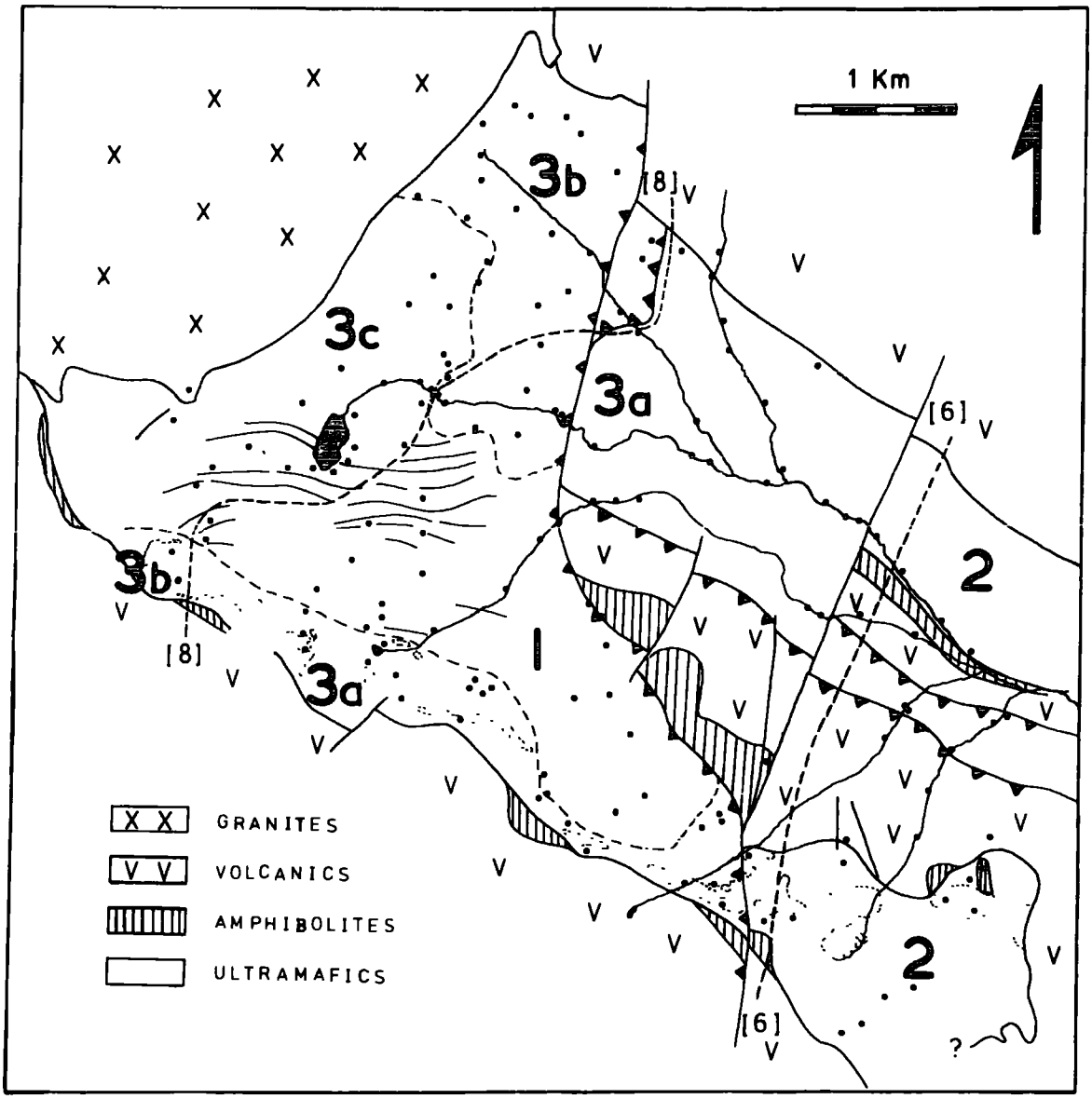

Figure 3.1 A sketchmap of the Blue River Ultramafic Body, showing sample location points, and the ultramafic units defined in the text. Reactions (6) and (8) are given in Table 5.4. They represent metamorphic isograds.

gradational, based on a uniform olivine matrix, and individual bands often die out along the strike. The layering, or "flow banding", as it was termed by Gabrielse (1963), is enhanced by the concentration of spinel grains into planar lenses and stringers parallel to the pyroxene bands.

The primary assemblage appears to be superficially unaltered, and fresh "apple-green" dunite weathers to a buff brown rind, with a smooth sandy surface. The rock is granular, coarse to fine, and it has a distinct tectonic fabric in hand specimen.

Pyroxene phenocrysts in the harzburgite interlayers weather out into relief as rusty red "warts", on an otherwise smooth weathering olivine surface. The rock is similarly deformed, and pyroxenes may be visibly fractured.

Although Unit (1) is essentially primary, the rocks have undergone minor interstitial serpentinization. This has affected rocks within Unit (3c) to a far greater extent. Although the character of Unit (3c) is unquestionably primary, it has undergone some serpentinization, and also subsequent thermal metamorphism. The pyroxenes and spinels are largely altered, but the granulated primary olivine matrix remains, and the tectonic fabric is retained. Compositional banding is still recognizable, as shown by

Wolfe (1965), although harzburgites look appreciably more rusty and altered than they do in Unit (1). Units (1) and (3c) form a primary core region within the ultramafic body, Figure 3.1. The distribution of primary olivine, which defines the core region, is given in Figure 3.2.

Wolfe (1965) notes that the compositional banding bears no obvious relationship to the present day contact, and it bears no relation to a recognizable fold pattern. North of Heazlewood Creek, Figure 1.3, the banding displays a moderate to steep south to southwesterly dip, discordant to observed contacts. South of the Creek, the foliation appears to be subparallel to the contact between Unit (1) and Unit (3a). This latter Unit, Figure 3.1, represents a serpentinized and later metamorphosed band, which was probably originally dunite. Spinel textures and chemistry will be shown to support this assumption. This band has acted as a locus for intrusion of bodies of gabbro, and both they, and the foliation probably originally paralleled the intrusive contact. The dunite band, and the gabbro, appear to be cut out north of Heazlewood Creek.

Gabrielse (1963) attributed "flow banding" to flow differentiation of the type observed in salt domes. This study shows that tectonic differentiation following equilibration is unlikely, and the layering probably represents flow differentiation of a crystal mush, followed by

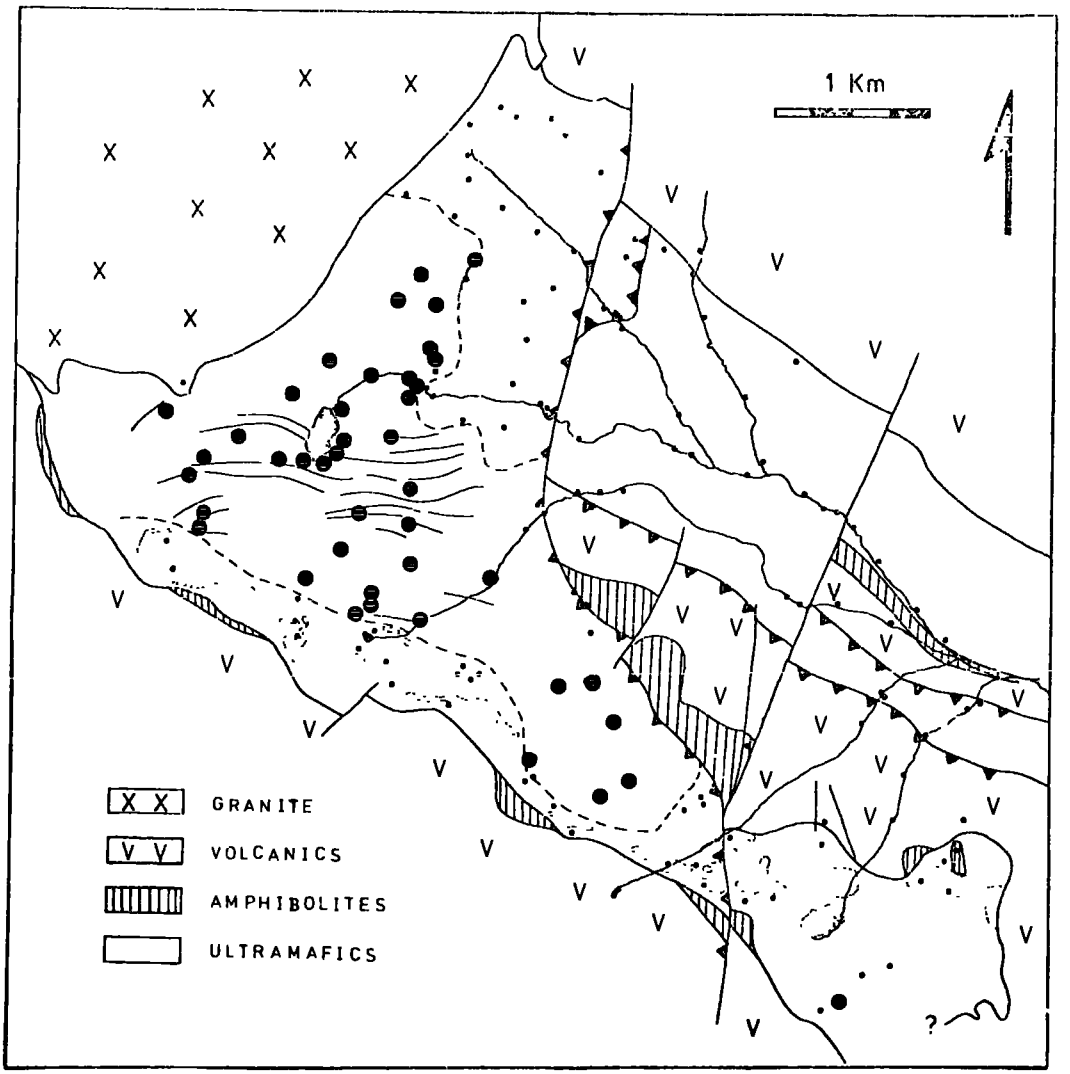

Figure 3.2 Distribution of olivine (1).

equilibration with a fluid phase, (gabbro).

3.2 Mineralogy and Mineral Chemistry

(i) Olivine (1)

There is no sensible difference between olivine which occurs as a matrix within harzburgite, and olivine which occurs as dunite. Deformation is a constant feature throughout the core region, and olivine textures reflect varying degrees of cataclastic deformation. Least deformed samples, such as 60874 and 60886, appear to be found at a distance from recognizable faults, and the more highly deformed samples, such as 60893 and 60902, were collected close to zones of dislocation. Where least deformed, as in Samples 60874, 60886, (Plate 3.3), the olivine is seen to be elongated within the plane of the deformational fabric. Crystal outlines are irregular, and grain sizes are variable. Grains with a length to breadth ratio of 10:1 were observed in some samples. These large, strained, granulated crystals are very often set in a matrix of fine grained polygonal granoblastic fragments, (Plate 3.3). The larger fragments display shadow extinction, and have strain lamellae parallel to (100). Strain lamellae and associated kink bands grade from diffuse to sharp, Wolfe (1967), and they eventually yield by fracturing parallel to the lamellae, as in Samples 60196, 61615 and 60893, (Plate 3.4). Some

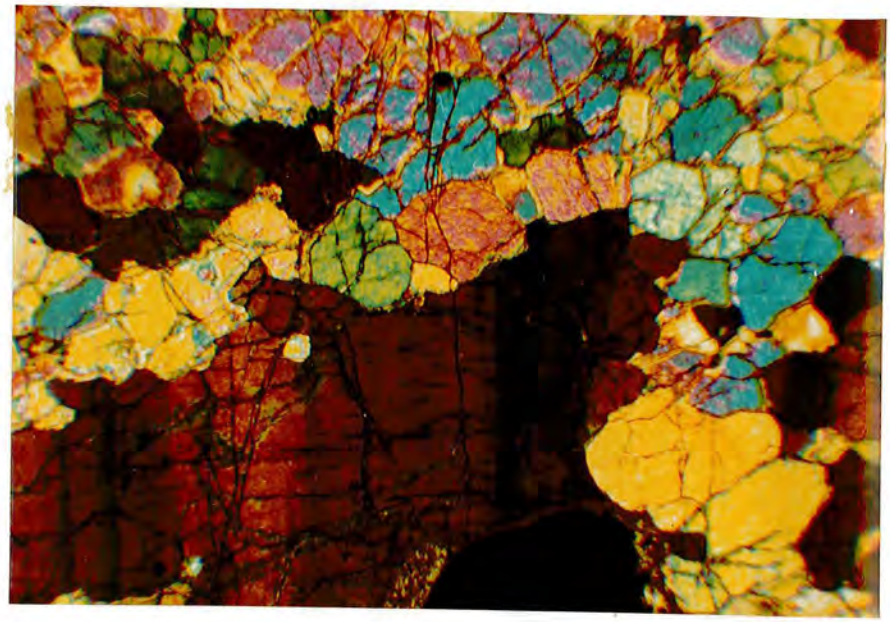

Plate 3.3. Photomicrograph: Primary olivine (1) in Sample 60886. Note the large strained olivine "megacryst", in a mosaic of small olivine polygons. Note also the "megacryst" fractures, perpendicular to the strain lamellae.
Crossed polars. Field width 1.7mm.

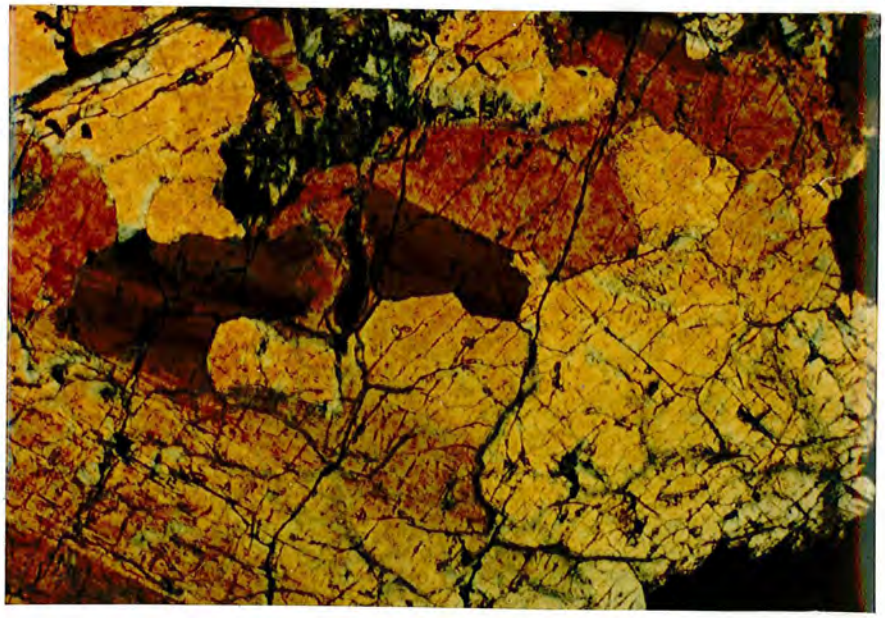

Plate 3.5. Photomicrograph: "Domain" formation in a large olivine (1) "megacryst" in Sample 60876. Note the polygonal fracturing and the localised strain effects. Crossed Polars. Field width 1.7mm.

samples also display fractures parallel to (001), perpendicular to the lamellae. These fractures are less well developed, and they tend to form "en echelon" rather than as continuous planes (Plate 3.3), Ragan (1963).

With increased granulation, large strained crystals disrupt to form domains, within which stress-strain effects are accommodated in isolation from the parent grain. In the early stages, areas of constant birefringence define original grain outlines, (Plate 3.5). With increased disruption, original relationships are lost, and the domains themselves granulate into smaller subdomains. Fracture induced polygonization tends to homogenize the rock, and reduce the sense of planar orientation in the rock fabric.

Some olivine crystals and domains appear to have been "shattered" into micro-domains or platelets, which retain the overall crystal outlines of their hosts. In Samples 60893 and 61615, (Plate 3.6), shattering evidently post-dates kink-band formation, as individual lamellae and kink-bands are shattered.

Some small olivines in the groundmass of the deformed rock show no sign of internal strain, and they have sharp, straight or curved, (concave inward), faces. Intergrain contacts give angles around 120°, the angle of minimum interfacial energy, and they resemble the annealed olivines described by Ragan (1969).

The main period of deformation must have predated Stage II serpentinization, as intergranular serpentine has exploited the deformational fabric. Sample 60196 contained intergranular serpentine. This was subsequently transformed into Al serpentine, and in Sample 60186, intergranular serpentine was regenerated as olivine (3), (Plate 3.2).

Much of the regenerated olivine formed above the talc isograd is also granulated and deformed, Samples 60202, 61600, (Plate 3.8). This, and the occurrence of antigorite serpentinite breccias along the Nickel Creek thrust, indicates subsequent deformation during Stage IV reserpentinization, (Chapter 7). The deformation did not include formation of lamellae, or internal crystallographic distortion, but it resulted in granulation of regenerated, and perhaps also primary olivine.

Experimentally deformed olivines were found by Raleigh (1967), to form kink bands orientated parallel to (010) and (001), when the crystals were deformed below 1,000^{o}C. Above 1,000^{o}C kink band orientations parallel (100) and (001). Perhaps the original deformation was at high temperature and later shattering occurred, on the third orthogonal axis, in response to lower temperature deformation.

Olivine (1) Chemistry

Primary olivine analyses are given in Table 3.1, and compositional data is displayed in Figures 3.3, and 3.4. Average olivine analyses for those samples which coexist with analysed spinel, and/or orthopyroxene, are given in Table 3.2.

The main chemical variable in natural olivine is the Fe content, as defined by the Mgx100/(Mg+Fe) ratio, or "forsterite" content. The Blue River olivines appear to be homogenous, not only at the scale of a single polished thin section, but also on the scale of the body as a whole. Figure 3.3 shows that the average forsterite content is relatively constant throughout the core region of the body. There is no evidence for systematic cryptic variation across the foliation trend.

The two histograms in Figure 3.4 show that there is little difference between dunite and peridotite derived olivine. The overall compositional range is Fo_{89}-Fo_{95}, which compares with a range of Fo_{87}-Fo_{95} determined by Wolfe (1967), from a study of olivine X-ray diffraction data. The effective range is somewhat less, from $Fo_{90.5}$-$Fo_{92.5}$, with a mean composition around Fo_{91}. This data is consistent with forsterite ranges observed in other "alpine" type peridotite bodies.

'TABLE 3.2 PRIMARY OLIVINE (1) ANALYSES AVERAGED'

	1	2	3	4	5	6	7	8
	60237	60902	60075	60196	60160	60094	60876	60163
OXIDE WEIGHT PERCENTAGE								
SIO2	41.67	41.37	41.28	41.07	40.94	41.12	41.08	41.10
TIO2	0.04	0.04	-	0.03	0.04	0.01	0.04	0.04
AL2O3	0.06	0.18	0.18	0.12	0.04	0.05	0.12	0.15
CR2O3	0.03	0.02	0.06	0.05	0.03	0.02	0.05	0.05
FEO	5.40	7.58	7.70	8.96	9.49	9.24	9.14	8.84
MNO	0.09	0.13	0.12	0.14	0.16	0.12	0.13	0.13
MGO	52.55	50.57	50.85	49.66	49.37	49.50	49.50	49.73
CAO	0.02	0.02	-	-	-	-	0.01	0.01
NIO	0.45	0.32	0.29	0.27	0.32	0.28	0.30	0.31
TOTAL	100.31	100.23	100.48	100.30	100.39	100.34	100.37	100.36
ATOMIC PROPORTIONS ON THE BASIS OF 4 OXYGENS								
SI	0.999	1.001	0.997	1.000	0.998	1.001	1.000	0.999
TI	0.001	0.001	0.000	0.001	0.001	0.000	0.001	0.001
AL	0.002	0.005	0.005	0.003	0.001	0.001	0.003	0.004
CR	0.001	0.000	0.001	0.001	0.001	0.000	0.001	0.001
FE2	0.108	0.153	0.156	0.182	0.194	0.188	0.186	0.180
MN	0.002	0.003	0.002	0.003	0.003	0.002	0.003	0.003
MG	1.877	1.824	1.831	1.801	1.795	1.797	1.796	1.802
CA	0.001	0.001	0.000	0.000	0.000	0.000	0.000	0.000
NI	0.009	0.006	0.006	0.005	0.006	0.005	0.006	0.006
END MEMBER COMPOSITIONS								
MG	94.46	92.12	92.05	90.67	90.11	90.40	90.49	90.81
FE	5.54	7.88	7.95	9.33	9.89	9.60	9.51	9.19

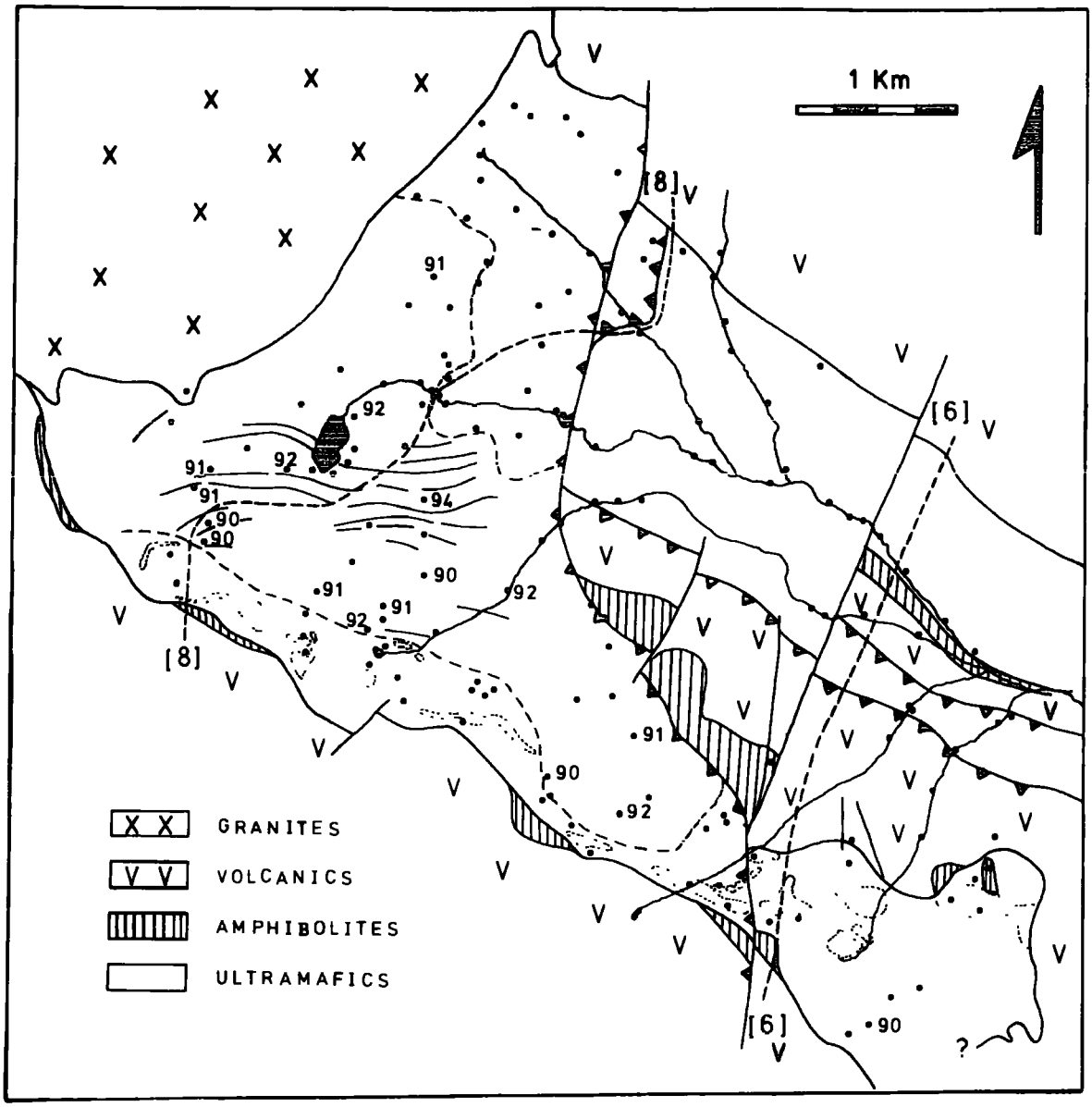

Figure 3.3 A sketchmap showing the distribution of the average olivine (1) forsterite content. Values have been rounded to the nearest percent.

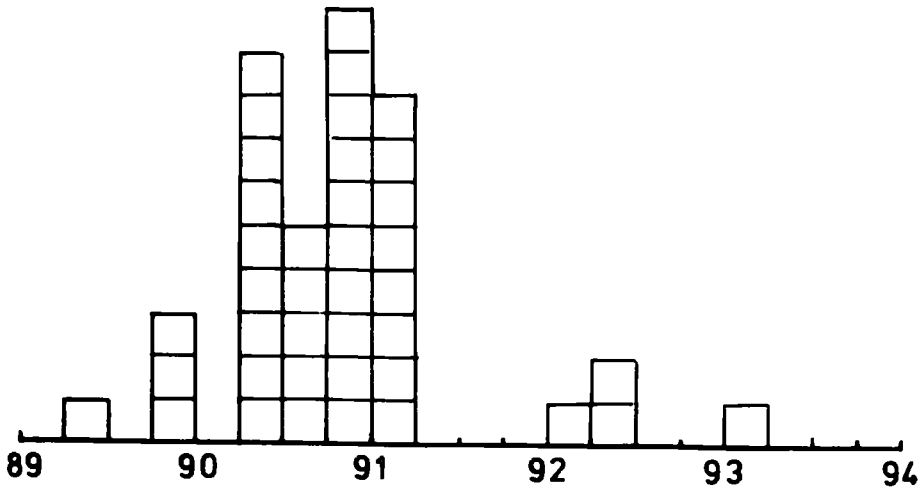

FORSTERITE
in
PERIDOTITE

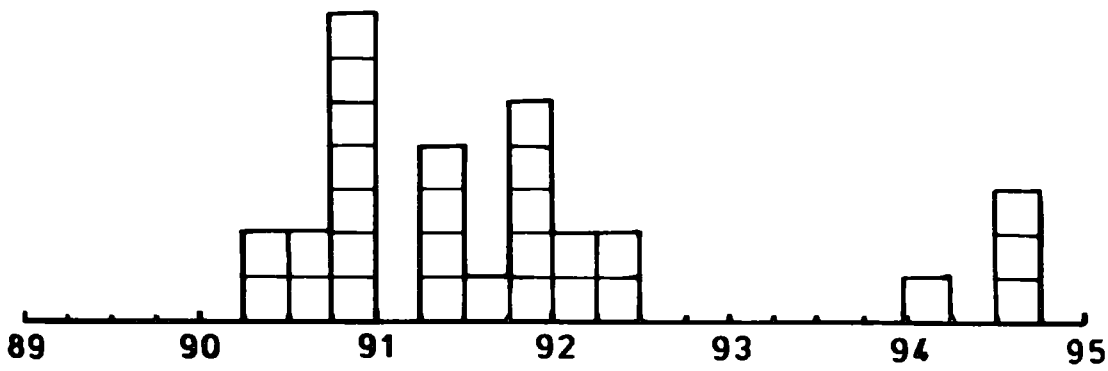

FORSTERITE
in
DUNITE

Figure 3.4 A frequency distribution plot of olivine (1) forsterite content, in rocks of dunite, and of peridotite composition. The sample lithology is as defined in Table 1.2, and the olivine (1) data is from Table 3.1.

One exceptional sample, 60237, has a far higher Fo content than the rest, Figure 3.4. The sample is a spinel rich dunite, and in having a Fo-rich olivine, it resembles similar olivines from olivine bearing chromitites, noted by Challis (1965), and Rodgers (1973). Irvine (1967) accounts for this Mg enrichment by local re-equilibration between olivine and spinel on cooling. The Fe partitions in favour of spinel, and Mg in favour of olivine. This effect will only be noticeable where the model proportion of spinel is high, and olivine correspondingly low.

Simpkin and Smith (1970), show that igneous olivines systematically increase their Ni content, and decrease their Mn content, with increase in forsterite. They established trends of Mn and Ni depletion, and enrichment, based on naturally occurring igneous olivines. The Blue River olivines contain amounts of Mn and Ni compatible with their igneous origin, Figures 3.5 and 3.6. The amount of Mn, as MnO, is low; between 0.08% and 0.23% MnO. The amount of Ni, as NiO is slightly variable; between 0.19% and 0.47% NiO. Table 3.3 contains comparable data from other bodies.

Olivine contains negligible amounts of Ti, Cr, and Ca, as might be expected from its petrogenetic environment, Simpkin and Smith (1970). The amount of Al allowed in the olivine structure is negligible, and no significance is

Table 3.3

"Alpine" peridotite olivine compositions

	Fo	NiO%	MnO%
1. Blue River	89.5-94.6	0.19-0.47	0.08-0.23
2. Burro Mt.	90.7-92.7	0.28-0.47	0.14-0.19
3. Vulcan Peak	88.8-94.4	0.25-0.47	0.05-0.10
4. Oregon	90.0-90.5	-	0.13-0.14
5. Papua	91.6-93.6	0.2 - 0.4	-

1 = This study; 2 = Loney et al (1971); 3 = Himmelberg and Loney (1973); 4 = Medaris (1972); 5 = England and Davies (1973).

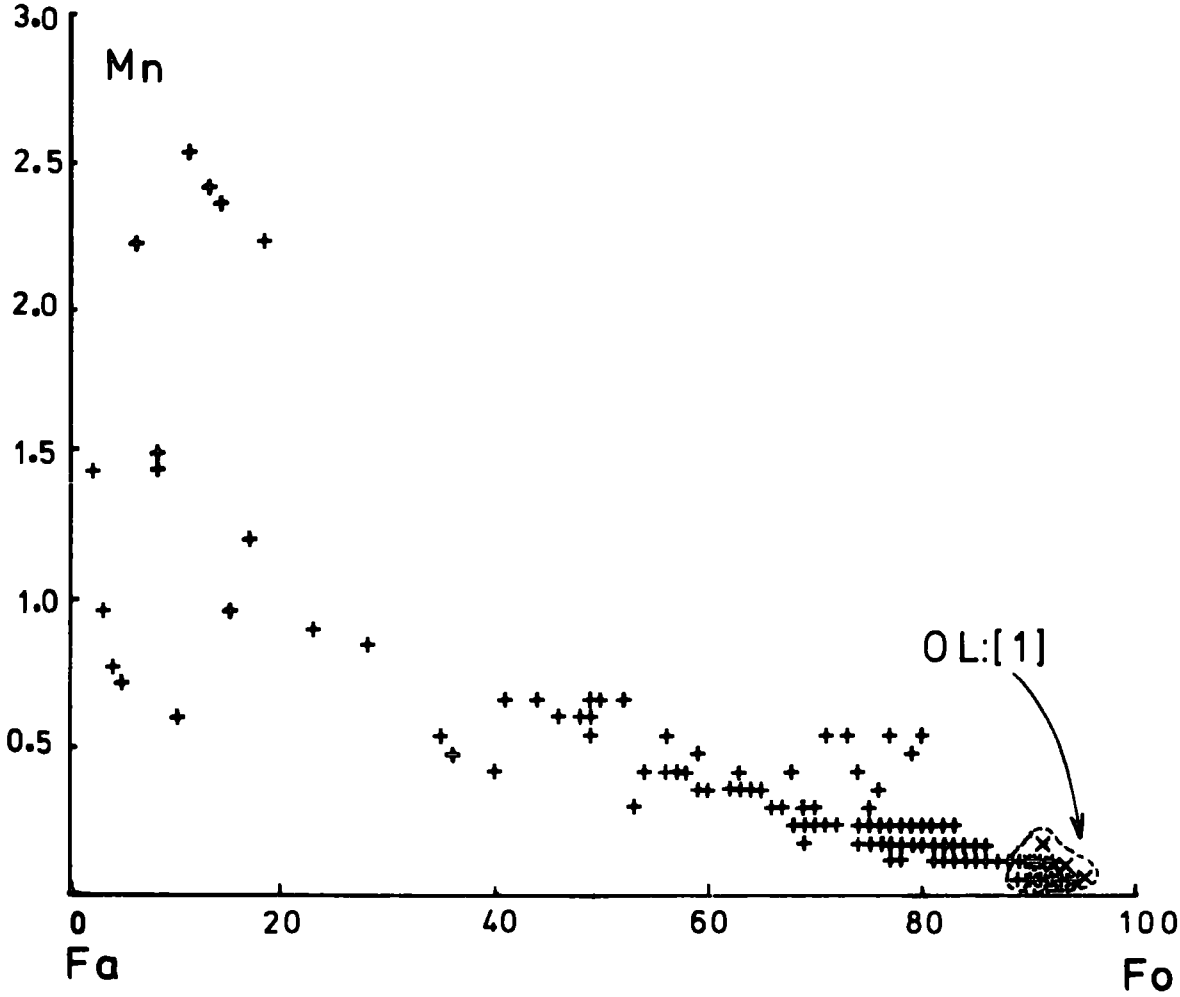

Figure 3.5 Mn variation with olivine forsterite content. Primary Blue River olivines, (denoted as (X)), are plotted with igneous olivines given by Simpkin and Smith (1970). These are denoted as (+).

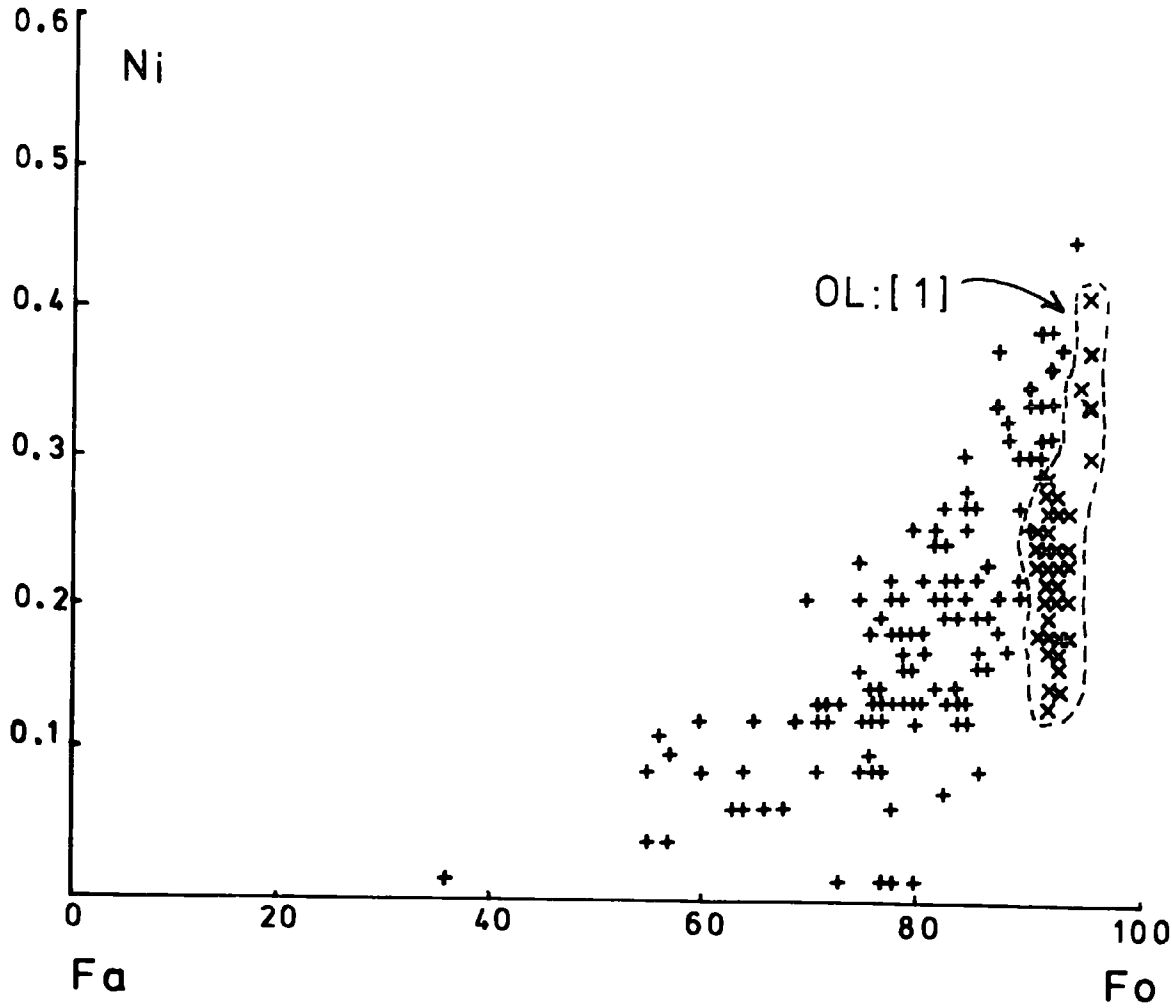

Figure 3.6 Ni variation with olivine forsterite content. Primary Blue River olivines (denoted as (X)), are plotted with igneous olivines given by Simpkin and Smith (1970). These are denoted by (+).

attached to the Al traces observed in some samples. Similarly the amount of Fe^3 allowed in the structure is limited, and all the Fe is calculated as FeO.

(ii) Orthopyroxene (1)

Primary enstatite phenocrysts occur as single crystals, and as crystal clusters, within the harzburgite and lherzolite components of the ultramafic assemblage. Stable enstatite grains are restricted to Unit (1), Figure 3.7. They are subeuhedral to subrounded, and 1.0-1.5 mm in width. Minor amounts of relict enstatite were also observed in Sample 60226; the relicts occur within talc.

The enstatites contain exsolution lamellae, and some also contain exsolved blebs of clinopyroxene. Both appear to be orientated parallel to (100). As noted by Wolfe (1967), this textural feature is similar to that shown by Bushveld enstatites. Exsolution lamellae are commonly observed in "alpine" peridotite enstatites, as by Challis (1965), and by Loney et al. (1971). Exsolution presumably reflects inability to accommodate Ca in the enstatite structure, as in Samples 60163, and 60168.

Enstatites are commonly deformed, and the cleavage parallel to (100) is often warped. Some show strained extinction, and kink bands occur in Samples 60163 and 60874, Plate 3.9 . Fracturing may occur perpendicular to (100),

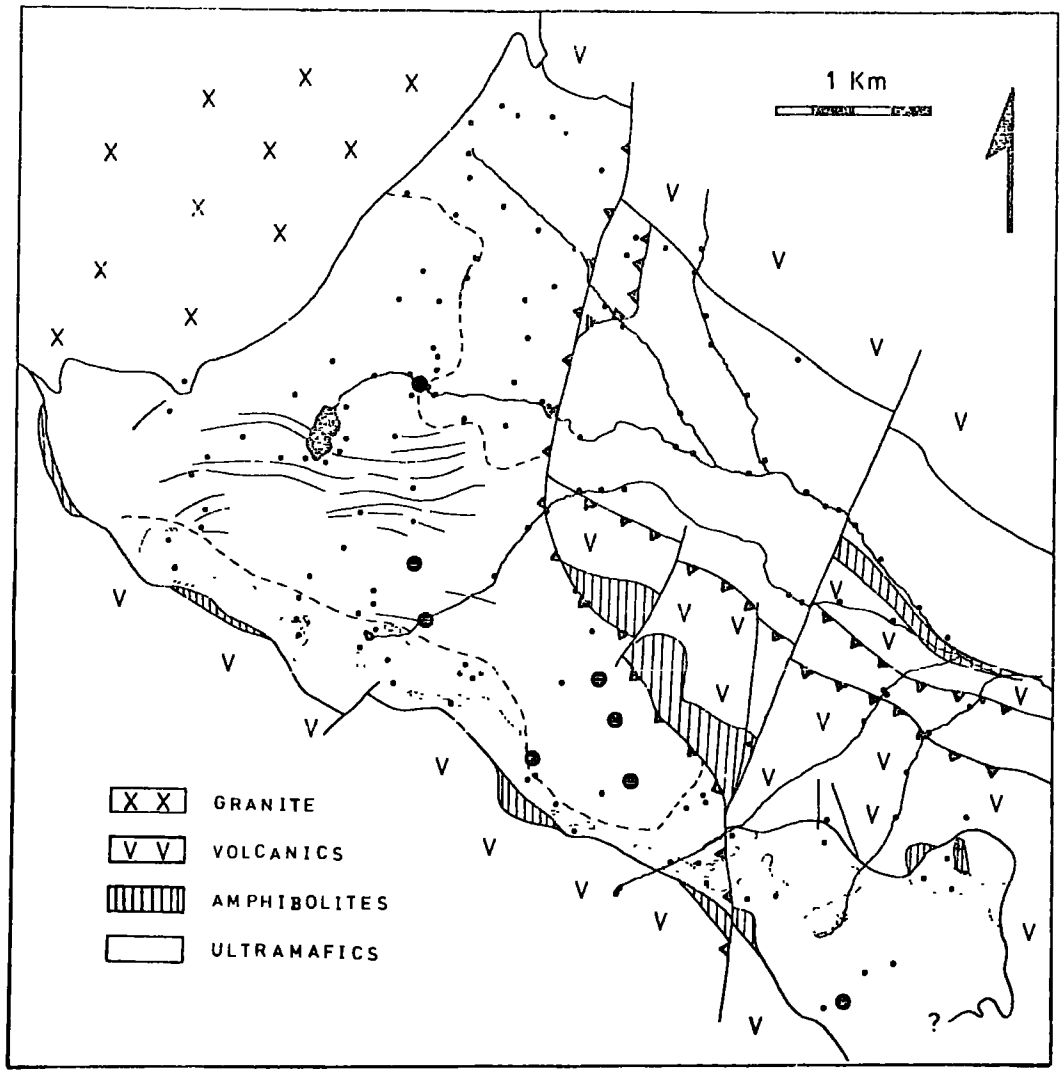

Figure 3.7 Distribution of enstatite (1).

and parallel to the (001) kink band. Deformation appears to post-date exsolution of the lamellae.

Many enstatites enclose rounded crystals of olivine, and a few enclose small subeuhedral grains of spinel. Similar textural relationships were observed by Jackson (1961), in the Stillwater Complex, and Challis (1965), in New Zealand ultramafics.

Orthopyroxene (1) Chemistry.

Orthopyroxene analyses are given in Table 3.4, and averaged analyses are given in Table 3.5. The compositional range is small, and although the pyroxene lies within the field of enstatite, it lies close to the field of bronzite.

The enstatite component, as defined by the Mgx100/(Mg+Fe) ratio, ranges from $En_{90.4}$-$En_{91.4}$. This range compares well with a range of En_{89}-En_{92} given by Wolfe (1967). This range was obtained by refractive index studies on six enstatites. The range of Fe, or ferrosilite substitution is clearly restricted, and the actual Mgx100/(Mg+Fe) ratio is similar to that of the coexisting olivine. Figure 3.8 shows that near 1:1 partitioning of Mg and Fe occurred, with a slight excess of Mg going into enstatite. This relationship is fairly common in "alpine" peridotites, and similar data from a number of comparable bodies are also plotted. The Mg:Fe ratio, and its distribution between the two phases, is remarkably constant, O'Hara (1963).

'TABLE 3.5 ENSTATITE(1) ANALYSES AVERAGED'

	1	2	3	4
	60160	60163	60876	60094
OXIDE WEIGHT PERCENTAGE				
SIO2	55.68	56.23	56.27	55.51
TIO2	0.07	0.09	0.06	0.02
AL2O3	3.17	2.76	2.73	2.82
CR2O3	0.63	0.61	0.69	0.90
FEO	6.07	5.90	5.70	5.85
MNO	0.14	0.14	0.14	0.14
MGO	33.48	33.95	33.28	32.60
CAO	0.63	0.64	1.29	1.90
NIO	-	-	-	-
TOTAL	99.87	100.32	100.16	99.74
ATOMIC PROPORTIONS ON THE BASIS OF 6 OXYGENS				
SI	1.924	1.932	1.938	1.928
TI	0.002	0.002	0.002	0.001
AL	0.129	0.112	0.111	0.115
CR	0.017	0.017	0.019	0.025
FE2	0.175	0.170	0.164	0.170
MN	0.004	0.004	0.004	0.004
MG	1.724	1.739	1.708	1.687
CA	0.023	0.024	0.048	0.071
NI	0.000	0.000	0.000	0.000
END MEMBER COMPOSITIONS				
CA	1.21	1.22	2.47	3.66
MG	89.47	89.81	88.78	87.33
FE	9.32	8.97	8.75	9.01

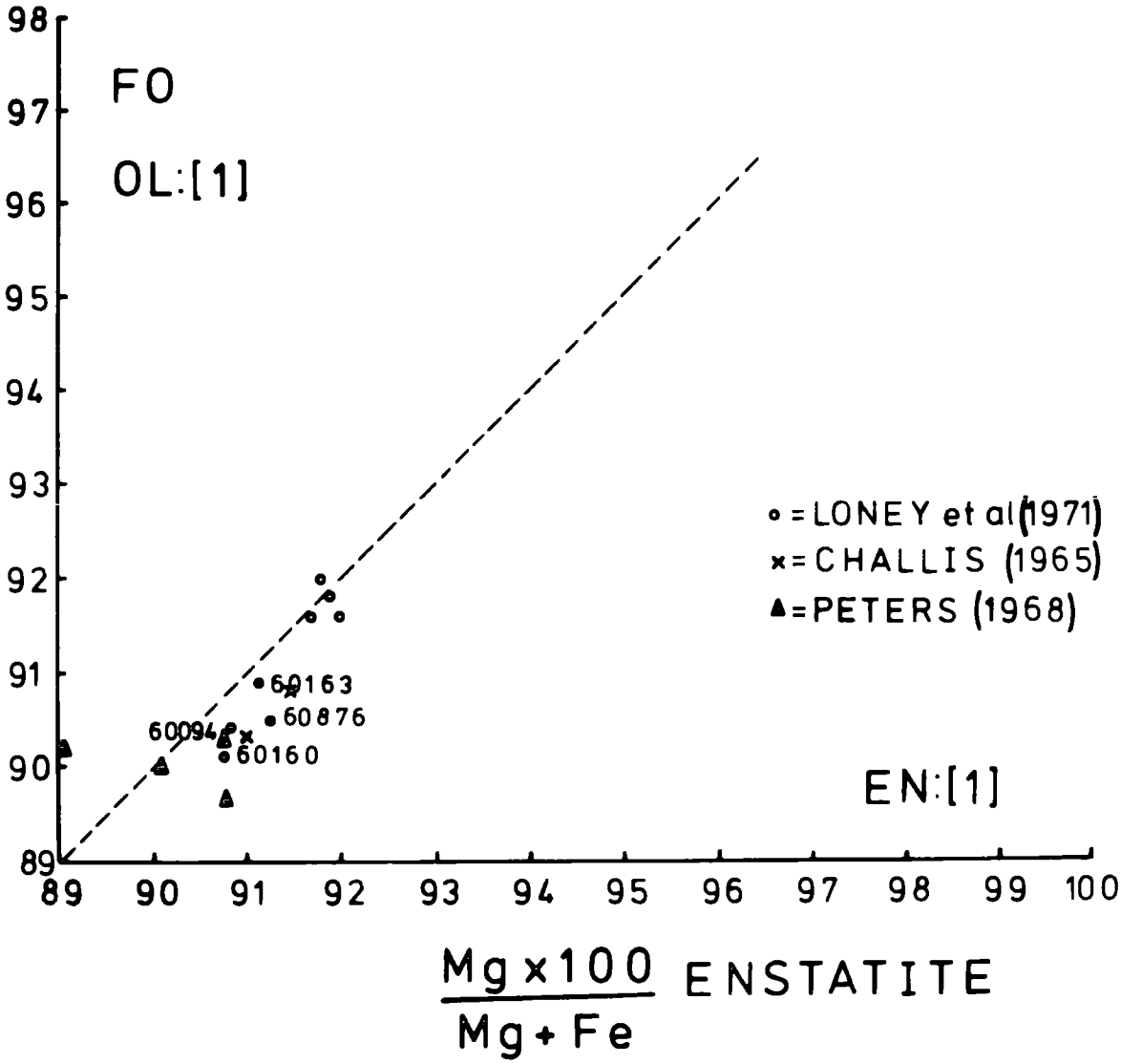

Figure 3.8 A plot of olivine (1) forsterite content against enstatite (1) enstatite content. Additional data from Loney et al (1971), Challis (1965), and Peters (1968) are also given.

Medaris (1972) has shown that the distribution of Mg and Fe is a useful guide to equilibrium, but that it is not a reliable temperature indicator.

The analyses given in Table 3.4 are of host enstatite that has already exsolved clinopyroxene. They are not representative of the initial enstatite formed, and they should not be compared directly with wet chemical analyses. In practice the proportions of Fe, Mg and Al do not differ substantially between host and lamellae, and the only major influence will be on Ca. Probe analyses should be somewhat lower than wet chemical analyses. Loney et al. (1971) discuss this point. They record a range of 0.7-1.1% CaO in probe analysed Burro Mountain enstatites. The somewhat higher Blue River values, up to 2.5% CaO in Sample 60094, may reflect incipient "rodingitization", as discussed in Chapter 7. Textural evidence supports this.

A major potential variable in the enstatite composition is reflected in the Al_2O_3 content. This covers a range from 2.25-3.25% Al_2O_3. The Al_2O_3 content is shown on Figure 3.9 with a range in additional analysed "alpine" enstatites, derived from a variety of differing occurrences, Green (1964), Kornprobst (1969), Loney et al. (1971), England and Davis (1972), Challis (1965), Medaris (1972) and Himmelberg et al. (1973).

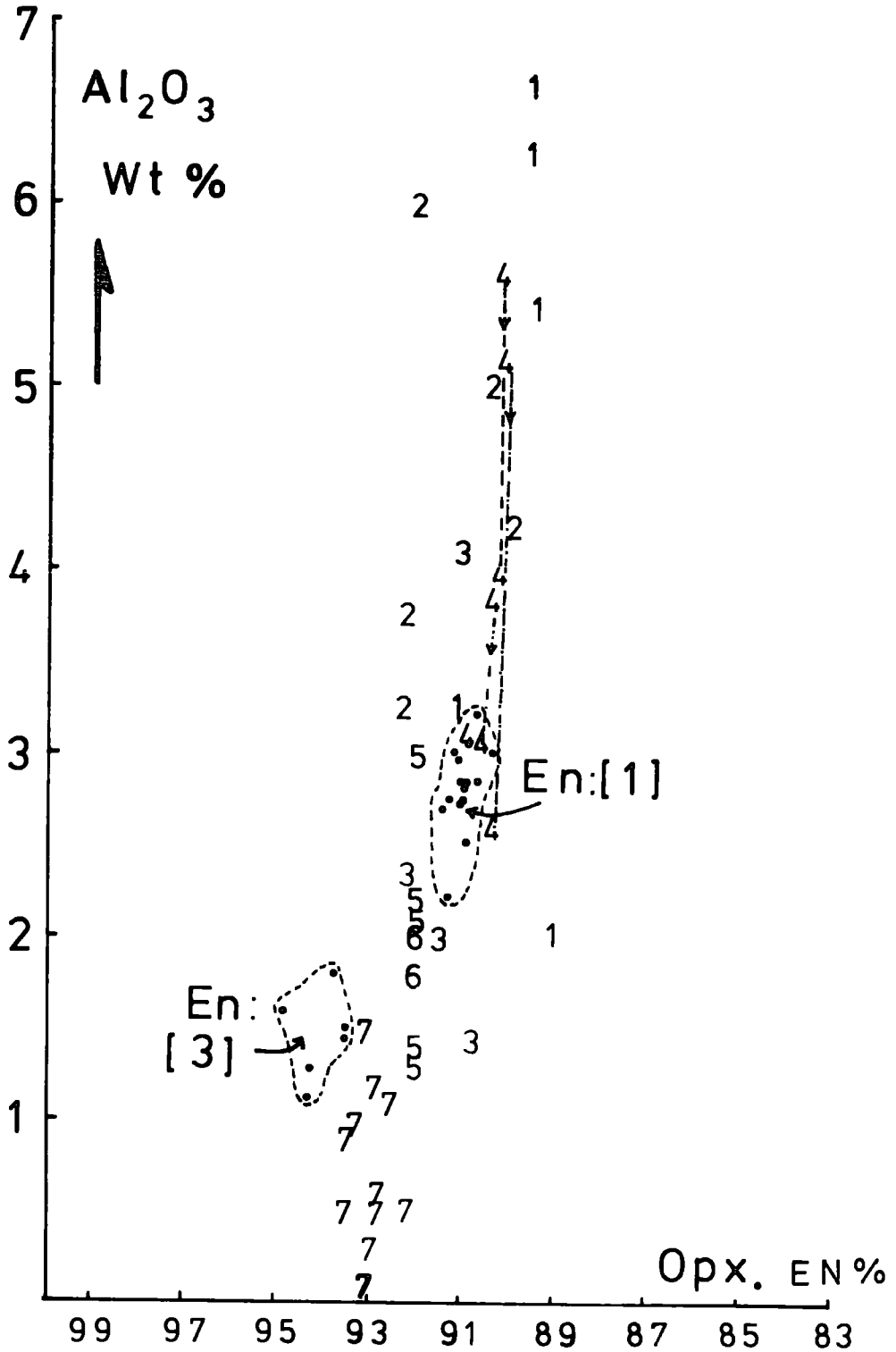

Figure 3.9 Al_2O_3 solubility in orthopyroxene. En(1) and En(3) refer to primary and metamorphic Blue River enstatites respectively.

Additional data: 1 = Lizard, England, Green (1964)
2 = Ben Bouchia, Morroco, Kornprobst (1969)
3 = Dun Mt., New Zealand, Challis (1965)
4 = Oregon, U.S.A., Medaris (1972), (zoned core to margin)
5 = Burro Mt., U.S.A., Loney et al. (1971)
6 = Vulcan Peak, U.S.A., Himmelberg et al. (1973)
7 = Papua New Guinea, Davis and England (1973)

The Al_2O_3 content appears to be independent of the coexisting spinel Al_2O_3 content, and the enstatite thus appears to be saturated in Al, Figure 3.10. This contrasts with the observations of Loney et al. (1971), on the Burro Mountain body, and Himmelberg et al. (1973), on the Vulcan Peak intrusive.

(iii) Clinopyroxene (1)

Small, euhedral, primary, clinopyroxene crystals are intimately associated with enstatite. Granular diopside crystals, up to 0.4 mm in diameter, occur around the margins of some of the larger enstatites, as in Sample 60094. In a few cases the diopside forms discrete 1.0 mm phenocrysts, as in Sample 60226, but these are rare, and subordinate to enstatite.

Diopside also occurs in lamellae, and as exsolved blebs, in orthopyroxene. Possibly much of the granular diopside was also originally exsolved, as it bears a strong affinity for enstatite. Challis (1965) describes a similar relationship between the two phases.

Diopside appears to remain as a stable phase below the level of the tremolite isograd (Chapter 5). Lamellae in a "bastite", in Sample 60067, have survived serpentinization, regeneration, and reserpentinization, Plate 3.10. Similarly Sample 60033 contains apparently original, granular,

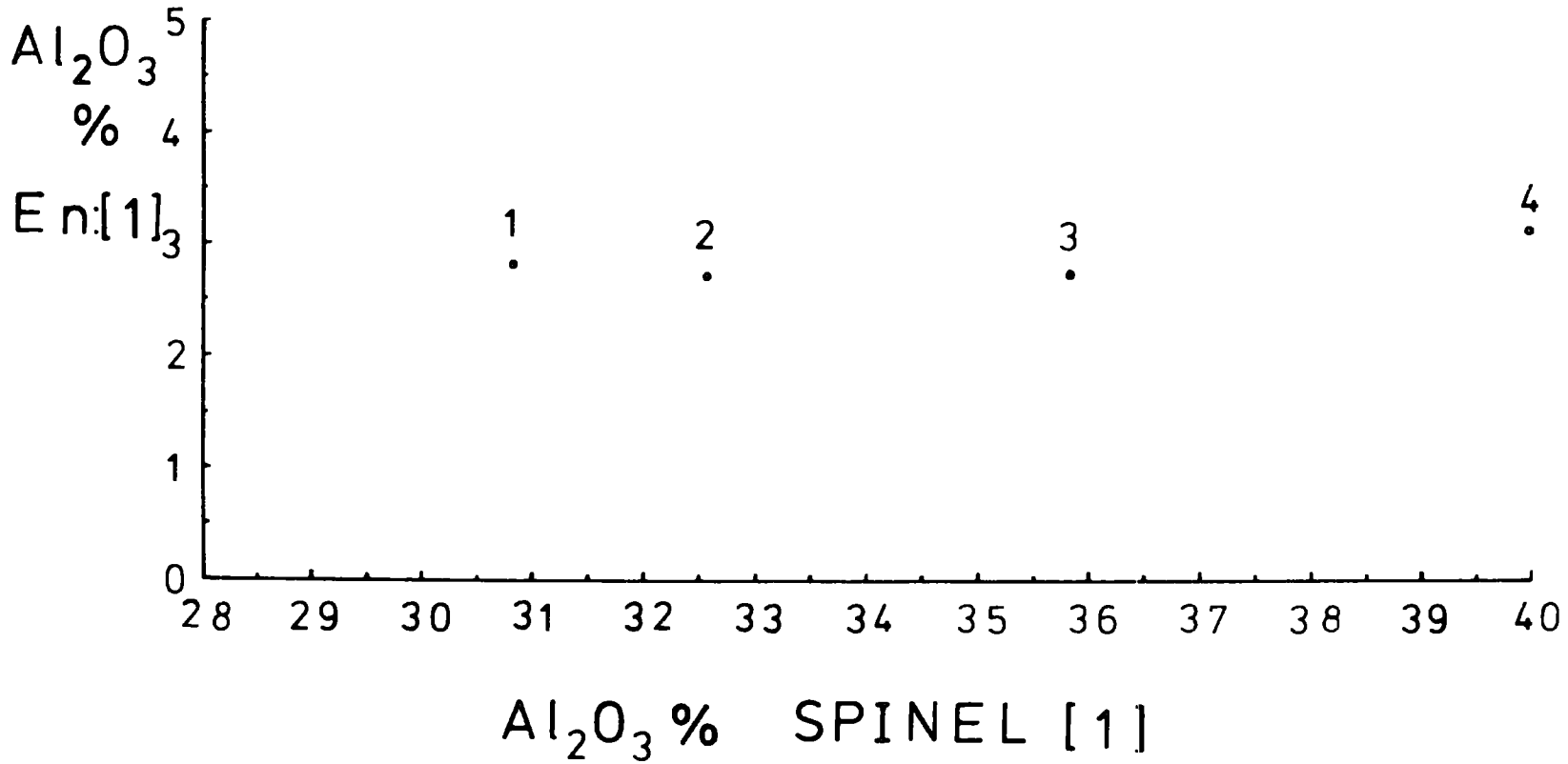

Figure 3.10 The solubility of Al_2O_3 in enstatite (1). The average Al_2O_3 content in enstatite, (Table 3.5), is plotted against the average Al_2O_3 value for the coexisting spinel (1) phase. (Table 3.10).
1 = 60094, 2 = 60876, 3 = 60163, 4 = 60160.

diopside. Elsewhere, in Sample 60041, the diopside appears to have been remobilised into scattered lozenges. The stability of diopside contrasts with the instability of the gabbro clinopyroxene during serpentinization, and it makes the Ca source problem during rodingitization difficult to explain. Gabbros in serpentinized harzburgite have been Ca metasomatized to rodingite.

The solubility of diopside in enstatite is a function of temperature, and Al_2O_3 content. An increase in the Al_2O_3 content results in a decrease in the mutual solubility, MacGregor (1967).

Clinopyroxene (1) Chemistry

Clinopyroxene analyses are given in Table 3.6, and are displayed in Figure 3.11, (a pyroxene quadrilateral). The analyses may be grouped in terms of textural form into granular , matrix diopsides, and lamellae diopsides within enstatite. Averaged analyses for each variety are given in Table 3.7. The lamellae population appears to be lower in SiO_2, and MgO, and correspondingly enriched in Al_2O_3, and Cr_2O_3. There is insufficient data to delineate two distinct populations. The observed differences may represent disequilibrium, or possibly stages of exsolution. Once exsolved, matrix diopside might be influenced by the other coexisting phases.

'TABLE 3.7 DIOPSIDE(1) ANALYSES AVERAGED'

	1	2	3	4	5	6
	60067M	60067L	60094M	60094L	60876M	60160L
OXIDE WEIGHT PERCENTAGE						
SIO2	53.63	52.16	53.85	51.76	52.62	51.70
TIO2	0.11	0.14	0.05	0.02	0.13	0.14
AL2O3	2.05	3.41	2.23	3.00	2.80	3.53
CR2O3	0.44	0.99	1.17	1.31	0.92	1.10
FEO	2.04	2.11	1.79	2.38	1.99	2.14
MNO	0.09	0.09	0.07	0.13	0.09	0.08
MGO	17.11	16.35	17.38	18.02	17.07	16.22
CAO	24.38	24.40	23.56	24.04	23.63	23.53
NIO	-	-	-	-	-	-
TOTAL	99.85	99.65	100.10	100.66	99.25	98.44
ATOMIC PROPORTIONS ON THE BASIS OF 6 OXYGENS						
SI	1.950	1.907	1.948	1.880	1.925	1.910
TI	0.003	0.004	0.001	0.001	0.004	0.004
AL	0.088	0.147	0.095	0.128	0.121	0.154
CR	0.013	0.029	0.033	0.038	0.027	0.032
FE2	0.062	0.065	0.054	0.072	0.061	0.066
MN	0.003	0.003	0.002	0.004	0.003	0.003
MG	0.927	0.891	0.937	0.976	0.931	0.893
CA	0.950	0.956	0.913	0.936	0.926	0.931
NI	0.000	0.000	0.000	0.000	0.000	0.000
END MEMBER COMPOSITIONS						
CA	48.92	49.94	47.90	47.08	48.23	49.20
MG	47.74	46.54	49.14	49.08	48.45	47.17
FE	3.34	3.52	2.95	3.84	3.32	3.63

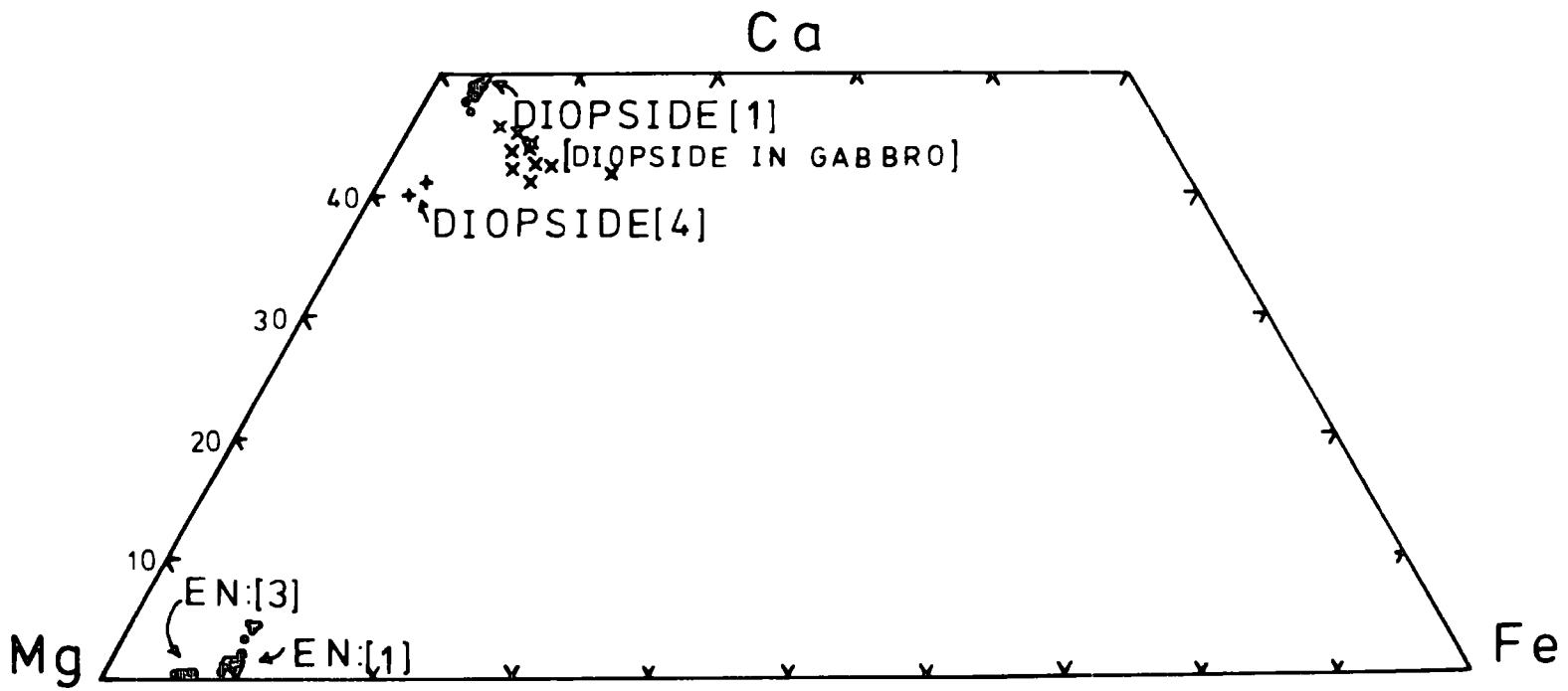

Figure 3.11 A pyroxene Quadrilateral, showing primary and metamorphic enstatite, primary diopside, and diopside (4) formed from enstatite (1). Clinopyroxenes from Blue River gabbros are also shown.

As enstatite and olivine are in equilibrium with spinel, Figure 3.20 and 3.21, it is likely that they are in equilibrium with each other, and that diopside lamellae are more or less in equilibrium with olivine.

The analyses are relatively homogeneous, in terms of the pyroxene quadrilateral, Figure 3.11, and they are similar to diopsides analysed by Loney et al. (1971), from the Burro Mountain.

(iv) Chrome Spinels (1) (Picrochromite)

An estimated 1-2% of the primary ultramafic material consists of discrete, disseminated, crystals of chrome spinel (Wolfe, 1967). The spinel conforms to the pyroxene based compositional banding in the rock, and it locally concentrates into disseminated and massive lenses a few centimetres across, which lie in the plane of the rock foliation. Within such concentrations the spinel is often fractured, and serpentine forms a matrix for disrupted chrome spinel, and for granulated primary olivine (60237, Plate 3.11).

Discrete spinel crystals are found disseminated throughout both peridotite and dunite, in the primary core region of the intrusive, and they also occur in regions of serpentinite, and metamorphosed serpentinite, Figure 3.12. They vary slightly in both form and size. Small, 0.25- 1.0 mm

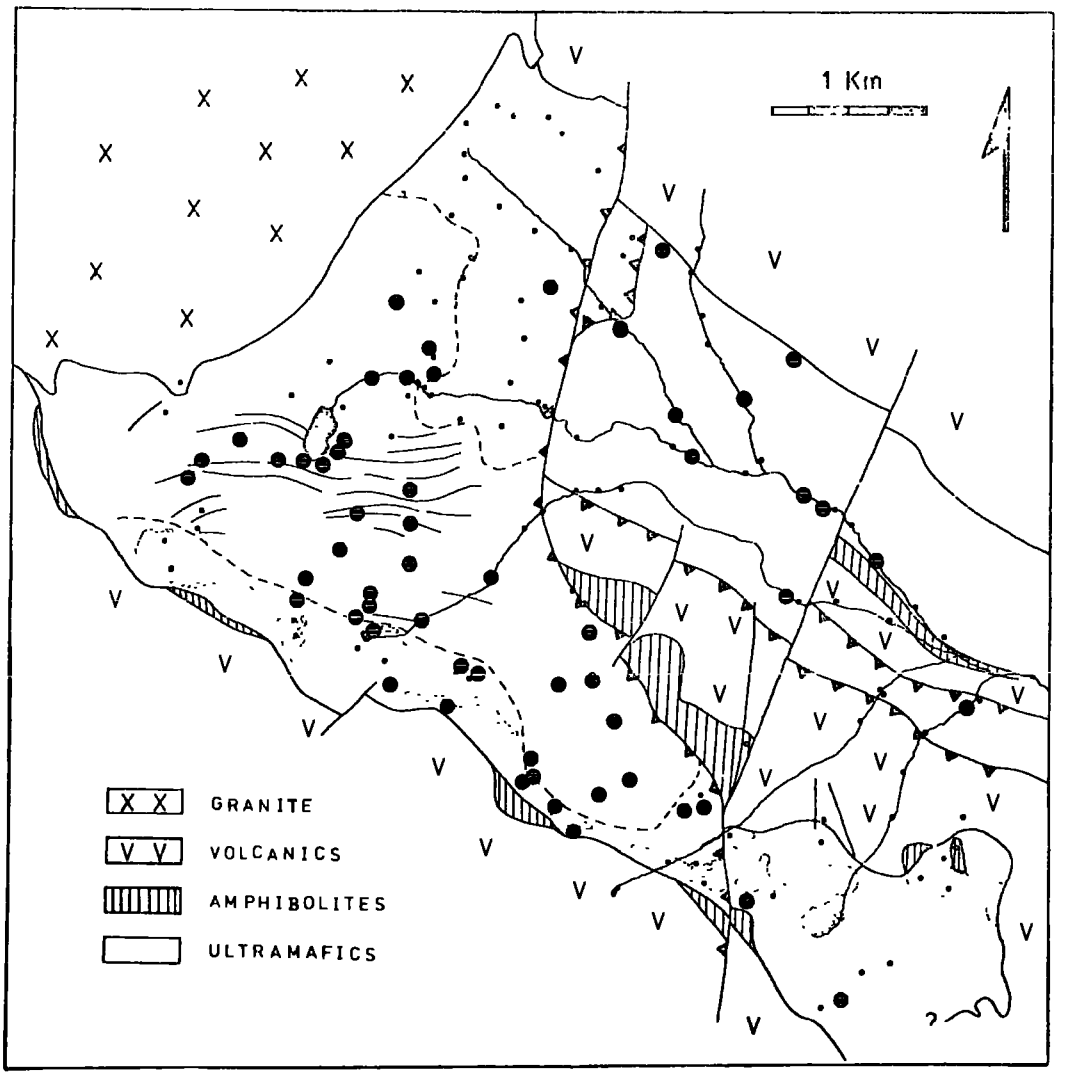

Figure 3.12 Distribution of spinel (1).

euhedral, translucent red spinels are found in all the dunite samples, and some of the harzburgite samples. The spinels are rarely fractured, but most have rounded corners, presumably acquired during the main period of olivine granulation, see Samples 60152, 61615 (Plate 3.12). The spinels show no sign of internal zonation, and rarely contain inclusions. A second variety of disseminated spinel occurs in rocks of peridotite, (harzburgite and lherzolite), composition. The spinels are larger, ranging from 0.5-4.0 mm in diameter. They are characteristically interstitial in form, and they are irregular in outline. The association between pyroxene and this spinel is locally strong, and this variety of spinel is occasionally found to poikilitically enclose both enstatite, and olivine, Samples 60094, 60163 (Plate 3.13). The association is best displayed in those "lherzolitic" samples which contain recognisable diopside. There is a range of transitional textural varieties, which show a progressive development of an interstitial texture, associated with pyroxene in peridotites. Large irregular spinels are not found in dunites, but small euhedral spinels may coexist with large irregular ones in peridotite, as in Sample 60168.

Textural evidence suggests that small euhedral chrome spinels formed early with olivine, and that both pyroxene and irregular spinels formed somewhat later.

Spinel (1) Chemistry

Primary spinel analyses are given in Table 3.8, and average spinel analyses are given in Table 3.9. The spinel composition lies close to the field of picrochromite, as defined by Simpson (1920), and it falls within the compositional prism utilized by Stevens (1944), and by Irvine (1965, 1967), Figure 3.13. Both Stevens and Irvine show that natural spinels deviate little from the stoichiometric formula, $R^{++}R_2^{+++}O_4$. They attribute observed deviation to impurity, analytical error, and subsequent hydrothermal alteration. This last may cause an imbalance in the $Fe^2:Fe^3$ ratio. Addition of appreciable Ti may also influence the stoichiometry of the spinel structure. In practical terms spinel is considered to acheive the "ideal" formula, which requires a $Ro:R_2O_3$ ratio of 1:1. The distribution of Fe (total), as determined by electron microprobe analysis, may be calculated using the "ideal" formula, by assigning appropriate amounts of FeO to the tetrahedral site, and Fe_2O_3 to the octahedral site. The distribution was achieved using the method of Carmichael (1967), in which Ti traces are assigned to the ulvöspinel molecule. Structural formulae, based on 32(O), are given in Tables 3.8 and 3.9.

The amount of Fe^3 contributing to the total trivalent cation content, Figure 3.14, is small, and the spinel

'TABLE 3.9 PRIMARY SPINEL(1) ANALYSES AVERAGED'

	1	2	3	4	5	6	7	8
	60237	60902	60075	60196	60160	60094	60876	60163
OXIDE WEIGHT PERCENTAGE								
SIO2	-	-	-	0.07	-	-	-	-
TIO2	0.24	0.19	0.16	0.17	-	-	0.06	0.01
AL2O3	8.89	10.37	13.48	21.58	39.92	30.82	32.55	35.81
CR2O3	59.56	54.06	53.25	41.29	27.67	37.00	35.36	31.65
FE2O3	2.80	5.03	4.38	5.15	2.36	2.09	2.16	2.65
FEO	17.52	19.11	18.49	21.56	13.00	15.54	14.50	13.39
MNO	0.29	0.51	0.36	0.27	-	0.24	0.18	0.19
MGO	10.34	9.14	10.14	8.81	16.42	13.68	14.62	15.71
CAO	0.02	0.01	-	-	-	-	-	-
NIO	-	-	-	-	-	-	-	-
TOTAL	99.66	99.42	100.26	98.90	99.37	99.37	99.43	99.41
ATOMIC PROPORTIONS ON THE BASIS OF 32 OXYGENS								
SI	0.000	0.000	0.000	0.018	0.000	0.000	0.000	0.000
TI	0.048	0.038	0.031	0.033	0.000	0.000	0.011	0.002
AL	2.790	3.271	4.132	6.527	10.650	8.656	9.023	9.744
CR	12.533	11.434	10.946	8.374	4.950	6.968	6.573	5.775
FE3	0.561	1.214	0.857	0.994	0.402	0.375	0.382	0.460
FE2	3.900	4.276	4.021	4.626	2.460	3.096	2.852	2.585
MN	0.065	0.116	0.079	0.059	0.000	0.048	0.036	0.037
MG	4.101	3.644	3.929	3.368	5.537	4.856	5.123	5.404
CA	0.006	0.003	0.000	0.000	0.000	0.000	0.000	0.000
NI	0.000	0.000	0.000	0.000	0.000	0.000	0.000	0.000

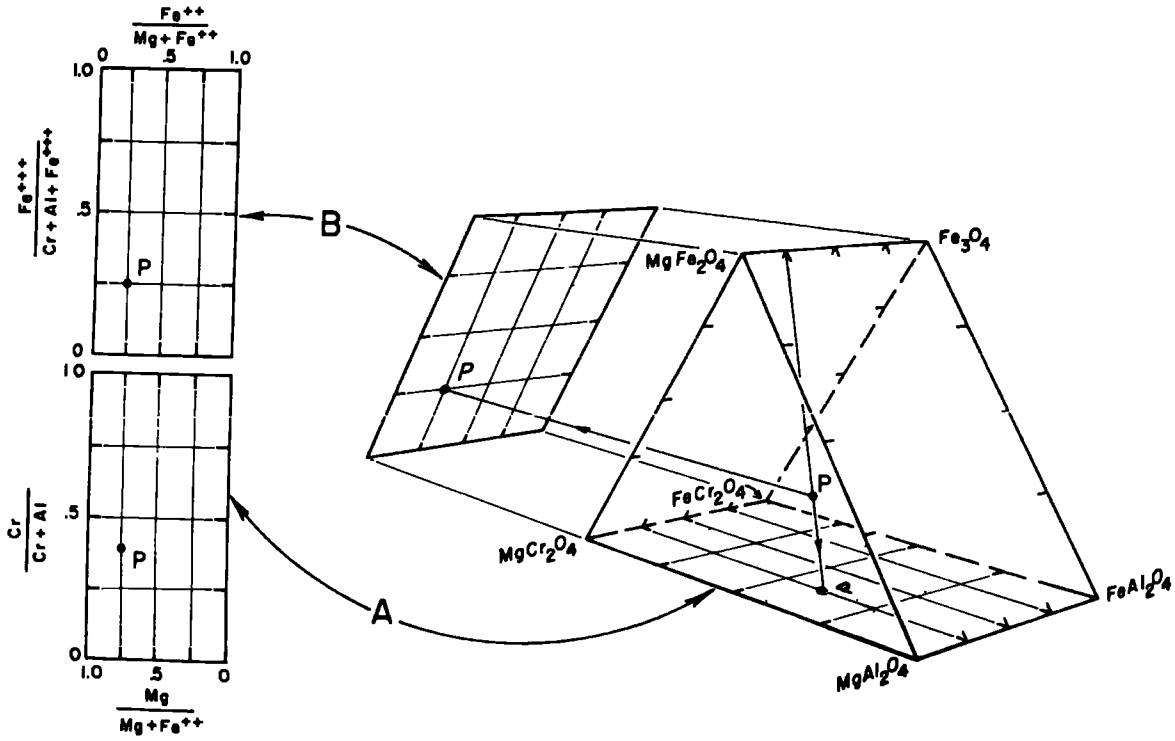

Figure 3.13 A spinel compositional prism, from Irvine (1965). The prism shows the principle compositional end members, and the main spinel ratio plots.

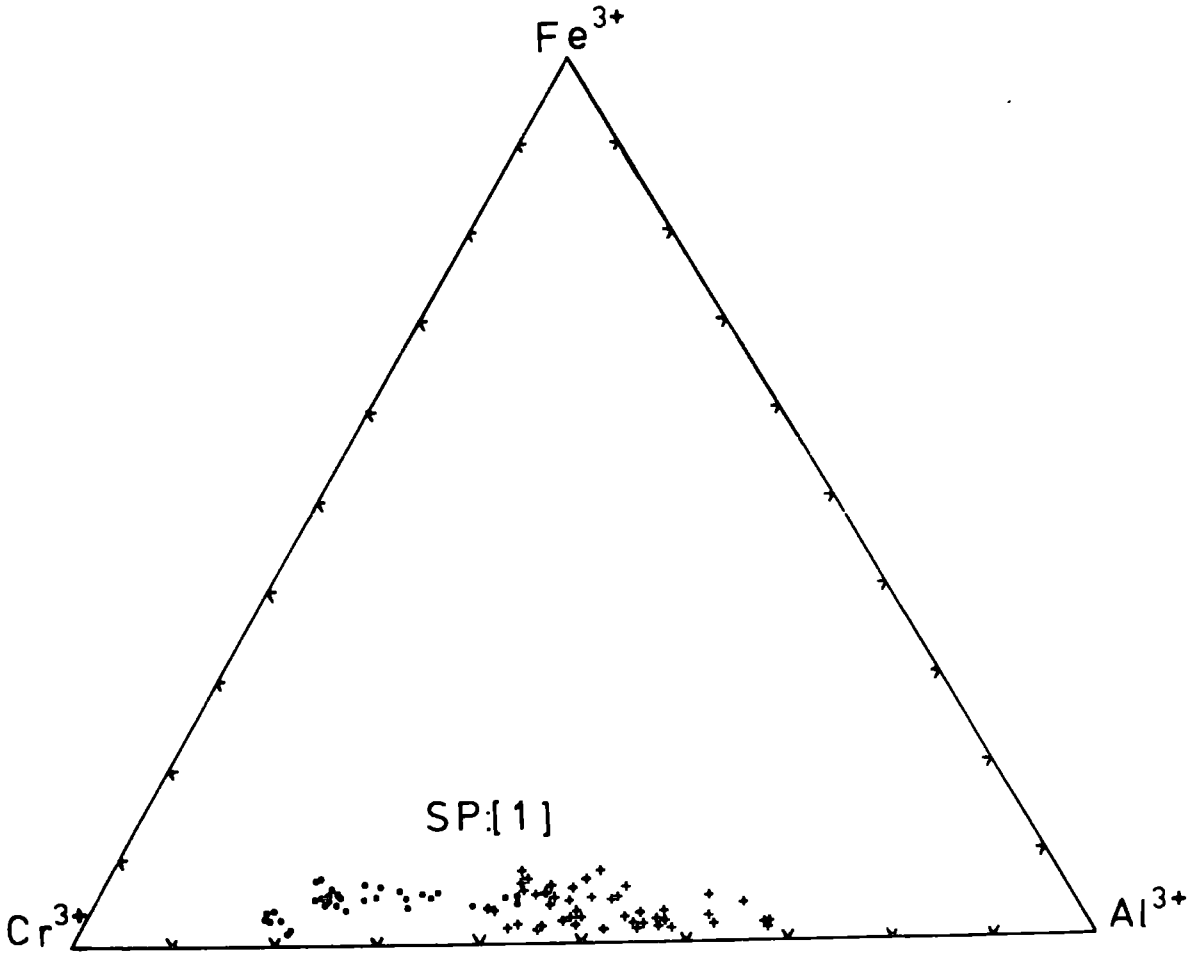

Figure 3.14 A trivalent cation plot.
Primary spinel (1) inferred to have been derived from a dunite host is given as a closed circle, and spinel derived, or thought to have been derived from a peridotite host, is shown as a cross.

usually contains less than 10% Fe^3 in octabedral coordination. This presumably substitutes for Al and Cr, within the "normal" spinel structure. The main substitution trend involves Al and Cr, and a solid solution series was observed between Cr rich and Al rich spinels.

There are two separate, but sympathetic substitution trends, which give a compositional spread within the four phase system, $FeCr_2O_4$-$MgCr_2O_4$-$FeAl_2O_4$-$MgAl_2O_4$. Substitution of Al for Cr in the octahedral site, as noted above, is the main substitution trend, Figure 3.14. In addition Mg substitutes for Fe in the tetrahedral site, Figure 3.15. Mg substitution is only readily apparent at high values of Al.

The only other significant cation is Mn, which occurs as traces of up to 0.5% MnO. The Mn content appears to be highest in those spinels enriched in Fe and Cr, and least in those enriched in Mg and Al.

The variable Crx100/(Cr+Al) ratio in Figure 3.15, reflects a range in Al_2O_3 content from 8.5-40.0% Al_2O_3, and a concomitant Cr_2O_3 range from 60.5-27.5% Cr_2O_3. The average Al_2O_3 content shows no obvious systematic relationship to primary banding, across the body as a whole, and compositional extremes are often closely distributed, Figure 3.16.

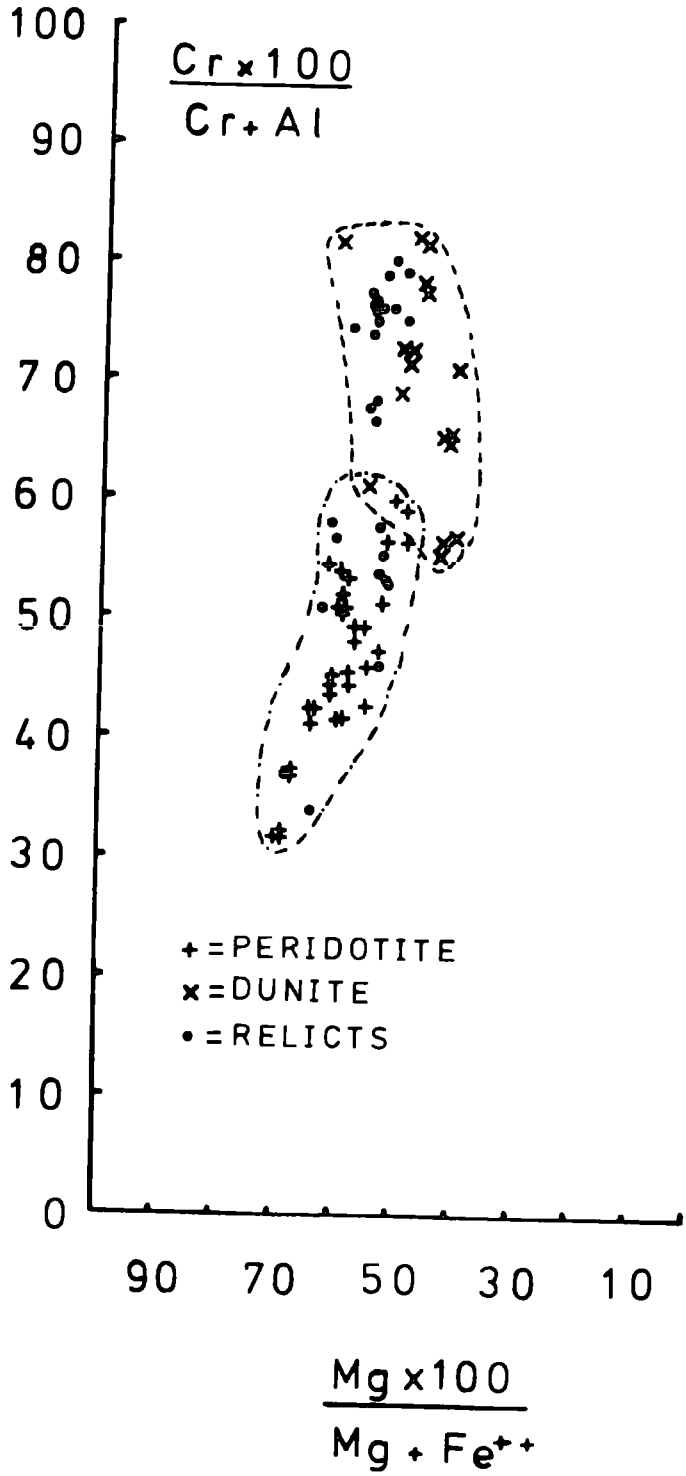

Figure 3.15 Cation ratio plot, after Irvine (1965,1967). Spinel (1) is differentiated according to the host lithology, as defined in the text.

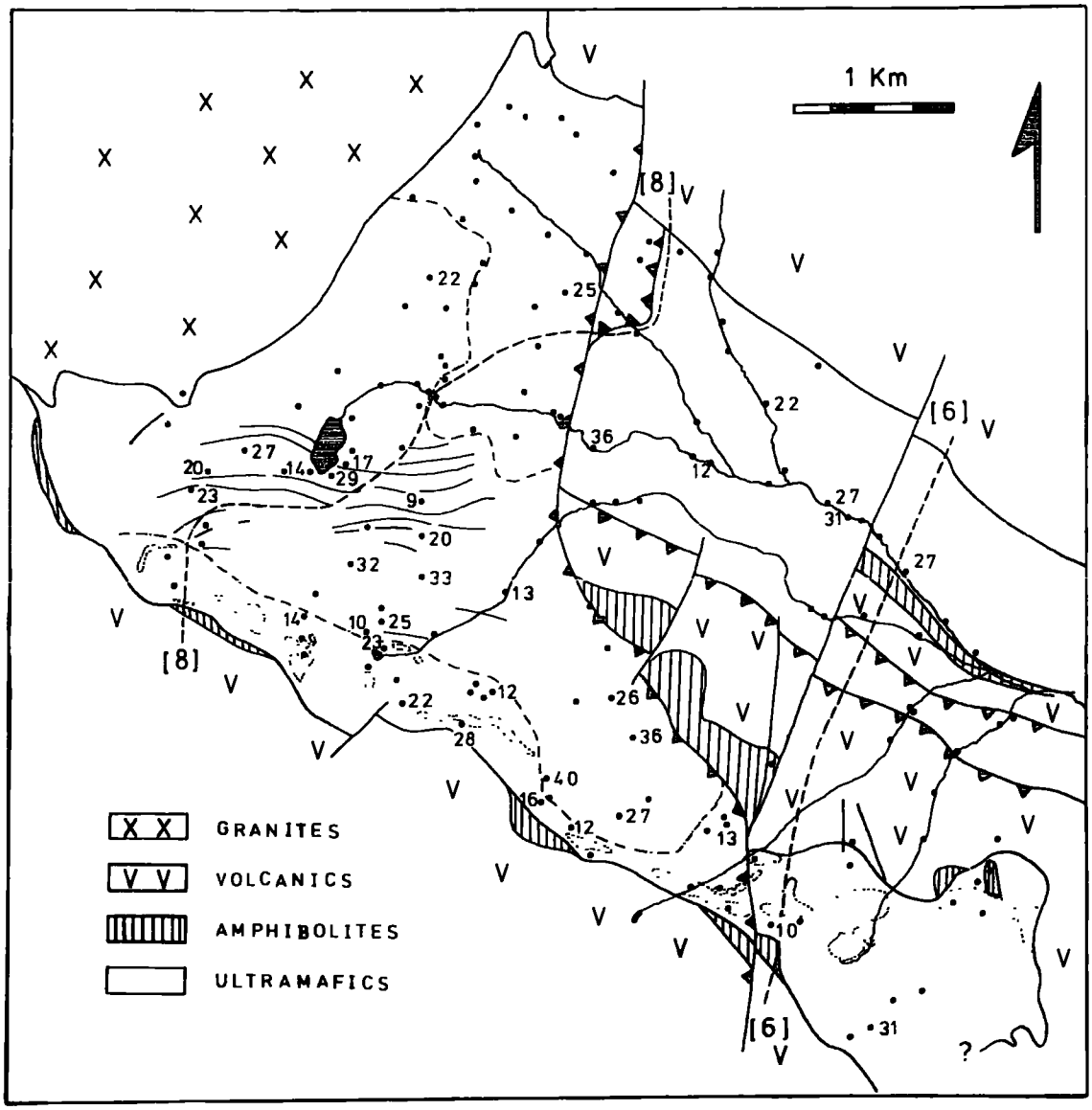

Figure 3.16 Sketchmap showing the distribution of the average Al_2O_3 content in spinel (1). Values are rounded to the nearest percent.

The spinels are homogenous, and consistent at a scale of the individual thin section, but they are very variable across the body as a whole. Compared with other spinel suites from "alpine" assemblages, quoted by Irvine (1967), the Blue River spinels cover almost the entire recorded compositional range, and have a wider spread than most suites, Figure 3.17. This is remarkable in a body of at most 25 km^2 areal extent.

The spinel chemistry shows a strong correlation with host rock lithology. The sample population was subdivided into two primary and one secondary group, and they are plotted accordingly on Figure 3.15.

1. Peridotite: Any sample containing recognizable pyroxene, bastite, or other pseudomorph after pyroxene, within the area of the polished thin section, Table 1.2.
2. Dunite: Samples in which no pyroxenes, or pyroxene pseudomorphs, were observed, Table 1.2.
3. Regenerated Dunite: Samples of metamorphosed serpentinite which retain relicts of primary spinel.

The textural distinction between spinels of dunite and peridotite host, and the progressive textural change from small euhedral to large and interstitial, is reflected in a chemical change from Cr to Al rich spinel.

Although similar trends have been recorded, for instance by Aumento and Loubat (1971), for Mid-Atlantic

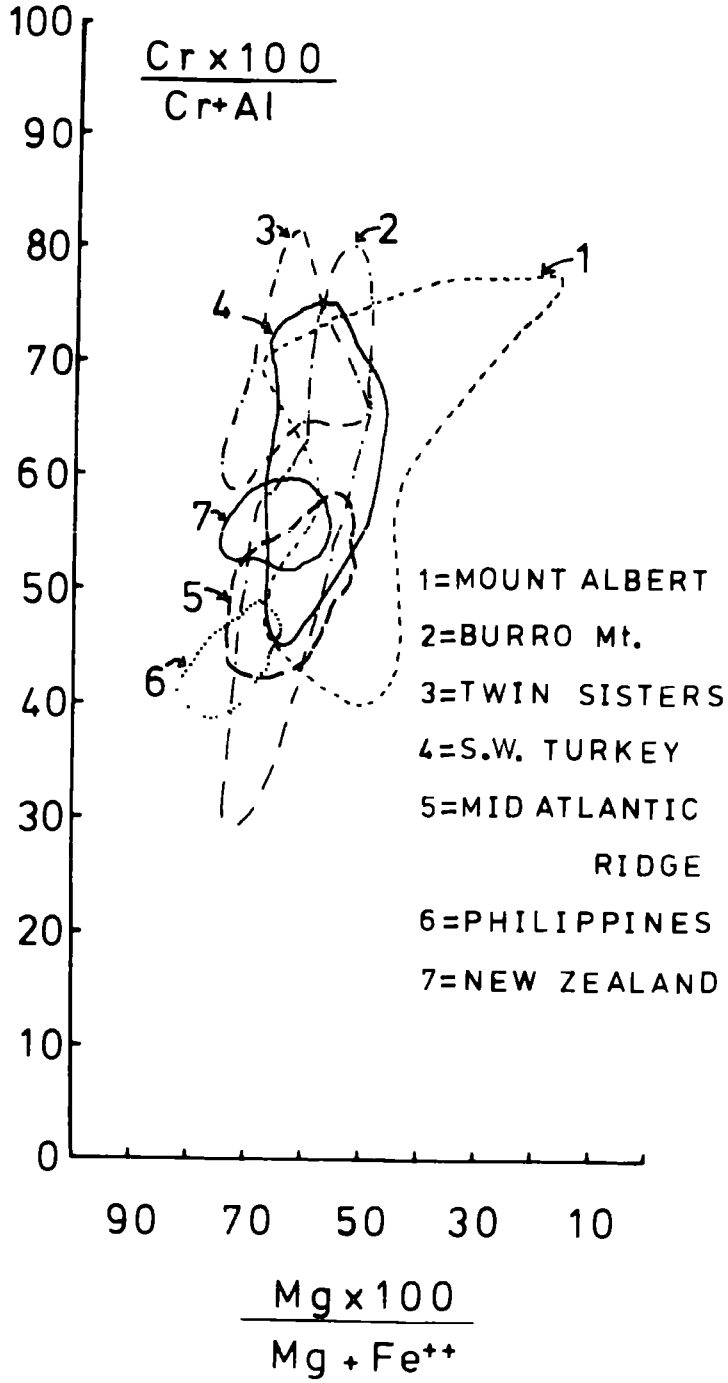

Figure 3.17 The compositional range observed in spinels from a number of ultramafic bodies.
1=MacGregor and Smith (1963)
2=Loney et al. (1971)
3=Onyeagochi (1974)
4=Engin and Hirst (1970)
5=Aumento and Loubat (1971)
6=Stoll (1958)
7=Challis (1965)

Ridge material, most "alpine" spinel populations are either too small, or are given with insufficient host rock data to interpret the significance of host rock lithology. In the case of the Mount Albert intrusion, Quebec, MacGregor and Smith (1960) relate the spinel composition to the country rock contact, and not to compositional banding.

It is apparent from Figure 3.15 that there is very little overlap between the dunite and the peridotite derived spinels. The two populations are transitional, and they break at a Crx100/(Cr+Al) ratio of 57.5 ± 2.5. Dunite spinels have a value above this, and peridotite spinels have somewhat lower ratios. Table 3.10 gives the spinel compositional range of both populations, in terms of structural formulae. Spinels 60196C(1), and 60874A(1), mark the transition point from dunite to peridotite. The slightly high Fe^3 content of the former probably reflects incipient hydrothermal alteration during Stage III. The excess Fe^3 appears to be substituting for Al, rather than Cr, Table 3.10

The critical Al content in Sample 60874A(1), is 24.5% Al_2O_3, and dunites can readily be differentiated from peridotites in Figure 3.16 on this basis. Similarly spinels in the third population must either be dunite or peridotite derived. A combination of chemistry and texture should be adequate to decide which. Samples 60157, 60159,

Table 3.10

Limiting Spinel Compositions

1. 60237 C(1)*

$Fe^{2+}_{4.3}\ Mg_{3.7}\ (Fe^{3+}_{0.5}\ Al_{2.9}\ Cr_{12.6})O^{x}_{32}$ Dunite

2. 60196 C(1)

$Fe^{2+}_{4.6}\ Mg_{3.4}\ (Fe^{3+}_{1.0}\ Al_{6.5}\ Cr_{8.4})O_{32}$ Dunite

3. 60874 A(1)

$Fe^{2+}_{4.9}\ Mg_{3.1}\ (Fe^{3+}_{0.3}\ Al_{7.1}\ Cr_{8.5})O_{32}$ Peridotite

4. 60160 A(1)

$Fe^{2+}_{2.5}\ Mg_{5.5}\ (Fe^{3+}_{0.5}\ Al_{10.5}\ Cr_{5.0})O_{32}$ Peridotite

*Details of composition and nomenclature are given in Table 3.8.

[x]Structural formulae, based on the generalized formula $R^{2+}_{8}\ R^{3+}_{16}\ O_{32}$.

and 60035, contain small euhedral spinels enriched in Cr and Fe, they are in all probability dunite derived. The spinels in Samples 60209, and 60907, are far more irregular, and as they are Mg and Al enriched, their host meta-serpentinite is thought to have been derived from peridotite. The apparent bias towards dunite derived relicts probably reflects the greater susceptibility of Al rich spinel to alteration during Stage III metamorphism. Much of the ferritchromit observed in the vicinity of the batholith is considered to be altered peridotite spinel.

A large number of samples containing relict dunite spinel were found along the western contact, in Unit (3a). They probably represent a thick band of dunite formed along this contact. The band appears to have acted as the locus for the intrusion of a number of gabbroic bodies.

The structural formulae in Table 3.9, and the Mgx100/(Mg+Fe) ratios given in Figure 3.15, show that dunite derived spinels have a relatively scattered range, from 40 to 60. This scatter may in part result from olivine spinel re-equilibration, as attributed to Sample 60237. Variable amounts of Fe may substitute in the spinel on cooling. peridotite spinels show a more marked trend towards Mg enrichment.

In Figure 3.18 the Fe^3 content, in relation to the total trivalent cation content, is plotted against the

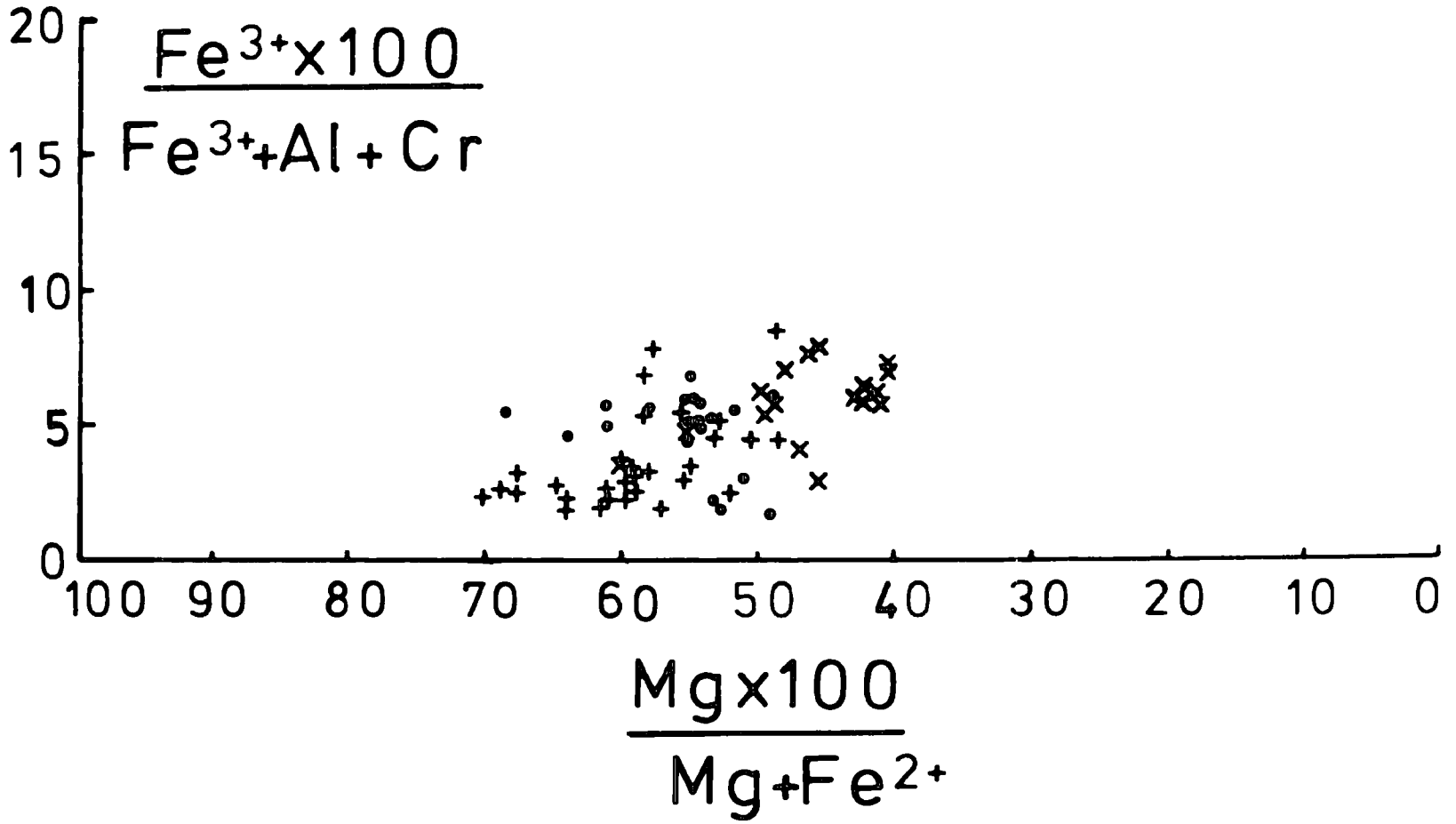

Figure 3.18 Cation ratio plot for primary spinel (1). Spinels are differentiated as in Figure 3.15.

Mgx100/(Mg+Fe) ratio. The dunite and peridotite populations overlap, but the Fe and Cr rich dunite-spinels appear to have a lower Mgx100/(Mg+Fe) ratio. The regenerated dunite spinels, which may show some incipient alteration, appear to have lower ratios still. The Fe^3 content appears relatively fixed, and relatively low, suggesting a low activity of oxygen.

(v) Cation distribution and Equilibration

Irvine (1965), discusses the thermodynamic basis for partitioning between spinel and olivine, and Jackson (1969) has extended the theory to enable usage of equilibrium data as a geothermometer. The distribution of Mg and Fe is complicated by the presence of trivalent cations in the spinel structure, nevertheless, the following Mg and Fe exchange reaction has been established:

$$Fe^{++}Si_{0.5}O_2 + Mg(Cr_\alpha Al_\beta Fe^{+++}_\gamma)_2O_4 = MgSi_{0.5}O_2 + Fe^{++}(Cr_\alpha Al_\beta Fe^{+++}_\gamma)_2O_4$$

The values α, β, and γ, refer to the fractions of Cr, Al and Fe, respectively in octahedral coordination in the spinel structure, and they sum to unity. The thermodynamic equilibrium coefficient (K_D) may be defined by the following equation, if one assumes ideal solid solution

behaviour, Irvine (1965), Jackson (1969).

$$K_D = \frac{X\ ol\ Mg.\ X\ chr\ Fe^{++}}{X\ ol\ Fe^{++}.X\ chr\ Mg}$$

where X ol Mg and X ol Fe^{++} are mole fractions of the end members, $MgSi_{0.5}O_2$ and $FeSi_{0.5}O_2$ respectively, and X chr Mg and X chr Fe^{++} are the fractions of divalent cations in the spinel.

Using the following equation, presented by Jackson (1969), it is possible to deduce the temperature of formation of an analysed equilibrium pair, using Gibbs free energy data; or alternatively it is possible to obtain the compositions which will coexist, at a given temperature.

$$T^{o} = \frac{5580\alpha + 1018\beta - 1720\gamma + 2400}{0.90\alpha + 2.56\beta - 3.08\gamma - 1.47\ LnK_D^{*}}$$

$$(Lnk = logn\ K_D)^{*}$$

The value T is in degrees Kelvin. Analytical error, deviations from stoichiometry, and uncertainties in Gibbs free energy values, are obvious sources of error, and Jackson suggests a reliability of no more than $\pm 300^{o}C$.

The Blue River primary assemblage is thought to represent an equilibrium assemblage, and temperature estimates are presented in Table 3.11. The estimates

Table 3.11

Spinel - olivine Geothermometer

Sample	KD	T°C	Rock-type
60075	12.01	1160	Dunite
60196	13.59	1030	Dunite
60237	16.53	1106	Dunite
60902	13.99	1140	Dunite
60094	6.09	1159	Peridotite
60160	4.11	1231	Peridotite
60163	4.79	1213	Peridotite
60876	5.38	1210	Peridotite

Comparative Temperature Ranges

Location	Temperature Range °C	Source
Blue River	1030-1231	This study
Burro Mt, USA	1098-1335	Loney et al. (1971)
Vulcan Peak, USA.	915-1365	Himmelberg et al. (1973)
Oregon, USA	1200-1410	Medaris (1972)
New Caledonia	1180-1300	Rodgers (1973)

Temperatures based on thermodynamic data from Irvine (1965) and Jackson (1969). Mineral data is shown in Tables 3.2 and 3.9.

range from 1030°C - 1230°C (±300°C) with a slight compositional bias towards higher values associated with peridotite pairs. Whether this difference is real, or it represents some systematic difference related to the appreciably lower K_D values is not known. The assemblage is considered to have equilibrated at a more or less constant temperature and pressure. In view of the silicate-spinel equilibration, which is inferred to occur on cooling, some of the temperature range, in particular the low value of 1106°C recorded for Sample 60237, may reflect a minimum value.

The other temperature ranges given in Table 3.11 were derived by a number of workers, using the same method. The similarity is striking, although the range in material is large. The somewhat higher values given by Medaris (1972), for some unusual harzburgites in southwest Oregon, are reasonable in view of the Al rich nature of the orthopyroxene, and its other high T and P features, Figure 3.9. The effect of pressure on the K_D value, representing equilibrium between olivine and spinel, is apparently small, Irvine (1965), and it is possible to construct theoretical equipotential surfaces, which represent equilibrium compositions for a given temperature.

Theoretical and observed olivine compositions are compared in Figure 3.19, after Loney et al. (1971). The

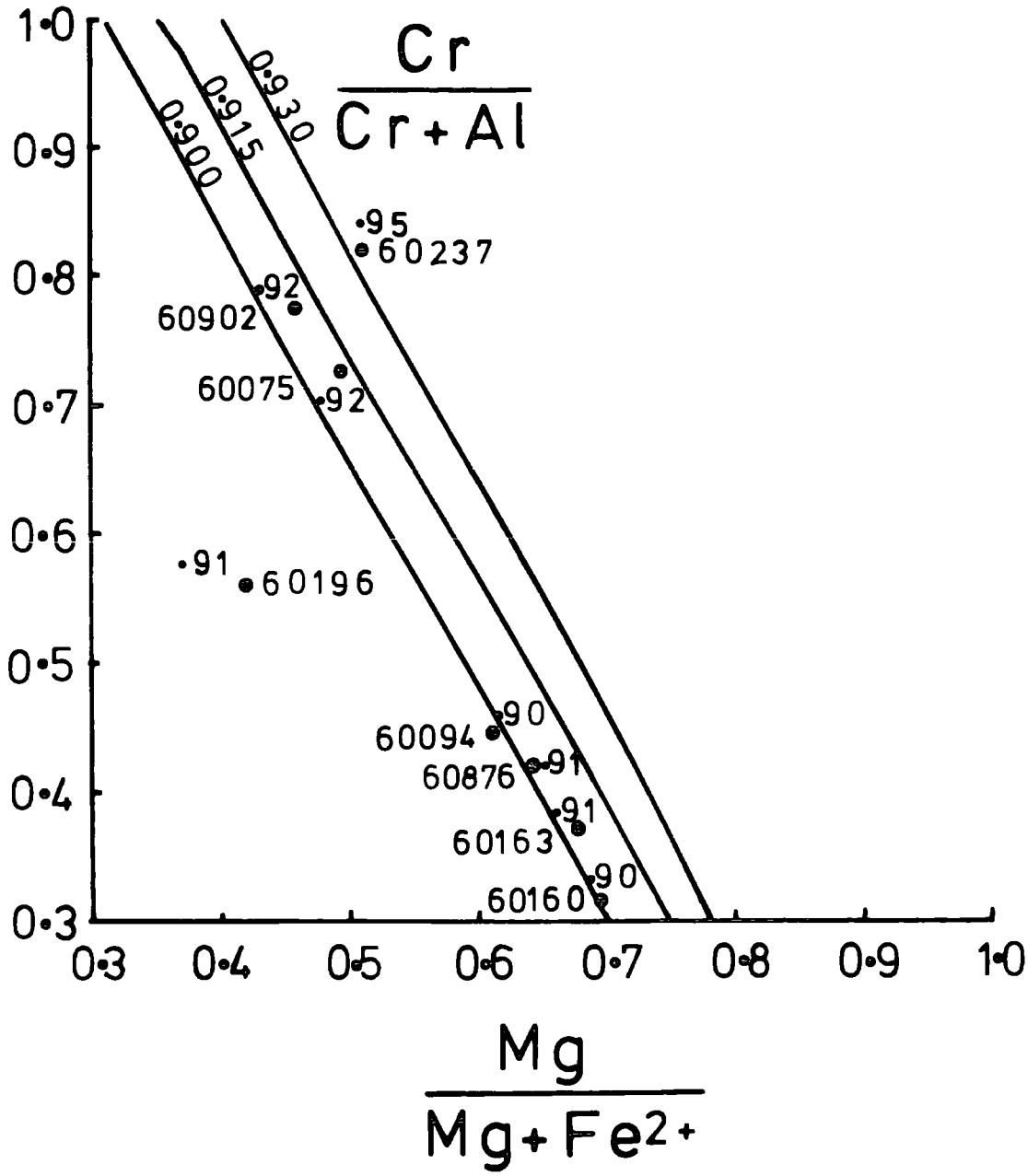

Figure 3.19. A spinel cation ratio plot, after Loney et al (1971). The plot has been contoured to give the theoretical coexisting olivine Mg cation fraction at 1200°C. The contours are for values of 0.900, 0.915, 0.930. Observed olivine Mg cation fractions are given for each analysed coexisting pair.

observed olivine, coexisting with a given spinel composition, lies close to the theoretical composition. This argues in favour of an equilibrium assemblage. Figure 3.19 has been contoured according to spinel compositions, which at a given P and T, will equilibrate with olivine or pyroxene of fixed Mg/Fe ratio.

The above contours are in part a function of the Fe-Mg distribution coefficient, attained by equilibrium partitioning between spinel and olivine. Figure 3.20, after Irvine (1965), and Rodgers (1973), shows the Cr fraction in the spinel, Y_{Cr}^{sp}, plotted against an Fe-Mg distribution coefficient, ln $X_{Mg}^{ol}(1-X_{Mg}^{sp})/(1-X_{Mg}^{ol})X_{Mg}^{sp}$. According to Irvine this relationship should give a straight line, slope K, if the conditions attained are equilibrium, and the amount of Fe^{3} is constant. The Blue River data indicates that equilibrium was attained, at a coefficient of K = 2.9, which compares with the value of K = 3 used by Irvine to construct his equipotential lines; based on Mount Albert data. The deviation of Sample 60196 from what is otherwise a remarkably straight line, is a function of the abnormal Fe^{3} content, and incipient alteration. A similar plot shows the equilibrium relationship between orthopyroxene and spinel. The Cr content is directly related to the Al content of the spinel, and the equilibrium distribution of Al between these two phases is

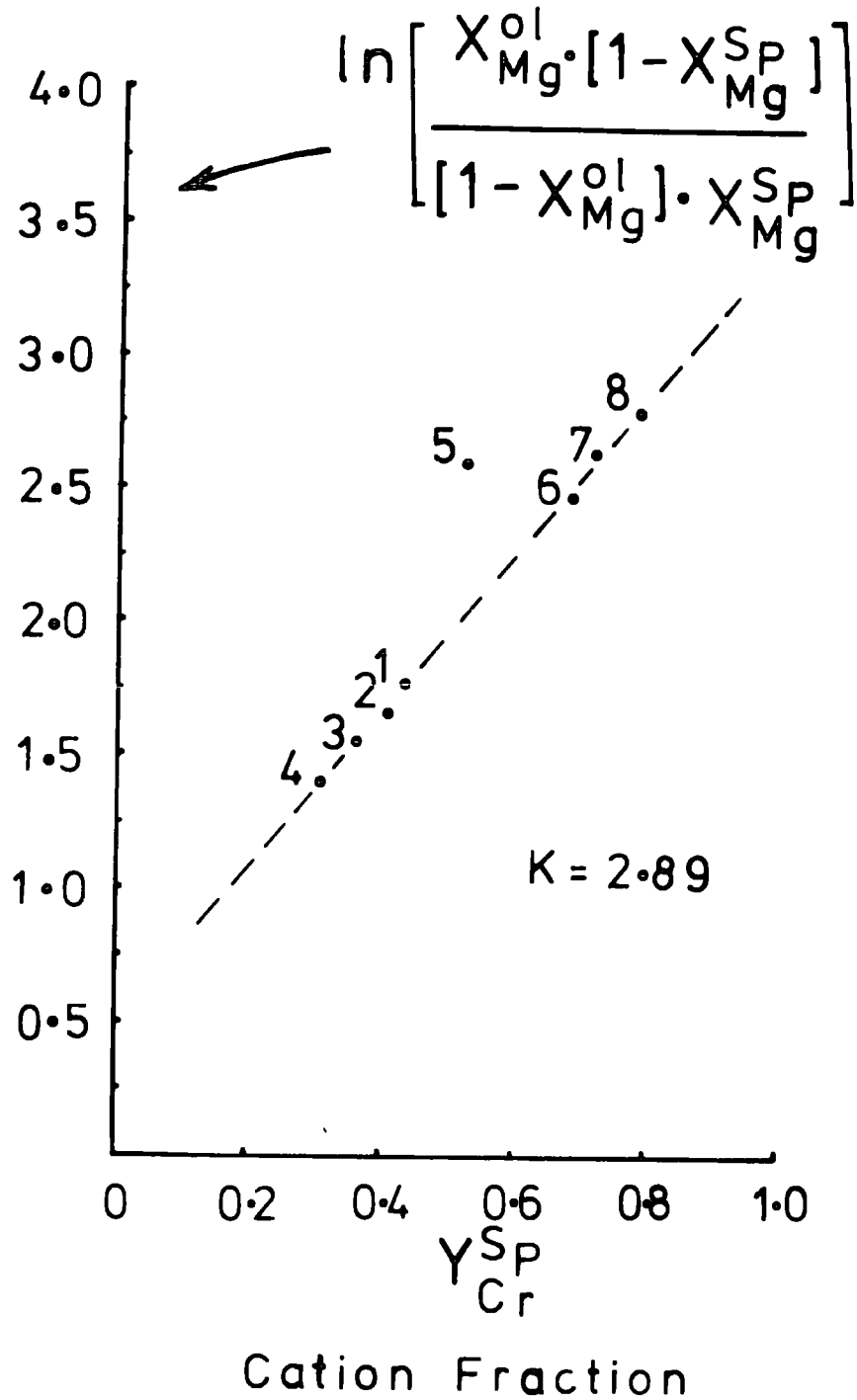

Figure 3.20 An olivine (1) - spinel (1) equilibration plot, after Irvine (1965), and Rodgers (1973). An Mg-Fe distribution coefficient is plotted against the Cr cation fraction in spinel. The value (K) represents the slope of the line. 1 = 60094, 2 = 60876, 3 = 60163, 4 = 60160, 5 = 60196, 6 = 60075, 7 = 60902, 8 = 60237.

important, Fig.3.21.

Powell and Powell (in press), have established an exchange reaction between olivine and clinopyroxene.

$$2CaMgSi_2O_6 + Fe_2SiO_4 = 2CaFeSi_2O_6 + Mg_2SiO_4$$

The content of the clinopyroxene MI site is non-ideal, and it is expressed as a regular solution. Mixing parameters were obtained, and calibrated against iron-titanium oxide temperatures. These enable equilibrium olivine-clinopyroxene pairs to be used as geothermometers. The pressure dependence of the geothermometer has been calculated at $5^{o}C$ per kilobar.

The following equation may be used to determine temperature (T), in degrees Kelvin, at a given pressure (P).

$$T = \frac{-2XAl(920000+3.6P)-0.0435(P-1)+10100}{8+2R\ln\frac{XMg,ol}{XFe,ol}\frac{XFe,MI}{XMg,MI}-714.3(2XAl)}$$

The symbols XMg, XFe and XAl denote the mole fractions of these elements in olivine, and in the clinopyroxene MI site. The value for Al includes other trivalent cations in octahedral coordination . The value for R is the gas constant.

The equation defines P-T lines, and assuming a pressure of between 5 and 10 Kbars, it is possible to estimate olivine-clinopyroxene equilibration temperatures. These are shown in Table 3.12. The value of $1050 \pm 50^{o}C$ is probably

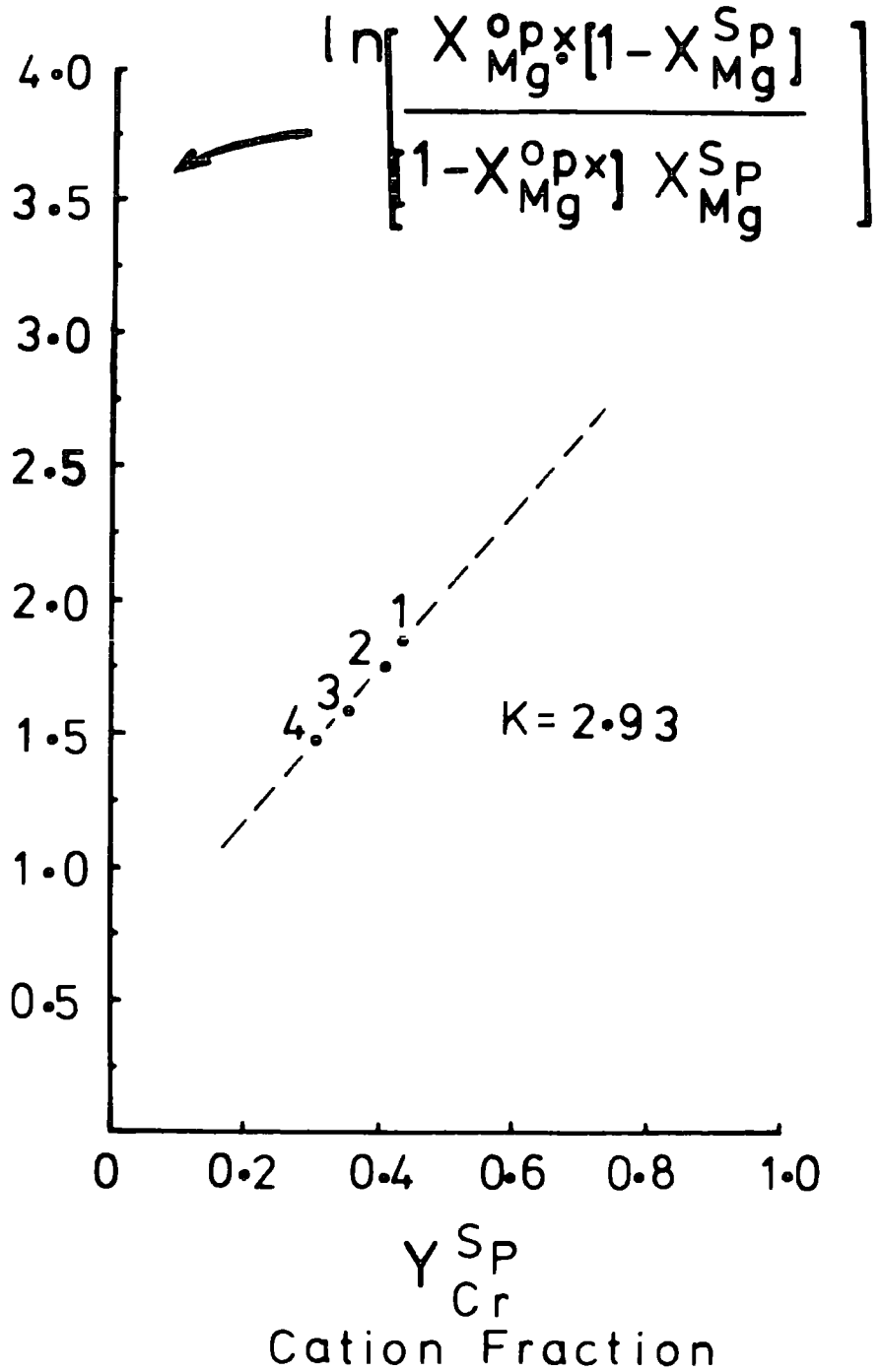

Figure 3.21 A spinel (1) - enstatite (1) equilibration plot, after Irvine (1965), and Rodgers (1973). An Mg-Fe distribution coefficient is plotted against the Cr cation fraction in the spinel. The value K is the slope of the line. 1=60094, 2=60876, 3=60163, 4=60160.

Table 3.12

Clinopyroxene - olivine Geothermometer

	Temperature °C		
Sample	5 Kbars	10 Kbars	15 Kbars
60160 L	1066	1094	1122
60094 M	1047	1077	1106
60094 L	1066	1094	1123
60876 M	1058	1087	1116

Temperatures based on thermodynamic data from Powell and Powell (in press). Mineral data is shown in Tables 3.2 and 3.7.

a realistic exsolution temperature. The diopsides which occur in peridotite, are more calcic, and less aluminous than the gabbroic diopsides, Table 8.1. They do however contain approximately equal amounts of trivalent cations. The lamellae diopsides probably exsolved after segregation of the gabbro into bodies and lenses.

(vi) Discussion

The Blue River Ultramafic body is classified as an "alpine" peridotite. As noted by Wolfe (1967), it displays many of the characteristic features of this ultramafic group. It consists of granulated and deformed dunite and harzburgite, and it has evidently been tectonically emplaced into a greenstone assemblage.

The olivine forsterite content, Fo_{91}, is normal for "alpine" peridotite, but slightly high for stratiform cumulate material. In addition it is homogenous, and there is no evidence for Fe enrichment across the body. Similarly the Ni content is homogenous, Figure 3.22. The Ni content is a sensitive indicator of magma fractionation, and in a stratiform sequence a marked depletion might be expected, as was found by Irvine and Smith (1967), for the Muskox body. Wager and Mitchell (1951) estimate that Ni partitions in favour of olivine, out of basalt magma, at a ratio of 12:1. Primary sulphide might influence this, but

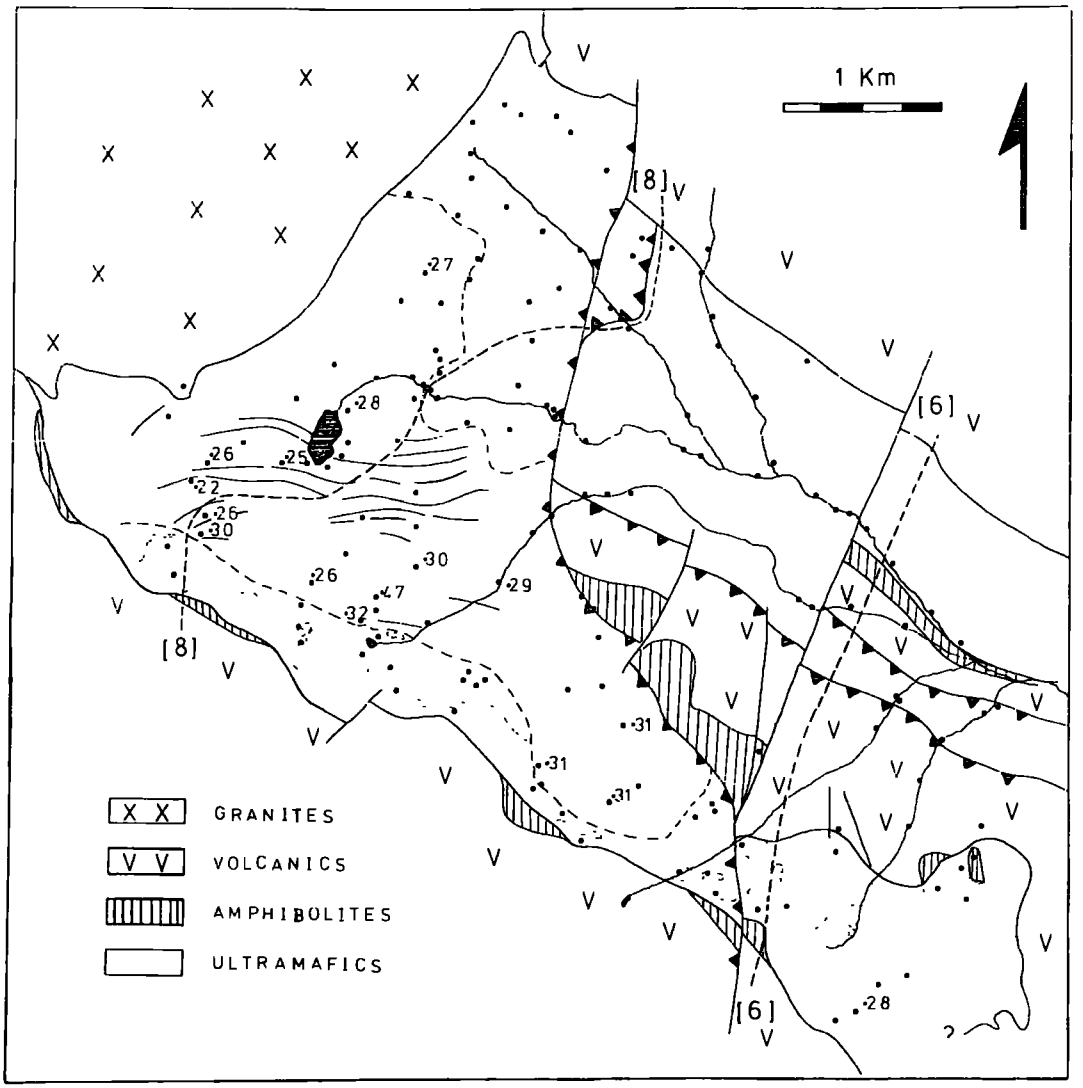

Figure 3.22 Plot of the distribution of the average NiO content in olivine (1).

none was found in the Blue River body.

Irvine (1967) recognized that "alpine" type bodies have a far wider range of spinel composition than do stratiform cumulate bodies. In this sense also, the Blue River body is typically "alpine".

Irvine (1967) shows that spinels which have unquestionably precipitated from a basaltic magma are invariably enriched in Cr and Fe. He presents data from the Stillwater, Bushveld and Great Dyke of Rhodesia intrusives to support this. His data shows that spinels within stratiform cumulate sequences have Crx100/(Cr+Al) ratios of 58.0 and above. This ratio almost exactly marks the break between Blue River dunite and peridotite derived spinels, Figure 3.15. Dunite derived spinels are similar to stratiform and they could thus be magma equilibrated. Peridotite derived spinels are too Al and Mg enriched to be derived directly from basalt magma, under comparable P-T conditions.

This relationship may be fortuitous, but there should be an explanation for the spinel textures, chemical range, and the somewhat coincidental occurrence of gabbro. This invites speculation.

The presence of two Al_2O_3 bearing phases in harzburgite, suggests that the body may not be homogenous,

and the harzburgite layers may be significantly enriched in Al. Wolfe (1967) quotes nine dunite analyses, and four peridotite analyses, derived by X-ray fluorescence. The former give an average value of 1.5% Al_2O_3, and the latter a value of 2.4% Al_2O_3. In spite of interlayering, there is a detectable difference.

Figure 3.9 shows that primary enstatite contains a constant value of 2.75-3.0% Al_2O_3. Any excess Al, over that required to "saturate" the enstatite present, appears to be within the spinel. Dunite spinels never contain excess Al over the basalt equilibration value; thus the presence of enstatite appears to be significant in the process which enriches the spinel. There are two possible processes, one metamorphic and one magmatic, which might influence the spinel.

Green (1964) and Medaris (1972) both present data on the metamorphic re-equilibration of Al rich enstatite, according to the following reaction:

Al enstatite + olivine = Al spinel + enstatite.

This process does not involve a wholerock chemical change, and it presupposes flow banding of Al rich enstatite or spinel, with later equilibration between the two. This equilibration would presumably form a P-T controlled enstatite, with a fixed Al_2O_3 content. This

relationship is not inconsistent with the data, but it does not explain the spinel textures.

Irvine (1967) proposed that Al rich spinels might be derived from original Cr rich spinels, by continuous reaction between minor amounts of trapped interstitial magma, and the primary mineralogy. This process accounts for the interstitial form of the spinel in peridotite, but it is less easy to reconcile with the primary banding.

The two processes are not irreconcilable, flow banding of olivine with both Al enriched enstatite and a spinel, may have been followed by equilibration with magma, and possibly incomplete magma segregation.

England and Davis (1973) describe harzburgites, from Papua, New Guinea, that contain enstatites with a very low Al_2O_3 content, Figure 3.9. The coexisting spinel is similarly low in Al, and the rock, which floors an ophiolite sequence, resembles an Al depleted residuum left after partial melting.

Hancock (1964) described a harzburgite slab, similar to the one above, in Borneo. His X-ray determinations of Al_2O_3 content in spinel and enstatite show a systematic variation across the Mt. Tawai ultramafic body. Basal (?) harzburgites give the following; Enstatite, 6.0% Al_2O_3, spinel 40.0% Al_2O_3. Topmost (?) values are 2.4% Al_2O_3, and 18.0% Al_2O_3 respectively. This systematic decrease implies

compositional change, possibly by increased partial melting, or Al partitioning on equilibration with magma.

Unlike the Mt. Tawai occurrence, which is a slab, probably with a P-T gradient from top to bottom, the Blue River body reflects a constant P-T environment, as it is such a small occurrence. The variable here is rock chemistry, perhaps the result of incomplete partial melting, prior to intrusion. Peridotite is thus "contaminated" with excess Al that it has not been able to shed into the magma. It is envisaged that the original flow differentiated harzburgite contained Al rich enstatite, and possibly also spinel. During the equilibration process Al partitioned into magma, where available, or, if not, into spinel. The The overall trend is probably one of Al depletion, leading to the basalt-equilibrated harzburgite described by Davis and England (1973). The dunite is already Al depleted.

CHAPTER 4. TECTONIC EMPLACEMENT AND SERPENTINIZATION

4.1 Tectonic Emplacement

The simple tectonic model, proposed in Chapter 2, suggests that hot, anhydrous, peridotite "mush" was emplaced into wet "ocean floor basalt", immediately prior to obduction of the greenstone assemblage, onto McDame Group carbonates, and Sylvester Group sediments.

The ultramafic body was probably transported from deep in the earths crust, to relatively shallow depths. Movement was accompanied by local tectonism, and the formation of the breccias referred to in Chapter 2. This change in level was presumably accompanied by cooling, and as suggested by Wolfe (1967), a temperature gradient was probably set up between the core and the contact.

Gabrielse (1969), notes that the Blue River body is the only ultramafic body within the Greenstone belt to have retained a significant "core" region, of unaltered primary peridotite. This is in spite of the marginal serpentinization. Possibly the body retained enough residual heat to prevent all but marginal serpentinization during Stage II.

4.2 Serpentinization

The only indisputable evidence that serpentinization occurred prior to the intrusion of the granite, comes from

the metamorphic textures described in Chapter 5. Metamorphism in Units (3a) and (3b), Figure 3.1, presupposes a pre-existing serpentine-brucite assemblage. Figure 3.1 brings out the marginal nature of this process.

Units (3a) and (3b) can be extrapolated to the southeast, into Unit (2). This lies beyond the influence of the granite, and thus on the hydrational side of the olivine isograd, shown in Figure 2.6. It is not possible to date the time of serpentinization in Unit (2), except to say that it could have continued throughout Stages II, III and IV. Sample 60094 was the only specimen found to retain primary olivine, all other samples are serpentinites. Water released during metamorphism in Units (3a) and (3b) may actually have contributed to serpentinization in Unit (2), during Stage III.

Unit (2) contains serpentinite formed from the primary peridotite mineralogy, and as such it is probably fairly representative of the material metamorphosed in Units (3a) and (3b).

Two varieties of serpentinite were found. Most of the area is underlain by "bastite serpentinite" derived from harzburgite, but sheared contacts are comprised of a darker, brittle, fibrous serpentinite.

Shiney, light-green, "bastite" pseudomorphs after enstatite (1) occur in a light grey-green, mottled, matt

textured serpentine, (Plate 4.1). The bastite serpentine appears to retain the prominent (100) cleavage of enstatite, and in some cases primary diopside exsolution lamellae remain. In other cases the lamellae appear to be replaced by magnetite, (Plate 4.2). The discrete lozenges of diopside shown in Plate 4.3, are thought to represent a younger generation of diopside, for the reasons given in Chapter 7. Similarly the chlorite found in some samples is thought to result from spinel (1) oxidation during Stage III, (Plate 4.4).

Sample 60094, Plate 3.14, contains highly granulated olivine relicts set in a matrix of interstitial serpentine. The serpentine forms a mesh around relict olivine granules, and these are pervasively altered from margin to core. Where total replacement has occurred, vein serpentine surrounds a mesh, which displays the characteristic "hour-glass" texture, Plate 4.5. Magnetite grains appear to concentrate in the early vein serpentine, rather than within the mesh itself.

Sheared serpentinites, found near present-day contacts, are matt textured, fibrous, foliated and very often slickensided. Dark green-black lenticular masses of brecciated serpentinite are enclosed within polished blocks. In thin section the fibrous nature of the serpentine is apparent, and the mesh texture is missing. The serpentinite characteristically contains appreciable magnetite.

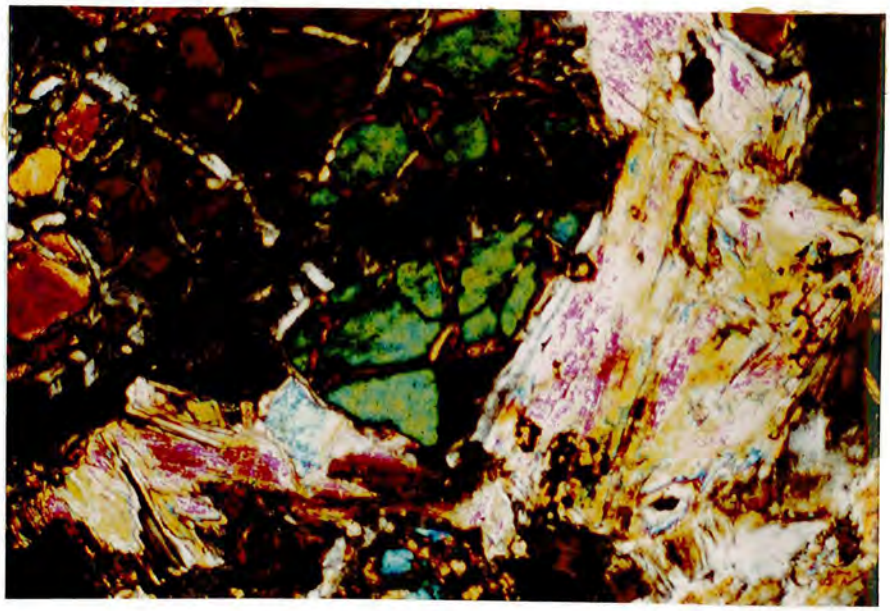

Plate 7.9 Photomicrograph: Olivine (3) in a matrix of recrystallized talc (pink) and chlorite (grey-brown). Note the minor serpentine veins cutting olivine. Sample 60199. Crossed polars. Field width 1.7mm

Plate 4.1 Massive serpentinite at location point 60041 on Claim Jumper Creek. Note the white rectangular bastite pseudomorphs after enstatite.

In Units (1) and (3c) alteration of enstatite (1) to bastite is inferred from the subsequent metamorphism, and remaining serpentine relicts. Minor interstitial serpentinization, and asbestos formation,is also inferred from the metamorphic textures described in Chapter 5.

4.3 Serpentine Chemistry

Table 4.1 lists serpentine analyses, from those samples in which the serpentine can be shown to be formed from the primary assemblage. As noted, these may not be strictly Stage II serpentines, but they are serpentines presumably formed from the same primary material, under similar conditions. The chemistry appears to be fairly consistent throughout.

CHAPTER 5: PROGRADE METAMORPHISM

5.1 Intrusion of the Cassiar Batholith

The batholith intrudes along the southwest margin of the McDame Synclinorium, Gabrielse (1963), Figure 5.1. It intrudes rocks belonging to both the miogeosynclinal McDame Group, and the overlying eugeosynclinal Sylvester Group.

The batholith contact is sharp, and, apart from the local occurrence of aplitic dykes cutting metasedimentary rocks, there is little recorded evidence of country rock contamination. Hornfelsed sediments near the contact appear to have a steep, tectonically induced, easterly dip, suggesting forcible emplacement. Contacts are locally schistose, Wolfe (1967).

A number of small sattelite stocks crop out along the batholith contact. Due west of the Cassiar Mine a small stock is notable for its high xenolith population, Gabrielse (1963).

The contact between the Cassiar batholith and the Blue River ultramafic body, Figure 5.2, is well displayed along the back wall of the Nickel Creek Corrie, Plate 2.4. The contact is planar, and it can be traced for a distance of 2 miles, (3.2 km) and over a relief of 1000 ft, (307 m), Wolfe (1965). It trends N.35°E and dips 77°NW, and is thus markedly discordant to the regional structure. The

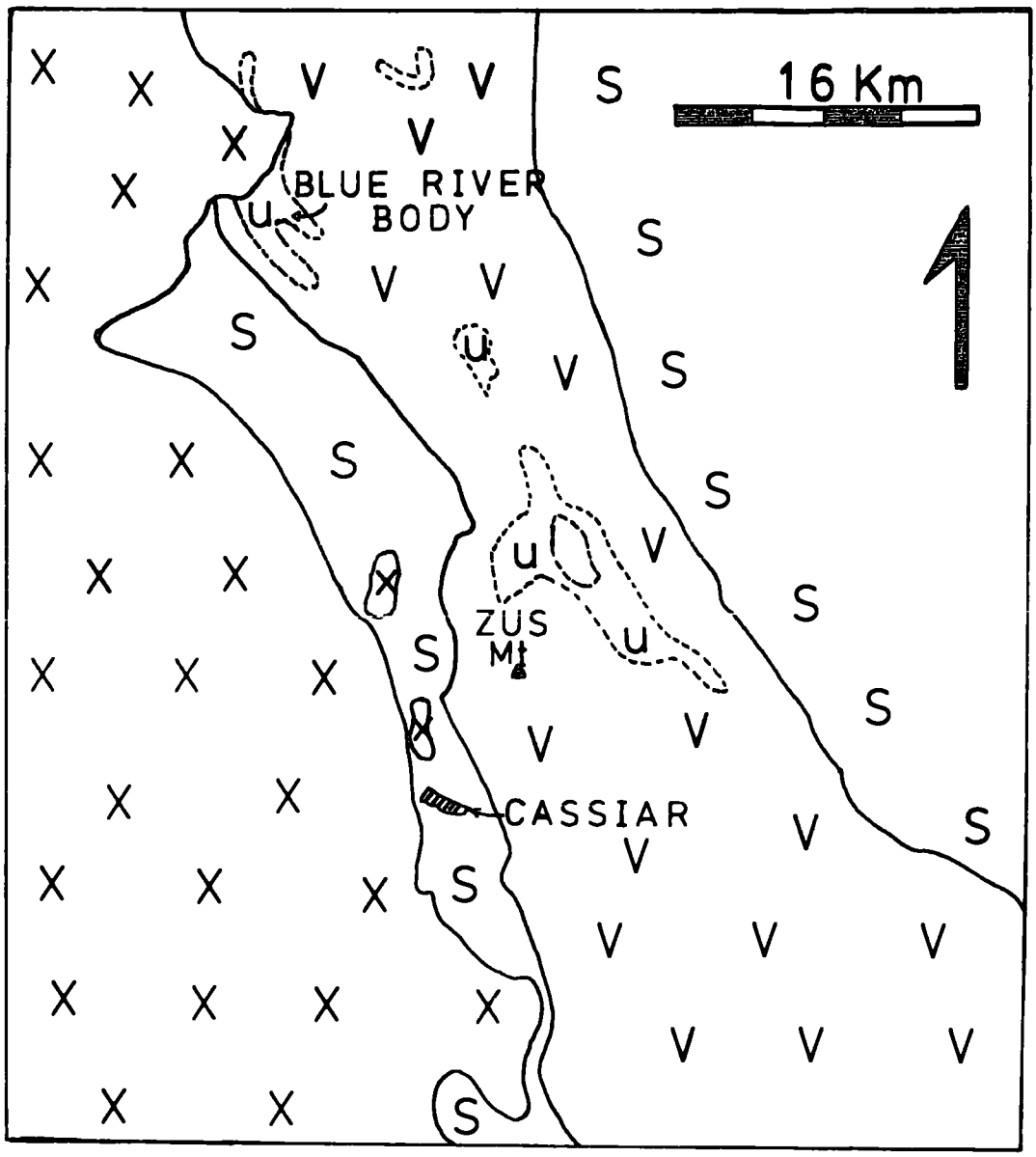

Figure 5.1 A sketch map showing the regional geology in the vicinity of Cassiar Townsite, (arrowed). Data from Gabrielse (1963), McDame Map area, and from Gabrielse (1969), Jennings River Map area.

S=McDame Group sediments
V=Sylvester Volcanics and Cherts
U=Ultramafic rock
X=Cassiar batholith

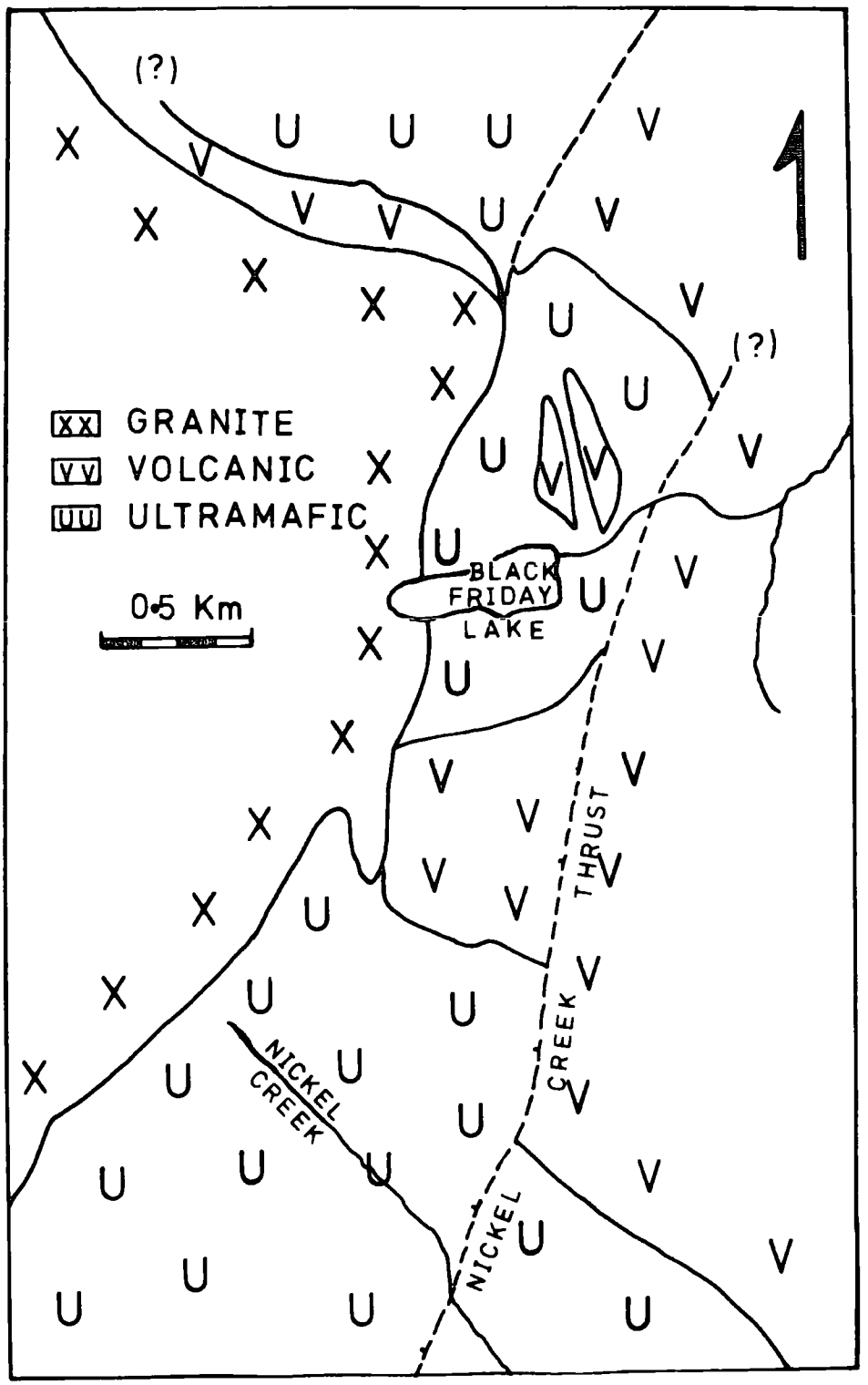

Figure 5.2 A sketchmap showing the northeast corner of the Blue River Ultramafic Body, (adapted from Wolfe (1965)), showing the location of the ultramafic intrusives in the vicinity of Black Friday Lake.

direction is consistent, as a trend of N.30°E, dip 70°SE was observed, offset 4 km along the strike to the southwest. The batholith may have intruded along a fault plane, as it closely parallels a dominant regional joint set, perpendicular to the axis of the synclinorium, Gabrielse (1963). The occurrence of and isolated body of ultramafic rock in the vicinity of Black Friday Lake, in the extreme northeast corner of the map area, Figure 5.2, favours this argument. There is no evidence for movement along the contact after emplacement of the batholith.

5.2 Batholith Composition

The Cassiar batholith consists of medium to coarse, pinkish-grey, homogeneous, granitic rock with varying proportions of plagioclase, (oligoclase to andesine), quartz, and microperthite. Modal proportions quoted by Gabrielse (1963), and Wolfe (1967), are plotted on Figure 5.3. Biotite and chlorite are the principle mafic minerals, except near contacts and inclusions, where assimilation leads to the development of hornblende and sphene. Inclusions of diorite, consisting of "hornblende-plagioclase-biotite sphene" assemblages are locally common near contacts. Microperthite phenocrysts preferentially develop in the vicinity of such inclusions, Gabrielse (1963).

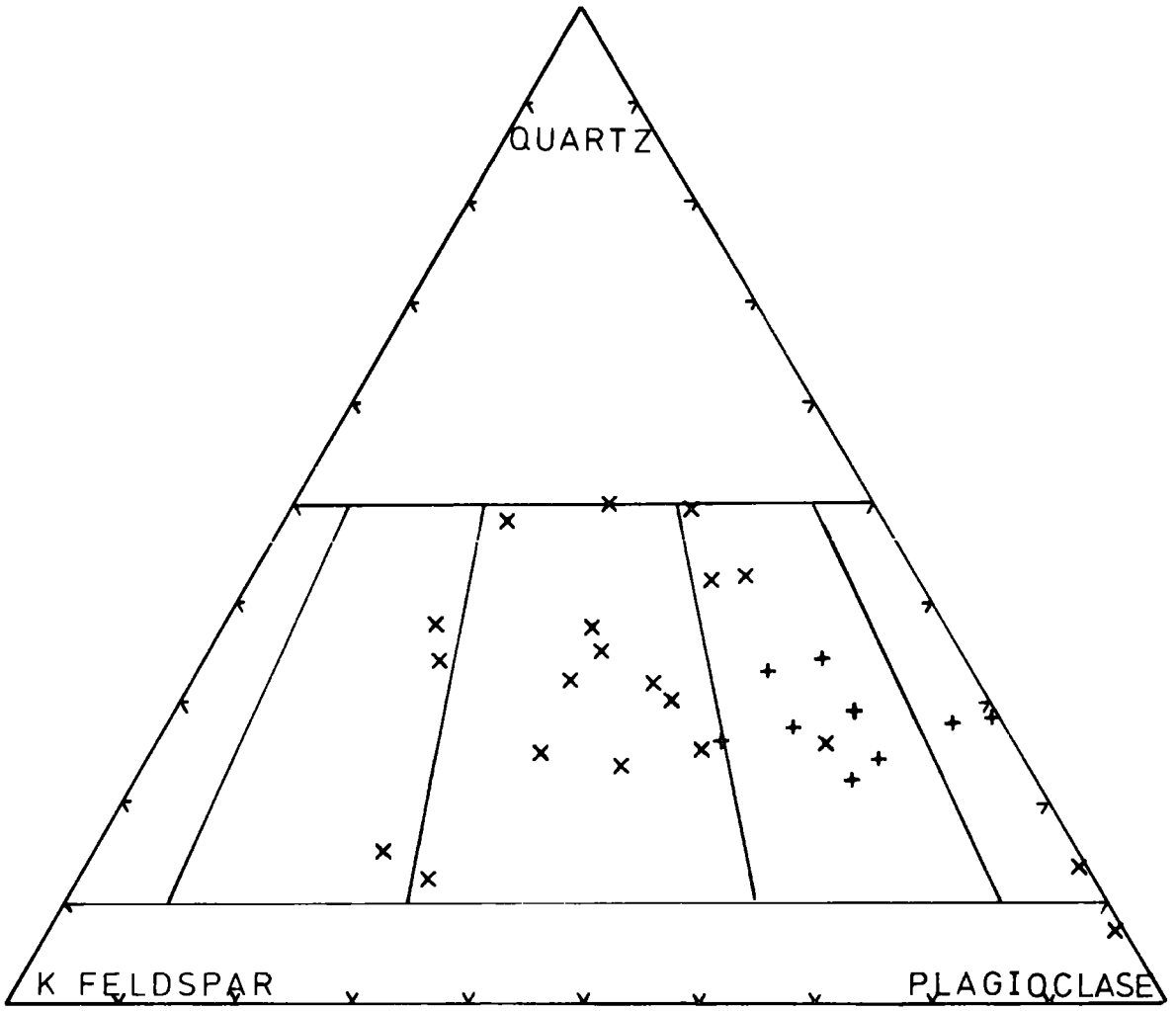

Figure 5.3 The modal composition of the Cassiar batholith. Estimates denoted (X) are from Gabrielse (1963), and estimates denoted (+) are from Wolfe (1967).

Assimilation of limestone along some contacts has basified the intrusive, which develops zoned calcic plagioclase, and a green-blue pleochroic hornblende, Wolfe (1967).

5.3 Contact Metamorphism

The batholith intrudes a variety of different rock types, and their varied response to thermal metamorphism should act as a guide to the P-T conditions operative during emplacement of the batholith. By extrapolation it should be possible to fit the metamorphism of the ultramafic body into a more generalized contact metamorphic framework.

Data on the thermal metamorphism is limited. Gabrielse (1963) quotes the work of MacDougall on the "Contact" Group of Mining claims, adjacent to the contact, west of Cassiar Mine, and he also gives generalized data for the northeast batholith contact. Wolfe (1967) gives more specific data about the contact in the vicinity of the ultramafic body.

Rocks within the aureole have been subdivided into four lithologic categories, which reflect the extreme range of primary rock composition, they are (i) metamorphosed sediment, (ii) metamorphosed carbonate and skarn, (iii) metamorphosed volcanic rock, and (iv) metamorphosed ultramafic rock. The first three are discussed on the

basis of the available data, and the fourth is an integral part of this study.

(i) Metamorphosed Sediments

Argillaceous sediments have been hornfelsed and recrystallized within an embayment separating the main batholith from a stock, due west of the Cassiar Mine. The embayment, which constitutes the "contact" Mining claim, thins from 500 m to 170 m, and forms a pendant within the batholith.

Bedded Al-rich shales have altered to a black, spotted hornfels, consisting of the assemblage "cordierite-orthoclase-quartz-biotite". This assemblage also contains a biotite rich variety, which occurs as angular inclusions within the stock, Gabrielse (1963).

Near the ultramafic body pelitic sediments are schistose parallel to the contact, Wolfe (1967). This foliation locally extends for 100 ft, (31 m), either side of the contact, and is used as evidence for forcible emplacement. The schist contains the following assemblage within 50 ft, (15 m), of the contact:

"Quartz-staurolite-almandine-muscovite-biotite"

Further out the following assemblages are recorded;

"Quartz-biotite-muscovite-orthoclase $\pm$ garnet"

"Quartz-epidote-hornblende-plagioclase"

"Quartz-hornblende-biotite-andesine".

The first two assemblages are recorded by Wolfe (1967), and the third by Gabrielse (1963). How far out these assemblages extend is not clear, as, although the sediments are hornfelsed for 1000 ft, (307 m), from the contact, Gabrielse (1955) records actinolite and chlorite in the matrix of sediments, "away from granite".

Rocks within the embayment presumably formed cordierite and orthoclase by the following reaction:

(1) 6 muscovite + 1 biotite + 15 quartz = 3 cordierite + 8 K feldspar + $8H_2O$.

This assemblage defines the "K-feldspar-cordierite" contact metamorphic facies of Winkler (1967). The reaction should proceed at $640^{\circ} \pm 20^{\circ}C$ at 2 Kbars, according to Winkler; and this would indicate such a temperature within the batholith embayment.

Staurolite and almandine together define a subfacies of the almandine amphibolite facies of regional metamorphism. The increase in pressure required to attain such a facies is unlikely, although tectonic overpressures may occur. Staurolite has been recorded in metamorphic aureoles, Pitcher and Read (1960); and Winkler (1967) states that staurolite and muscovite will replace cordierite in rocks of suitable composition. Similarly Chinner (1962) suggests a restricted, but stable, field of almandine in a thermal environment.

The stable association of "muscovite-biotite-quartz" precludes K-feldspar-cordierite hornfels conditions. Both hornblende and plagioclase are stable, and albite and chlorite absent. The sediments are thus assigned to the hornblende hornfels facies. These sediments, which extend for an unknown distance from the contact, have probably been subjected to the following reaction.

(2) Chlorite + tremolite + quartz = hornblende + anthophyllite + H_2O

This reaction, which marks the onset of hornblende hornfels facies conditions, proceeds at $560^{\circ} \pm 10^{\circ}C$ at 2 Kbars, Choudhuri et al. (1967). The true temperature was probably lower, as the original rock contained actinolite not tremolite.

Within the inner aureole of the batholith, sediments probably did not reach $640^{\circ}C$, in the vicinity of the ultramafic intrusion, but they were presumably heated to around $560^{\circ}C$.

(ii) Metamorphosed Carbonates and Skarns

Limestones have recrystallized to a sugary "marmorized" limestone within the embayment area. This is finely interbedded with sedimentary hornfels and skarn. A mixed sequence has been metamorphosed to the following laminate assemblage.

"Garnet-diopside-calcite"

"Orthoclase-cordierite-biotite"

"Diopside-orthoclase"

These confirm the K-feldspar-cordierite hornfels conditions indicated for this area. The absence of wollastonite may be a compositional phenomenon.

Near the ultramafic body Wolfe (1965) reports that limestones, dolomites, and calcareous dolomites are recrystallized for 1000 ft,(307 m),from the contact; and silicious dolomites form a "calcite-forsterite" assemblage for a distance of 75 ft,(23 m),from the contact.

Winkler (1967) uses this assemblage to mark the onset of hornblende hornfels conditions, provided the ratio $CO_2:H_2O$ in the fluid phase is above 1:3. When this condition is satisfied, the following reaction will proceed at $530^{o}\pm10^{o}C$, at 1 Kbar, Metz (1967).

(3) Tremolite + 11 dolomite = 8 forsterite + 13 calcite + 9 CO_2 + H_2O.

Tremolite was not reported by Wolfe, and the following, anhydrous, reaction probably gave rise to this assemblage, under similar P-T conditions.

(4) 2 dolomite + 1 quartz = forsterite + 2 calcite + CO_2

The temperature indicated is compatable with hornblende hornfels conditions within the inner aureole of the batholith.

(iii) Metamorphosed volcanic rocks

Although outcrop is poor in the immediate vicinity of the batholith, Wolfe (1967) reports the following hornfels within 500 ft ,(153 m), of the contact.

"Quartz-hornblende-biotite-plagioclase"

This assemblage passes outward into the following hornfels, which itself passes into typical type I Sylvester volcanic rock, as defined by Gabrielse (1963). This exhibits a similar mineralogy, (see Chapter 8).

"Quartz-actinolite-albite-epidote-calcite $\pm$ chlorite"

This assemblage belongs to the albite-epidote facies of thermal metamorphism, and it is also transitional to the regional "spilite" mineralogy discussed earlier. Onset of this facies is established by the following reaction, Winkler (1967).

(5) 1 kaolinite + 2 quartz = 1 pyrophyllite + 1 H_2O

This reaction proceeds at 400°C at all geologically realistic pressures; and thus the ambient regional maximum temperature attained was probably, (on this basis), in excess of 400°C at some stage.

(iv) Metamorphosed ultramafic rocks

Blue River ultramafic rocks in the aureole of the batholith have been metamorphosed for a distance of 5000 m from the nearest exposed contact, which is

along the back of the Nickel Creek Corrie, Figure 5.4, (Plate 2.4).

The batholith truncates Stage II structures, and it cuts both the relatively unaltered "core" region, defined by Units (1) and (3c),on Figure 5.4,and also the highly serpentinized marginal regions, defined by Units (2), (3a) and (3b). The compositional differences between the two are reflected in the metamorphic mineralogy, and although the pattern of metamorphism is similar in each case, there are significant differences. Figures 5.5 to 5.10 show the spatial distribution of the following prograde metamorphic phases, olivine (3), tremolite-anthophyllite, talc, ferritchromit (spinel (3)), Al serpentine (including chlorite), and enstatite (3).

The body is subdivided on the basis of the talc isograd into an "outer aureole", defined by Units (1) and (3a), and an "inner aureole" defined by Units (3b) and (3c), Figure 5.4. These represent metamorphic zones based on the incoming of olivine (3), according to the two classic olivine producing reactions,established by Bowen and Tuttle (1949). Within the "outer aureole" it is possible to define an additional isograd, based on the first appearance of tremolite. Similarly within the "inner aureole" the first appearance of prograde enstatite (3) marks a further isograd.

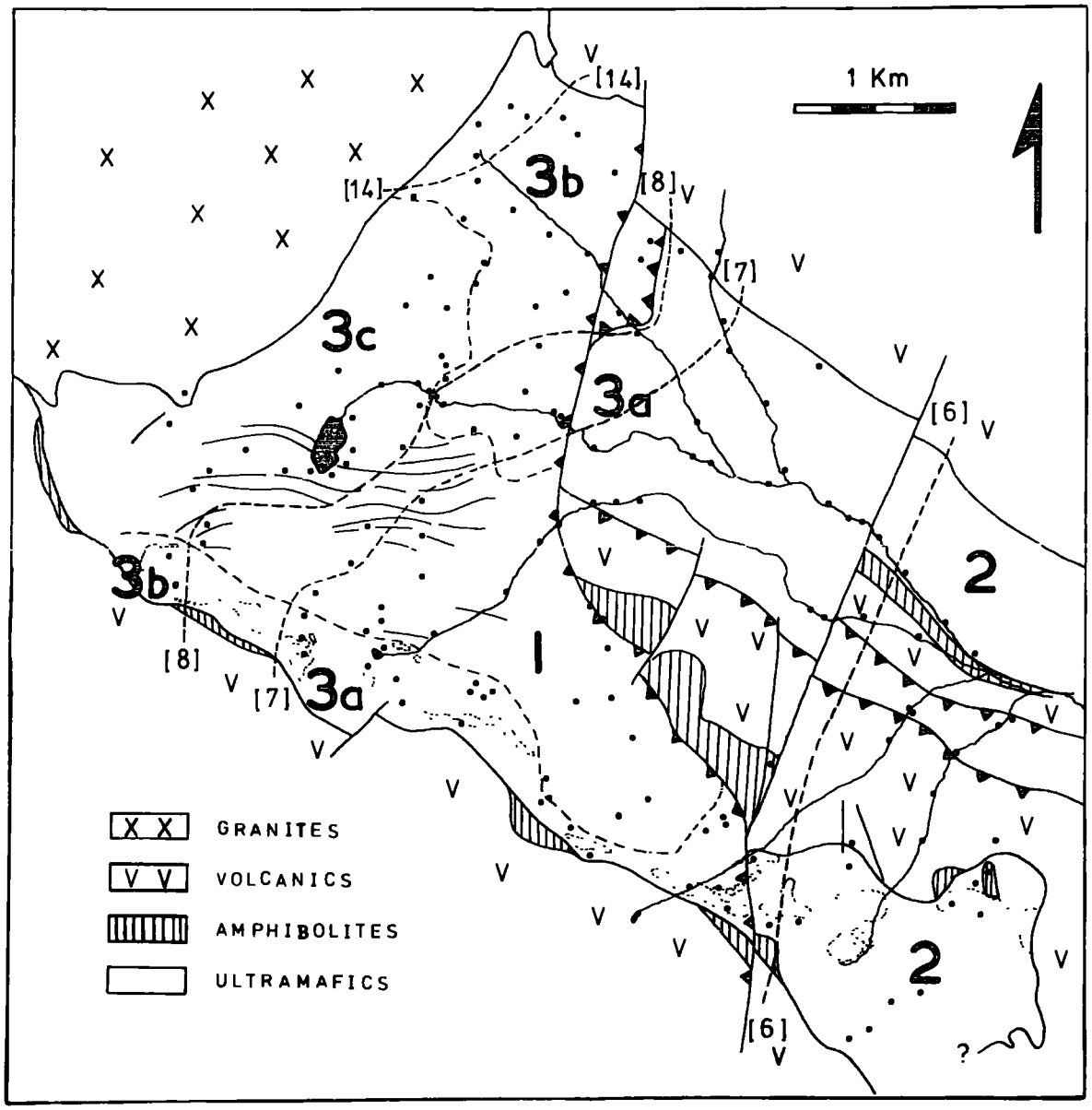

Figure 5.4 A sketchmap showing the location of prograde metamorphic isograds. Isograd reactions are given in Table 5.4.

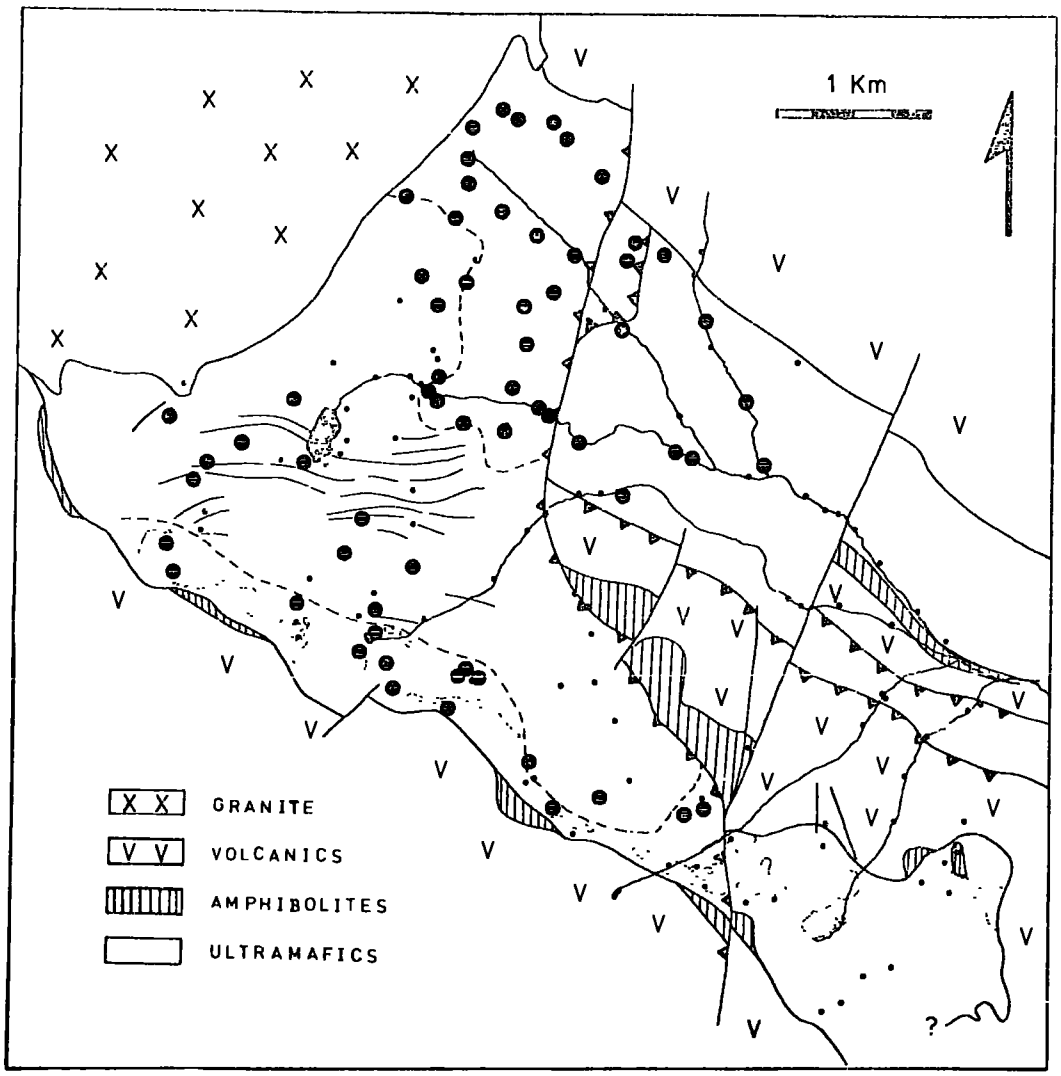

Figure 5.5 Distribution of metamorphic olivine (3).

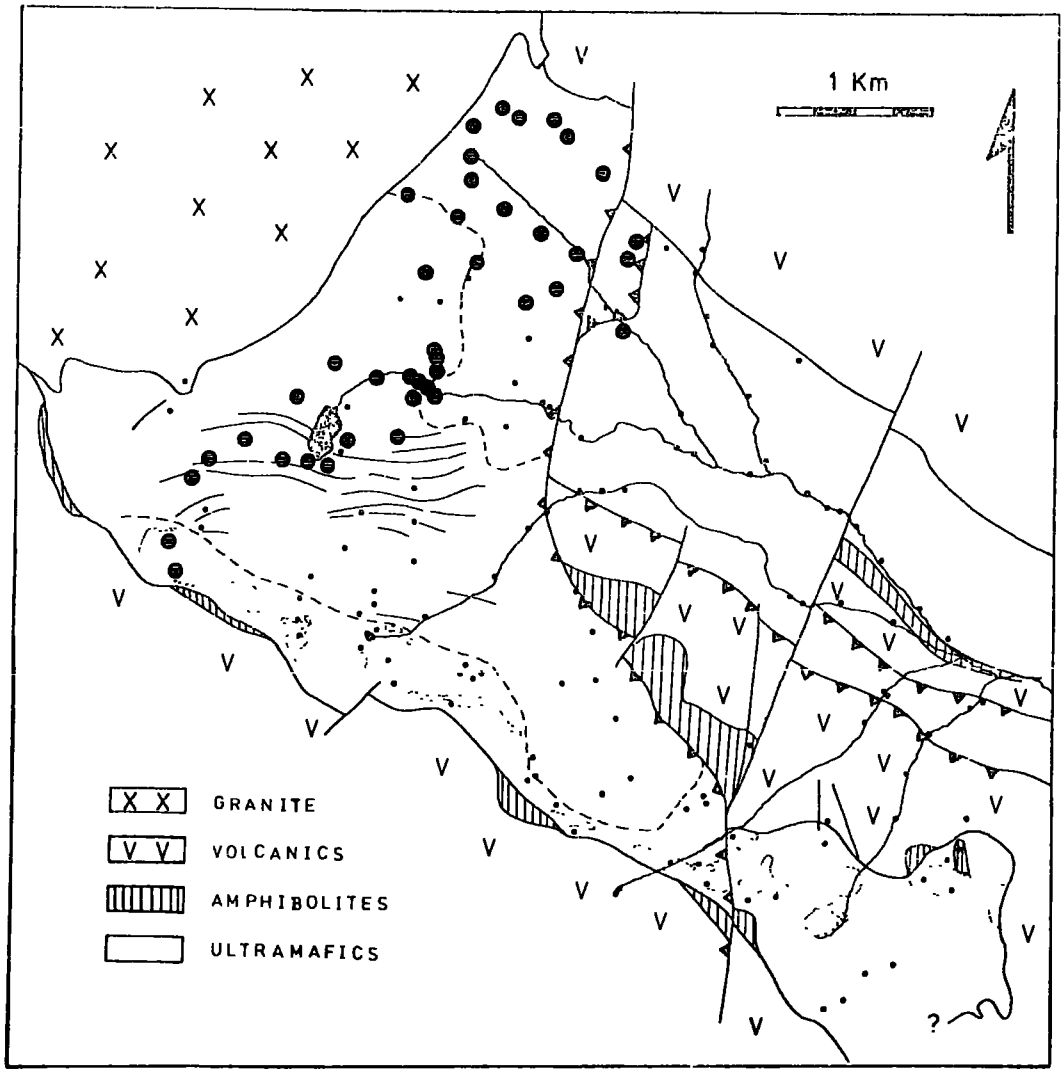

Figure 5.6 Distribution of talc.

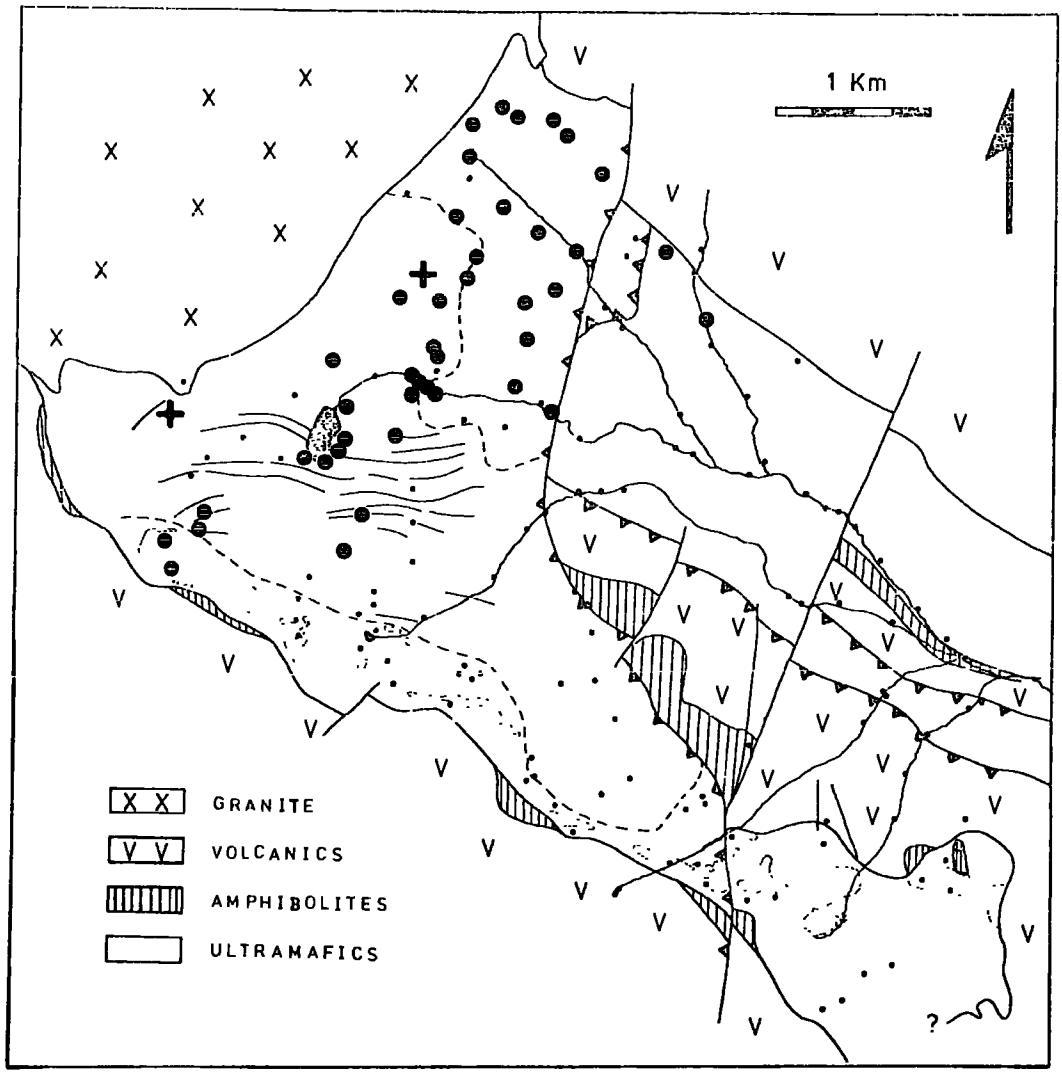

Figure 5.7 Distribution of tremolite, (closed circles), and anthophyllite, (crosses).

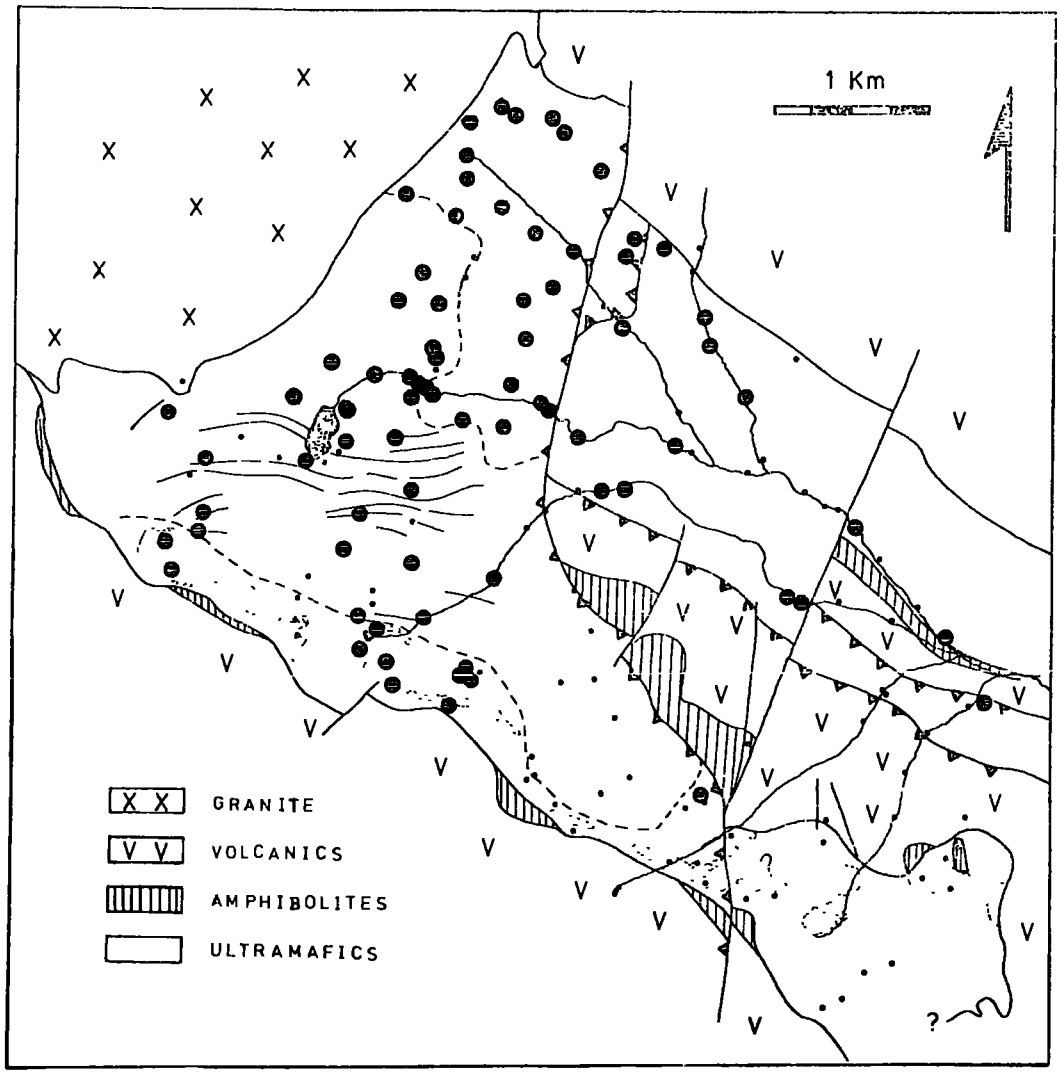

Figure 5.8 Distribution of ferritchromit and chromium magnetite, (spinel (3)).

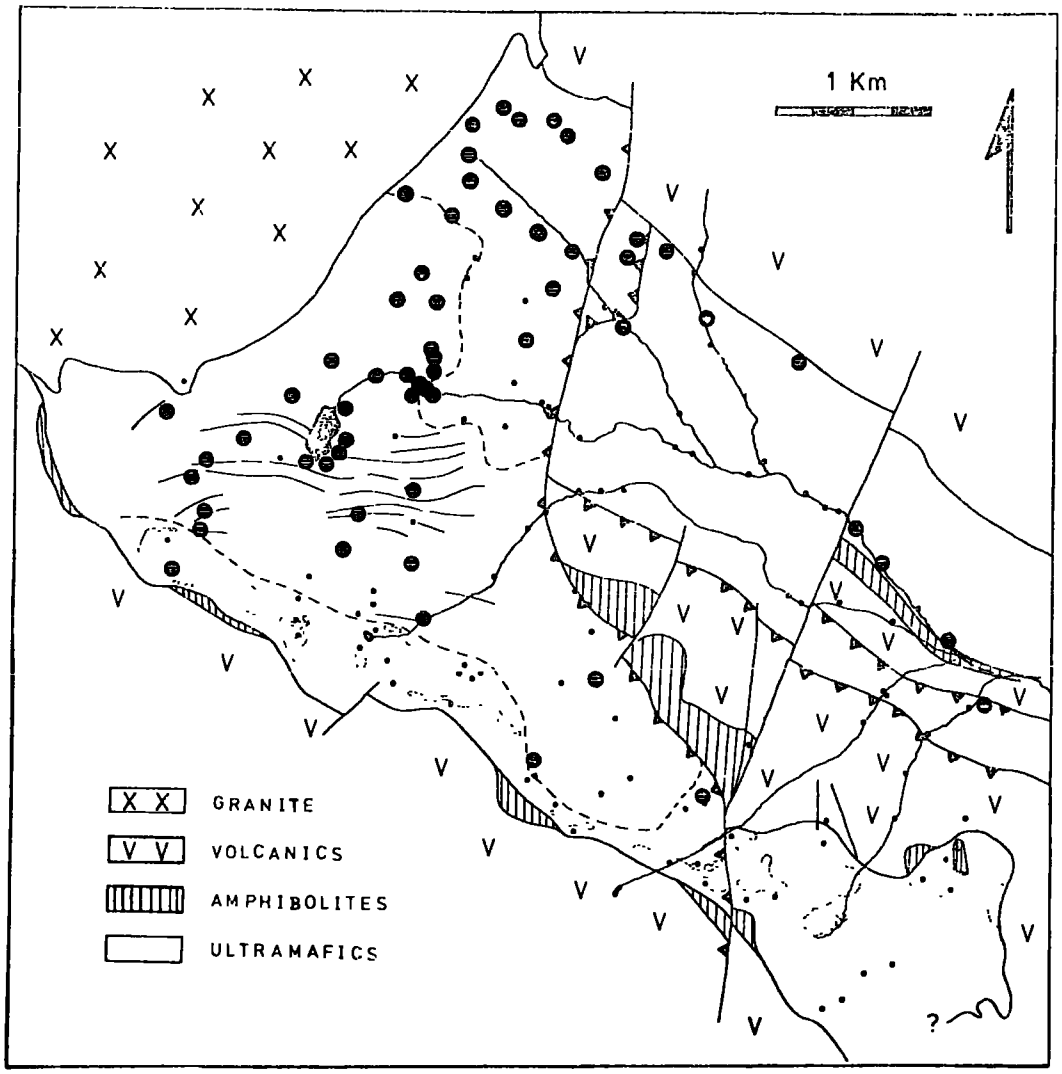

Figure 5.9 Distribution of Al-serpentine and chlorite.

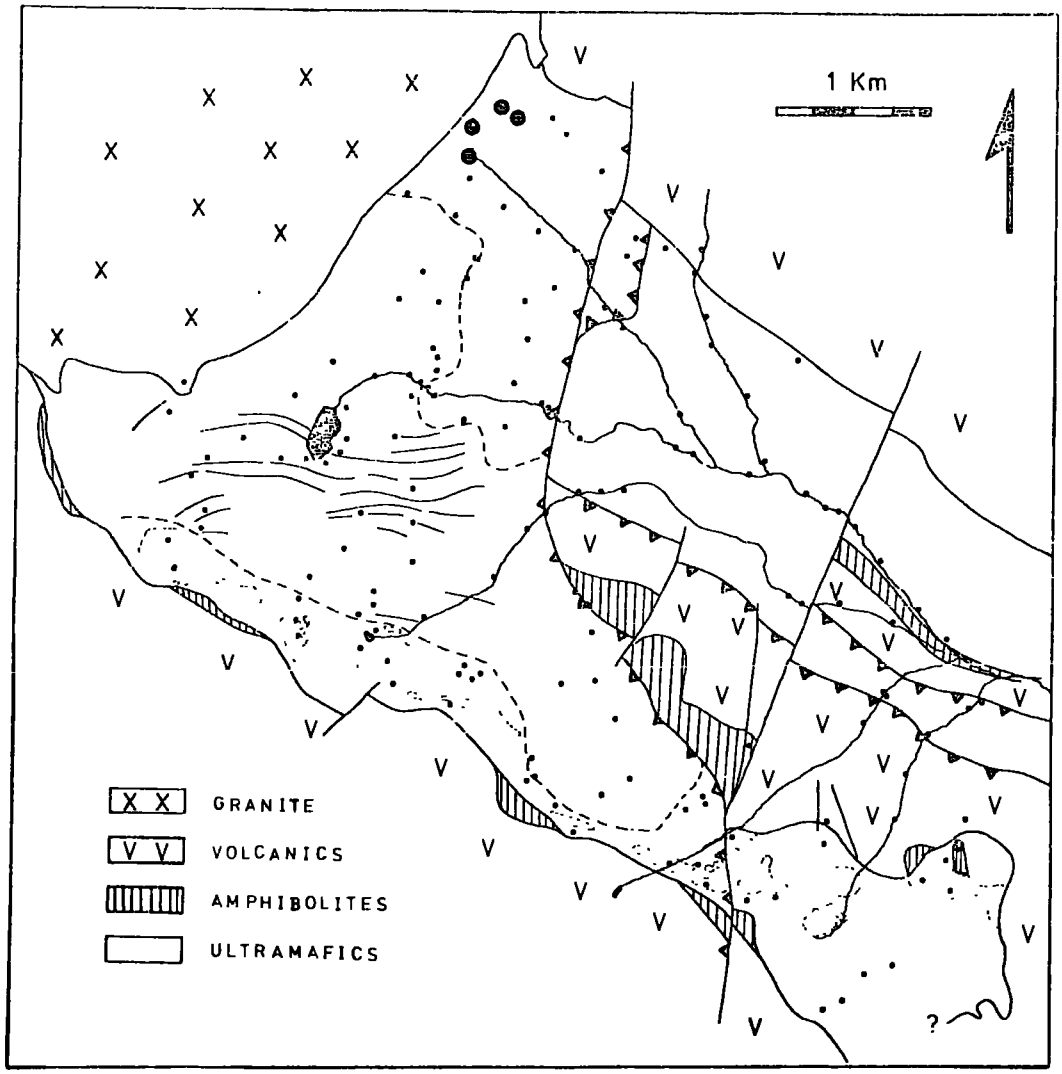

Figure 5.10 Distribution of metamorphic enstatite (3).

Meta-Peridotite (Unit (1))

Contact metamorphism is barely discoverable in Unit (1), which retains its primary, Stage I assemblage. It remained essentially anhydrous during Stage II, and was consequently inert during prograde metamorphism. A few "bastite" pseudomorphs after enstatite (1) were formed during Stage II, especially along the northern contact of Unit (1), and these show partial to complete regeneration to an olivine (3) pseudomorph. The Stage II bastite retained the outline and internal structure of the host pyroxene, and in particular, it retained the pronounced cleavage parallel to (100). This cleavage controls much of the later olivine growth. In samples 60874 and 61552 olivine has nucleated around the margin of the bastite, and has started to grow inward ,(Plate 5.1). Inward growth is controlled by the inherited cleavage, and a patchwork of short elongate olivine crystals replace the serpentine. Relict serpentine within the growing olivine fringe recrystallizes, and coarse euhedral magnetite crystals are invariably found within the pseudomorph, (Plate 5.1).

In sample 60153, large olivine (3) mosaics, pseudomorphing bastite, attain diameters of up to 4.0 mm. The replacement olivine appears to show a greater crystallographic control by the original fracture pattern,than by

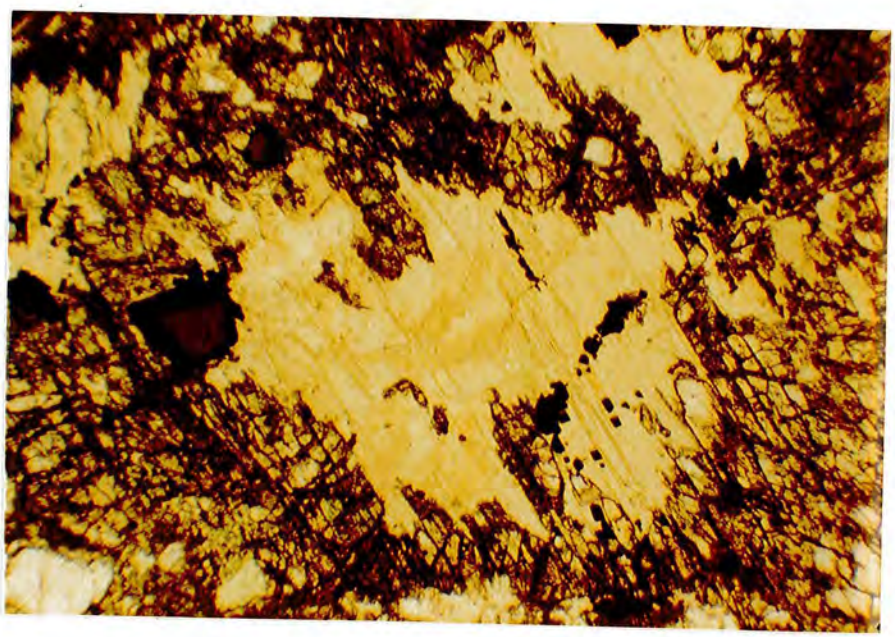

Plate 5.1 Photomicrograph: A fringe of olivine (3) growing around a bastite pseudomorph. Growth is controlled by the original cleavage. Note the magnetite granules. Sample 60874. Plane polarised light. Field width 1.7mm.

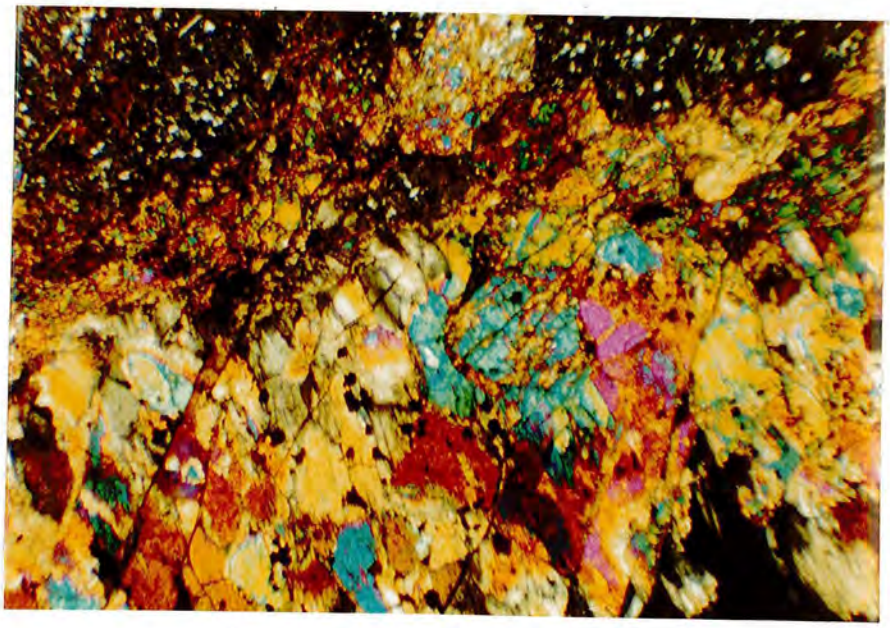

Plate 5.2 Photomicrograph: Olivine (3) and granular magnetite replacing a bastite pseudomorph in Sample 60153. Note the preferentially altered primary olivine, now serpentine. Crossed polars. Field width 1.7mm.

enstatite cleavage. The replacement olivine, (Plate 5.2) is clear, fresh, and unaltered, although the matrix olivine (1) is largely serpentinized at a later stage, (see Chapter 7). The extra stability is thought to be a function of mineral chemistry, (see Chapter 6).

Irregular access of water during Stage II evidently led to the formation of bastite in rocks which contain relict enstatite (1). In Samples 60876 and 60160, partial regeneration has occurred close to primary unaltered enstatite.

Table 5.1 shows the assemblages attained in Unit (1), and Table 5.2 summarizes the probable reactions involved.

The development of olivine without talc implies that the pseudomorphs are formed by reaction (6), which presupposes a brucite component to the original rock.

(6) Serpentine + brucite = olivine (3) + H_2O

Clinopyroxene lamellae are stable in primary enstatite throughout much of Unit (1), (Plate 3.10), but cease to be stable above the tremolite isograd. Samples 61552, and 61556, contain tremolite needles and blades, overprinted on the primary lithology. They commonly occur in the vicinity of bastite pseudomorphs.

The occurrence of tremolite below the talc isograd, Figure 5.7, suggests a serpentine-diopside reaction, such as that indicated by Evans and Trommsdorff (1970), Table 5.2.

TABLE 5.1

Metamorphosed Ultramafic Rocks

Unit (1) and Unit (3c)

Assemblages, and representive Samples

outer aureole

Reaction (6)

(Ol(1), ± En(1), Spinel(1), Serp, Magnt) ± Ol(3)
(60153, 60874)

Reaction (7)

(Ol(1), Spinel(1), Serp, Magnt) ± Ol(3) ± tremolite
(61552, 61556)

inner aureole

Reactions (8,9,10)

(Ol(1), ± Spinel(1)), Al serp, Ferritchromit, tremolite
(60186, 60174)

± Ol(3) ± talc

Reaction (11)

(Ol(1), Spinel(1)), Al serp, Ferritchromit,
(60196)
Anthophyllite

Reaction (12,13)

(Ol(1)), Ol(3), Tremolite, Ferritchromit, Chlorite
(60341)

Hornblende, anthophyllite

Relict primary mineralogy, and metamorphic assemblages in the "core" region of the ultramafic body. Underlined phases represent their first occurrence according to the associated reaction.

TABLE 5.2

Metamorphosed Ultramafic Rocks

Unit (1) and Unit (3c)

Reactions:

outer aureole

(6) Serpentine + brucite = 2 olivine (3) + $3H_2O$

(7) 5 serpentine + 2 diopside = tremolite + 6 olivine (3) + $9H_2O$

inner aureole

(9) Spinel + serpentine = Ferritchromit + Al serpentine + SiO_2

(10) Enstatite + diopside + SiO_2 + H_2O = tremolite

(8) 5 serpentine = 6 olivine (3) + talc + $9H_2O$

(11) 9 talc + 4 olivine = 5 anthophyllite + $4H_2O$

(12) Al serpentine = chlorite

(13) Chlorite + talc + tremolite + SiO_2 = Anthophyllite + hornblende + H_2O

(7) 5 serpentine + 2 diopside = tremolite + 6 olivine (2)

$+ H_2O$

The tremolite isograd is placed 2000 m from the batholith contact, Figure 5.4 and 5.6.

Meta-Peridotite (Unit (3c)).

Above the talc isograd, in Unit (3c), there is a marked increase in the degree of alteration. Excepting Sample 60226, enstatite is completely lacking, Figure 3.7, and primary spinel shows a far greater degree of alteration. There is an overall increase in the apparent degree of hydration, and the effect of this is shown by the observed assemblages and reactions in Tables 5.3 and 5.4.

Above the isograd some, although not all, bastites show sign of regeneration, and those that do, may show either partial development, as described for Samples 60195 and 60341, or complete replacement as in Samples 60174 and 60186 (Plate 5.3). Complete replacement forms a controlled mosaic approximately 3.0 mm in diameter, with flecks of talc intimately associated with the replacement olivine. Complete replacement may be inhibited by the formation of Al serpentine and chlorite at the expense of primary serpentine. The bastite is thus "poisoned" structurally. In Sample 60341 (Plate 5.4) regenerated olivine granules form stringers within a chlorite pseudomorph, which itself has replaced Al

TABLE 5.3

Metamorphosed Ultramafic Rocks

Unit (3a) and Unit (36)

Assemblages

outer aureole

Reaction (6)

(Spinel (1), Serp., Magnt.), $\pm$ Ol(3)

Reaction (7)

(Spinel (1), Serp., Magnt.), Ol(3), Tremolite

inner aureole

Reaction (8,9,10)

Ol(3), Al serp., Ferritchromit, Talc, $\pm$ Tremolite

Reaction (12,14)

Ol(3), En(3), Chlorite, Tremolite, Ferritchromit.

Relict primary mineralogy, and metamorphic assemblages within the marginal serpentine. Underlined phases represent their first occurrence, according to the associated reaction.

TABLE 5.4

Metamorphosed Ultramafic Rocks

Unit (3a) and Unit (3b)

Reactions:

outer aureole

(6) Serpentine + brucite = 2 olivine (3) + $3H_2O$

(7) 5 serpentine + 2 diopside = Tremolite + 6 olivine (3) + $9H_2O$

inner aureole

(9) Spinel (1) + serpentine = Ferritchromit + Al serpentine + SiO_2

(10) Enstatite + diopside + SiO_2 + H_2O = tremolite

(8) 5 serpentine = 6 olivine (3) + talc + H_2O

(12) Al serpentine = chlorite

(14) Talc + olivine (3) = enstatite (3) + H_2O

serpentine.

Original bastites retain their outline, and those that show only partial, or no regeneration of olivine, are replaced initially by an intimate association of Al serpentine and fibrous tremolite, with or without talc. In Samples 60185 and 60186, bastites consist of an outer fibrous tremolite fringe, and an inner anomalous "berlin blue" birefringent Al serpentine.

The primary, olivine (1) based texture of the rock is retained, although intergranular serpentine changes its chemistry, but not its structure. In Sample 60196 "typical" intergranular serpentine is Al rich. X-ray diffraction data (Appendix IV) confirms the structural state of the mineral. The development of Al serpentine is related to the hydrothermal alteration, and oxidation of primary spinel to "ferritchromit", a name applied by Engin and Aucott (1971). The degree of alteration appears to depend on the proximity to the batholith, and the composition of the primary spinel. Large, irregular, Al rich primary spinels, as described from peridotites in Chapter 3, show signs of incipient alteration as far south as Samples 60071, and 60160, below the talc isograd. Above the isograd alteration is far more pervasive, although, as noted earlier, Figure 3.12, relict red spinels do remain. Halos of Al serpentine start to

develop around primary spinels, as the first stage in the oxidation process, (Plate 5.5). Al serpentine replaces interstitial serpentine and olivine (1), and forms a felty fringe around the spinel (1). Wolfe (1967) notes that an inner halo of dirty fibrous "kammererite" forms around the spinel, and an outer clear zone of "penninite" forms along the contact with olivine (1). The former is birefringent grey, and the latter an anomalous "berlin blue" colour, Samples 60071, 60226, (Plate 5.6). In fact, (Chapter 6), there is little compositional variation; they fall with a limited Al solid solution range, and the feature is probably one of crystallinity. Thus oxidation of Al spinels, and later oxidation of Cr spinels, leads to the conversion of all the serpentine from Stage II, not already regenerated to olivine (3), into Al serpentine. In addition, the halos indicate a direct reaction with olivine in the presence of water. During oxidation the spinels become blackened and irregular, and loose their red translucency in thin section. Alteration proceeds inwards, and red cores often remain.

Tremolite is a common metamorphic mineral above the talc isograd, laths and needles between 0.2 mm and 2.0 mm long, occur as individual blades, and as clusters, imprinted on the primary olivine and secondary serpentine,

(Al serpentine), matrix. They are often broken and fractured as a result of minor intergranular movement, but they are rarely disorientated, (Plate 5.7).

Anthophyllite blades and needles, similar to tremolite in mode of occurrence, appear in Sample 60196, a sample which, on the basis of its spinel (1) chemistry, is dunite, and thus deficient in Ca.

Although talc is widespread above the isograd, it is not abundant, and it occurs principally as small flakes disseminated between granulated olivine (1) relicts, within the remnant matrix. It also occurs with tremolite and Al serpentine in bastite pseudomorphs, and in Sample 60226, replacing relict enstatite (1).

Alteration of serpentine to Al serpentine undoubtedly hinders olivine (3) generation in the "serpentine" matrix, and thus reduces talc formation. Interstitial olivine (3) overgrowths on olivine (1) were observed in Samples 60186, 61615, (and possibly in Sample 61560, below the isograd). The overgrowths form a meshwork replacing serpentine. They are in optical continuity with their enclosed fragment, they form sharp intergrain contacts between rounded and granulated fragments, and they stand out as a result of preferential serpentinization of olivine (1), during

Stage IV, (Plate 3.7). This latter feature suggests a compositional difference, analogous to that observed in the bastite pseudomorphs in Sample 60153. The amount of interstitial serpentine which has been regenerated in Units (1) and (3c) is small, which suggests that very little water got into the "core" region, inspite of the highly serpentinized nature of the marginal zones.

Retrogressive reserpentinization, which reverses the talc forming reaction, may locally account for the scarcity of talc.

Talc and olivine (3) were probably formed by reaction (8), Table 5.2, the higher temperature reaction established by Bowen and Tuttle (1949).

(8) 5 serpentine = 6 olivine (3) + talc + $9H_2O$

This reaction is probably inhibited by reaction (9), which alters the composition of the serpentine.

(9) Primary spinel (1) + serpentine = ferritchromit + Al serpentine + SiO_2

Substitution of Al for Si in the serpentine structure produces an excess of Si, which is probably absorbed by the following reaction, (10).

(10) Enstatite (1) + diopside (1) + SiO_2 + H_2O = tremolite.

As noted, (excepting Sample 60226), neither primary pyroxene phase was observed above the isograd. Although

considered a high temperature reaction by Boyd (1959), a reaction like this explains the formation of tremolite in a system in which serpentine is contaminated by Al, preventing reaction (7).

Anthophyllite produced in Sample 60196 presumably forms by the experimentally determined reaction (11), discussed by Greenwood (1963).

(11) 9 talc + 4 olivine = 5 anthophyllite + 4 H_2O

The reaction temperature suggested for this is around 670°C at 2 Kbars. This is unrealistic in terms of the associated rock types, and a lower temperature is suggested. This is probably reasonable, as the anthophyllite formed contains appreciable Fe, (Chapter 6).

Samples 60199 to 60174 were collected along a sharp ridge that forms the back wall of the corrie complex. The back wall of this ridge falls away into a granite-floored corrie, (Plate 5.8), which drains to the northeast, and is largely scree covered and inaccessible. For this reason Unit (3c) was only sampled in the vicinity of the contact in one location, that of Sample 60341. This sample displays a slightly higher grade mineralogy.

Partially regenerated bastites appear to be forming colourless anthophyllite, and a green pleo-

choric hornblende (Plate 5.9), according to reaction (13), established by Choudhuri and Winkler (1967).

(13) Chlorite + talc + tremolite + SiO_2 =

anthophyllite + hornblende + H_2O

This reaction proceeds at a temperature of $540^{\circ} \pm 10^{\circ}C$, below 1 Kb P_{H_2O}, the reaction is however pressure sensitive, Figure 5.11, and above this pressure anorthite becomes a stable phase. This reaction, close to the contact, is in good agreement with the observed countryrock data, and it suggests hornblende hornfels conditions within the "inner aureole". The reaction also suggests a low P_{H_2O}, below 1 Kb.

As noted earlier, Al serpentine has completely recrystallized to chlorite in this sample. Chlorite pseudomorphs replace bastite (Plate 5.4), and sharp crystalline laths replace a halo of Al serpentine (Plate 5.10). Whether chlorite is formed by reaction, or structural transformation, is not directly apparent. As it pseudomorphs an original Al serpentine halo, it may result from a structural transformation from a 7 Å septachlorite, or serpentine lattice, to the true 14 Å chlorite structure. This transformation has been observed by a number of workers, including Yoder (1952), who suggested a transformation temperature of 500° - $520^{\circ}C$, Nelson and Roy (1958), Gillery (1959), and Velde (1973). Velde suggests

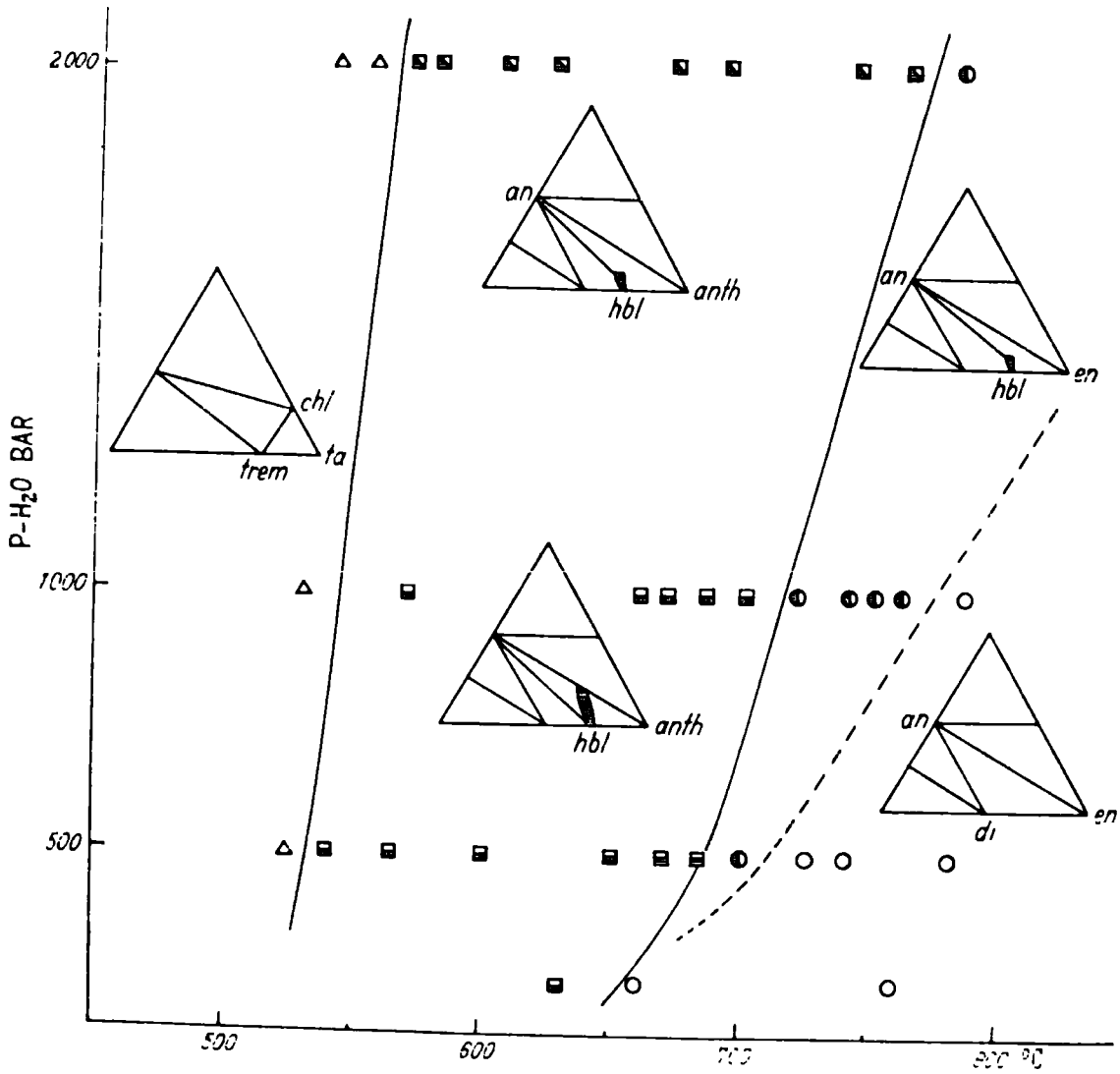

Figure 5.11 The stability of the assemblage "Tremolite (trem) - Talc (ta) - Chlorite (chl)," as a function of P_{H_2O} and temperature, in rocks of "ultrabasic" composition. The data are from the experimental work of Choudhuri and Winkler (1967). Anorthite=(an), Enstatite=(en), Anthophyllite=(anth), Hornblende=(hbl), Diopside=(di).

lower transformation temperatures, but also a compositional control.

Meta-serpentinite (Unit(3a))

The two bands of marginal serpentinite which flank the "core" region have both been subjected to the same metamorphic process, and they display similar rock textures and isograds on either side of the core.

In marked contrast to Unit (1), Unit (3a) is strongly metamorphic in character, consisting largely of secondary regenerated olivine (3), in a relict serpentine matrix. Retrogressive serpentinization during Stage IV has markedly reduced the amount of surviving olivine (3), especially in the east, Figure 5.5, but it has not influenced the texture of the rock, and enough remains to establish the pattern of metamorphism below the talc isograd. Textural evidence suggests that metamorphism regenerated olivine up to 5000 m from the batholith contact in the west, and for 4000 m in the east, Figure 5.4. A few weak textural traces were detected below the transverse fault which cuts the body across Claim Jumper Creek.

The main metamorphic feature is the characteristic "oolitic" texture noted by Gabrielse (1963),and Wolfe (1965, 1967). This is well developed in Unit (3a), particularly in the west, and along Spudusob Creek in the east. The texture derives from the development of evenly

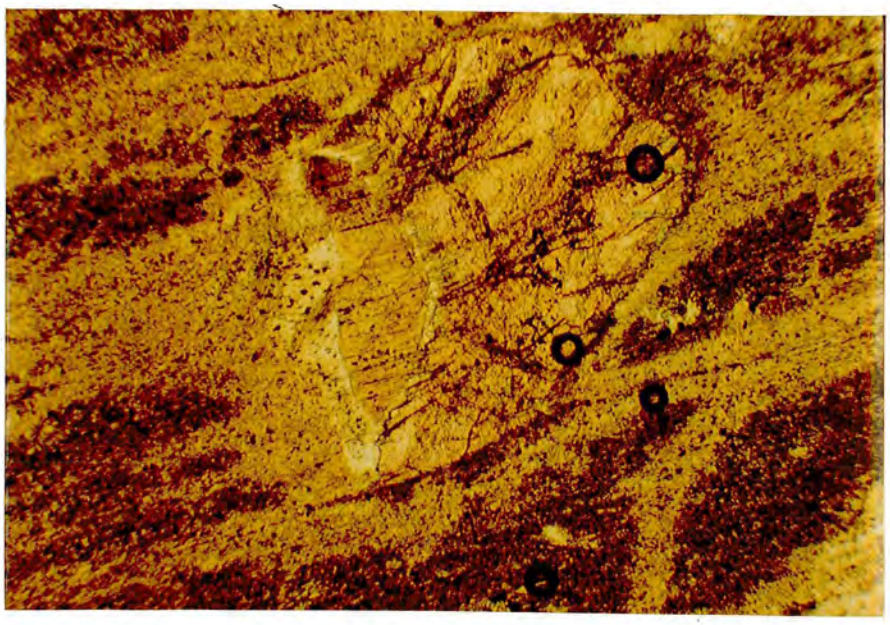

Plate 5.9 Photomicrograph: Green hornblende enveloped by fibrous white anthophyllite, adjacent to a large olivine. The assemblage is in a bastite consisting of chlorite and tremolite, in Sample 60341. Plane polarised light. Field width 1.7mm.

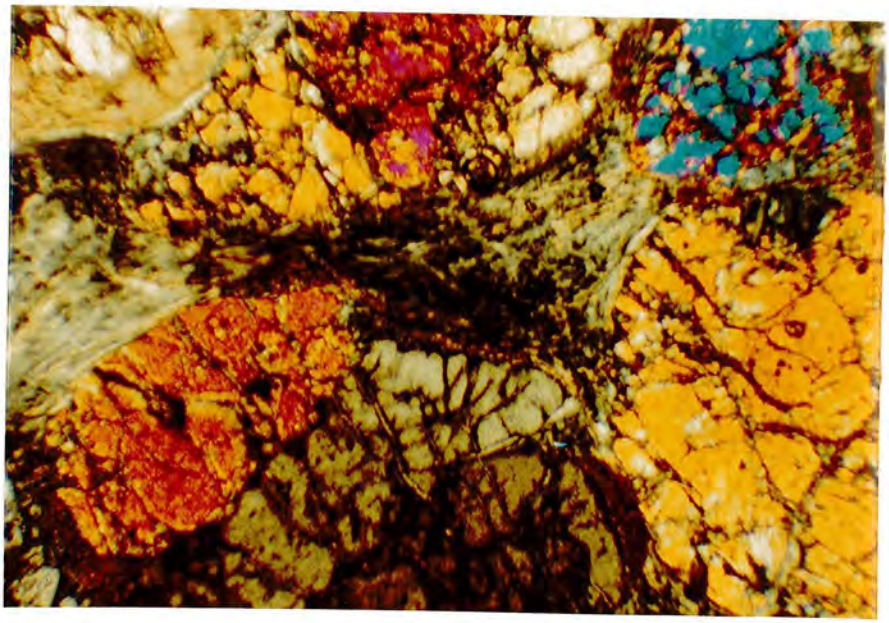

Plate 5.15 Photomicrograph: A composite cored metamorphic olivine, set in modified matrix serpentine, in Sample 61632. Crossed polars. Field width 1.7mm.

spaced olivine porphyroblasts, which grow at the expense of serpentine into either a mutually interfering mosaic, in which most of the serpentine has been exhausted, Samples 60171, 60206, or into descrete crystals with sharp euhedral outlines, as in 60157 and 60035 (Plates 5.11). A third variety, no longer preserved as olivine, developed in samples such as 60055 and 60056. Scattered, rounded cores of olivine (3) were formed, but sharp euhedral outlines were never attained, (Plate 5.12). The size and number of secondary olivine porphyroblasts is seen to increase from Sample 60143, on Spudusob Creek, to Sample 60038, and conversely the amount of recognisable bastite is seen to decrease.

Granules of relict primary clinopyroxene appear to have remained stable in Samples 60029 and 60033, and lamellae remain unaltered in a distinct bastite, within Sample 60067. This suggests that "harzburgite" serpentinite regenerates to secondary dunite, but perhaps not as readily as original dunite derived serpentinite. The development of olivine (3), in Samples 60029 and 60033, is not as good as in Samples 60035 and 60102, which are nearby. Bastites are thus lost during progressive metamorphism.

In hand specimen olivine "kernels", or porphyroblasts, are found to be small, 1.0 mm to 3.0 mm in length, and approximately uniform in grain size. They appear spherical

or elongate-euhedral in outline, and they give the rock a coarse granular appearance. The rock is usually foliated, with olivine grains orientated in planes, and separated by planes of apple-green translucent serpentine. The retrogressive serpentinization of olivine to a dark green serpentine imparts a distinctive mottled appearance to the rock, a feature which first drew attention to the rock, (Gabrielse, 1963). In addition, weathering of exposed surfaces hydrates magnetite to rust, in the porphyroblast; and brings out white weathering brucite, coating the interface between regenerated olivine (3), (or a serpentine pseudomorph thereafter), and the matrix serpentine, as in Samples 60102, and 61592 (Plate 5.13).

The metamorphic foliation is irregular and distorted, but parallel to the western margin, within that zone. Along Heazlewood Creek there is a strong foliation subparallel to the floor of the Heazlewood Thrust. The foliation may be partially inherited from the Stage II serpentinite, but it may also reflect activity along these contacts during regeneration. In the northeast, Samples 60128 and 60109, foliation is subparallel to the Nickel Creek thrust, and the batholith contact. The variation in foliation is thus a complex result of inherited foliation, and operative tectonic relations at the time of metamorphism. No simple, single, factor appears to be responsible.

Plate 5.13. Dark serpentine (4) pseudomorphs after olivine (3), set in a matrix of light green serpentine (3). The old olivine porphyroblasts are enveloped by a white coating of brucite. Outcrop joint surface, location point 60102, Unit (3a).

Plate 5.23. Strongly foliated regenerated dunite from Unit (3b). The foliation, which is enhanced by "chlorite" layers, is subparallel to the contact of the batholith. Location point 61597, northeast of Nickel Creek.

In thin section most of the larger olivine (3) porphyroblasts appear to be strongly zoned, with a dark, turbid, circular, inner core, and an outer clear margin. The turbidity appears to result from the concentration of minute gas bubbles, and the inclusion of minute crystals of magnetite, which occasionally hydrates and stains the core region brown. Turbid cores vary in intensity, some samples such as 60171, 61567, and 60157, are particularly strongly cored. A single turbid "core" may centre one crystal of olivine (3), or several, (Plates 5.14, 5.15). Growth was evidently point centred, and depending on the scatter of nucleation centres, single or multiple crystalled kernels were developed. Sample 60157 contains a few large crystals, where as Sample 61636 contains a mosaic of small weakly cored granular crystals. Continued growth leads to mutual interference, and a polygonal mosaic, Sample 60227, (Plate 5.16). Patches of serpentine may remain, and in these patches euhedral growth continues, with slightly rounded corners, Sample 61632 (Plates 5.17, 5.18).

Samples 60894 and 61531 are crossed by a number of planes which consist of strongly cored olivine porphyroblasts. In Sample 60894, (Plate 5.19), the amount of marginal olivine formed within the plane is limited, and it would appear that the cores were continuous within the plane. It is interpreted as a fracture along which gas flowed

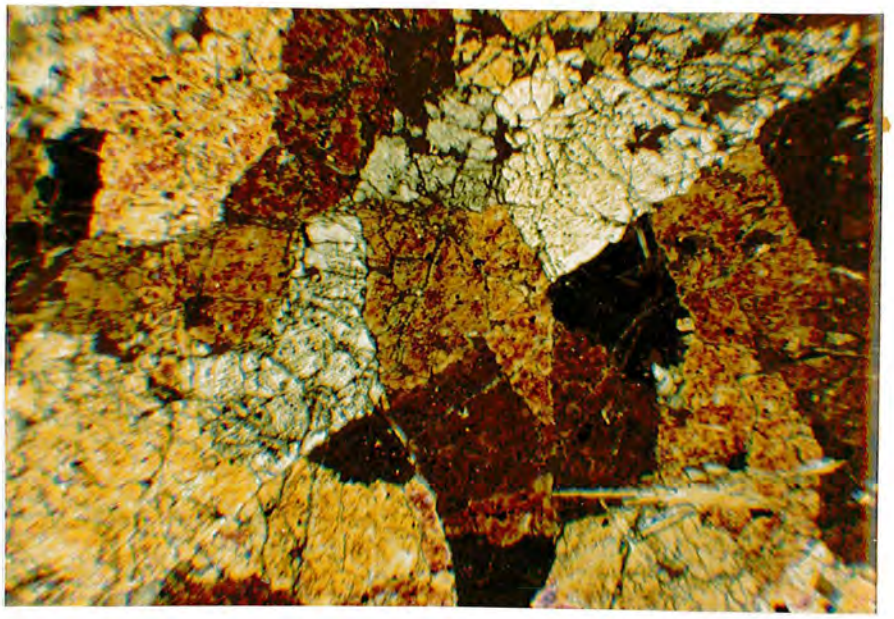

Plate 5.16 Photomicrograph: A completely recrystallized mosaic of olivine (3). Note the crystal outlines, and the control by a fracture interface. Sample 60227. Crossed polars. Field width 1.7mm.

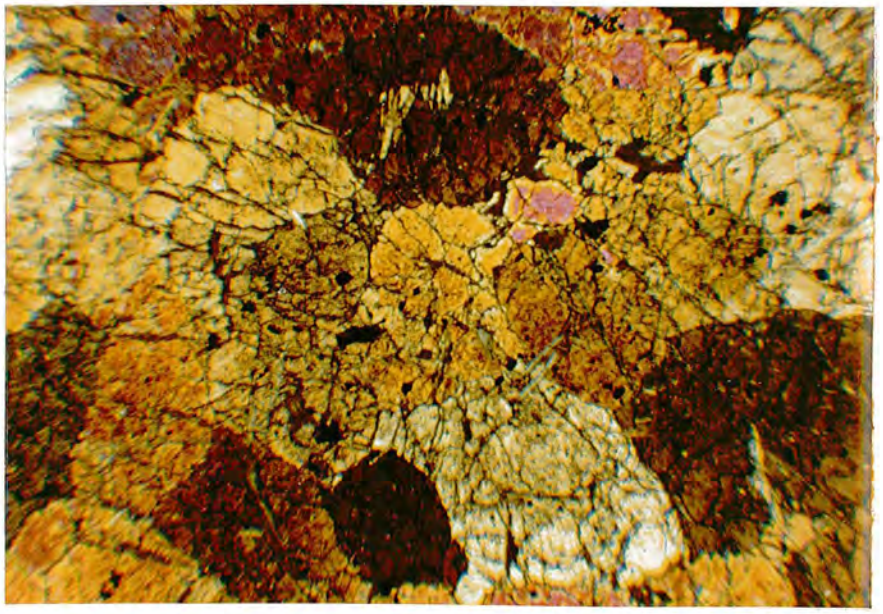

Plate 5.29 Photomicrograph: A completed mosaic of recrystallized olivine (3). Note the curved crystal outlines, and the mild fracturing. Sample 60172. Crossed polars. Field width 1.7mm.

during the initial period of dehydration. Fast crystallization of core olivine, along the fracture, led to the development of cored olivine, within a generally less strongly mottled rock. Possibly small flecks of serpentine, trapped during fast early growth of core olivine, dehydrated to develop the observed gas bubbles. Spherical cores of olivine are enclosed by clear crystalline olivine margins, (except as noted in Samples 60055, 60056), and this suggests a slower more controlled period of olivine growth, with gas released during dehydration diffusing out through the serpentine matrix, and established fractures.

Although some samples, such as 60171, display evenly-spaced, uniformly cored olivines, presumably representing one nucleation period, others, such as 60157 and 60035 contain a range of sizes and intensities, representing continuous nucleation. Sample 60157 in particular, has small interstitial "marginal type" olivine grains among the cored porphyroblasts, (Plate 5.20).

The initial dark green serpentine formed in bastite-serpentinite during Stage II is progressively altered by the development of olivine porphyroblasts during Stage III. The characteristic "hourglass" texture is lost, and a felty, fibrous serpentine is developed, that envelopes the porphyroblasts, and forms a relict serpentine matrix below the talc isograd. The nature of this matrix is obscured by retro-

gression to antigorite during Stage IV, above its retrogressive isograd. In Samples 60035, 60102 and 60157, the matrix remains, isolating euhedral crystals, (Plate 5.21).

The regeneration process is independent of the spinel phase, and relict red primary spinels remain scattered through Unit (3a). Some Al rich spinels show partial alteration to ferritchromit and Al serpentine, Sample 60143, but the alteration tends to be minor and superficial; particularly for small euhedral Cr rich spinels, such as those found in Samples 60157, 60159, 60021, and 61577. Alteration increases towards the talc isograd, and becomes significant in the area now retrogressed to antigorite, Sample 60907, 60109 and 60069. Some spinels are altered to, or coated by, magnetite, presumably formed during Stage II.

The contact between Unit (1) and Unit (3a) is remarkably sharp, and as noted, there is little material transitional between the two. The contact is easily traced in the west, as the weathering pattern differs. The change appears to be sharp and transitional, as between Samples 60241 and 60160, two neighbouring but totally different rocks. Similarly the contact between Unit (3a) and Unit (3c) is sharp and well exposed up the waterfall section below Ice Lake. Samples 60226 and 60227 fall on different sides of the line. A weakly mottled regenerated rock appears to pass into a granulated primary rock with little or no

tectonic break. Minor evidence for tectonism along that contact comes from control of olivine (3) by fractures, in Sample 60227, gas flow fractures, in 60894, and recrystallized asbestos, in Sample 61525.

Close to the Unit (1) contact, (Heazlewood thrust?), Sample 61525 contains a distorted vein of recrystallized asbestos. The vein reaches a maximum width of 1.0 cm, and a length of approximately 12.0 cms, tapering to each end. It has a coarse olivine orientation perpendicular to the vein walls, as in chrysotile asbestos cross-fibre. In thin section, coarse, clean, granular olivine (3) crystallize an off-centred medial partition of fine magnetite dust (Plate 5.22). This in particular is indicative of prior asbestos veining.

All the olivine (3) produced below the talc isograd is assumed to have formed according to reaction (6). Early, fast, crystallization of core olivine on crossing the isograd, was followed by a slower development of later olivine, presumably as the serpentine-brucite assemblage attained equilibrium with olivine, under the prevailing P-T conditions. The amount of relict serpentine decreases towards the talc isograd, and even asbestos (chrysotile(?)) has recrystallized just below the isograd. Samples 60109, 60117, 61623 and 61625, all contain tremolite without talc, overprinted as blades on the secondary olivine. This is

taken as evidence for reaction (7), within the regenerated unit.

Meta-serpentinite (Unit (3b))

The small area of marginal serpentinite in the west, that lies above the talc isograd, has undergone retrogressive metamorphism to a talc-antigorite assemblage consequently most of this section refers to the well exposed eastern area of talcose, regenerated dunite. The talc isograd appears to cross the Nickel Creek thrust, and a distinct block of talcose rock, (Plate 3.1) appears at the entrance to the Nickel Creek Corrie. The white to brown weathering of the rock, and its rounded outcrop, is characteristic of talcose rock. Some rocks retain a distinct foliation, Samples 61597 and 61611, and this is defined by parallel planes of distinct but weakly cored olivine (3), with intervening planes of Al serpentine, (chlorite), or talc. The trend of this foliation appears to be consistent, subparallel to the batholith contact, and also to the Nickel Creek thrust, Figure 5.2, (Plate 5.23).

In hand specimen the rock is faintly mottled, and sandy textured. The amount of matrix is usually small, and except where retrogression has occurred, the rock resembles dunite. Broken rock is black inside, with fine flakes of talc disseminated about dark coloured olivine

kernels, both set in a dark green Al serpentine matrix. Tremolite, which is a common to abundant metamorphic mineral in most rocks, such as Samples 61600 and 61607, is rarely visible in hand specimen. Patches of tremolite, talc and Al serpentine appear in "clots" within the rock, very often close to, or associated with, a spinel phase. These, in thin section, appear to represent bastites, which have acted as centres for the development of these phases. Otherwise tremolite needles occur, as they do throughout Unit (3c), randomly distributed over regenerated, (but not primary), olivine. Blades and needles, singly and in clusters, are often broken and fractured, but again they do not appear to be disorientated (Plate 5.24).

Talc and Al serpentine are intimately associated with each other, and with highly irregular oxidised crystals of ferritchromit, (Plate 5.25). Relicts of fresh red spinel(1) are remarkably rare, small euhedral relicts were observed in Samples 60209 and 60894.

The talc and Al serpentine associated with diffuse and highly altered ferritchromit is poorly crystalline and intergrown. Talc, which tends to be present in greater amounts than in Unit (3c), also occurs separating discrete olivine grains, (Plate 5.26). Retrogressive alteration of olivine (3) to serpentine during Stage IV appears to correlate with greater interstitial talc and Al serpentine

(chlorite), crystallinity, Samples 61535, 60137, 61598. Brown birefringent laths and bundles of Al serpentine recrystallize from the "berlin blue" birefringent, felty matrix, Al serpentine. Such recrystallization is seen in Samples 60202 and 61607.

Olivine (3) in Samples 60894 and 60206 appears to be transitional, with cores formed by the lower temperature reaction (6), and margins formed by the higher temperature, talc producing reaction, (8). Evidence for this consists of a pronounced inclusion ring, and crystallographic break surrounding the olivine core, (Plate 5.27). The olivine is typical of that found below the isograd, except for this inclusion ring, which also marks the locus of a number of crystal lattice defects, (Plate 5.28). Areas of matrix serpentine in Sample 60894 have been converted into talc, (Plate 5.27); as the rock contains a stable primary spinel, and no excess Al.

Above the isograd olivines tend to be smaller, up to 1.0 mm in diameter, less strongly cored, and mutually interfering, except around original bastites. They thus form a mosaic of irregular polygons, (Plate 5.29). Samples 60172, 61607 and 60209, are texturally not dissimilar to lower grade olivines in Sample 60171. The olivine, along with the tremolite, has undergone granulation (and minor reserpentinization), which complicates the mosaic, but does

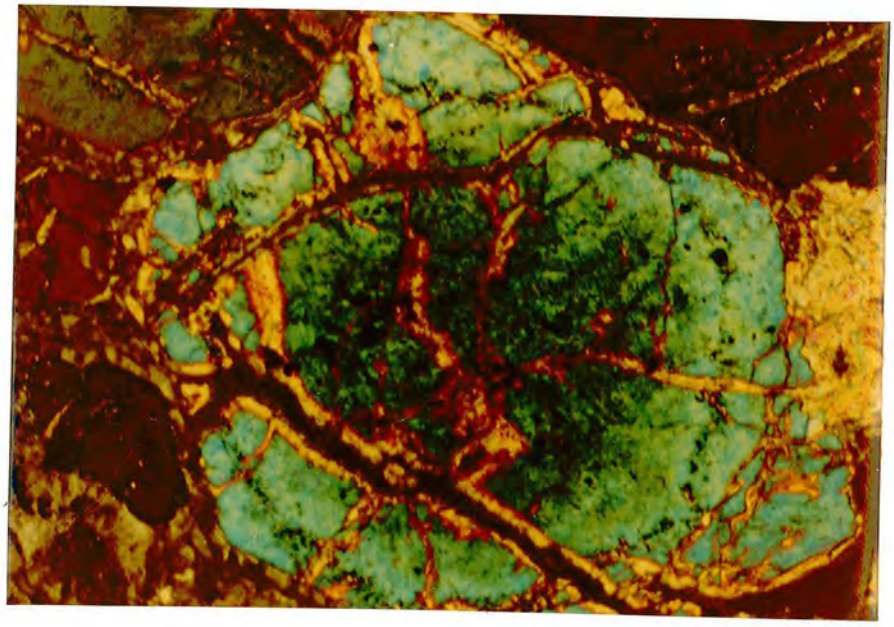

Plate 5.27 Photomicrograph: A single cored metamorphic olivine in Sample 60894. Note the circular core, inclusion ring, and additional growth (bottom right). The matrix is talc. Crossed polars. Field width 1.7mm.

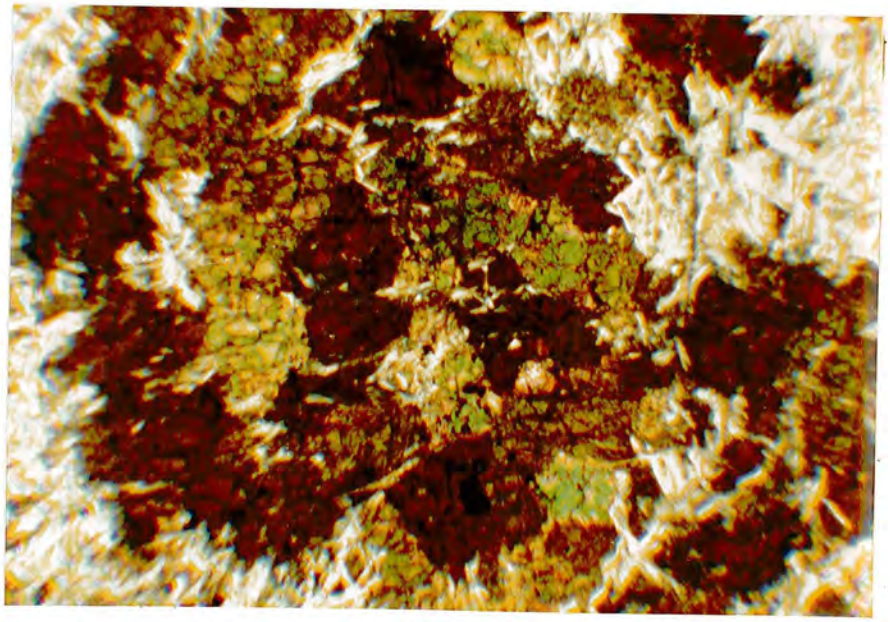

Plate 6.1 Photomicrograph: A mosaic of small non cored metamorphic olivine crystals, in Sample 61637. Note the tectonic fabric, and the feathers of antigorite, (white), Crossed polars. Field width 1.7mm.

not induce strain in the crystal lattice.

In the extreme northeast corner of the map area, orthopyroxene is stable within 300 m of the batholith contact, Figure 5.10. Above the orthopyroxene (enstatite (3)) isograd, olivine is coarser grained, up to 2.0 mm in diameter, Sample 60215, and homogeneous. There is little or no evidence for core formation. The polygonal olivine mosaic has been more or less exploited by retrogressive serpentine, (Plate 5.30), Samples 60213, 60215, although the coexisting enstatite seems to remain stable. During retrogression black spinel, ferritchromit, has partially altered to magnetite and small cubes of green spinel (Plate 7.7). Al serpentine has altered to chlorite, Samples 60213, 60215, 61603, and talc has largely been removed.

Enstatite (3) distribution is very restricted, and none was observed in Unit (3c). The enstatite occurs as single crystals, and as clusters up to 5.0 mm in diameter. Crystal outlines are irregular, and some crystals, although fresh, display wavey extinction. Many crystals appear to pseudomorph bastite, in which magnetite was deposited parallel to what were the original lamellae, similar to bastites in Samples 60041 and 60094, (Plate 4.2). The new pyroxene thus replaces the old, (Plate 5.31), and the bastite was not converted to Al serpentine.

Plate 5.30 Photomicrograph: A large metamorphic enstatite, (grey), in a mosaic of non-cored olivine (3). Note the minor reserpentinization of olivine, and traces of fibrous tremolite. Sample 61603. Crossed polars. Field width 1.7mm

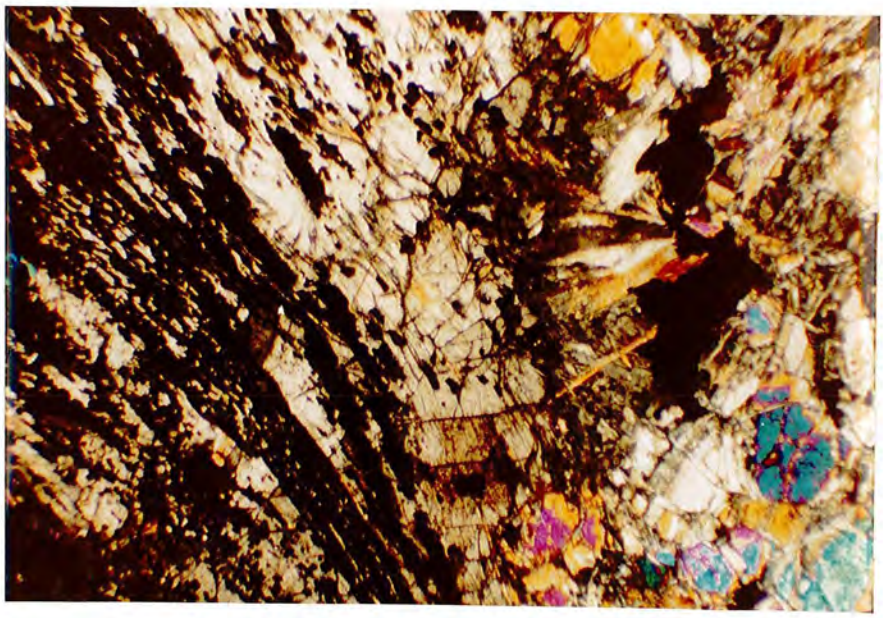

Plate 5.31 Photomicrograph: Similar to 5.30, note the magnetite deposited in enstatite, and the large size of the crystal. Sample 61603. Crossed polars. Field width 1.7mm.

Enstatite was probably formed according to reaction (14), Table 5.4, as described by Bowen and Tuttle (1949).

(14) Talc + olivine (3) $\rightleftharpoons$ En(3) + H_2O

Possibly olivine pseudomorphs after bastite were subsequently converted back into enstatite (3) according to the above reaction, suggesting that regeneration near the granite predated oxidation of the spinel.

Tremolite is found in the assemblage, much as it occurs below the enstatite isograd, overprinted as laths and needles on the olivine (3) matrix. There is no evidence for anthophyllite and hornblende formation according to reaction (13), although reaction (14) might suggest a temperature in excess of 600 ^{o}C at 1-2 Kbar P_{H_2O}, Bowen and Tuttle (1949). Recrystallized talc and chlorite occur in Samples 60199 and the ex-dunite Sample 60218, although whether by a prograde reaction, or a retrograde reaction is uncertain.

The formation of enstatite is not attributed to the chlorite break-down reaction established by Fawcett and Yoder (1966), reaction (15), inspite of the presence of traces of green spinel.

(15) FeMg chlorite = olivine + enstatite + spinel.

This reaction would require a temperature in excess of 700°C, at a pressure of above 3.5 Kbars P_{H_2O}. At lower pressures cordierite should form. The unrealistic P-T conditions, and the modal proportions of the phases make this reaction unsuitable.

CHAPTER 6: METAMORPHIC MINERALOGY

6.1 Mineral Chemistry

Regenerated olivine Unit (3a)

The electron microprobe analyses given in Table 6.1 and illustrated in Figures 6.1,6.7, indicate the compositional range found within this metamorphic olivine population as a whole, and also within individual analysed samples.

The population has a variable Mgx100/(Mg+Fe) ratio, as defined by the forsterite content, and Mn is seen to increase sharply with increase in Fe.

The physical core to margin zonation observed for these olivines is reflected by a pronounced chemical zonation. Turbid olivine cores are enriched in Fe and Mn, and the clear outer margins are Mg rich, with local enrichment of Ni.

Simpkin and Smith (1970) have documented a trend towards Mn enrichment with Fe, and Ni increase with Mg, in "igneous olivines", Figure 6.1. & 6.2. Although olivine (1) adheres to the trend pattern, olivine (3) evidently does not. In particular the trend towards Mn enrichment is far faster and greater than is anticipated in igneous olivines. The anomalous trend is chemical support for a metamorphic origin. In addition the zonation is from an Fe rich core to a Mg rich margin, which is counter to most olivine

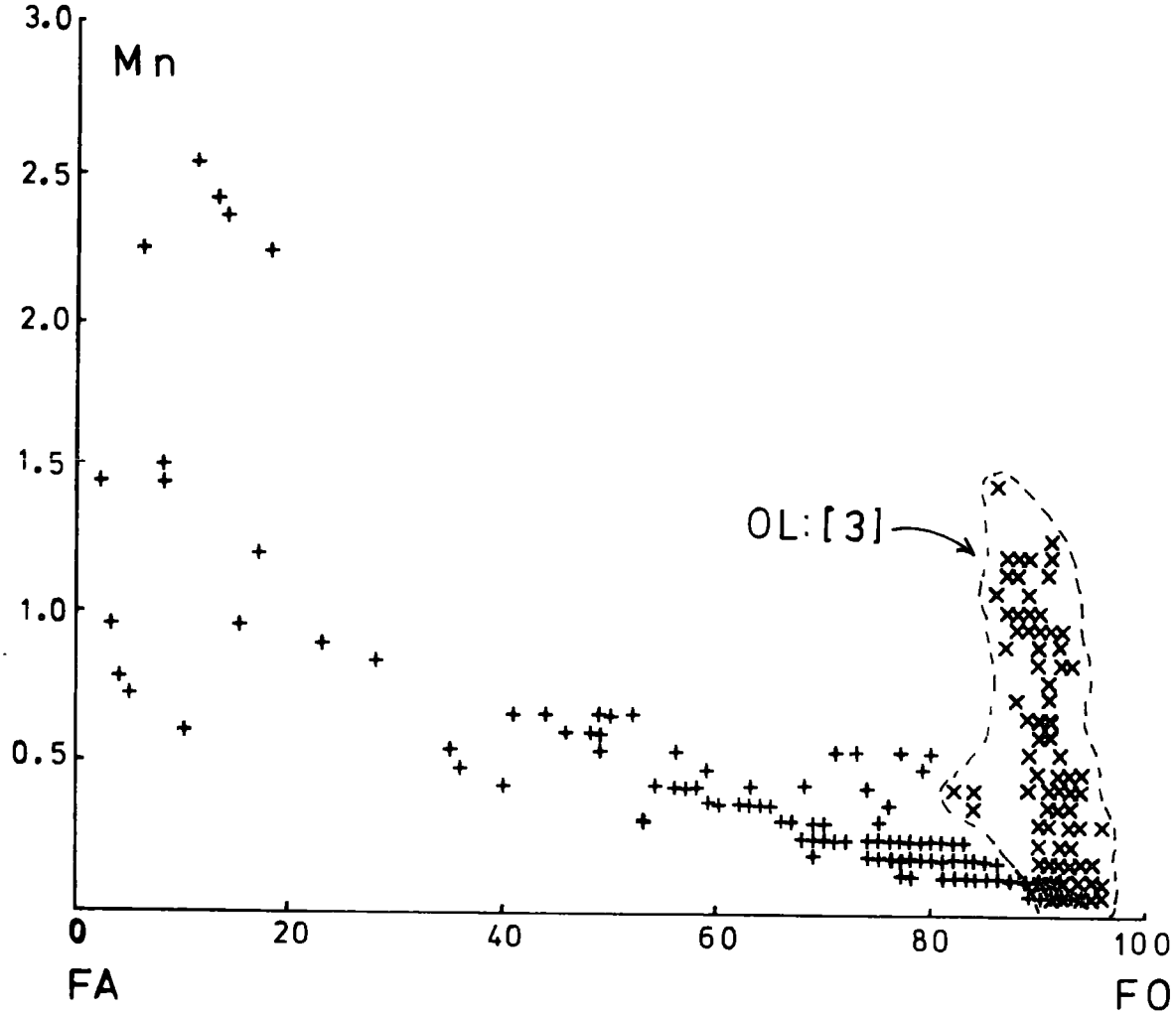

Figure 6.1 Mn variation with olivine-forsterite content. Metamorphic olivines from the Blue River (denoted as (X)), are plotted with igneous olivines from Simpkin and Smith (1970). These are denoted as (+).

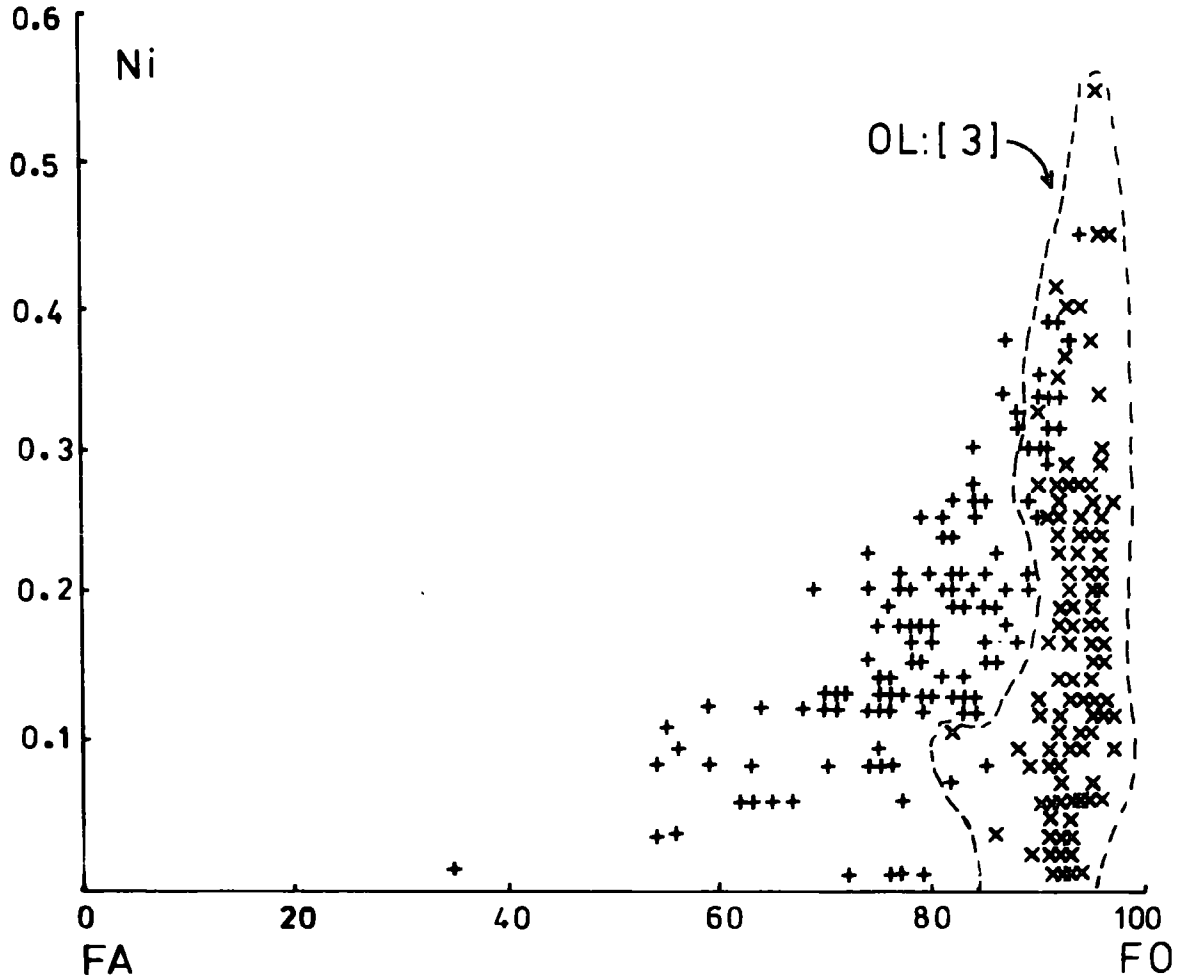

Figure 6.2 Ni variation with olivine forsterite content. Metamorphic olivines from the Blue River, (denoted as (X)), are plotted with igneous olivines given by Simpkin and Smith (1970). These are denoted as (+).

zonation in igneous rocks, which relates to cooling of the rock. In a metamorphic environment the reverse is true, and prograde metamorphism is concerned with heating.

There is a strong correlation between the intensity of the core turbidity and the degree of chemical zonation. Sample 60157, (Plate 5.20), shows a maximum range in forsterite content from Fo_{85}-Fo_{97}, and others such as Samples 60035, and 60171 cover a similar range. Figure 6.3 shows the range of forsterite content found in each analysed sample. Most appear to straddle the mean olivine (1) compositional value of Fo_{91}, but a few are either depleted or enriched in Fe relative to this composition. Sample 60109, (Fo_{94}), is infact the only analysed sample that gives consistently high values, relative to the original olivine (1) value of Fo_{91}. This sample is weakly cored, it contains recognisable magnetite dust, and thoroughly altered spinels. These spinels have evidently taken up excess Fe and Mn, depleting the silicate system, Table 6.9. Secondary spinels, ferrit-chromit, analyses illustrate this point. Perhaps significantly the sample lies close to the talc isograd, as its chemical characteristics are similar to that of the Unit (3b) olivine population.

In contrast, Samples 60067, 60021, and 61637 appear to be enriched in Fe, as no olivine above Fo_{89} has been detected. In the case of Sample 60021, preferential

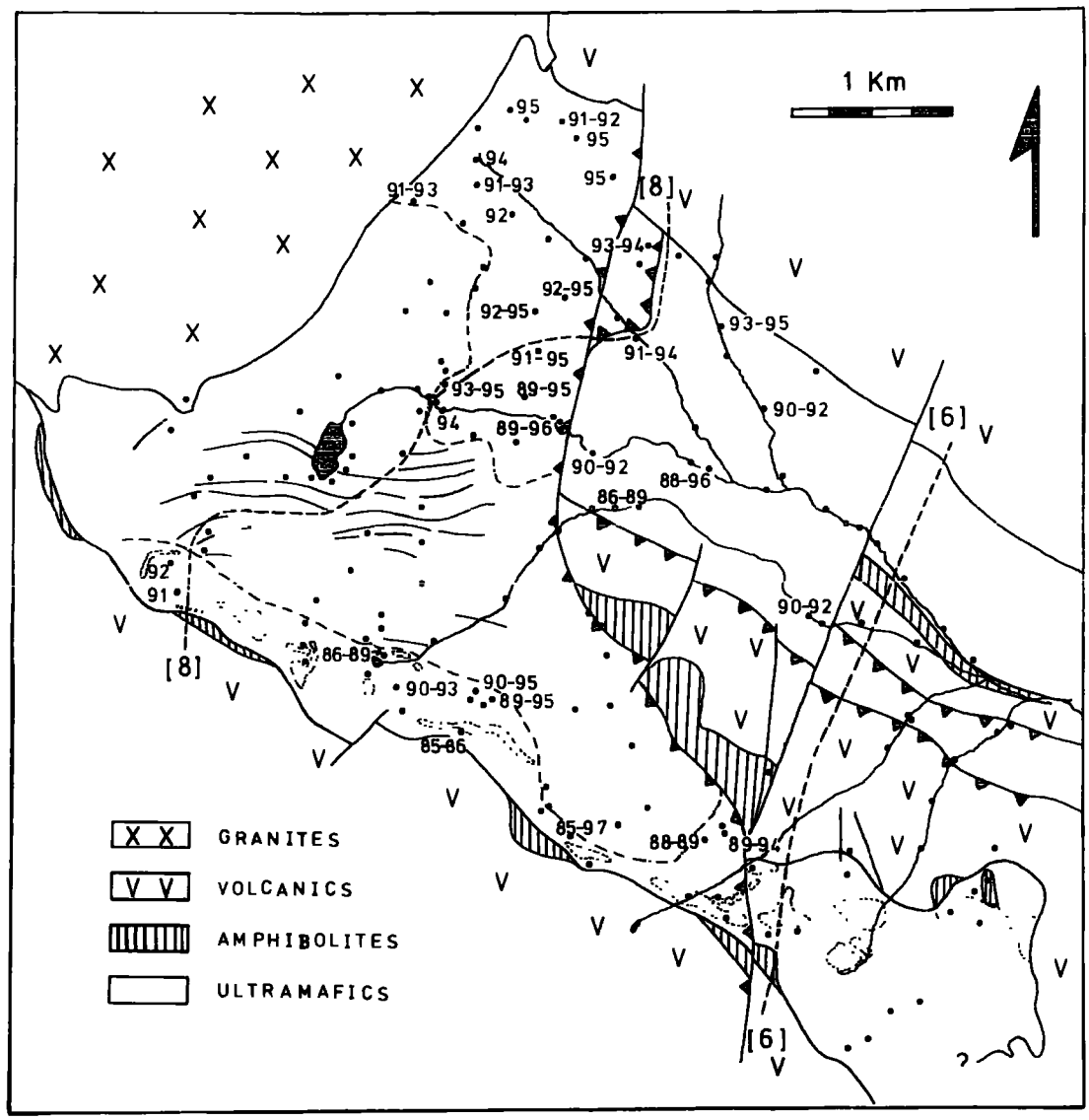

Figure 6.3 Olivine (3) forsterite ranges across the intrusive.

serpentinization and alteration has probably removed all the Mg rich end member olivine, as cores appear to be surrounded by a pronounced serpentine reaction halo. Metamorphism perhaps did not go so far, and produce so much Mg rich olivine, or that produced has been removed. Table 6.1, Samples 60021 and 61577 are similar in their olivine chemistry, only in the latter, remnants of Mg rich olivine remain.

This argument cannot apply to Samples 60067 and 61637. Sample 61637 consists of a large area of olivine (3) in the form of a complete polygonal mosaic. Some has been retrogressively altered to serpentine, (antigorite), but the texture of the rock, (Plate 6.1), suggests a large area of homogeneous Fe and Mn enriched olivine. There is no core formation, and the mosaic has a very strong foliation across it. This fabric, and the close proximity to a major lithologic contact, suggests recrystallization of a schistose serpentinite, depleted in Mg relative to Fe and Mn. Similarly Sample 60867, a serpentinite breccia, contains mosaic fragments similar to those in Sample 61637. These areas of Fe and Mn olivine mosaic are set in serpentine within which a second generation of olivine (3), the marginal Mg rich variety, is nucleating. Presumably serpentine depleted in Mg formed early Fe Mn rich olivine, which got caught up in a breccia of less Mg depleted

serpentine. This later nucleated Mg rich olivine. This suggests a strong correlation between composition, time, and temperature.

Similarly, in Sample 60067, a relatively homogeneous mosaic of Fe Mn enriched olivine was formed throughout the rock. In this case the original sample was unquestionably harzburgite. The absence of Mg again correlates with an area of tectonic activity, below the Heazlewood thrust. Removal of Mg, presumably as brucite or carbonate, is favoured over enrichment of Fe and Mn, as both retain a similar level to that reached in "normal" cored olivine . Similarly the retention of bastite outlines in Sample 60067 argues against mobility of appreciable Si.

As noted, bastite pseudomorphs in Unit (1) show partial alteration to olivine (3). In Sample 60153, this leads to the formation of markedly Fe enriched olivines, Table 6.2. The composition is slightly anomalous, even for Mn enriched olivines, as the Mn:Fe ratio is wrong, Figure 6.1. Being set in relatively unaltered peridotite, Mg was probably able to deplete, without the opportunity for Mn to enrich.

Core to margin zonation in Sample 60157 appears to be representative, and the evidence suggests simple alteration of composition with time. No oscillations or composition breaks were detected in the samples analysed, although granulation and reserpentinization has upset the spatial

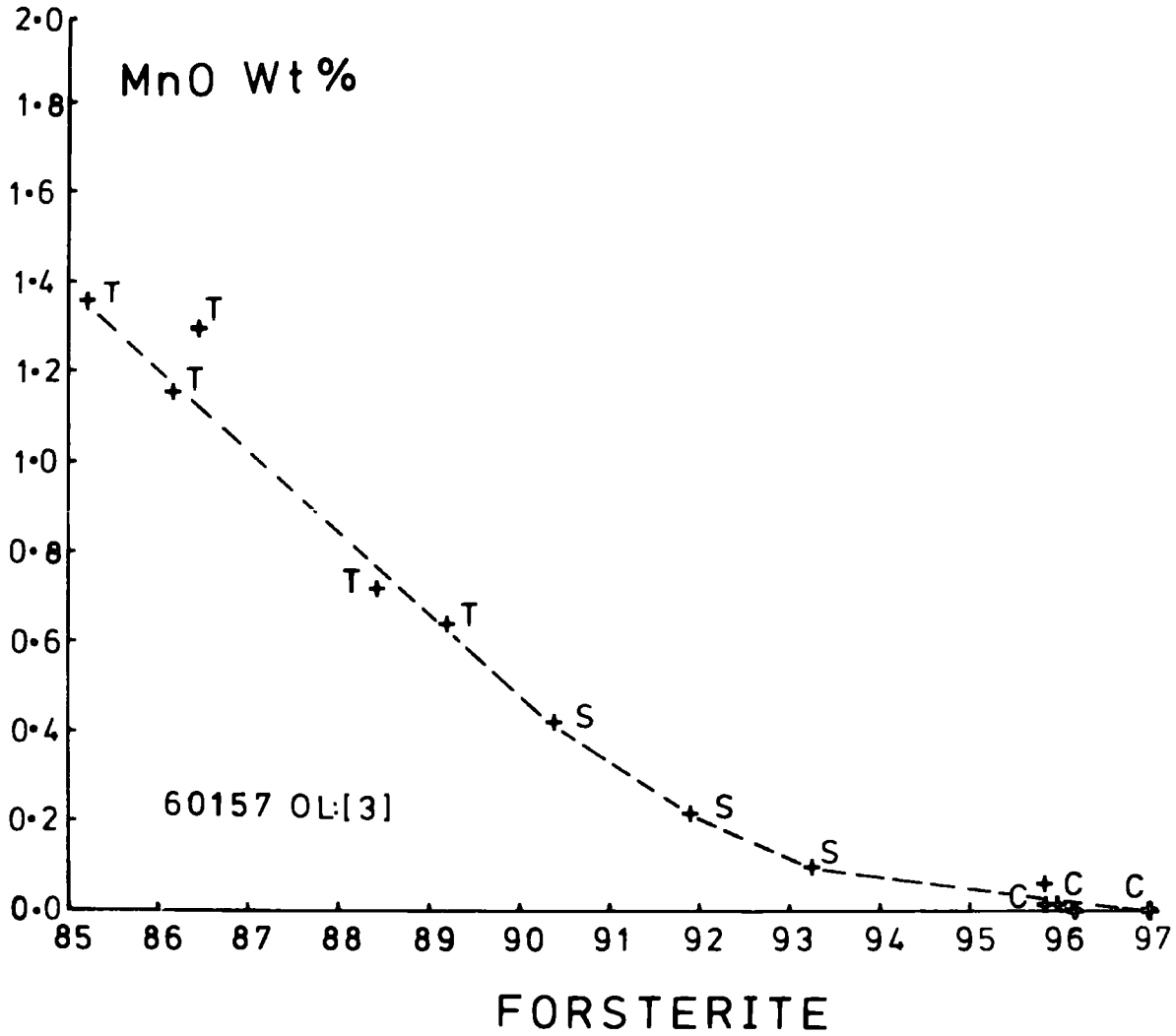

Figure 6.4 MnO variation with olivine (3) forsterite content, in Sample 60157. The MnO content depletes from an inner, turbid, "core" region(T), through "marginal" olivine,(C). Data from a number of spot analyses made on several crystals, Table 6.1.

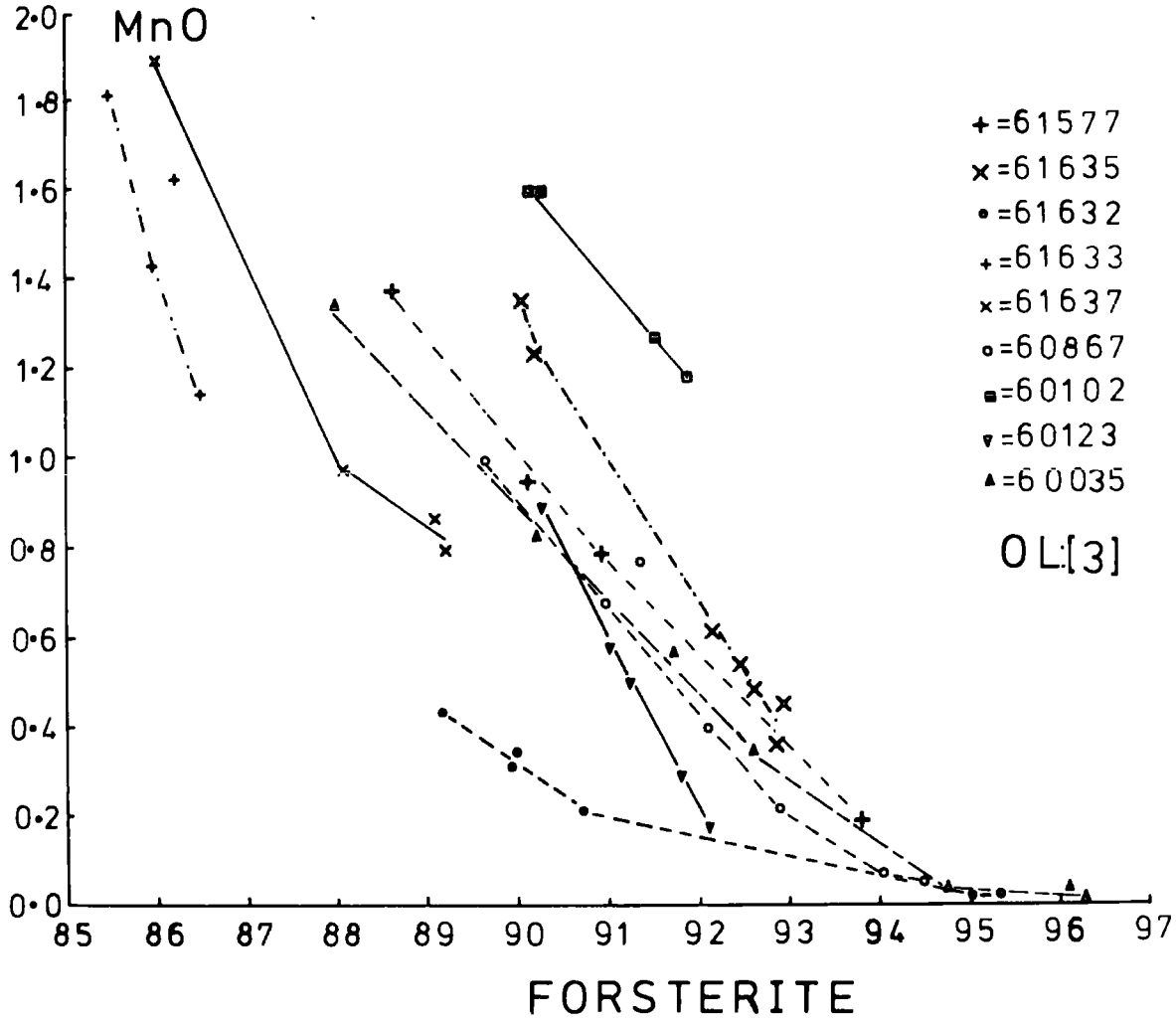

Figure 6.5 MnO variation with olivine (3) forsterite content. MnO depletion, from "core" to "margin", is shown for a number of zoned metamorphic olivines located in Unit (3a). Analytical data is shown in Table 6.1.

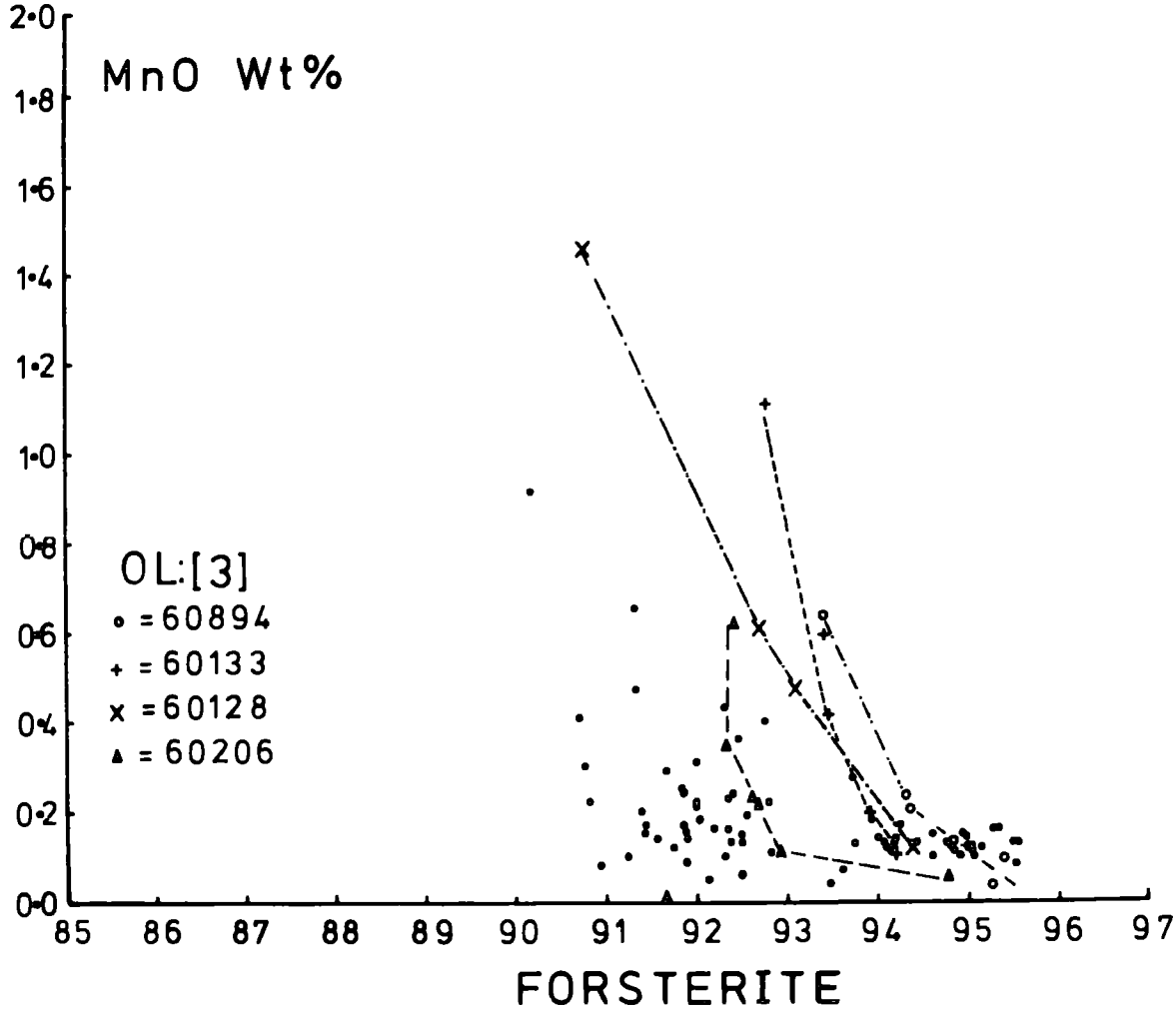

Figure 6.6 MnO variation with olivine (3) forsterite content. Strongly zoned olivines in Unit (3b) have been differentiated, and weakly or non zoned olivines are shown as closed circles.

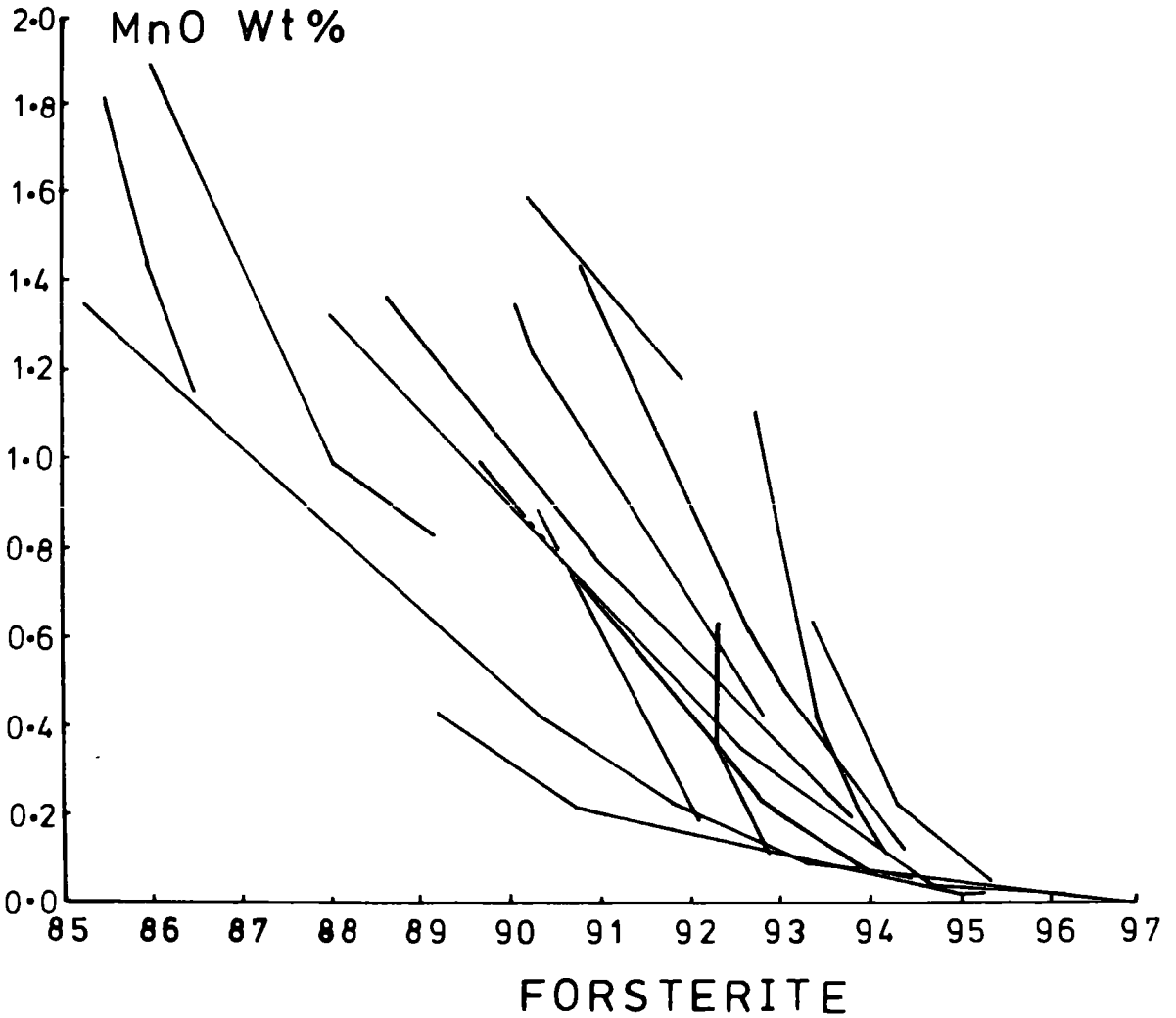

Figure 6.7 MnO variation with olivine (3) forsterite content. Composite diagram, taken from Figures 6.4, 6.5, 6.6. The figure illustrates the wide range in olivine (3) "core" composition, and the restricted range in "marginal" olivine composition.

relationships, and makes this difficult to prove.

In Figure 6.4 the MnO percentage is plotted against forsterite content. It is apparent that Sample 60157 has a uniform Mn depletion gradient, and that turbid cores have a high MnO content. The semi-turbid core region extends from Fo_{90} - Fo_{93}, and passes from the region of Mn enrichment into the region of Mn depletion, based on an average olivine (1) MnO value of 0.13 % MnO. At values of Fo_{96} and above, Mn is effectively absent. This simple relationship is found in other analysed samples, Figures 6.4 to 6.6. The data shows that within any given sample the gradient gives a remarkably even slope, but that the depletion gradient is variable from sample to sample. Figure 6.7 shows the various depletion gradients plotted together. It is apparent that high values of MnO correlate with a variable forsterite content, and in two extremes, 1.0% MnO occurs in Fo_{87}, Sample 60157, and Fo_{93}, Sample 60133. In each case the final, marginal type, olivine falls within a relatively restricted compositional field, and the important variable is not the amount of MnO in the system, but the amount of Fe, as reflected in the forsterite content. The initial core composition must depend on the bulk rock composition, at the time of initiation of reaction (6), and the oxygen fugacity, temperature and pressure will influence the trend thereafter, to marginal type olivine.

Removal of Fe through substitution in the ferritchromit lattice will influence the gradient, and cause a steepening of the slope. Significantly Samples 60133 and 60206, which lie close to the talc isograd, both have steep slopes. The important factors therefore, are initial availability of Fe, and the degree of oxidation.

Ni is not found in the Mn rich olivine core, but it does occur in variable amounts in the outer margin. Sample 60157, in particular, contains up to 0.67% NiO. Similarly marginal olivine in Sample 61632 contains 0.57% NiO. In spite of substantial Mg enrichment some samples contain no Ni in their outer marginal olivine, as in Samples 60867, 61635. Those that do contain traces, Samples 60035, 60171, 60102, contain little more than is found in olivine (1). There is little evidence for Ni concentration. The distribution of Ni-sulphide in Figure 6.8 shows that it tends to be concentrated in Unit (3a), and there is a strong negative correlation between availability of sulphur, and concentration of Ni in olivine margins. Sample 60157, and Sample 61632 contain no significant sulphide, whereas Sample 60867 is considerably enriched in sulphide. This suggests that Ni is not easily reincorporated into the olivine structure, and that it has a stronger affinity for sulphur, where present.

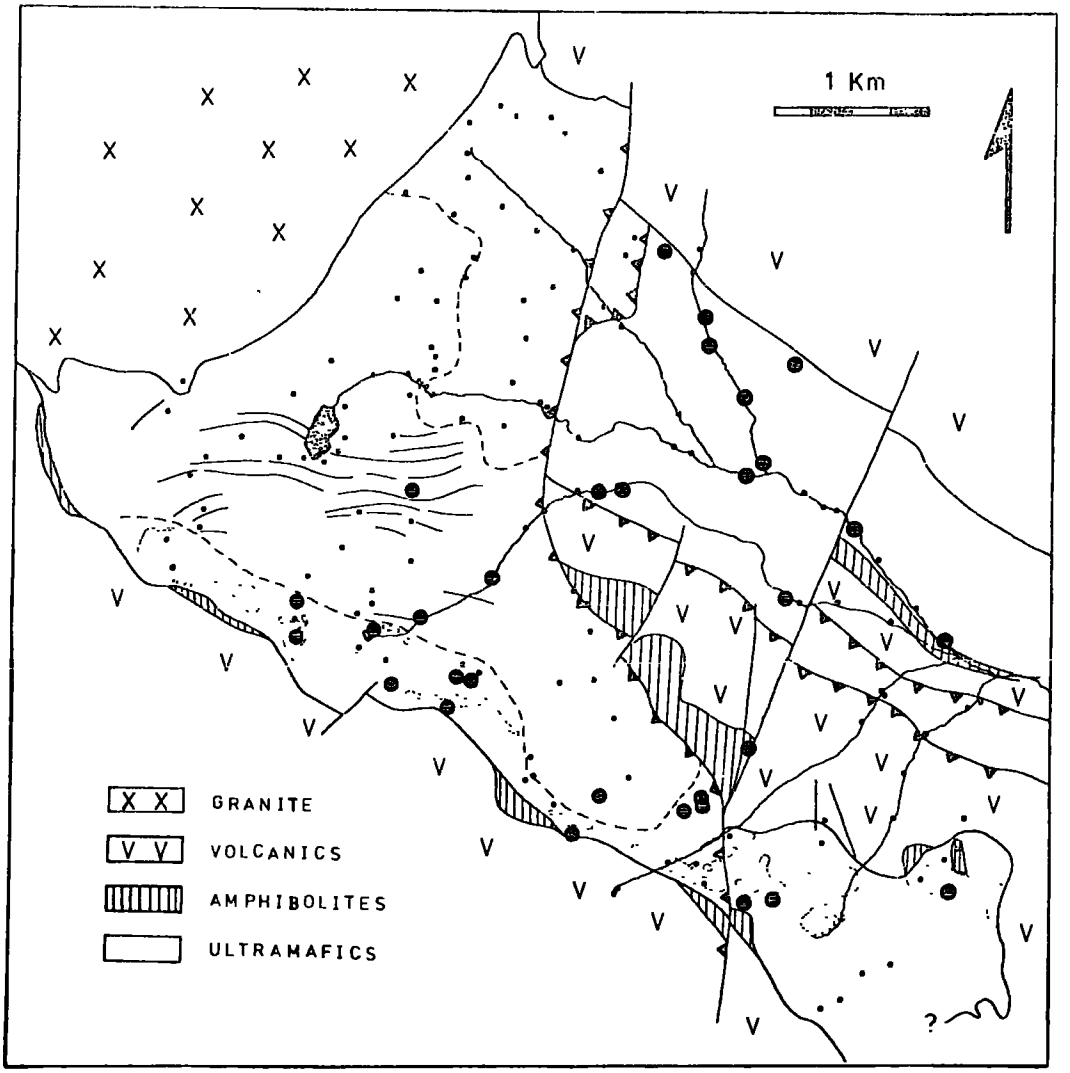

Figure 6.8 Distribution of samples containing a significant trace of sulphide.

Figures 6.9(a) and (b) show point sections across one, single, cored crystal of olivine (3), from Sample 60894. Although above the talc isograd, this sample has close affinities with those below, (Plate 5.27). The sections show the marked depletion of Ni in the inner core region of the olivine, and its early enrichment during the first stage of marginal olivine development. The same crystal shows a gradual but progressive Mn enrichment from margin to core, much as discussed earlier.

Metamorphic olivine analyses, given by Frost (1973), fall within the forsterite range Fo_{90}-Fo_{94}, with most around Fo_{91}. They indicate a variable, but significant trace of Ni, up to 0.47% NiO, and a generally low MnO content, up to 0.18% MnO. One exception however, contains 0.95% MnO at $Fo_{94.9}$.

Springer (1974) indicates a forsterite range of Fo_{89-97}, based on partial analyses of metamorphic olivines from the aureole of the Pine Hill intrusive. He also records MnO values of up to 0.3%.

Regenerated olivine (Unit (3b))

Above the talc isograd regenerated olivine is either Fo_{90} or above. The core to margin zonation is less evident physically, and also chemically. Samples close to the talc isograd do show some Mg enrichment, from Fo_{92}-Fo_{95} in

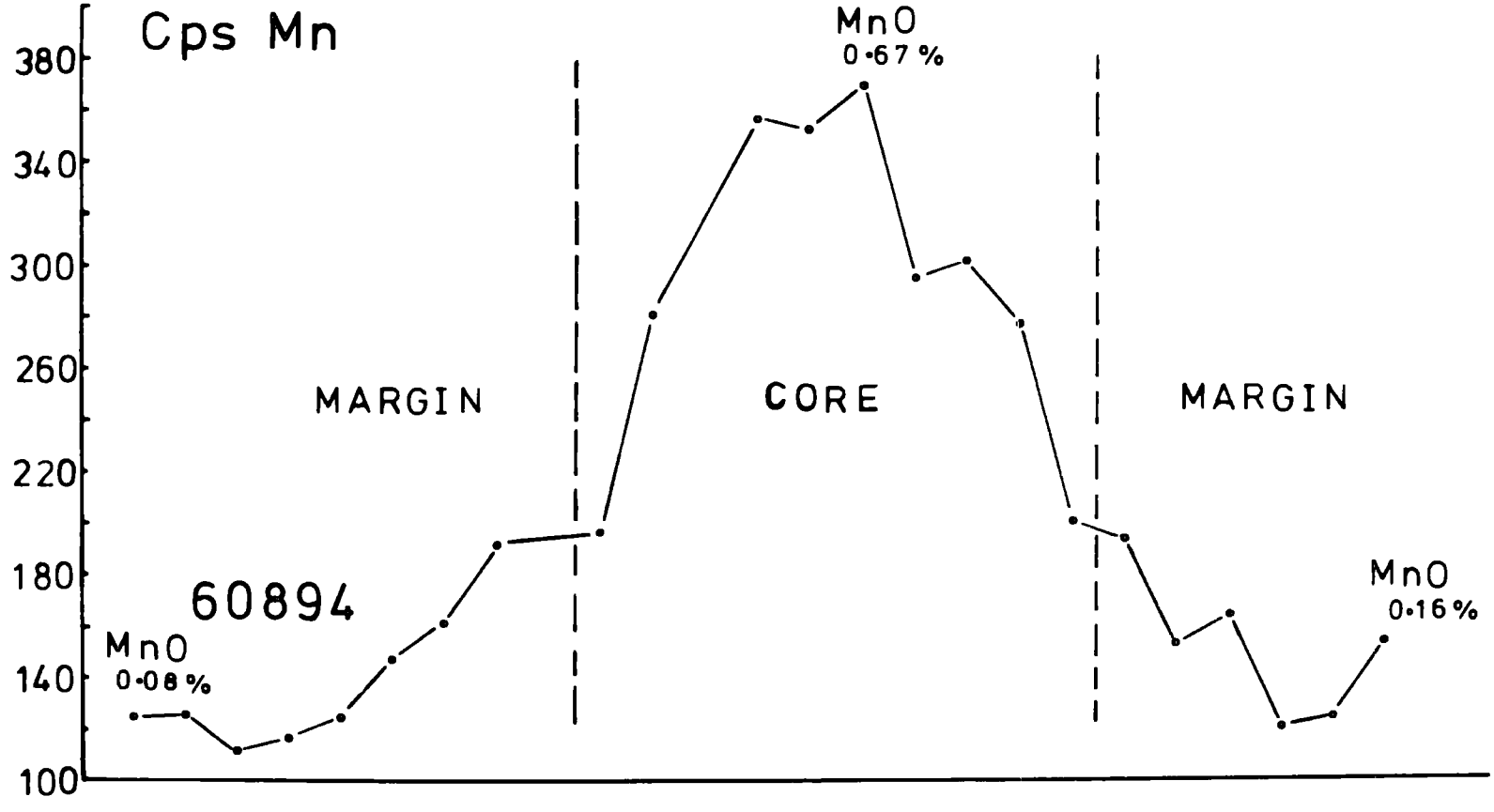

Figure 6.9(a) Mn variation across a single, zoned, olivine crystal in Sample 60894. Spot analyses, as counts per second, and weight percent MnO, are given for spaced points across a crystal of width 1.0 mm.

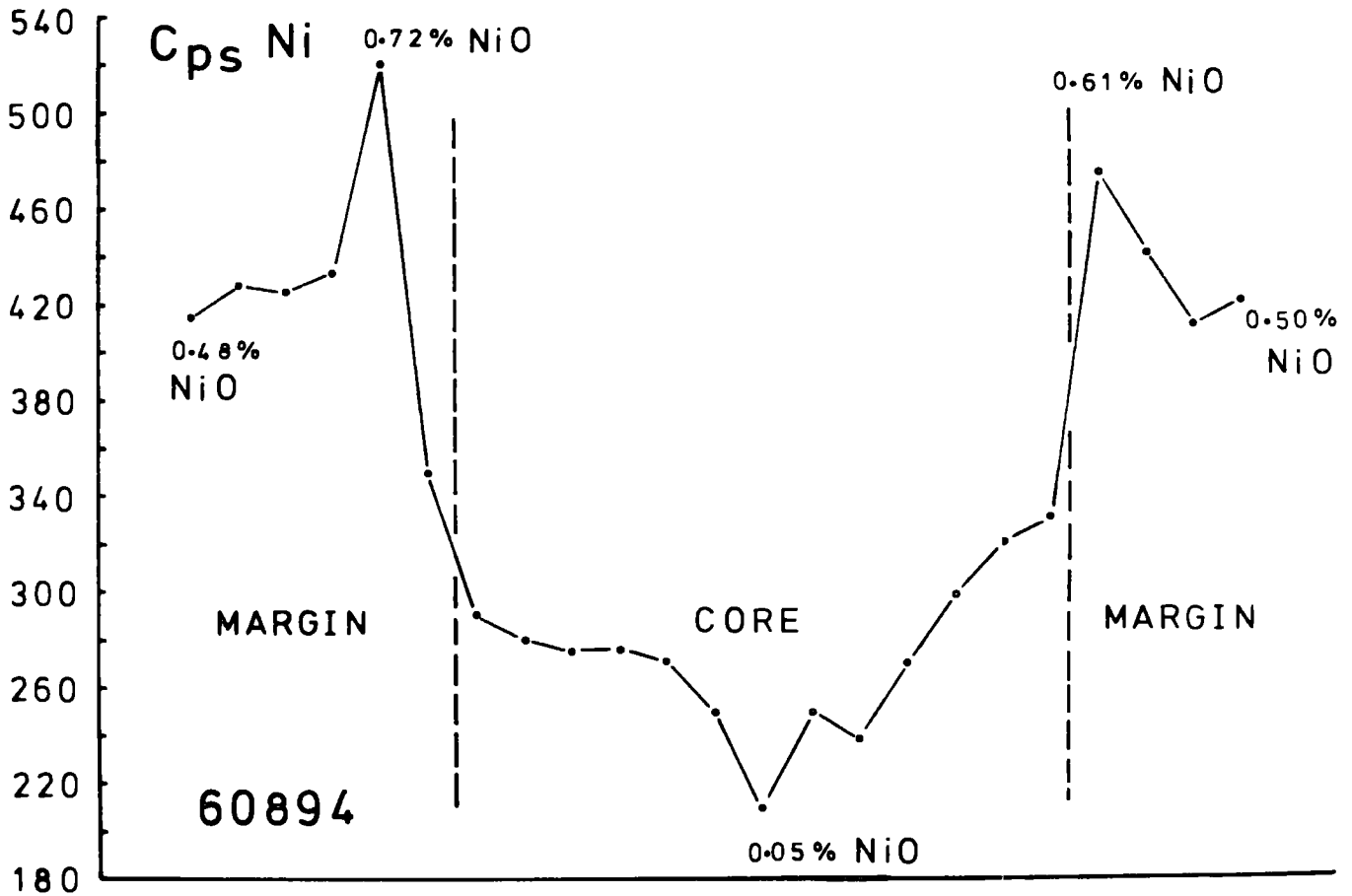

Figure 6.9(b) Ni variation across a single, zoned, olivine crystal in Sample 60894. Spot analyses, as counts per second, and weight percent NiO. The section is that shown in 6.9(a).

Samples 60206 and 60209. The amount of Mn enrichment is very small, and the distribution is far less regular, Table 6.3. The amount of Ni present in the rock is however significant, although again scattered. In neither case is sulphide present, and there is no evidence for Ni loss. Figure 6.10 shows a NiO histogram for Unit (3b) olivines, compared with Unit (3a) zoned olivines. Figure 6.11 shows a comparable MnO plot.

There appears to be a tendency for these olivines to attain a uniform composition, and a maximum value of Fo_{95} is found north of Nickel Creek, in Samples 60213, 61598, and 60137. This value is similar to that found in the outer margin of zoned Unit (3a) olivines, and the bulk of the talc isograd olivines would plot close to the cluster point on an MnO v Fo plot.

There would appear to be a trend towards Mg enrichment along the northeast contact of the body, and straight temperature control is unlikely. Once again the availability of Fe is crucial, and some Fe has to be removed to attain these values. Thus the Fo content correlates with degree of spinel oxidation, and modal percent ferritchromit. This feature is borne out in the succeeding sections, where it is shown that not only Fe, but Mn and Ni are also absorbed as divalent cations into the ferritchromit structure.

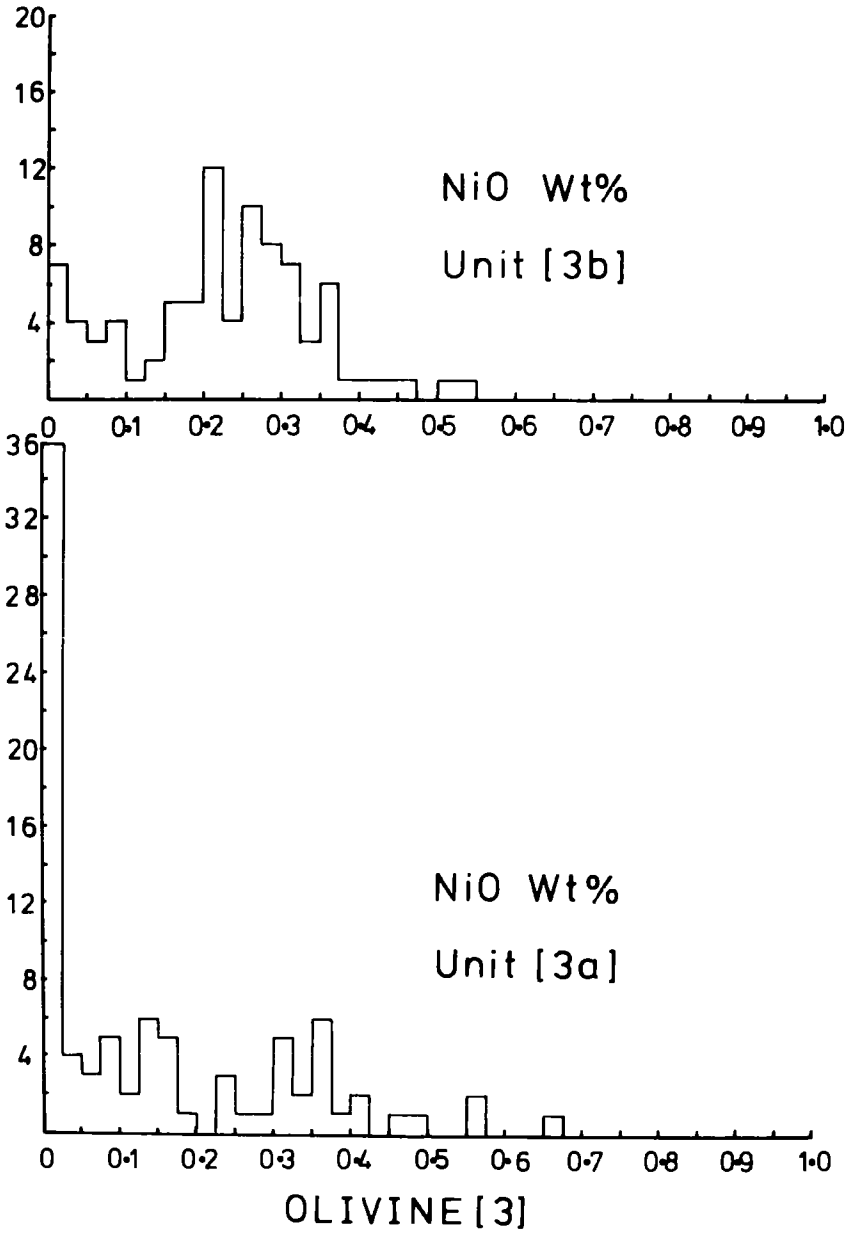

Figure 6.10 A frequency distribution plot, showing the NiO content of olivine (3) in Units (3a) and (3b).

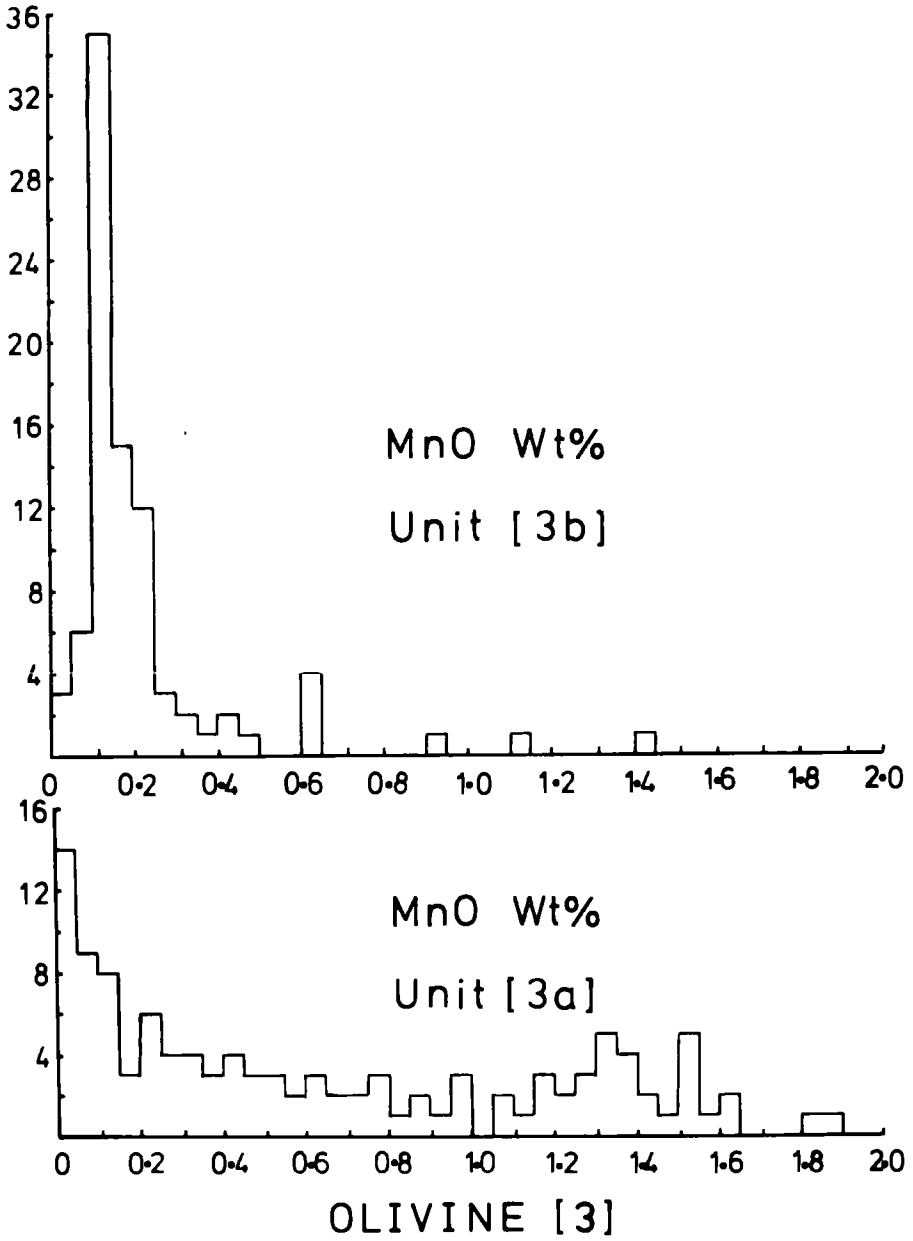

Figure 6.11 A frequency distribution plot, showing the MnO content of olivine (3) in Units (3a), and (3b).

In contrast, regenerated olivine pseudomorphing bastite in Unit (3c), Samples 60174 and 60186,is not dissimilar to primary host olivine. They are approximately Fo_{90}-Fo_{91}, Table 6.2, although they tend to be depleted in Ni, reflecting the initial host pyroxene chemistry. This is unlike the neighbouring olivine (1). Pseudomorphs in Samples 60179 and 60180 are from within regenerated dunite, and as such they are similar to "normal" regenerated material in those samples.

Oxidation of spinel above the talc isograd has evidently altered the Fe, Mg, Ni, Mn, distribution pattern, and consequently compositions are slightly erratic.

Enstatite (3)

Metamorphic enstatite analyses, Table 6.4, show that the regenerated phase is significantly different from the primary enstatite (1) phase,in terms of composition. The metamorphic mineral is depleted in Al_2O_3, Cr_2O_3, FeO and CaO, and it is enriched in MgO and SiO_2. The two populations are distinct, and a metamorphic origin is indicated by chemistry as well as texture.

The two analysed samples, Sample 60213 and 61603, give Mgx100/(Mg+Fe) ratios slightly above the coexisting olivine value, Figure 6.12. Ideal 1:1 partitioning of Fe and Mg was nearly attained, and a near equilibrium environment was probably reached.

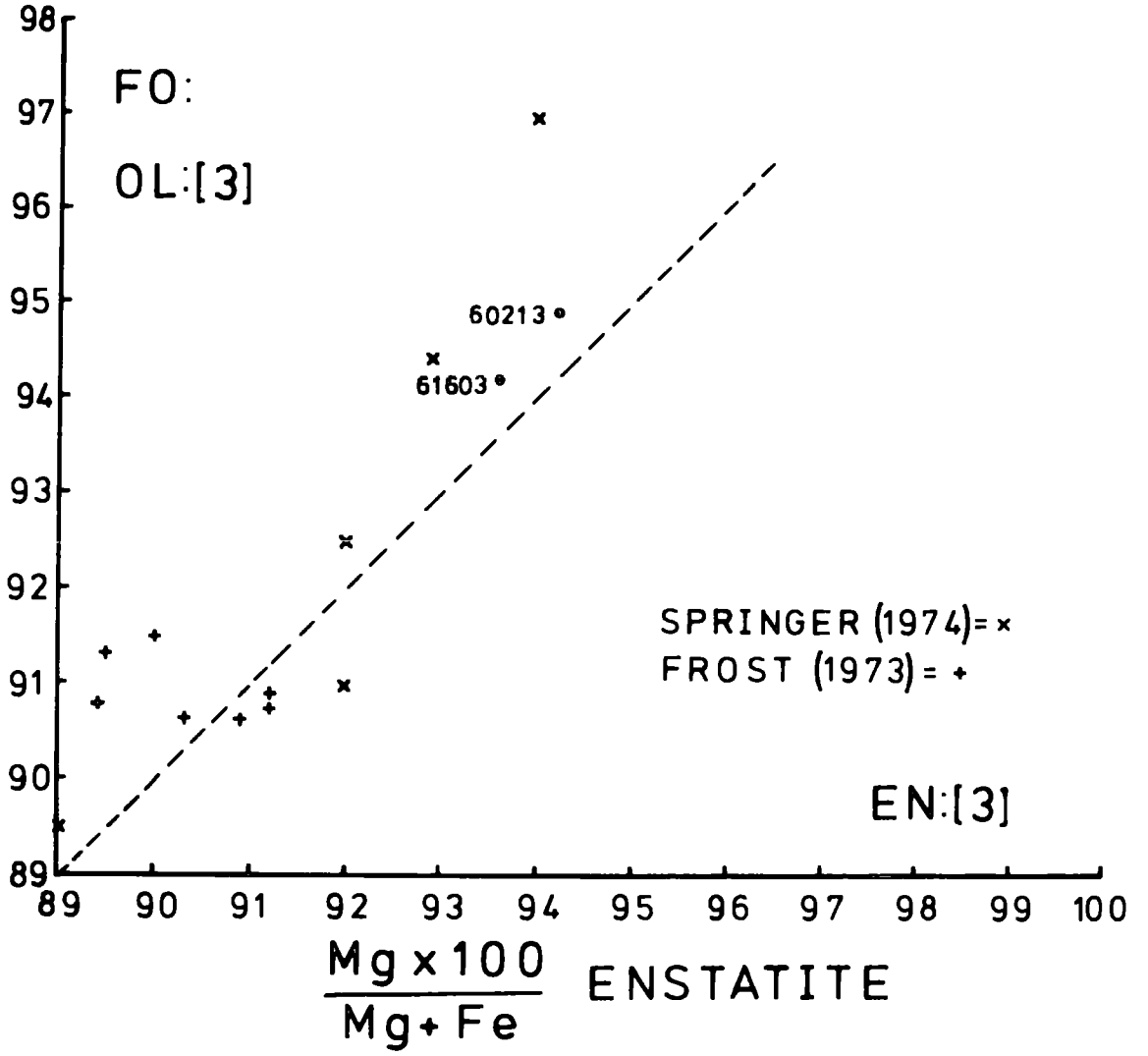

Figure 6.12 Olivine (3) forsterite content plotted against enstatite content in metamorphic enstatite (3). Comparable data from Frost (1973) and Springer (1974) is also shown.

Frost (1973) also gives metamorphic enstatite analyses, and these are plotted on Figure 6.12. They too have attained near equilibrium conditions with coexisting olivine, but they have recrystallized with a near primary Mgx100/(Mg+Fe) ratio. There does not appear to have been the same removal of Fe from the silicate system. Similarly partial analyses by Springer (1974) indicate an enstatite range of En_{89-94}. Figure 6.12. The primary enstatite composition is unknown. Springer also records a very low CaO content, and an Al_2O_3 value of 1.6%. This compares with an average Blue River value of 1.46% Al_2O_3.

Serpentine (Unit (3a))

Metamorphism of a serpentine-brucite assemblage has produced zoned olivine porphyroblasts within a modified serpentine matrix. This foliated matrix serpentine is presumably stable at the level of metamorphism which produces "marginal" olivine (3).

Retrogressive serpentinization has in many cases altered the porphyroblast olivine to a serpentine-brucite assemblage, but the two serpentines are texturally quite distinct. It is not known whether the chemistry of the matrix serpentine was altered during Stage IV, but crystallographically it has remained unaltered.

Matrix serpentine analyses, from Samples 60021, 60035, 60102 and 61632, are given in Table 6.5. An average value

along with data for other serpentine types, is given in Table 6.6. This Table includes an analysis of chrysotile cross-fibre asbestos from the Cassiar Asbestos Mine. This closely resembles matrix serpentine from Samples 60021 and 60102. Both are very reduced in FeO, and have approximately equal parts SiO_2 and MgO. Samples 60035 and 61632 contain significant traces of Al_2O_3 and Cr_2O_3. These are incompatable elements in the olivine structure, and they would be expected to concentrate in the serpentine. The amount of oxidation of the spinel is important in this regard, as is the amount of regeneration. Presumably with modal decrease in serpentine, the incompatable elements will concentrate in the lattice.

Above the antigorite isograd, it is difficult to differentiate between recrystallized matrix serpentine, (above), and antigorite derived from olivine. In a few samples it is possible. Samples 61623, 61625, 60206, and 61635(?) contain "antigorite" largely formed at the expense of matrix serpentine, as indicated by rock textures. These analyses are presented in Table 6.7. These "antigorites" contain appreciable Al_2O_3 and Cr_2O_3 in solid solution, and Sample 61525 contains over 4.0% Al_2O_3.

'TABLE 6.6 SERPENTINE ANALYSES'

	1	2	3	4	5	6	7
	'A'	'B'	'C'	'D'	'E'	'F'	'G'
OXIDE WEIGHT PERCENTAGE							
SIO2	40.71	36.15	42.61	42.24	41.02	41.53	42.14
TIO2	0.02	0.01	-	-	-	-	-
AL2O3	0.33	0.08	1.97	0.48	-	-	1.64
FEO	1.55	2.98	3.56	1.39	4.11	1.27	4.78
MNO	0.03	0.01	0.04	0.05	-	-	-
MGO	40.38	41.45	39.95	41.88	39.44	40.93	38.37
CAO	0.04	0.04	-	-	-	-	-
CR2O3	0.37	0.05	0.25	0.16	0.20	0.01	0.20
NIO	0.13	0.24	0.18	0.17	0.11	0.04	0.15
TOTAL	83.56	81.01	88.56	86.37	84.88	83.78	87.28
ATOMIC PROPORTIONS ON THE BASIS OF 28 OXYGENS							
SI	7.907	7.384	7.863	7.921	7.941	8.008	7.931
TI	0.003	0.002	0.000	0.000	0.000	0.000	0.000
AL	0.076	0.019	0.429	0.106	0.000	0.000	0.364
FE2	0.252	0.509	0.549	0.218	0.666	0.205	0.753
MN	0.005	0.002	0.006	0.008	0.000	0.000	0.000
MG	11.688	12.619	10.986	11.704	11.380	11.762	10.763
CA	0.008	0.009	0.000	0.000	0.000	0.000	0.000
CR	0.057	0.008	0.036	0.024	0.031	0.002	0.030
NI	0.020	0.039	0.027	0.026	0.017	0.006	0.023

A = Average modified matrix serpentine, Table 6.5; B = Average serpentine pseudomorph after olivine, Table 7.3; C = Average Malenco Antigorite, Trommsdorff and Evans (1972); D = Cassiar Asbestos, Gabrielse (1963); E = Average lizardite, Page (1968); F = Average chrysotile, Page (1968); G = Average Antigorite, Page (1968).

Al serpentine and chlorite Unit (3b), Unit (3c)

Above the talc isograd Al serpentine and coarsely crystalline chlorite show no sign of conversion to antigorite, and they very often coexist with a 'pure' serpentine derived from Stage IV olivine serpentinization.

Al serpentine and chlorite analyses, Table 6.8, indicate a variable Al_2O_3 content between 10.0% Al_2O_3 in Sample 60133, and 18.0% Al_2O_3 in Sample 61603 The Al_2O_3 content thus increases towards the granite, in both core and marginal units, and it can be contoured crudely parallel to the batholith contact, Figure 6.13. The values thus appear to be related to temperature.

The Al content is divided between tetrahedral and octahedral sites, and the following substitution trend appears to be operative.

$$Al^{IV}\ Al^{VI} = Si\ Mg$$

Al has been allocated to both octahedral and tetrahedral sites,in the following manner. Assuming a correct Si value, and no additional tetrahedral components, Al^{IV} is assigned to the site to complete site occupancy. Excess Al is assigned as Al^{VI} to the octahedral site. The sum of the trivalent cations in octahedral coordination should equal the amount of Al in tetrahedral coordination, in order to balance the charges. The amount of Fe^{3+} is unfortunately

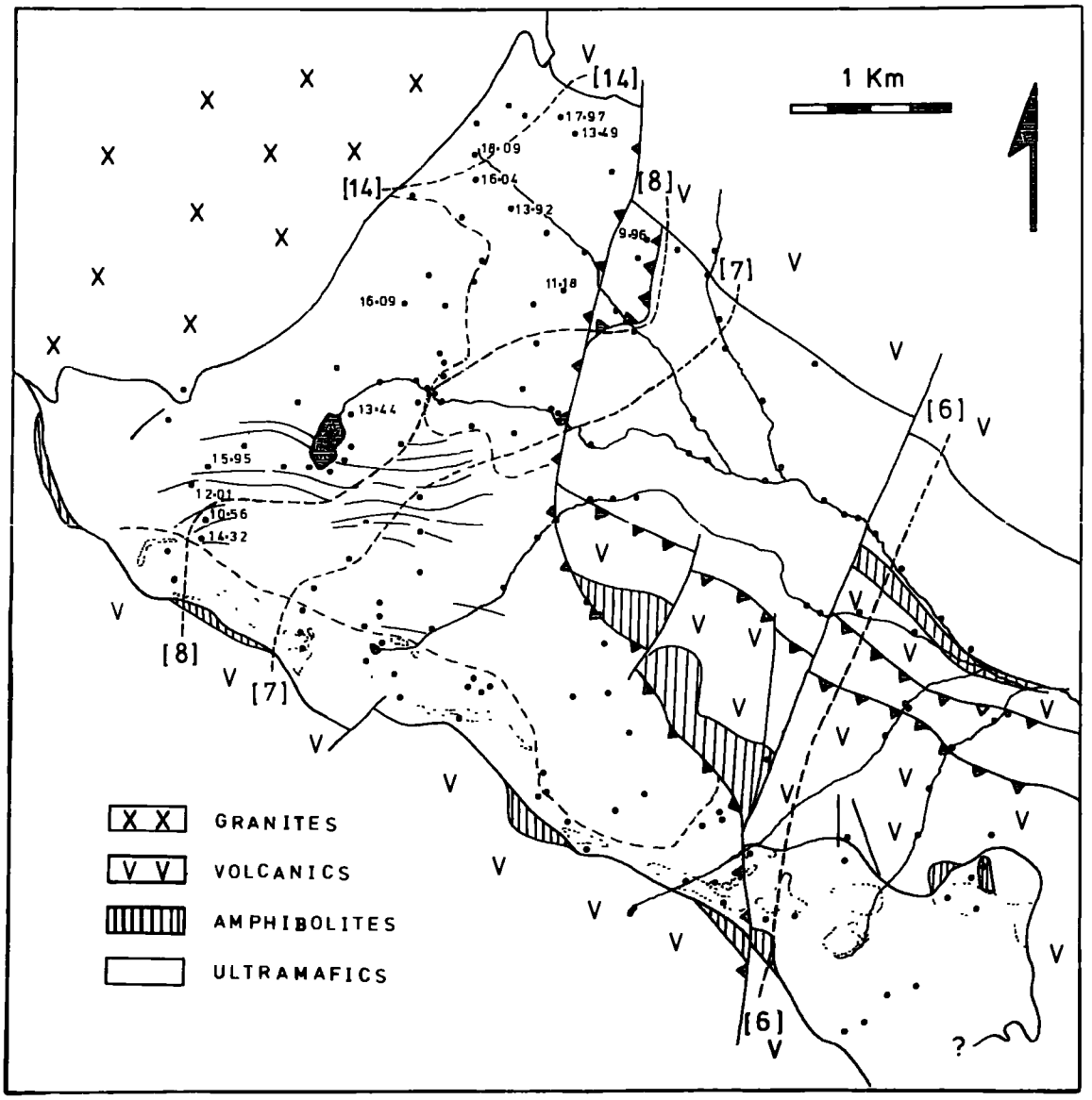

Figure 6.13 Plot of the distribution of the average Al_2O_3 content in Al serpentine and chlorite.

unknown, but there is a close correspondence between the total amount of cations in the two lattice sites, Figure 6.14.

The Al serpentine compositional range falls between the two following end points:

$$Mg_{11}Al([Si_7Al]O_{20})(OH)_{16}$$

$$Mg_{10}Al_2([Si_7Al]O_{20})(OH)_{16}$$

The poorly crystalline Al serpentines appear to be penninite, Deer, Howie, and Zussman (1962), although most of the recrystallized chlorites appear to be clinochlore, with a slightly higher Al content. Also plotted in Figure 6.14 are the matrix Al serpentines from below the isograd, chlorites from the Twin Sisters body. Onyeagochi (1974), and a suite of analyses from Frost (1973). The latter are "chlorites" from the Ingalls Ultramafic Complex in Washington, and are taken from a similar contact meta-peridotite. Frost also noted an increase in Al^{IV} towards the contact, and he considered that the chlorite structure broke down to form spinel, forsterite and enstatite, at the following composition.

$$Mg_{9.6}Al_{2.4}([Si_{5.6}Al_{2.4}]O_{20})(OH)_{16}$$

This level of substitution was not attained at the contact of the Cassiar Batholith, and there is no evidence for this break down reaction.

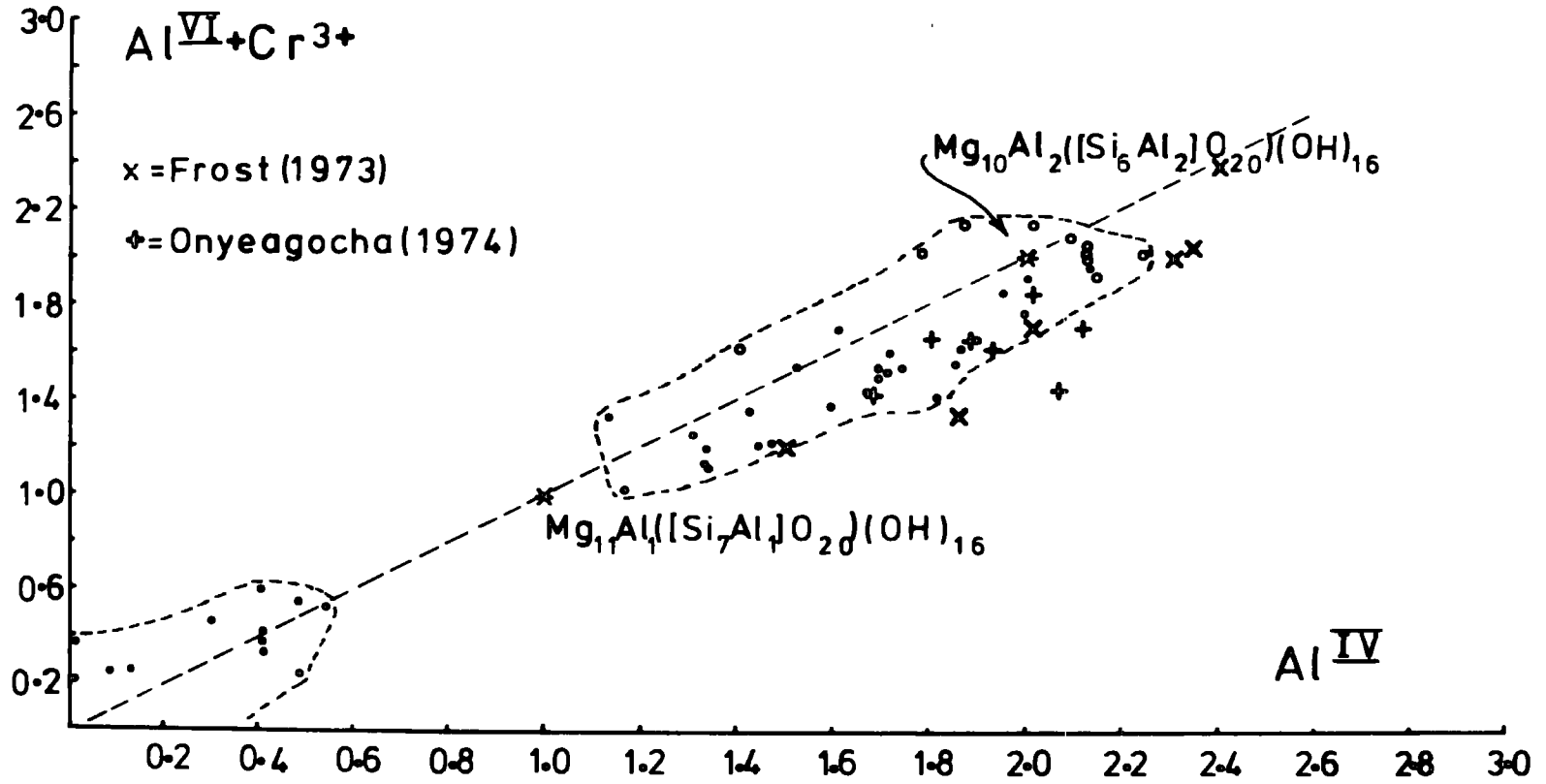

Figure 6.14 The distribution of Al in Al serpentine and chlorite between octahedral, and tetrahedral site. The value for Al^{VI}, (with Cr), compensates for the substitution of Al^{IV} for Si. Closed circles are from poorly crystalline Al serpentine, and open circles are from laths of recrystallized chlorite.

Velde (1973) has shown that Al serpentine is stable over a wide compositional range in the serpentine-amesite system, below 450°C. Below this temperature all the analysed samples could exist with the 7 Å serpentine structure.

Experimental work in the system $MgO-Al_2O_3-SiO_2-H_2O$ suggests that two fields exist above this temperature, one with a serpentine structure, and impure serpentine composition, and the other with a chlorite 14 Å structure, and an Al rich composition. The compositional break at the level of the talc isograd supports this, although conversion to the chlorite structure appears to be sluggish above the isograd. X-ray diffraction data indicates that many samples retain their serpentine structure, until either the higher temperature/Al content regime, near the contact, or the addition of a new serpentine phase aids recrystallization.

If data from the coexisting pairs in Samples 60184, 61598, and 61603, Figure 6.15, gives the minimum Al content allowable in the 14 Å structure, at a given temperature, then Sample 60184 suggests 450°C, and 61603 suggests a contact temperature of 550°C, by extrapolation of Velde's solubility data, Figure 6.16. This assumes no change in the Al_2O_3 content on reserpentinization. In effect the solubility gap increases with grade, and the olivine - "chlorite" - talc field, Figure 6.15, increases in size.

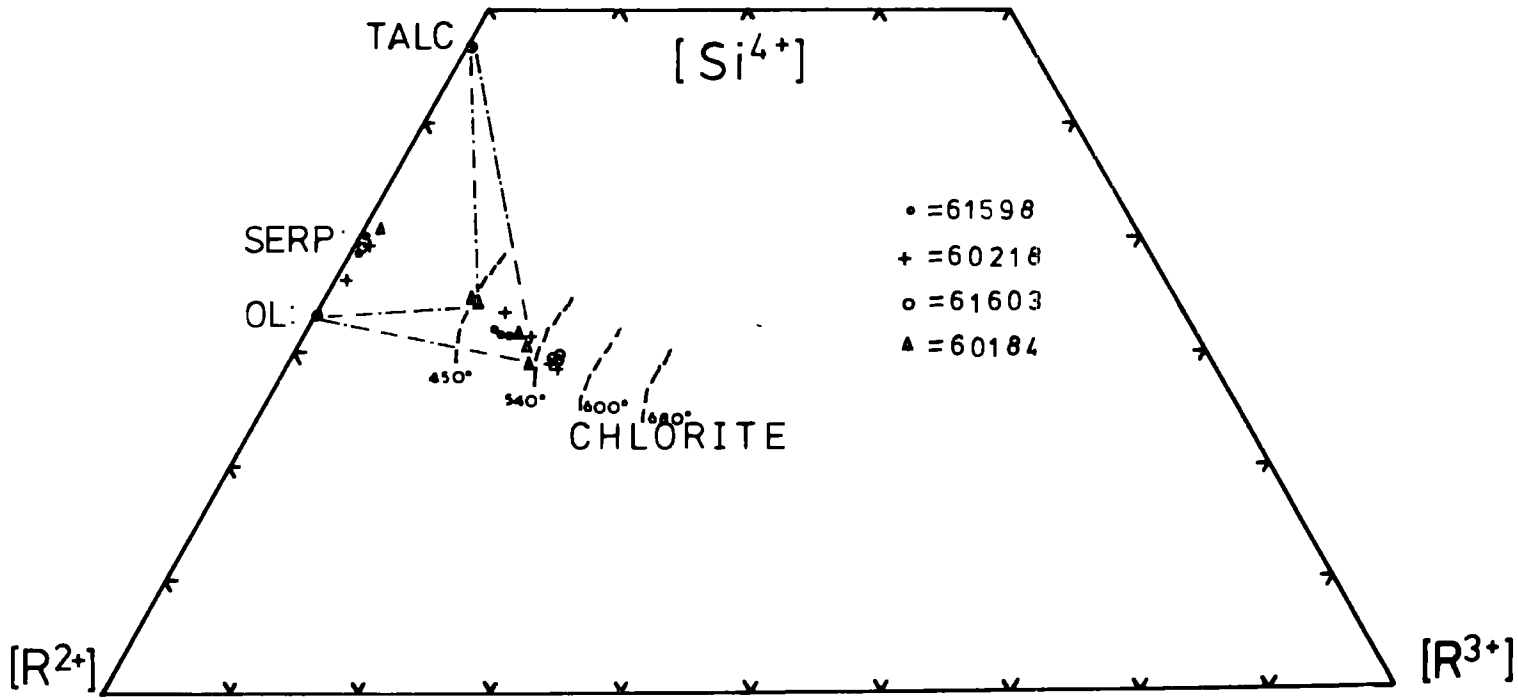

Figure 6.15 Part of an R^{2+} - R^{3+} - Si^{4+} plot, showing the compositions of coexisting serpentines and chlorites, and also the variable olivine-talc-chlorite field. Temperatures are extrapolated from Velde (1973), Figure 6.16.

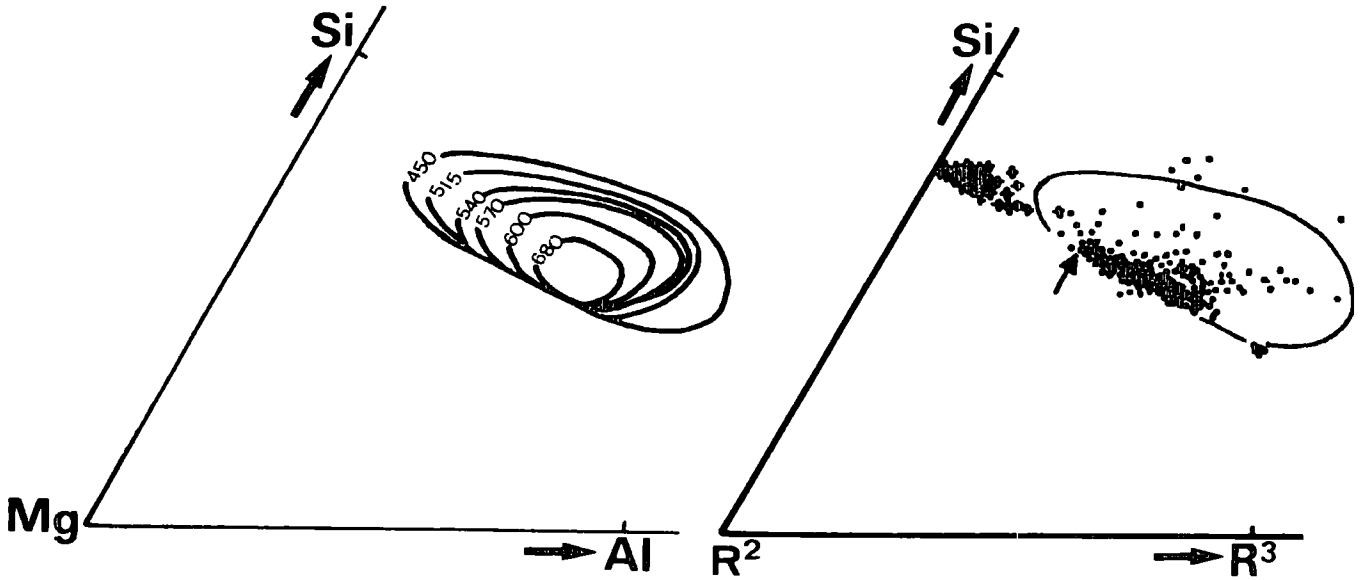

FIGS. 4 and 5: FIG. 4 (left). Solid solution observed at various temperatures and 2 Kb pressure for the 14 Å chlorites. FIG. 5 (right). Natural chlorite and serpentine analyses are plotted as a function of R^2–R^3–Si content. Dots are 14 Å chlorites, crosses are serpentines. Chemical analyses were not used if they contained > 0·10 Ca^{2+}, > 6·10 octahedral ions, or < 4·10 Si^{4+}. Formulae were calculated on the basis of $O_{10}(OH)_8$ using the method of Foster (1962). The solid line shows maximum solid solution of coexisting 7 Å and 14 Å chlorites in the Mg–Al–Si synthetic system.

Figure 6.16 Figs.4 and 5 from Velde (1973), showing the observed, and experimentally determined solubility of Al in the serpentine-chlorite system.

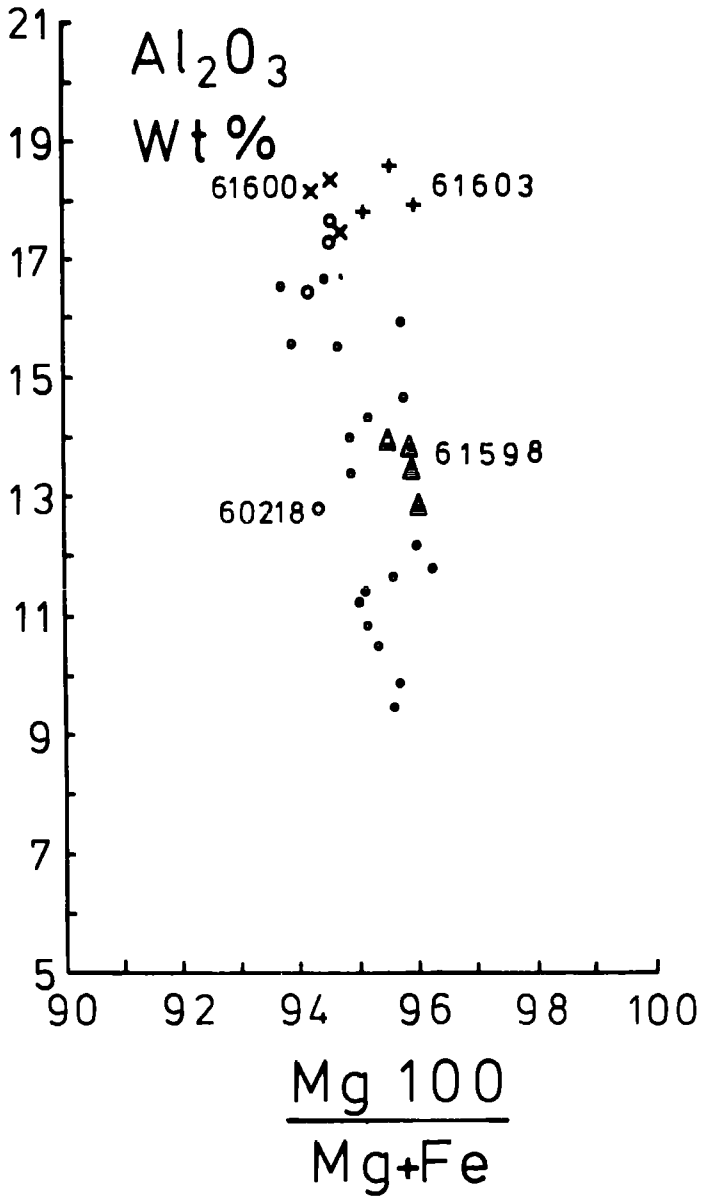

Figure 6.17 Al serpentine and chlorite composition plot, showing enrichment in Al_2O_3 content.

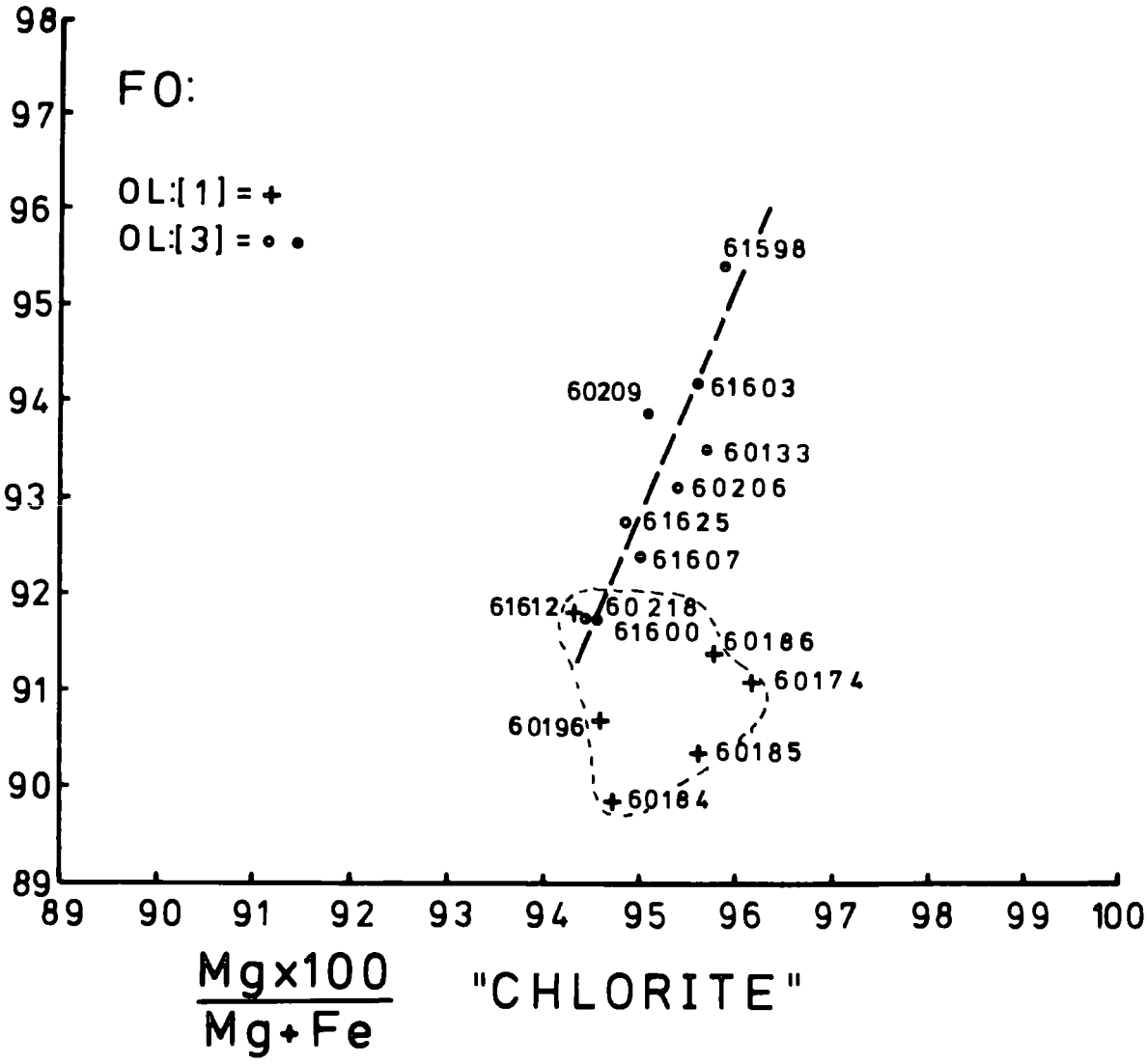

Figure 6.18 Olivine forsterite content plotted against "chlorite" Mg/Mg+Fe ratio, (closed circles and crosses). Al rich serpentine data are indicated by open circles.

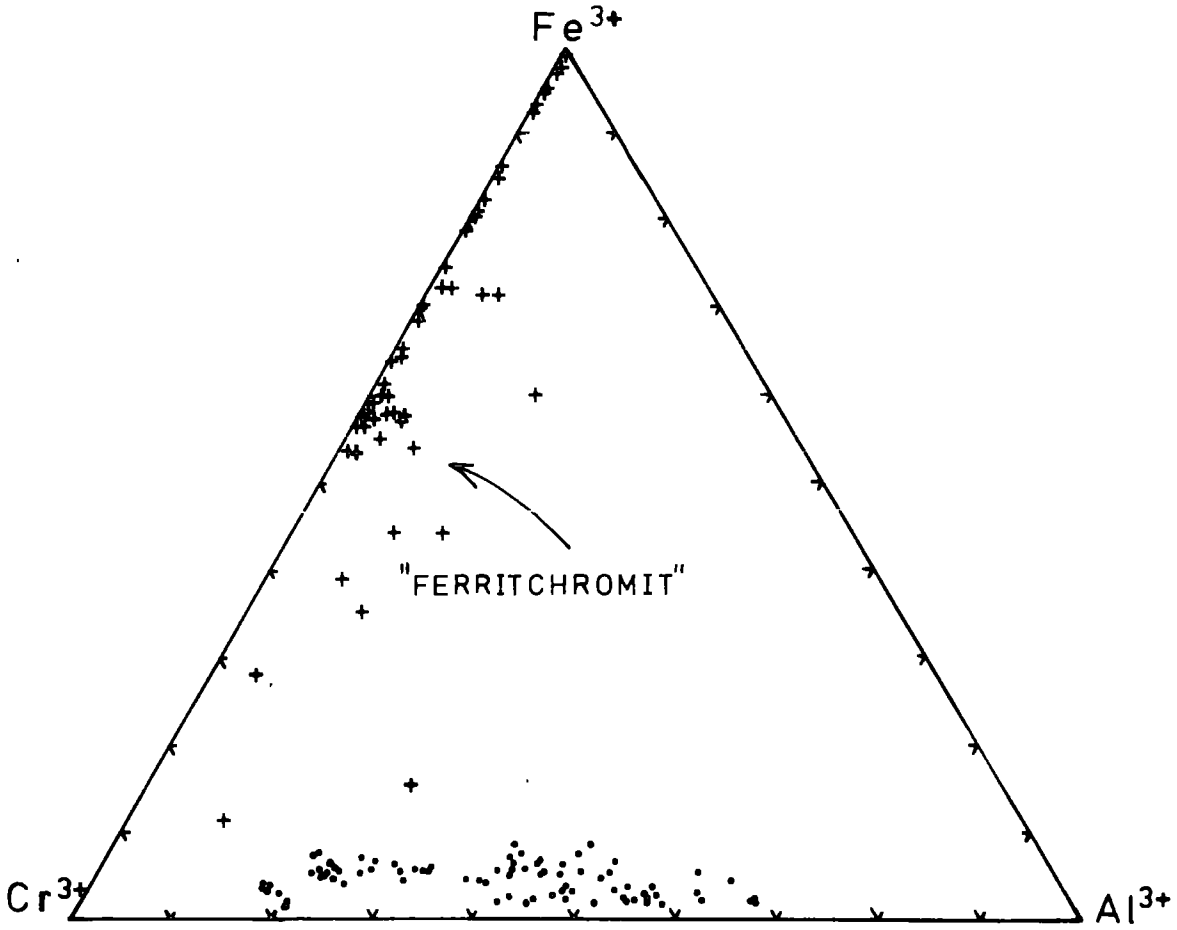

Figure 6.19 A trivalent cation plot, showing the compositional range observed in spinel (1), (closed circles), and the observed trend from "intermediate" ferritchromit to magnetite in spinel (3), (crosses).

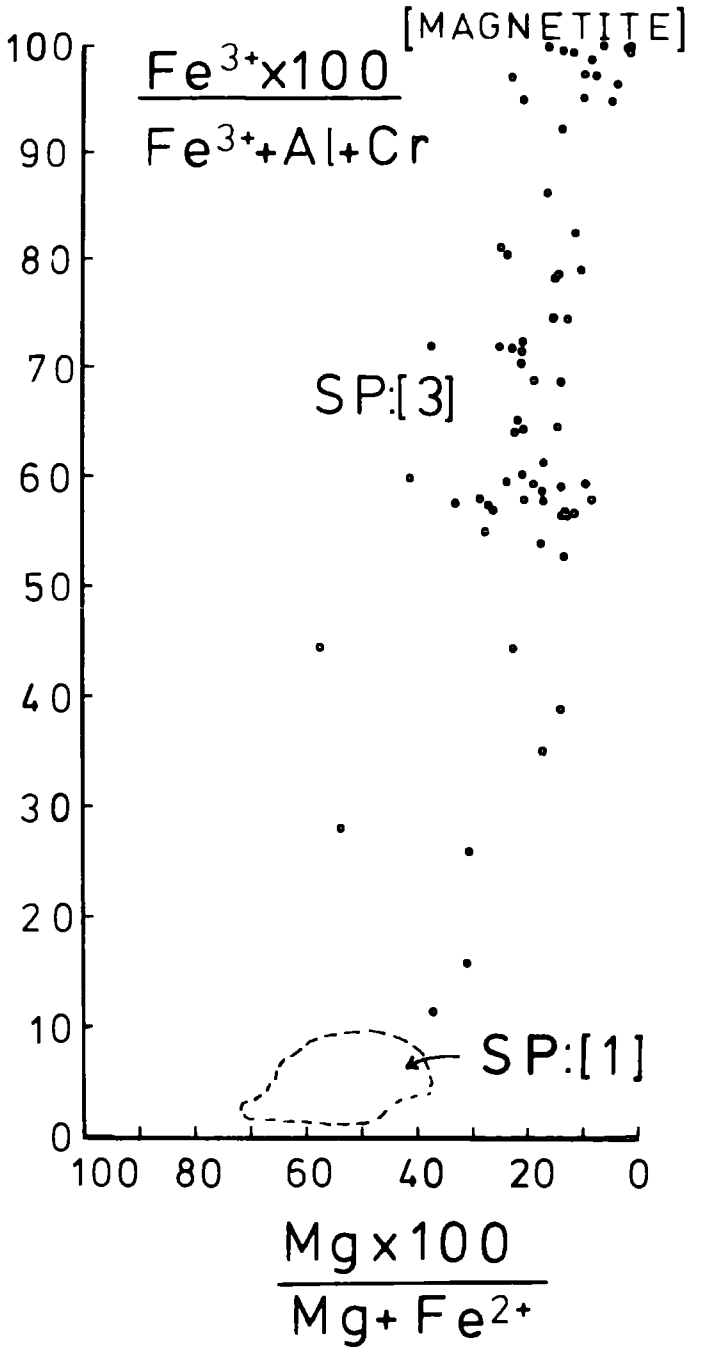

Figure 6.20 A spinel ratio plot, showing the development of ferrit-chromit, (spinel (3)), and the trend towards magnetite.

alteration trend is thus towards magnetite sensu stricto. The spinel structure starts out "normal", with $8R^2$ cations in four fold coordination, and $16R^3$ cations in six fold coordination, and it finishes with the "inverse" spinel structure of magnetite. This has $8R^3$ and $8R^2$ in four-fold cordination, and $8R^3$ in six-fold cordination. The alteration process thus involves structural change as well as chemical alteration.

The trivalent cation plot, Figure 6.19, shows that Al is readily replaced by Fe^3, and that little Al is retained in the spinel structure. This substitution is fundamental to the metamorphic development of the inner aureole, as Al is released into the silicate system, and Fe is removed from it.

Primary spinel (1) has a variable Al content, ranging from 20% of the trivalent cation content in dunite to 70% in some peridotites. This variation has been shown to influence the stability of the spinel, and a few relict chrome rich spinels, as in Samples 60209 and 60196, have remained relatively unaltered. These samples contain coexisting primary spinels and ferritchromites, and Figure 6.21 shows the essentially simple cation for cation substitution which occurs. Similarly Sample 61633 illustrates the simple replacement of Al^3 by Fe^3. If a constant Cr^3 content is retained in the structure, some dunites might be

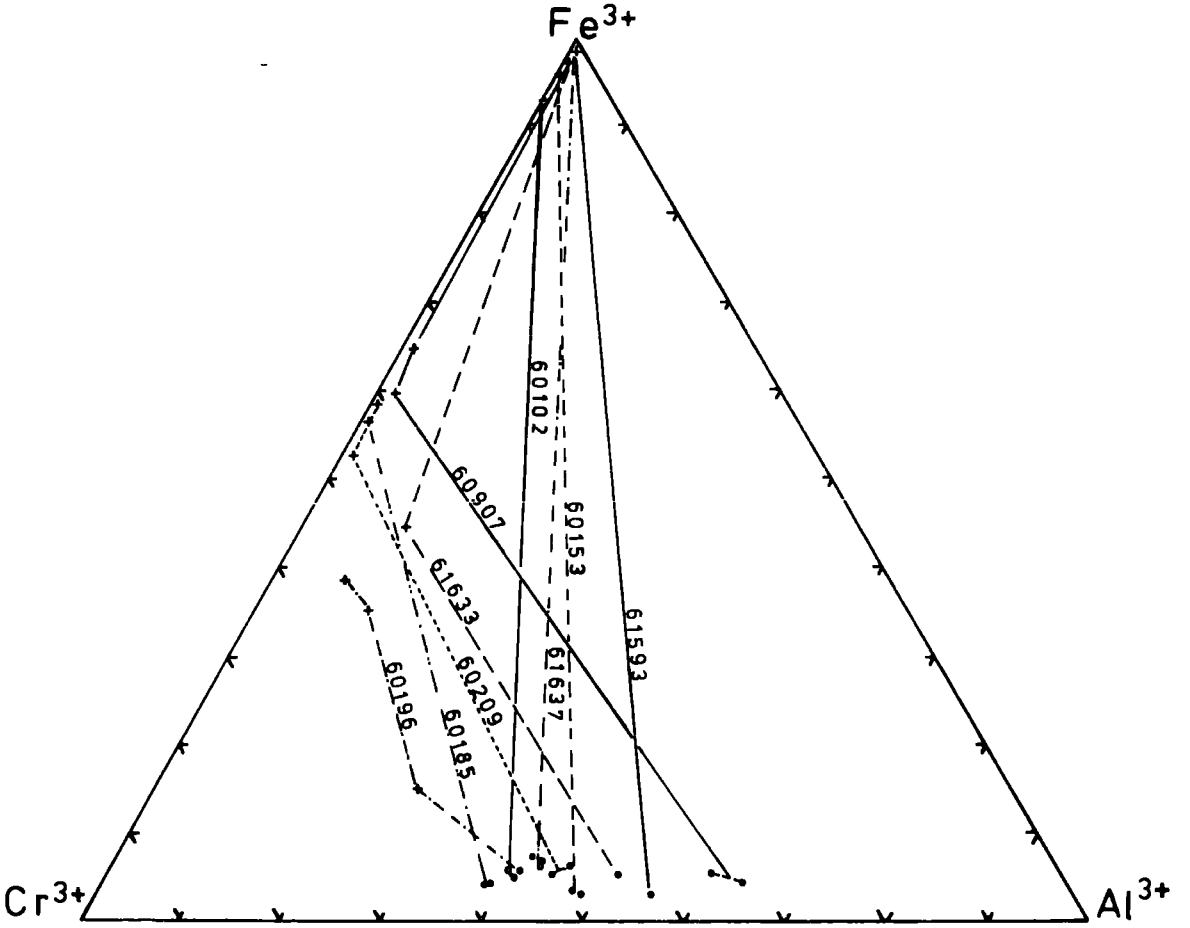

Figure 6.21 A trivalent cation plot, showing tielines between primary spinel (1), and coexisting ferritchromit, and/or magnetite.

expected to have lower contents of Fe^3. The fact that they do not, either indicates predominantly harzburgite derived spinel, or else minor replacement of Cr^3 by Fe^3. Although both factors may apply, and many are undoubtedly peridotite derived spinels, other samples give evidence for loss of Cr^3, e.g. Sample 60185, Figure 6.21.

The concentration of ferritchromit analyses with just in excess of 50% Fe in the trivalent state suggests an intermediate composition between that of spinel, and of magnetite, in the following manner.

1) $R^2_8\ (Al^3_8 Cr^3_8)O_{32}$ "normal" spinel(1)

2) $R^2_8\ (Fe^3_8 Cr^3_8)O_{32}$ "normal" ferritchromit

3) $Fe^3_8 (Fe^3_8 Fe^2_8)O_{32}$ "inverse" magnetite

Sample 60209 contains both primary and ferritchromit oxidized spinels, these illustrate the above "normal" varieties.

1a) $R^2_8 (Al^3_{7.2} Cr^3_{7.6} Fe^3_{1.0})O_{32}$. (60209B1)

2b) $Fe^2_8 (Al^3_{0.2} Cr^3_{7.1} Fe^3_{8.4})O_{32}$. (60209A3)

The distribution of samples containing this intermediate spinel is shown in Figure 6.22. It is perhaps significant that they define a band crudely parallel to the talc isograd. Samples 60209, 60206, 60137, 61525, 61552 and 60186 in particular contain a limited range of ferritchromit composition, equivalent to the cluster on

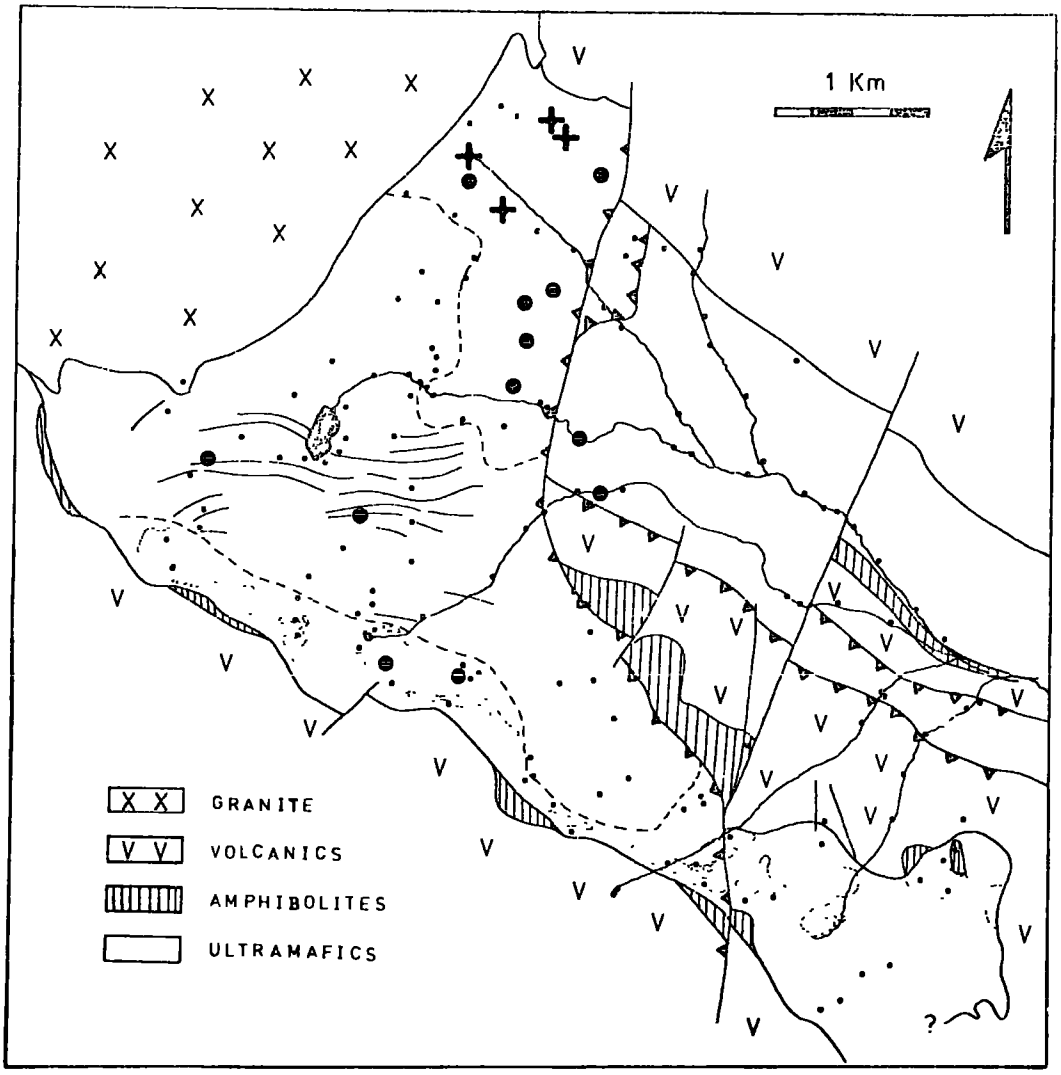

Figure 6.22 Distribution of samples which contain "intermediate" ferritchromit, (closed circles), and chromium magnetite, (crosses), as the main oxidation product of spinel (1).

Figure 6.19. This is further brought out in Figure 6.23 where the $Cr^3:Fe^3$ contents of these spinels are compared with the more highly altered population defined by Samples 61598, 61600, 61603 and 61607. These lie closer to the batholith contact, and they, and in particular Sample 61600, illustrate the simple Fe^3 for Cr^3 replacement which occurs. Magnetite is invariably Cr^3 enriched in this group.

Below the talc isograd there appears to be a similar gradient away from the above ferritchromit composition, as found in Samples 61635, and 60867, but commonly samples coexist with relatively pure magnetite, Samples 60907, 61633, 61635, 61637. Ultimately away from the contact, samples such as 60153, 60102, and 61637 contain primary spinel (1) with magnetite, and no intermediate phase, Figure 6.22.

Textural and chemical data suggests the following:

1) coexisting spinel (1) and magnetite during bastite regeneration (Samples 60153, 60874).
2) partial "oxidation" to ferritchromit margin (Sample 60196).
3) complete alteration at the talc isograd. (Samples 60206, 60209, 61625).
4) conversion of ferritchromit to Cr^3 magnetite with grade increase (Samples 61600, 61598).

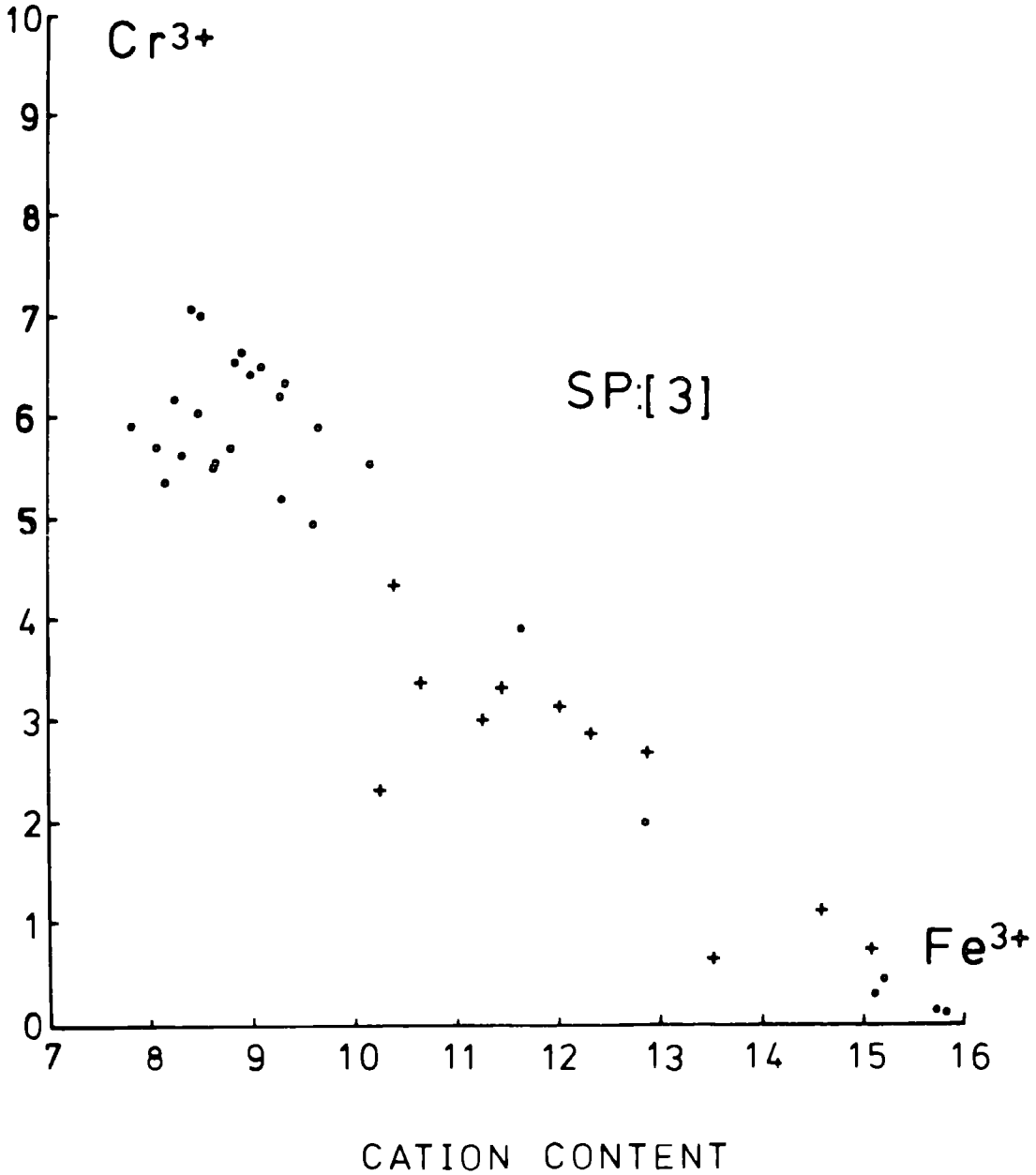

Figure 6.23 The octahedral Cr^3 and Fe^3 contents of the oxidized spinels shown in Figure 6.22. Closed circles are "intermediate" ferrit-chromit, and crosses represent chromium magnetite.

5) partial alteration to Cr^3 magnetite, and also pure magnetite generation during retrogressive serpentinization (Samples 61635, 60907).

Alteration in the trivalent cation site is accompanied by similar Fe^2 enrichment in the divalent cation component, Figure 6.20. The ferritchromit cluster, with an Fe^3x100/ (Fe^3+Al^3+Cr^3) value of around 57, appears to have an Mgx100/ (Mg+Fe^2) ratio between 10 and 30. Subsequent alteration reduces the ratio, and the composition of magnetite should be attained. In fact the ratio in any given sample appears to be variable, and no convincing Mg:Fe substitution trends can be established within a given sample. One reason for this may be the additional and variable content of Mn and Ni taken into the spinel structure. Table 6.9, and Figures 6.24 and 6.25, show that Mn and Ni both increase with degree of oxidation, or Fe_2O_3 content. The scatter in both cases is broad, but Mn and Ni appear to differ in one respect. Mn is enriched during early alteration to ferritchromit, as in Samples 60206 and 60209, and it reaches a maximum of around 1.0% MnO. It then depletes rapidly, and late magnetites contain only traces. The distribution in Samples 61600, 61635 and 61625 and others, Figure 6.24, illustrates this point. Mn presumably substitutes for Fe^2 in the spinel structure during early regeneration, as it does in olivine.

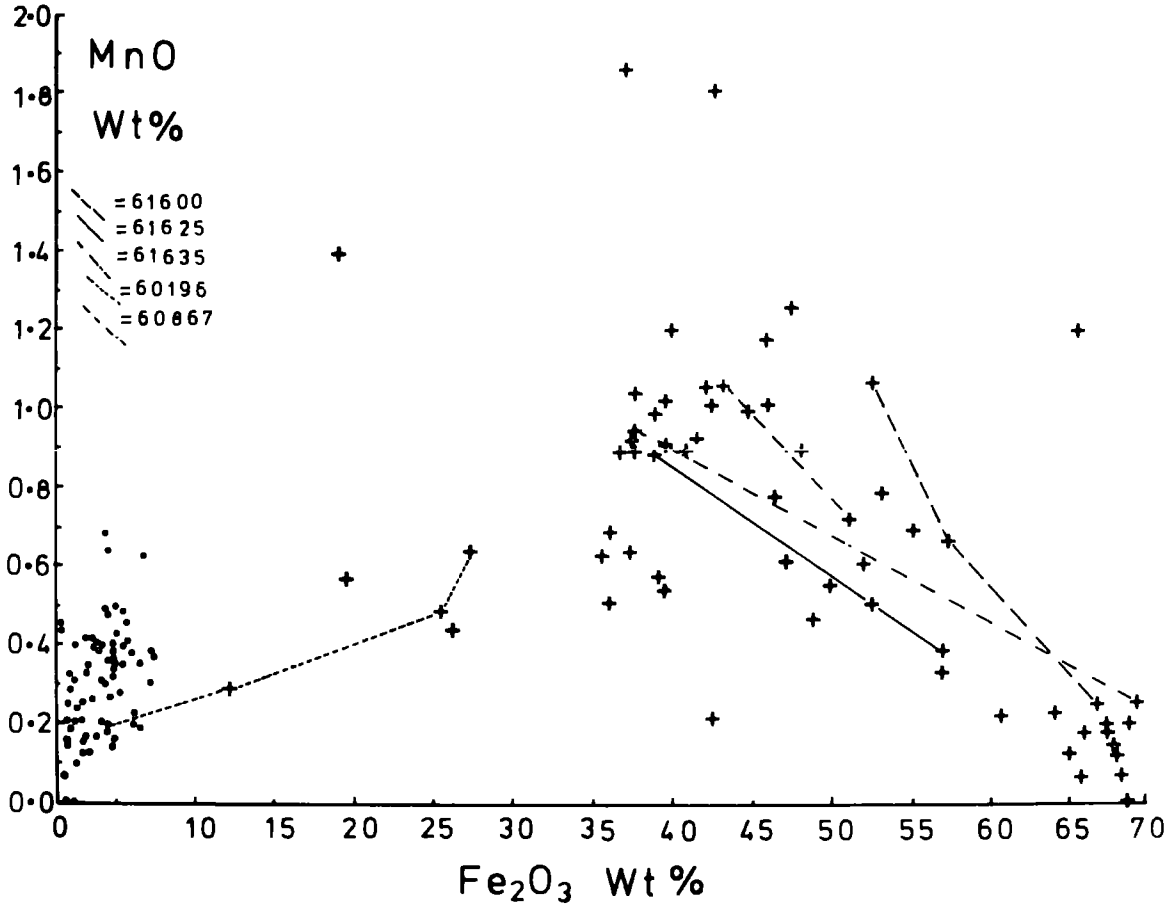

Figure 6.24 MnO variation with Fe_2O_3 content. Primary spinels are given as closed circles, and oxidized ferritchromit and magnetite (spinel (3)) are represented by crosses.

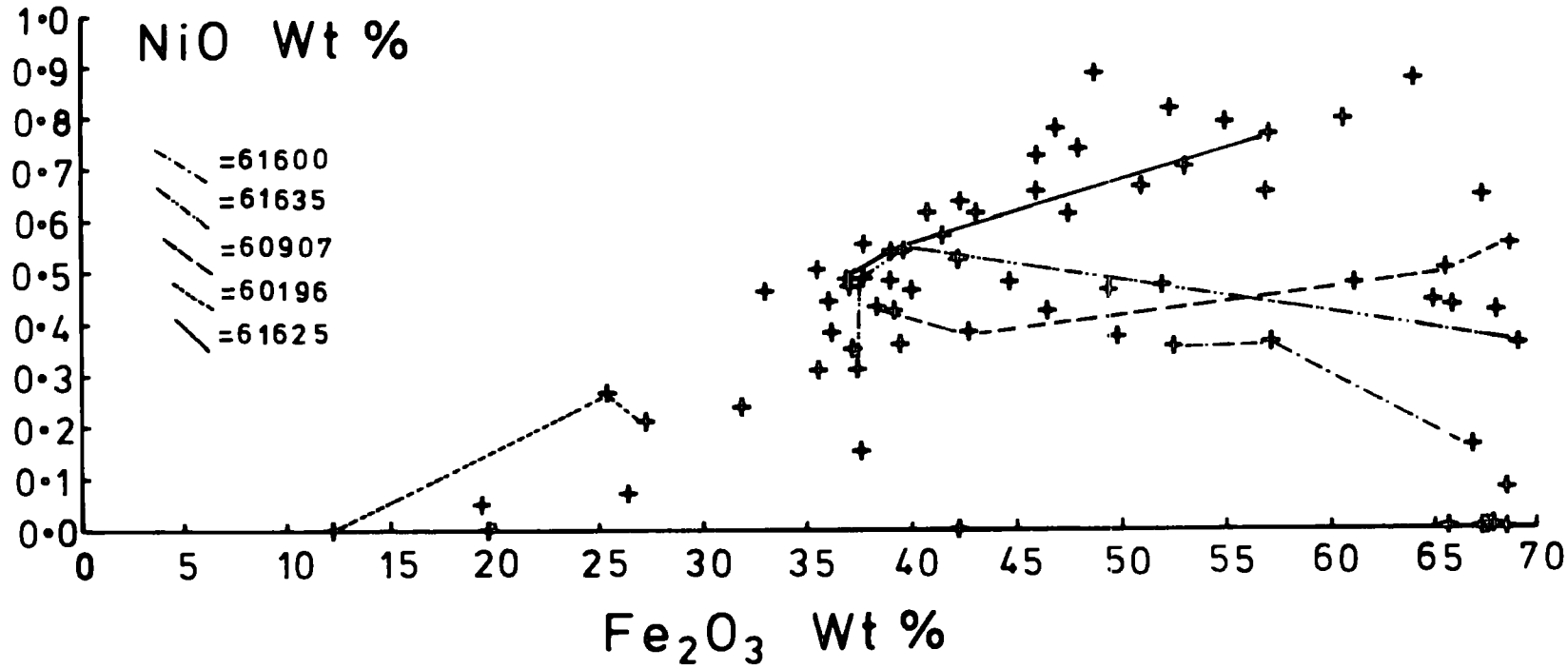

Figure 6.25 NiO variation with Fe_2O_3 content in spinel (3).

In contrast, Ni enrichment in ferritchromit, Table 6.9, Figure 6.25, is continuous, and there is only a slight suggestion that Ni, as NiO, declines with increase in Fe_2O_3. The points are scattered and only a general trend can be inferred from the data. It would seem that Ni is held in the matrix longer than Mn, and that it partitions between late olivine (3) and spinel (3). There is no free sulphide above the talc isograd, Figure 6.8, and Ni does not appear to be removed as a sulphide phase, it remains within the olivine and spinel structures.

A significant feature of the spinel alteration process is that it removes Fe from the silicate system. The modal proportion of spinel in the rock is therefore important in governing the olivine composition, as is the overall rock Fe content. High Fe and reduced spinel might account for the olivine Fe content in Sample 61600.

Amphiboles

The chemical analyses given in Table 6.10 show that two amphibole varieties are found in the inner aureole of the batholith. They both appear to be a stable product of prograde metamorphism. The most common phase is tremolite, as shown by the analyses. The tremolite composition is fairly pure, and the Mgx100/(Mg+Fe) ratio is high. Figure 6.26 shows that there is a slight trend towards Mg enrichment within regenerated rocks. Samples 60184 and 60185

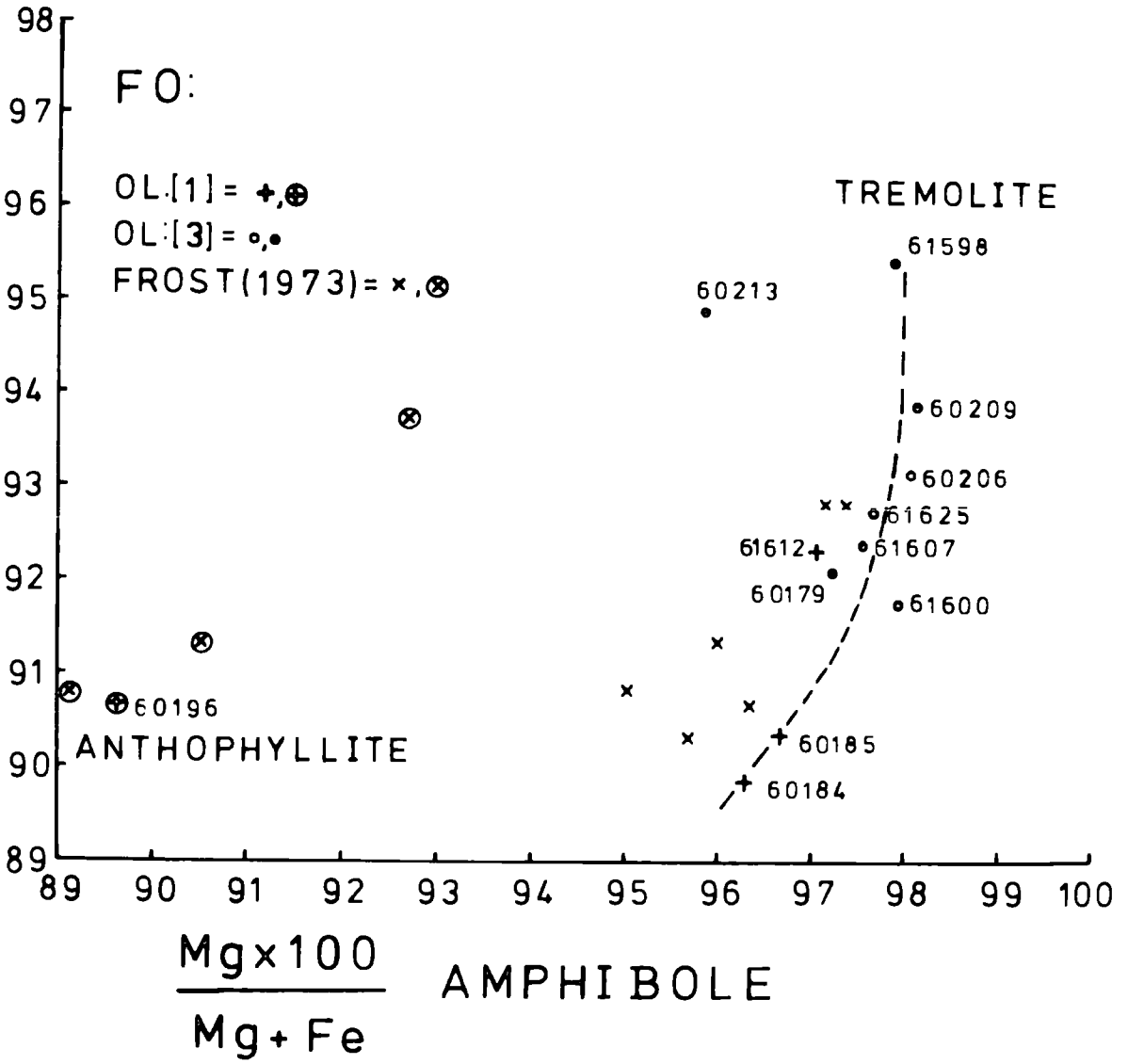

Figure 6.26 Olivine forsterite content plotted against the Mg/Mg+Fe ratio in amphibole. The symbols are as shown in Figure 6.18. Additional data from Frost (1973) are also plotted.

are lower in their Mgx100/(Mg+Fe) ratio, but Sample 61612, which contains slightly more forsteritic olivine than is usual, has a relatively high ratio in its tremolite.

Regenerated rocks in Unit (3b) are found to contain Mg rich silicates, and with the exception of Sample 60213 this holds true for the analysed tremolites, Figure 6.26. The reason for the anomalous Fe content in Sample 60213 is uncertain, it may relate to the addition of a new phase, enstatite, which is not found in any of the other analysed tremolite bearing rocks.

There is no apparent enrichment in trace elements, unlike the situation for olivine (3), and the analyses are largely free of Mn, Ni, and Ti. The only real variable is Al, which ranges from 0.12% to 2.18%. The Al is largely in the tetrahedral site, as Al^{IV}.

Six similar tremolite analyses from the thermally metamorphosed Ingalls Ultramafic Complex, are also shown in Figure 6.26. These give a similar trend towards Mg enrichment, and similar overall values, Frost (1973).

The two analyses from Sample 60196 indicate that the rock contains anthophyllite. These give an average Mgx100/(Mg+Fe) ratio of 89.62, slightly lower than the coexisting average olivine (1) value of $Fo_{90.68}$. Also plotted are three comperable analyses from Frost (1973).

Talc

The talc analyses in Table 6.11 indicate a fairly consistent talc composition. The amount of Fe in the structure is small, and the analyses indicate a Mgx100/(Mg+Fe) ratio of 98. This value appears to be independent of coexisting olivine composition. The talc structure appears to contain a trace of Al, presumably in the tetrahedral site. The amount is generally small. Talc also contains a significant trace of Ni in octahedral coordination. The overall totals are low, but distribution between the two lattice sites is reasonable. Again the composition is very similar to that observed by Frost (1973) in a similar thermal environment. Talc Mgx100/Mg+Fe ratio is plotted against coexisting olivine forsterite content in Figure 6.27.

6.2 Discussion

The outer aureole contains a stable olivine (3) - serpentine assemblage. This, in the absence of talc, is a strong indication of regeneration according to reaction (6). This reaction requires the presence of brucite in the original Stage II serpentinite, although this is difficult to prove directly.

Page (1967) records brucite within the Burro Mountain body in California. He shows that the brucites are Fe enriched, and that they contain between 18 and 32

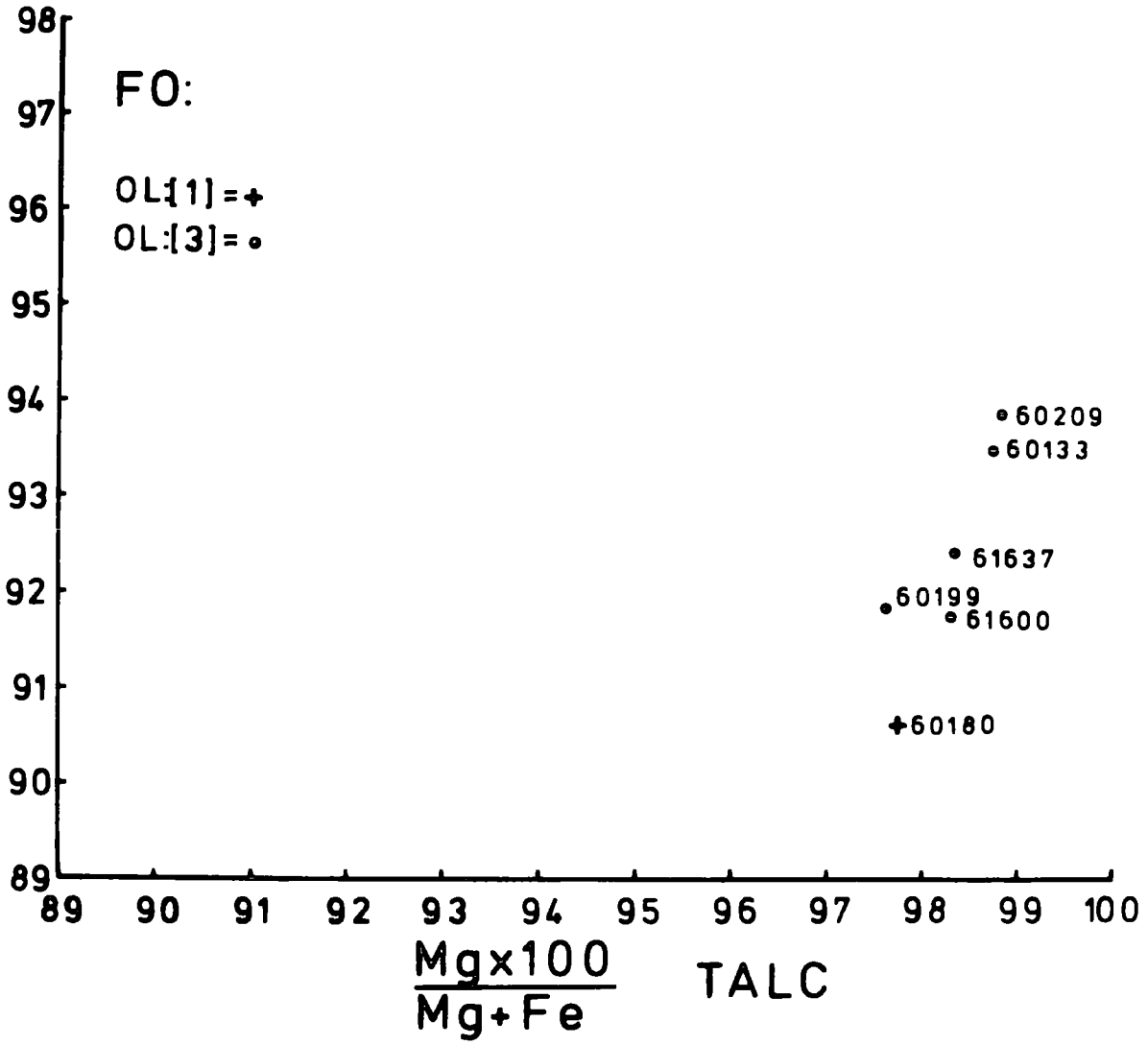

Figure 6.27 Olivine forsterite content plotted against coexisting talc Mg/Mg+Fe ratio.

mol percent $Fe(OH)_2$ in solid solution. They apparently display a uniform spatial distribution, with Fe rich brucites favouring low density marginal serpentinites. If this relationship is general, the Blue River Stage II brucite might also be expected to contain appreciable Fe. Whether Mn similarly concentrates in the brucite structure is not confirmed, but analyses quoted by Deer, Howie and Zussman (1962) indicate that it does. They record 0.38% MnO in brucite from serpentinite.

Ball and Taylor (1961) have shown that the brucite breakdown reaction to periclase can be considered in terms of cation migration, and a relatively constant number of oxygen atoms per unit volume. By their model, the original structure breaks down into "donor" and "acceptor" regions. "Donor" regions release water, and the cations migrate to "acceptor" regions, which only loose protons. This model is thought to account for lattice simularities between the phases, and the change from hexagonal close packing to cubic close packing within the lattice. They also note initial dehydration at 400°C, a somewhat lower temperature than recorded by Fyfe (1958), at around 550°C.

Ball and Taylor (1963) continue their argument for inhomogeneous dehydration, and the setting up of "donor" and "acceptor" regions, in a study of serpentine dehydration. They use a similar model to explain the topotactical

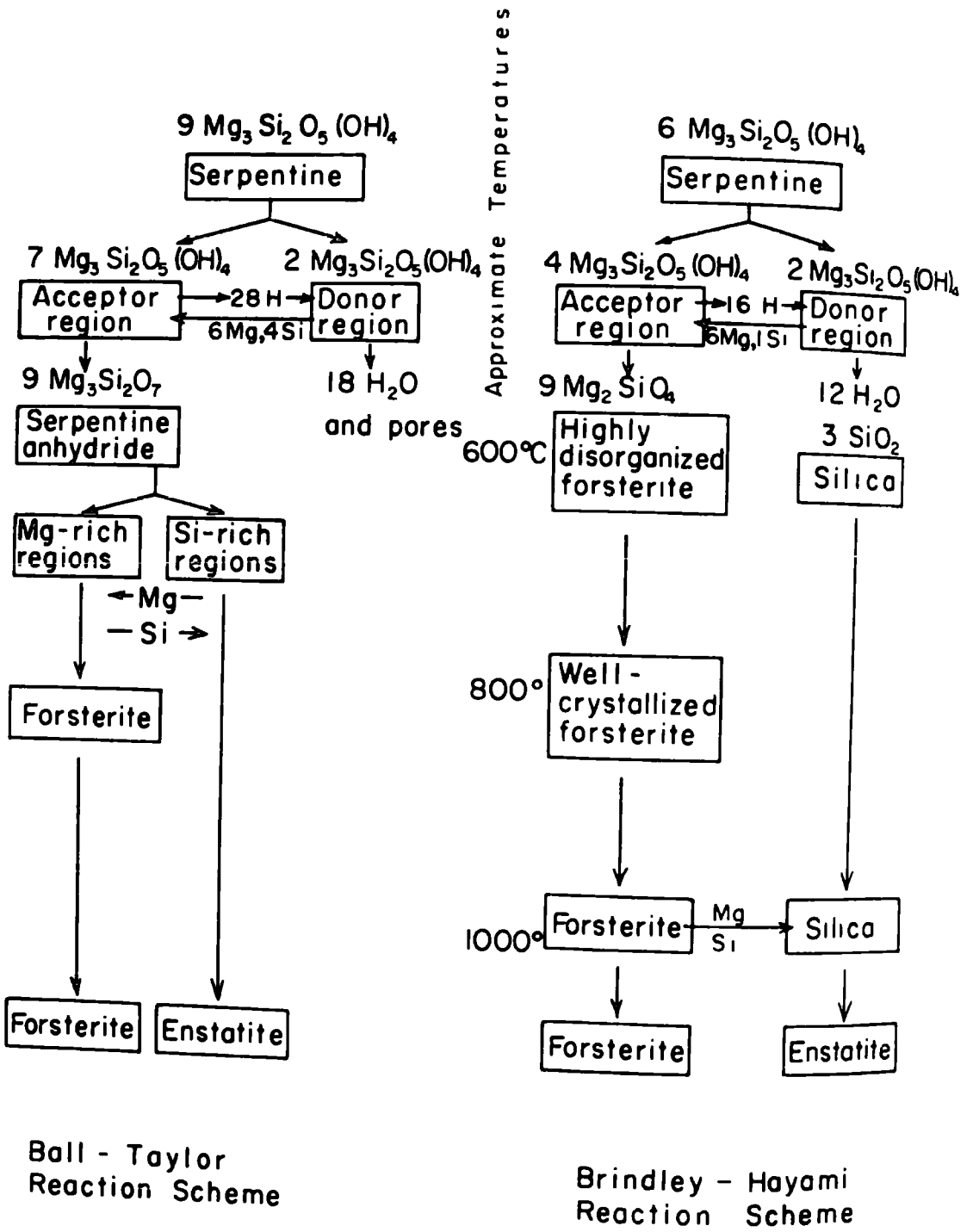

Figure 6.28 Reaction schemes proposed for the olivine regeneration process, from Brindley and Hayami (1965).

relationships between olivine pseudomorphs after a serpentine host. This model was adapted by Brindley and Hayami (1965), in order to account for the late occurrence of prograde enstatite, and the apparant requirement of excess Si. Their process is summarised in Figure 6.28 from Brindley and Hayami. This indicates that the following reaction occurs in a brucite free system.

$$(3MgO.2SiO_2) = 1.5(2MgO.SiO_2) + 0.5(SiO_2)$$

Anhydrous Serpentine	Forsterite 87.5%	Silica 12.5%

Eight unit cells of serpentine become nine unit cells of olivine. In so doing, "donor" regions release water, and donate (6Mg+1Si) to the "acceptor" region, in exchange for 16 protons. The "donor" region is left with an excess of Si. In a brucite bearing rock, which contains similarly mobile cations, the serpentine "donor" region might well become a brucite "acceptor" region, and form olivine by the following reaction.

$$2Mg(OH)_2 + SiO_2 = Mg_2SiO_4 + H_2^+$$

In reality, once nucleation has occurred Fe and Mn display greater cation mobility than Mg, and they concentrate preferentially in both "acceptor" and "donor" sites, leaving a Mg Ni enriched serpentine-brucite assemblage.

The temperature at which serpentinization occurred

is unknown, and although several estimates for reaction (6) have been made, the point is still open to debate. Similarly the regeneration temperature is open to question. Early experimental work in the system $MgO-SiO_2-H_2O$ indicates a temperature of around 365°C at 1 Kbar, Bowen and Tuttle (1949). Kitahara and Kennedy (1967) indicate a similar temperature.

Fe substitution in the olivine (1) structure is thought, by Page (1967), to considerably lower the reaction temperature, his thermodynamic data on brucite, (albeit at 1 atmosphere), indicates the Fe content strongly influences the stability of brucite. Further indications of low temperature serpentinization are given by a study on the oxygen isotope fractionation between serpentine and magnetite, Wenner and Taylor (1971). They suggest formation of lizardite-chrysotile assemblages at between 85°C and 185°C.

Scarfe and Wyllie (1967) also indicate a significantly lowered reaction temperature in an Fe buffered system. They suggest a temperature of around 320°C at 1 Kbar, comparable to serpentinite weakening temperatures recorded by Raleigh and Paterson (1965) for brucite serpentinite transformation from a ductile to a brittle state.

In addition Johannes (1968) indicates a lowering of the pure Mg brucite-serpentine reaction temperature and

this is considered to represent a more realistic maximum, as it was established using minerals rather than oxides.

The difference between the Scarfe and Wyllie, and Johannes plots, Figure 6.29, presumably represents all or part of the serpentine-brucite-olivine (3) stability range, and progressive metamorphism presumably alters the phase compositions, as illustrated in Figure 6.30. The matrix becoming progressively enriched in Mg and Ni, and the olivine (3) initially concentrated in Mn and Fe at low temperature, and depleted with T increase. Matrix serpentine remains in any of three situations.

1) Brucite depleted in the rock (Samples 61637, 60067)

2) Insufficient temperature to complete reaction (Samples 60055, 60021)

3) Al substitution blocks serpentine structure. (Samples 61625, 60171)

The serpentinization process produces magnetite, and following Hostetler et al (1966), peridotite probably reacted according to the following variant of reaction (6).

(6a) $9(Mg_{0.92}Fe_{0.08})_2SiO_4 + (Mg_{0.92}Fe_{0.08})SiO_3 + 12.595H_2O + 0.0885\ O_2 = 5(Mg_{0.96}Fe_{0.04})_3Si_2O_5(OH)_4 + 2.595(Mg_{0.85}Fe_{0.15})(OH)_2 + 0.177Fe_3O_4 + 0.874\ MgO.$

Textural evidence suggests that the magnetite is not reabsorbed into the olivine structure, and the rock should start out with an excess of Mg. In reality the availability

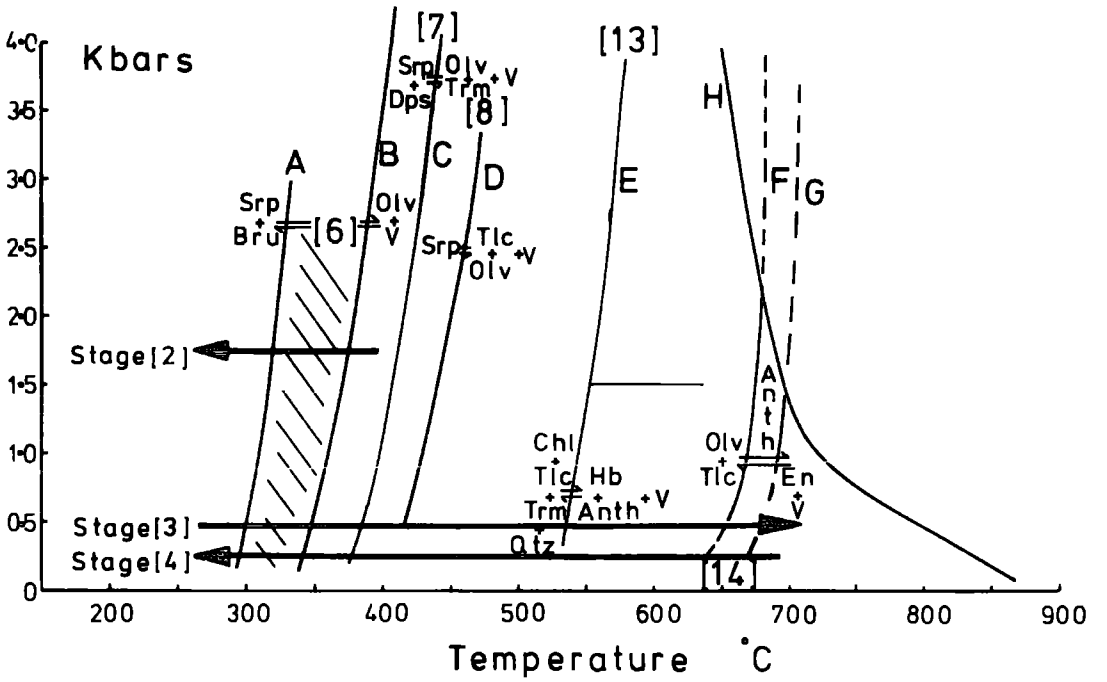

Figure 6.29 Experimentally determined stability fields in the system $MgO-SiO_2-Al_2O_3-CaO-H_2O$.

Reactions (6), (7), (13) and (14) are shown in Table 5.4.

A = Scarfe and Wyllie (1967)
B = Johannes (1968)
C = Evans and Trommsdorff (1970)
D = Scarfe and Wyllie (1967)
E = Chondhuri and Winkler (1967)
F = Greenwood (1963)
G = Greenwood (1963)
H = Wolfe (1967)

Line H is the "wet" fusion curve for granite.

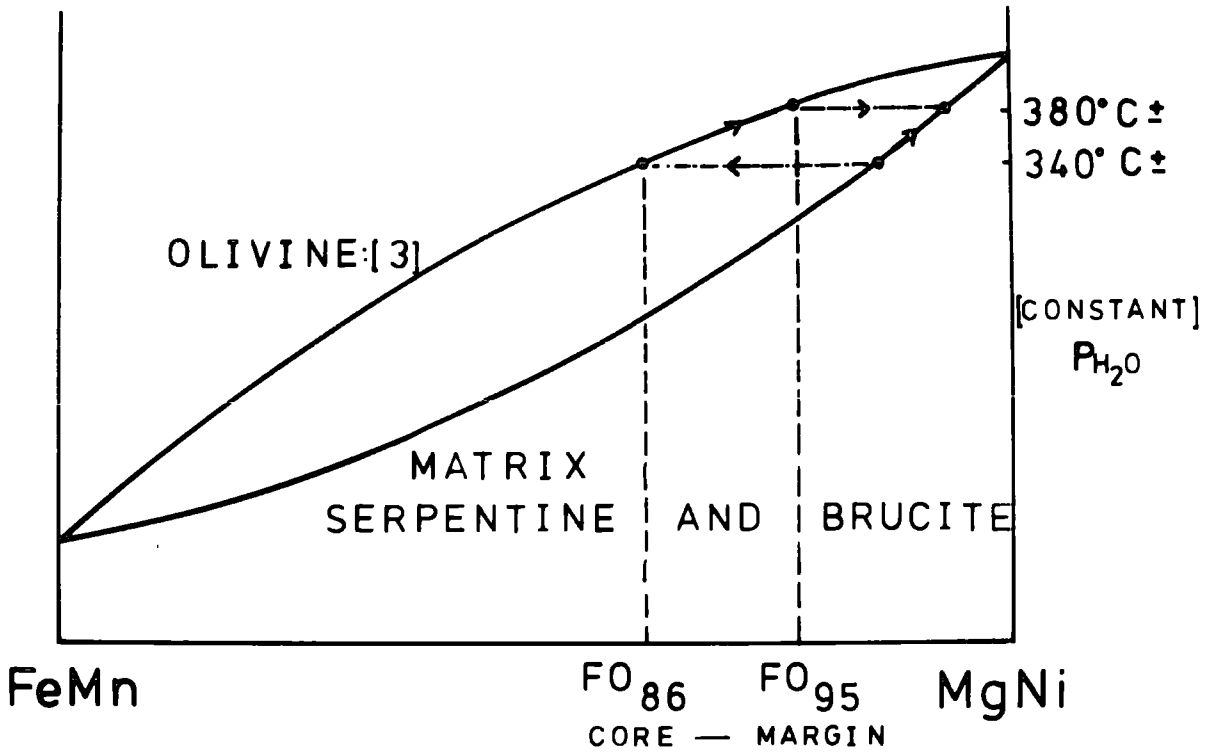

Figure 6.30 A schematic representation of the sub-solidus relations between serpentine and metamorphic olivine (3), during prograde metamorphism.

of oxygen is crucial to regeneration, as noted, the MnO content is a variable independent of olivine (3) forsterite content. The oxidation of spinel, and removal of Fe has established a series of depletion gradients. Possibly, below the talc isograd, Mn is a function of temperature and pressure, and Fe has a variable response to fO_2.

Above the talc isograd both Fe and Mn partition in favour of ferrichromit, possibly during initial heating at a relatively high fO_2. The rock presumably still contained a brucite component, and the body probably passed through the reaction field of reaction (6) to that of reaction (8). The relative importance of each is not known, although weak cores, and overgrowths in Sample 60894 indicate some influence of reaction (6). The reaction (8) temperature is as problematical as that of reaction (6). Bowen and Tuttle (1949) suggest 500°C, although Scarfe and Wyllie (1967) suggest a lower value of 450°C at 1 Kbar. The first is based on 'pure' Mg rich materials, and the second is conducted in an Fe buffered system. King et al. (1967) use thermodynamic data to create a theoretical reaction curve similar to that described by Scarfe and Wyllie (1967), Figure 6.29.

The experimental work of Velde (1974), into the stability of 7 Å and 14 Å "chlorites", is in good agreement with the above estimate for the talc isograd. After a

compositional break at the level of the isograd, the "chlorite" compositional range decreases towards the contact.

Increased oxygen activity above the isograd has, as noted, fundamentally influenced the mineralogy, and the following variants appear to have occurred, in addition to reactions (6) and (8).

(6b) Serpentine + brucite = olivine (3) + FeO + H_2O

(9a) spinel (1) + serpentine + FeO = Ferritchromit + Al serpentine + SiO_2 + MgO

(10a) Diopside + SiO_2 + MgO + H_2O = tremolite

(11a) talc + olivine (3) = enstatite (3) + H_2O

These reactions take place in Unit (3b), but similar reactions occur within Unit (3c).

(9b) Spinel (1) + serpentine = ferritchromit + Al serpentine + MgO + SiO_2

Spinel oxidation is not dependent on the olivine producing reaction, and ferritchromit can form by modal reduction, or release of Mg and Al. The formation of Al serpentine and tremolite occurs as before, but anthophyllite is formed in Sample 60196, not enstatite.

A survey of the relevant literature shows that there are only a few well documented occurrences of metamorphic olivine, and most of these are from a thermal environment. A number of studies in the last few years have contributed

to the understanding of the regeneration process, both in thermal metamorphism, Springer (1971, 1974), Frost (1973), Trommsdorff and Evans (1972), and in regional metamorphism, Evans and Trommsdorff (1970).

Bowen and Tuttle (1949) use the observations of MacDonald, that olivine 'kernels' are found in the aureole of the Sierra Nevada batholith, as evidence to support low temperature olivine regeneration.

Seki (1951) describes progressive metamorphism of the Miyamori ultrabasic body, Japan, in the aureole of a granodiorite batholith. He records metamorphism 4 km from the batholith contact, and suggests the simultaneous formation of zones 1, 2 and 3, Table 6.12. He considers antigorite to be retrogressive, analogous to the Blue River situation. Zone 2 is similar to the Blue River inner aureole. The enstatite-green spinel assemblage is interesting in view of the experimental work discussed, and the apparently retrogressive spinel found in this study. Seki compares the chemistry of fresh "diallagite" (clinopyroxenite?), with a tremolite-antigorite replacement, and concludes that FeO, Fe_2O_3, $K_2O + Na_2O$, Al_2O_3, and TiO_2 are depleted during contact metamorphism. This presupposes no loss during serpentinization.

Yamaguchi (1964) describes the regeneration of serpentinite to 'dunite' in the aureole of a granite

TABLE 6.12

Seki (1951)

Miyamori ultrabasic body (Japan)

1) Olivine-enstatite-(Al?) green spinel-cummingtonite-talc-tremolite

2) Olivine-tremolite-anthophyllite-talc-chlorite

3) Olivine-tremolite-antigorite

4) Antigorite.

intrusive and ring dyke complex at Obira Mine, in Kyushu, Japan. He describes and illustrates olivine veinlets and porphyroblasts, his descriptions fit the Blue River outer aureole occurrence very well. His mineral assemblages, Table 6.13, suggest regeneration by reaction (6), in a non-oxidising environment.

Yamaguchi also describes massive dunites from the crystalline schists of Higashi-Akaishi, Shikoku, Japan. These apparently contain two olivine types, one "clear", and one "turbid". The "clear" olivine contains up to 0.78% CaO, Yamaguchi (1964), in contrast to a maximum recorded "turbid" olivine value of 0.35% CaO. The description clearly fits that of a zoned olivine as discussed in this study. Granulation may have destroyed the core to margin relationship. CaO was not concentrated in the Blue River olivine, core or margin, possibly as CaO was either removed as tremolite, or else migrated into 'rodingite' during Stage II. Simpkin and Smith (1970) correlate high CaO content with a low pressure environment. Whether this holds for metamorphic olivines is not known.

Springer (1971) discusses the contact metamorphism of ultramafic rock within the aureole of the layered mafic, (olivine gabbro), Pine Hill instusive complex, in the foothills of the Sierra Nevada. An aureole which extends for up to 6000 m from the contact gives the metamorphic assemblages

TABLE 6.13

Yamaguchi (1964)

Obira Mine, Oita (Japan)

1) Olivine

2) Serpentine-tremolite-olivine

3) Serpentine

shown in Table 6.14. Springer estimates a contact temperature of $770^{o} \pm 25^{o}C$ at above 1.5 Kbar, based on experimental work. His assemblages correlate well with those of Seki (1951). An inner green (Al rich) spinel-enstatite assemblage passes outward into an assemblage containing anthophyllite, and this passes into a talc-chlorite-tremolite zone. Springer notes FeCr spinel, which presumably means oxidation in the aureole, as described in this study. This was not recorded by Seki, but it may have been present. The presence of chlorite in the outer zone suggests "inner aureole" conditions throughout, in comparison with the Blue River body. Textural evidence suggests that the green Al rich spinels described by Springer, are identical to those found in the Blue River body, and a similar origin is inferred.

Frost (1973) describes regeneration of a serpentinized peridotite in the aureole of the Mount Stuart batholith in the Central Cascades of Washington. The aureole apparently extends for 2 km, and it contains assemblages, Table 6.15, compatable with both inner and outer aureoles. Zones 5 and 6, correlate with the outer aureole of the Blue River body, and Zones 1-4 with the inner aureole. The contact temperature is taken to be $730^{o}C$ at 3 Kbars, based largely on the chlorite breakdown reaction to produce Al rich spinel and enstatite.

TABLE 6.14

Springer (1974)

Pine Hill Intrusive Complex (U.S.A.)

1) Olivine-enstatite-Al spinel-hornblende-
FeCr spinel

2) Olivine-anthophyllite-chlorite-tremolite
FeCr spinel

3) Olivine-talc-chlorite-tremolite-
FeCr spinel

4) Olivine-antigorite-chlorite-tremolite-
FeCr spinel

TABLE 6.15

Frost (1973)

Ingalls ultramafic body (U.S.A.)

1) Olivine-enstatite-spinel

2) Olivine-enstatite-chlorite

3) Olivine-enstatite-anthophyllite

4) Olivine-talc

5) Olivine-serpentine-tremolite

6) Olivine-serpentine-diopside

Trommsdorff and Evans (1972) describe progressive thermal metamorphism of antigorite schist in the aureole of the Bergell tonalite in Italy. They record the assemblages shown in Table 6.16, and they establish similar isograds to those observed in the Blue River body. There is however, one important difference between the two. The Malenco serpentinite had already undergone "alpine" regional metamorphism to an antigorite-olivine-diopside body prior to thermal metamorphism, Peters (1968). Trommsdorff and Evans state that antigorite-brucite is a stable pair prior to the formation of olivine, and as such, the following reactions are metastable relative to a slightly higher temperature "polymorph".

(6c) Chysotile + brucite = 2 forsterite + $3H_2O$

(7b) 5 chrysotile + 2 diopside = 6 forsterite + tremolite + $9H_2O$

(8b) 5 chrysotile = 6 forsterite + talc + $9H_2O$

Metastable or not, the above reactions do have application in natural situations, and on the basis of the present study, oxidation, and thus Al availability appears to be a stabilizing influence on antigorite.

Another occurrence of metamorphic olivine is recorded by Oliver and Nesbitt (1972) from altered ultramafic rock in the Western Australian greenstone belt south, of Kalgoorlie.

TABLE 6.16

Trommsdorff and Evans (1972)

Malenco serpentinite (Italy)

1) Anthophyllite-olivine-tremolite

2) Talc-olivine-tremolite

3) Antigorite-olivine-tremolite

4) Antirgorite-olivine-diopside

Olivine "megacrysts" up to 2 cms in diameter give a spotted appearance to the rock. They record relict "spinifex" quench textures preserved in regenerated olivine, which suggests a constant volume replacement. They also note the conversion of chlorite to olivine, with further generation of chlorite, a feature which may account for the progressive concentration of Al in serpentine in the system pertaining to the Blue River. They also record a variable, but low forsterite content, which they correlate with bulk rock chemistry.

CHAPTER 7: RETROGRESSIVE SERPENTINIZATION

7.1 High Temperature Serpentinization

Some of the ultramafic body underwent high temperature alteration to antigorite. Antigorite appears to be the principle retrogressive serpentine phase for a distance of 2400 m from the batholith contact, Figure 7.1. Minor lizardite-chrysotile serpentine formation occurred along the batholith contact, as noted earlier, but this probably post-dates the development of antigorite.

Feathery blades of antigorite overprint olivine (1) and tremolite in Unit (3c), and occur intimately associated with talc in Unit (3b). Above the Nickel Creek thrust antigoritization is weak and sporadic, but below the thrust, in Unit (3a), antigorization is pervasive down to its isograd. Thus although olivine (3) is well displayed above the fault, and in the talc zone, and also below the antigorite isograd, it is largely altered to antigorite in the footwall of the thrust.

The presence of a discrete antigorite isograd implies a thermal relationship to the batholith, and suggests that antigorite was not formed during cold, pervasive, late-stage serpentinization.

In Samples 61567, 61637, and 60171, matrix serpentine initially formed during Stage II, and modified during

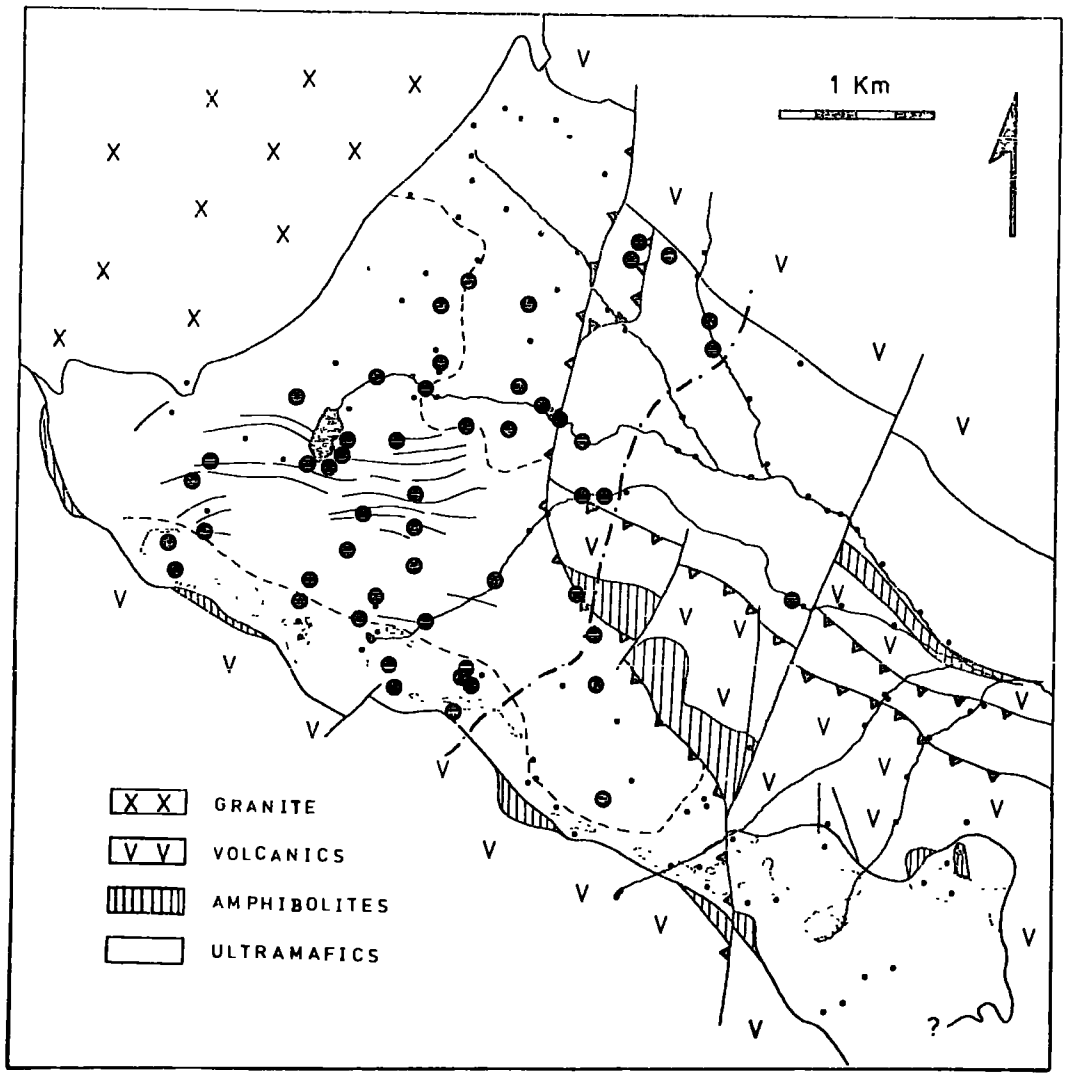

Figure 7.1 Distribution of antigorite serpentine, and the line of the (retrogressive) antigorite isograd.

Stage III, is recrystallized to antigorite, with little destruction of the olivine generated during Stage III. The amount of olivine converted directly into antigorite increases below the Nickel Creek thrust; Sample 60109 displays both matrix recrystallization and olivine alteration, and Sample 60907 is almost completely altered to antigorite, (Plate 7.1). In hand specimen samples are hard, dark green, matt textured, and very often jointed and sheared. Some joints are infilled with apple green amorphous serpentine, and others contain microveins of chrysotile asbestos (Plate 7.2). The original mottled and foliated regenerated texture may remain, although increased antigoritization reduces its intensity. The foliation of the rock is subparallel to the Nickel Creek thrust, along Heazlewood Creek, Samples 60066 to 61539, and similarly along Nickel Creek from Sample 60130 to 61611.

It seems likely that movement occurred along the thrust after, and perhaps during, the main period of olivine regeneration, and that antigorite formed in the waning stage of the thermal event. The occurrence of antigorite as the matrix for a tectonic serpentinite breccia at sample location point 61629 in Unit (1) also suggests that movement occurred along the fault at this stage (Plate 2.5). Had serpentine existed earlier, it should have regenerated

Plate 7.2. Mottled serpentinite (4), after regenerated dunite. Olivine (3) "kernels" are brought out by the rusty weathering. Asbestos veinlets are symmetrically arranged about a central fracture. Location point 61527, on Spudusob Creek.

Plate 7.12. A rodingite dyke, showing a chloritic reaction halo on contact with serpentine. The serpentinite is massive, brittle and sheared. Location point 61588, on Claim Jumper Creek.

to dunite prior to antigoritization. This was not the case, indicating late movement on the fault.

Further evidence for the retrogressive development of antigorite is found in Samples 60186 and 61560, where as noted earlier, antigorite has preferentially exploited the core region of olivine (1), leaving marginal olivine (3) unaltered (Plate 3.7). Textural evidence indicates that the formation of antigorite is thus retrograde, and not prograde. Within samples like 60907, which are almost completely altered to antigorite serpentinite, relict patches of olivine (3) appear to form a complete mosaic, supporting the view that the whole rock had been converted to olivine with only minor relict serpentine.

Along the western contact, in Unit (3b), olivine (3) has been replaced by a talc-antigorite assemblage, which again probably indicates movement and relatively high temperature serpentinization in the waning stage of the metamorphism, Samples 60179, 60180 (Plate 7.4)

The stable spinel phase during antigoritization would appear to be a ferritchromit, spinel (3), although many samples retain relict primary spinel (1). No samples containing antigorite also contain the small cubic green spinel, and its occurrence appears to be restricted to the low temperature serpentinization stage.

Gabrielse (1955, 1963) describes the occurrence

of antigorite in the aureole of the Cassiar batholith, and he studied the serpentine varieties extensively. He confirmed the occurrence of "feathery reticulate antigorite" using differential thermal analysis, X-ray diffraction data, and electron-photomicroscopy.

7.2 Low Temperature Serpentinization

Low temperature serpentinization to lizardite and chrysotile occurred above the enstatite isograd in Unit (3b), and below the antigorite isograd in Unit (3a). Serpentinization presumably also occurred in Unit (2), during Stage IV, but as these rocks were never heated above the reaction (6) threshold, they presumably underwent a continuous alteration process from Stage II. The largely pervasive, mesh texture, bastite serpentinite of Samples 60041 and 60040, are the norm, and relict olivine (1) found in Sample 60094 is exceptional. The only evidence of post Stage II activity is the formation of chlorite, and slight alteration of spinel. As the regeneration process is one of dehydration, excess water may well have moved into Unit (2), out of Unit (3a).

Good evidence for Stage IV serpentinization comes from those samples which contain serpentine pseudomorphs after olivine (3), Samples 60102, 60033, 60034, and 60157. Euhedral regenerated olivine porphyroblasts set in a matrix

of modified serpentine, from Stage II, are replaced by a serpentine-brucite pseudomorph. The outline of the original crystal is retained, and there is no evidence for volume expansion. Outer margins (Plate 7.5) are clearly defined, and the matrix and pseudomorph serpentines are quite distinct. The crystal margins are very often bordered by strongly birefringent flakes of brucite (Plate 7.5), which suggests a reaction relationship, and cation mobility.

Serpentinization exploits cracks and fractures, and it preferentially exploits outer Mg rich margins (Plate 5.20). Where both core and marginal olivine have been serpentinized, as in Sample 60035, magnetite dust is clearly concentrated in relict core regions, this reflects both Stage II magnetite, and also magnetite formed during re-serpentinization of a Fe rich core.

Samples 60102 and 60157 both have a pronounced brucite margin around the pseudomorph, and this also acts as a zone of magnetite deposition (Plate 7.6). These brucite bearing samples initially formed olivine (3) by reaction (6), and they then reverted to serpentine and brucite according to the same reaction. The distribution of brucite, as detected by X-ray diffraction methods, Figure 7.2, indicates brucite stability below the antigorite isograd, but not above.

Primary spinel (1) remains stable, although it is

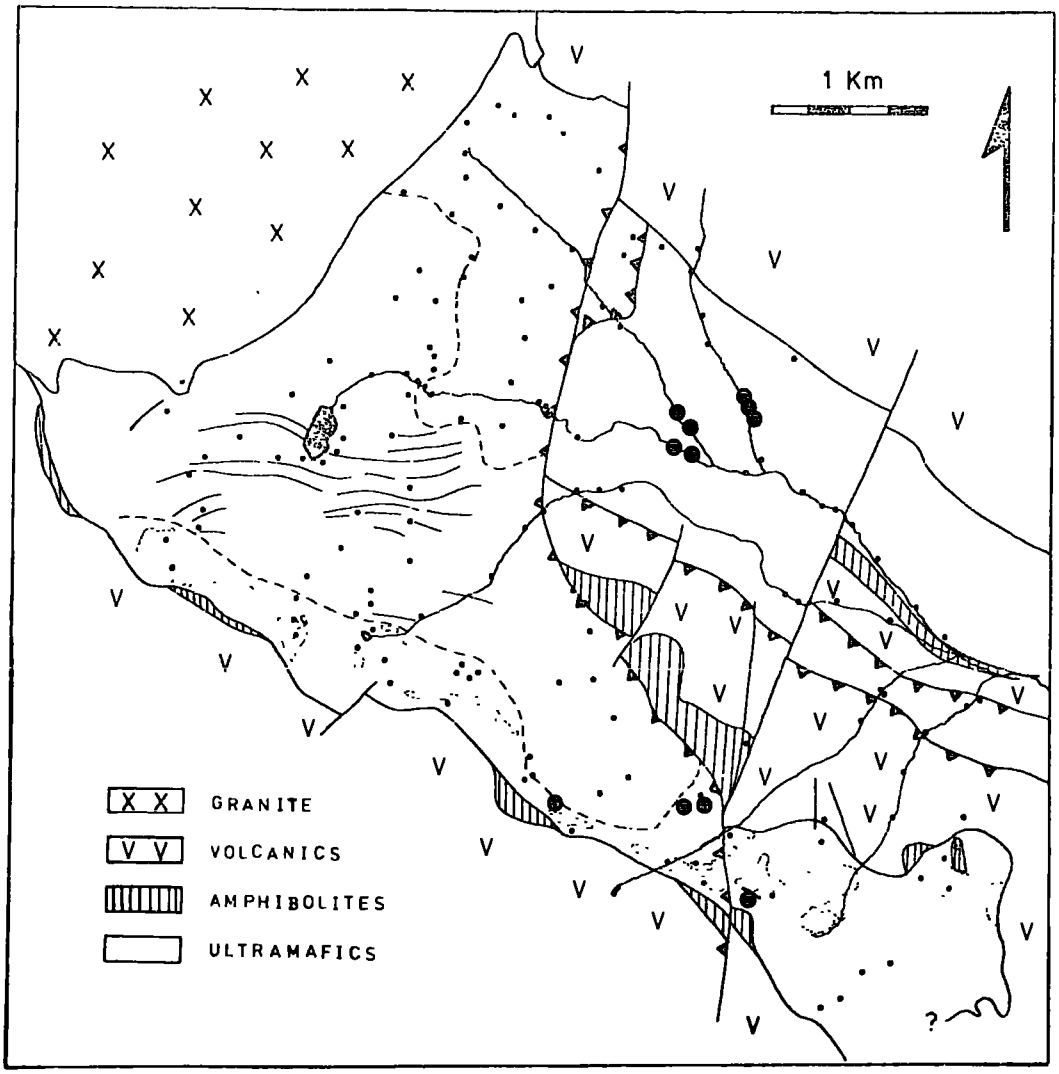

Figure 7.2 Distribution of samples containing anomalously large amounts of brucite; as determined by X-ray diffraction.

often coated with magnetite, Samples 60035, 60157. Some samples which contained, or contain, Al rich primary spinel, as in 60140 and 60143, were oxidized, and contain ferritchromit. This is now surrounded by a well crystalline chlorite. The occurrence of chlorite associated with altered spinel away from the batholith contact, Samples 60018, 60023, 60062 and 60041, is ubiquitous in serpentinite, in contrast to the Al serpentine found in regenerated and primary dunite nearer the contact. The occurrence of serpentine is thought to stimulate recrystallization of Al serpentine to chlorite.

A few samples, such as 60143, and 60140, contain an additional Al rich spinel phase intimately associated with chlorite and relict ferritchromit. The spinel is light green, translucent and granular , it occurs as cubes in the vicinity of an altered ferritchromit (Plate 7.7). Original relict spinel (1) in Sample 60143 remains, and its analyses, Table 3.8, indicate a high primary Al content.

Above the enstatite isograd, along the batholith contact, olivines have been altered to ribbon serpentine, subparallel to the batholith contact, which is the main fabric trend. Original olivine outlines remain, defined by magnetite dust. Regenerated enstatite (3) remains stable, although olivine (3) is largely altered. Ferritchromit and Cr^3 magnetite spinels are granular and

resorbed in texture, and original chlorite halos have recrystallized to a platey chlorite, Sample 61603, 60213, and 60215 (Plate 7.8). In Sample 60215 the chlorite is pleochroic and green, and other samples such as 61603 give a greenish tint. This is possibly a function of Cr^3 content. The ferritchromit and chlorite are both intimately associated with minor amounts of green cubic spinel (Plate 7.8). This very often nucleates on ferritchromit, and may pseudomorph ferritchromit, Samples 60199, and 61603. The assemblage also contains large clearly crystalline laths of talc, intimately associated with similar chlorite laths (Plate 7.9). These overprint the matrix component of the original rock, and reserpentinized olivines are locally enclosed by recrystallized matrix. Serpentine does not vein or cut through the matrix, Sample 60199 (Plate 7.10). This late talc appears to be recrystallized matrix talc from the regeneration process, or alternatively a new generation. If the latter case were correct it might be expected to overprint regenerated olivine, but it does not.

Throughout Unit (3b), east, there is a strong correlation between the amount of late serpentinization and the degree of crystallinity of chlorite and talc, Samples 61598, 60137.

Antigorite bearing rocks below the fault show little sign of low temperature alteration, except in the form of

veining by chrysotile asbestos (Plate 7.2). The formation of clean microveins of cross-fibre asbestos is a significant late stage feature, which also relates to a period of jointing.

7.3 Serpentinite Mineralogy

Antigorite

Antigorite is formed from pre-existing, modified, matrix serpentine, formed during Stage II, and also directly from olivine. A group of samples which are chemically related to Al serpentine, but are texturally related to antigorite have already been described. These antigorites, in Samples 61625 and 60206, show a marked depletion in SiO_2 and MgO, and increase in Al_2O_3, Cr_2O_3 and FeO, Table 6.7.

Throughout the rest of the area it is not possible to determine whether the antigorite is olivine derived, or derived from matrix serpentine, and a variety of analyses are often obtained within a single sample. Many closely resemble antigorites analysed by Trommsdorff and Evans (1972) from the Malenco serpentinite. An average of their analyses is shown in Table 6.6. Antigorite analyses in Table 7.1 show that Samples 60907, 61633 and 61635, closely resemble those recorded by the above workers, but they tend to have a lower FeO content. Others more closely resemble the Al rich matrix variety in Table 6.7, as in Sample 60171. Some samples such as 60109 have both types.

Discussion. Antigorite

Textural evidence both in this study and elsewhere indicates that antigorite is a distinct high temperature "polymorph" of serpentine. It has been recorded in areas of regional metamorphism, with or without brucite, Trommsdorff and Evans (1972), Jahns (1967), and it has also been recorded from regions of thermal metamorphism, Wilkinson (1953). Francis (1956) indicates that antigorite may replace enstatite and olivine directly, or alternatively may replace pre-existing mesh textured serpentine. His study at Glen Urquhart supports the contention of Hess et al. (1952), that the chrysotile-antigorite transformation is sluggish, and that shearing stress is a prerequisite for antigorite formation. This is not incompatible with the observed association of antigorite with the Nickel Creek thrust, and shear stress cannot be ruled out as a contributing factor to antigorite formation in the Blue River ultramafic body.

Whittaker and Wicks (1970) deduce from a statistical study by Page (1968), that antigorite contains a higher SiO_2, and lower MgO and H_2O contents than other serpentine "polymorphs", and it also allows considerable trivalent cation substitution in the octahedral sheet.

Recent experimental work by Iishi and Saito (1973)

suggests that the MgO to SiO_2 ratio is the critical factor, and not trivalent cation content. They synthesised "pure" antigorite between 450° and 550°C, with a MgO:SiO_2 ratio within the range 5.36:4 to 5.16:4. The formation thus favours an excess of SiO_2, or depletion in MgO. In addition they found that antigorite was favoured by increased load pressure.

The feathery antigorites identified by Gabrielse (1963) have been shown to display a varied chemistry, from almost "pure" antigorite to appreciably Al rich serpentine. Thus, although some well defined antigorite, Sample 60907 (Plate 7.1) is formed, much is appreciably contaminated. A variety of factors probably contributed towards antigorite formation, during the waning stage of thermal metamorphism.

Lizardite-Chrysotile

Table 7.2 contains analyses of serpentines derived from olivine (3) above the talc isograd. The analyses are remarkably constant, in contrast to the antigorites described above. Sample 60218 and 60199 contain slightly higher FeO values, and lower SiO_2 values. They may indicate contamination by brucite. Most samples are low in Al_2O_3 and Cr_2O_3 and relatively uniform in SiO_2 and MgO percentage. Some samples, such as 61603, give analyses not dissimilar to that of chrysotile asbestos Table 6.6 , and comparable to the "pure" modified matrix serpentine surrounding

porphyroblasts in Sample 60021, and 60102, Table 6.5.

In Sample 60035, two varieties of serpentine were identified and analysed, Tables 6.5, 7.3, and two impure brucite analyses were obtained, Table 7.4. The data shows that modified matrix serpentine approaches the composition of serpentine sensu stricto, whereas serpentine pseudomorphing olivine (3) is enriched in MgO, FeO, and depleted in SiO_2.

The SiO_2 depletion in Figure 7.3 suggests contamination by brucite. Page (1967) describes how similar mixtures define a trend between serpentine, and the composition of brucite within the assemblage. Extrapolation of the observed trend (based on very few points), suggests a brucite composition of around 24% FeO, markedly more than the content of the analysed (impure) brucites which margin the pseudomorph. These contain around 5% FeO. The constant volume of the olivine pseudomorph strongly suggests cation migration according to the following reaction, given by Hostettler et al. (1966).

(6) 5 olivine + $4H_2O$ = 2 serpentine + 4MgO + SiO_2

704 gms + 72 gms = 554 gms + 161 gms + 60 gms

(220 cc) (221 cc)

This reaction requires the removal of appreciable amounts of MgO and SiO_2. The marginal brucite presumably represents material removed from the structure. Whether migration of

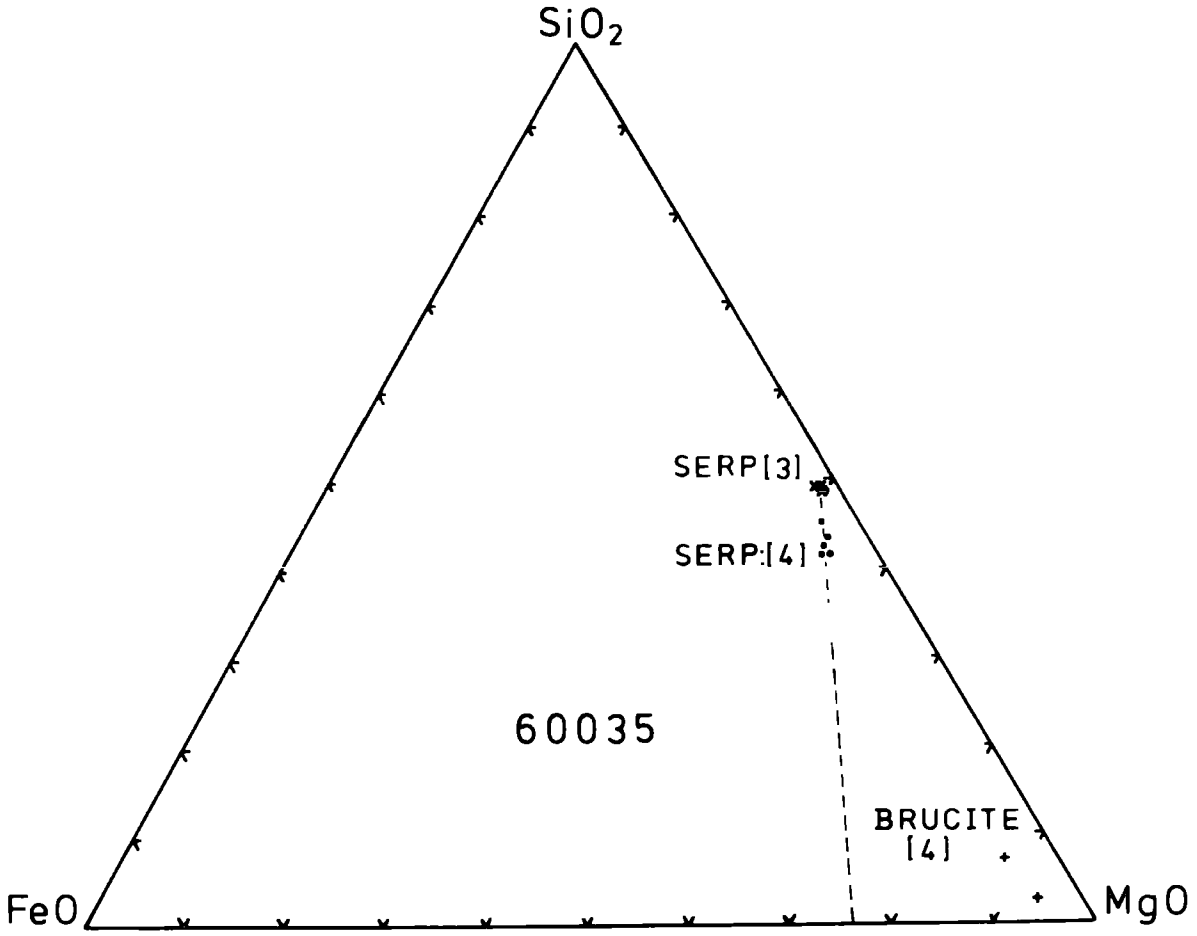

Figure 7.3 Simple oxide plot, after Page (1967), showing modified matrix serpentine (3), and pseudomorphous serpentine (4), in Sample 60035.

Table 7.4

Brucite Analyses

	60035J*	60035K*	A
SiO_2	2.56	5.05	-
FeO	3.54	3.73	1.37
MnO	0.07	0.08	0.38
MgO	78.47	60.67	67.96
NiO	0.20	0.22	-
	84.84	69.75	69.71

*Contaminated brucite, surrounding a serpentine pseudomorph after olivine (3), in Sample 60035.

A: Analysis 2, from Deer, Howie and Zussman (1962). Brucite in serpentinite, Mt. Ramazzo, Italy.

Mg is favoured over Fe, leading to the difference in inferred and observed composition of the brucite, or the FeO becomes reorganised as magnetite is not known. The latter seems most likely (Plate 7.6). As the pseudomorphs still contain brucite, excess SiO_2 must have been removed. Whether this enters the matrix serpentine structure, or is removed from the system is not known, although chemical evidence implies loss. Conceivably brucite could recombine with excess SiO_2 to form more matrix serpentine. There is however, no evidence to indicate this. The pseudomorph "serpentine" contains significantly more NiO than the matrix variety, indicating that NiO was absorbed into the olivine, and subsequently released.

In Sample 60102, Table 7.3 , there is no significant difference in composition between modified matrix, and pseudomorph. This suggests that serpentinization leads to the formation of a chrysotile-like serpentine by diffusion of excess SiO_2, FeO, and MgO (Plate 7.6).

Rocks which have undergone this form of retrogressive serpentinization are found to contain appreciable brucite, and this is easily detected by X-ray diffraction methods. Figure 7.2 shows those samples which were found to contain large amounts of brucite. Significantly they form a band below the antigorite isograd, and above the olivine (3) isograd.

Green Spinel (4)

Three green spinel analyses are given in Table 7.5. The analysis from Sample 60199 is from a green pseudomorph after ferritchromit, and those of Sample 61603 are of cubes encrusting ferritchromit. All three show a marked reduction in Fe^3 and Fe^2, and an increase in Mg and Al. The analyses, and three comparable Al spinel (4) - ferritchromit pairs from Springer (1974) are plotted on Figure 7.4, a trivalent cation plot, and Figure 7.5, Mgx100/(Mg+Fe) ratio plot. The analyses show markedly similar trends.

Textural evidence indicates that Al spinel is generated at the expense of ferritchromit, by substitution of Al for Fe^3 and to a lesser extent Cr^3, and in addition, of Mg for Fe.

Primary Al rich spinel (1), Figure 6.21, is stable during serpentinization, when it coexists with magnetite. Evidently ferritchromit is not stable during low temperature serpentinization to lizardite-chrysotile, and the magnetite-Al rich spinel (4) pair is re-established. This represents a reversal of the oxidation trend, during less oxidising serpentinization.

As noted, oxidation involves two stages, early formation of ferritchromit by substitution of Fe^3 for Al^3, and a later, slower, conversion to the "inverse" magnetite

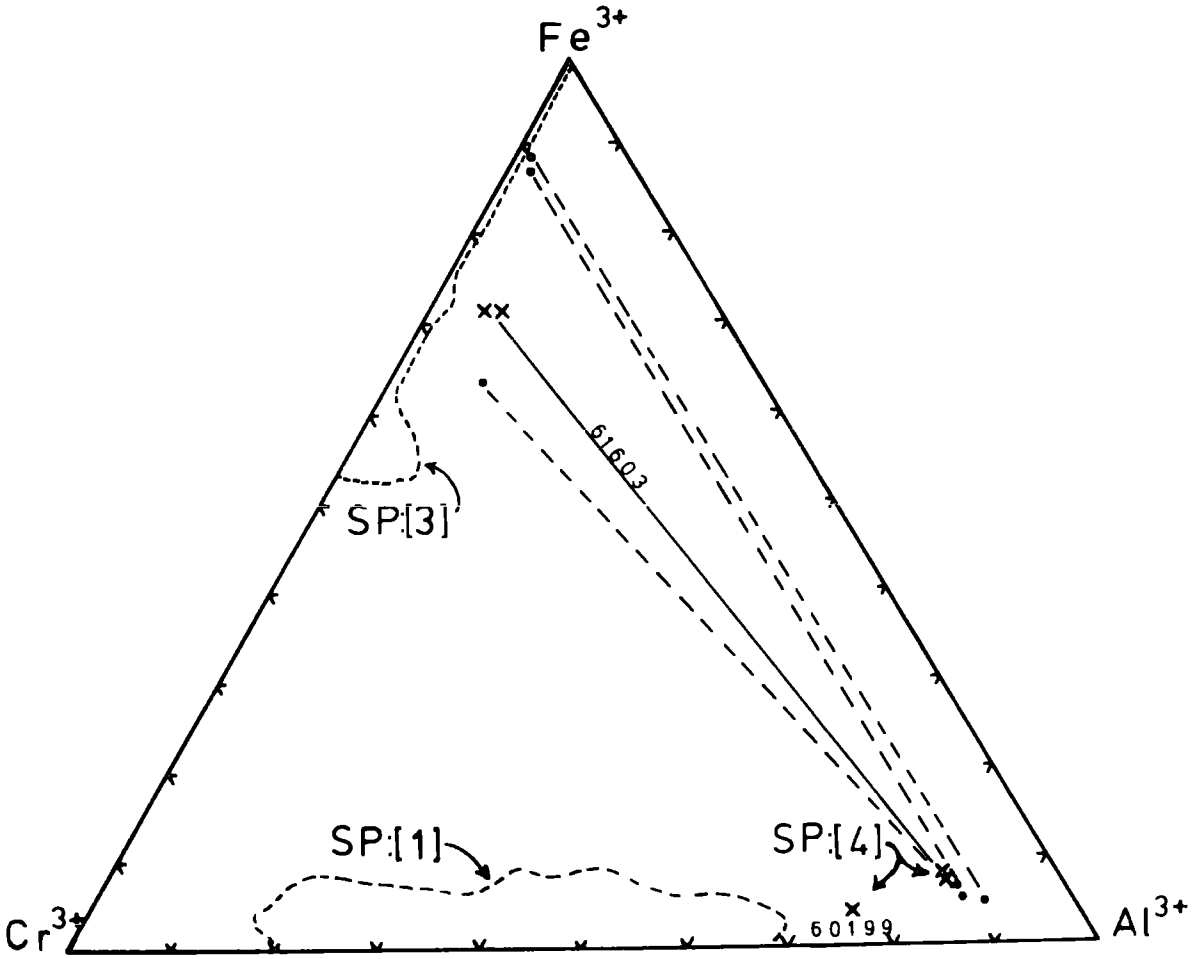

Figure 7.4 A spinel trivalent cation plot, with tie-lines joining coexisting chromium spinel (3), and green spinel (4), shown as crosses. Similar data from Springer (1974) are shown as closed circles.

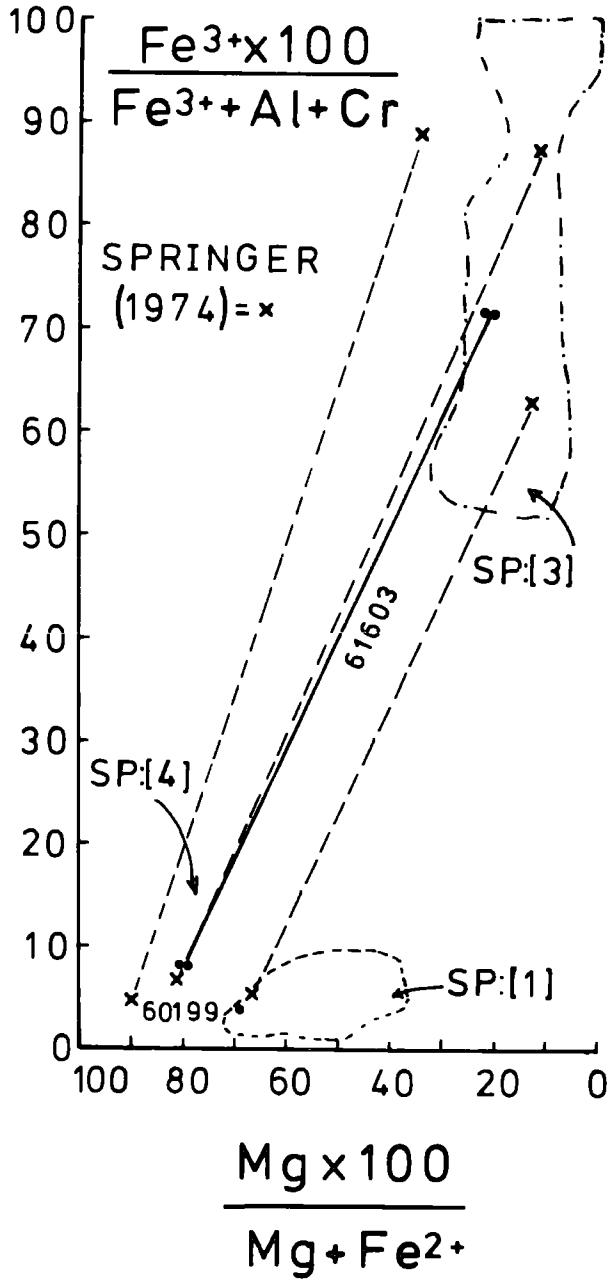

Figure 7.5 A spinel ratio plot, showing co-existing ferritchromit, spinel (3), and green spinel (4). Additional data, from Springer (1974), is also shown.

structure. Intermediate stages appear to be unstable, and they must react with chlorite, the only available Al rich phase, to produce a new Al rich spinel (4). The process is indicated schematically in Figure 7.6 . The following reaction is inferred.

Ferritchromit + chlorite = Al Spinel + serpentine + magnetite

Muir and Naldrett (1973) found a miscibility gap between magnetite and hercynite end members in igneous ultramafic rocks from the Giant Nickel Mine in British Columbia. Two spinels, one enriched in Al^3 and Mg, and the other enriched in Fe^3, Ti and Ni exsolved on cooling of the body. The Blue River body shows no sign of spinel immiscibility, rather stability obtained by reaction, in a system of variable $f.O_2$.

7.4 Carbonitization

Samples 60159 and 60241 consist of carbonate pseudomorphs after regenerated olivine, in a matrix of talc, carbonate, and rare serpentine. This is further evidence for SiO_2 mobility, and for the loss of SiO_2 from the system. The carbonate pseudomorphs of magnesite, very often consist of a clear well crystalline outer margin, and a less well crystalline core. The inner margin between the two is sharp (Plate 7.11) and the outer rim probably represents carbonatized brucite.

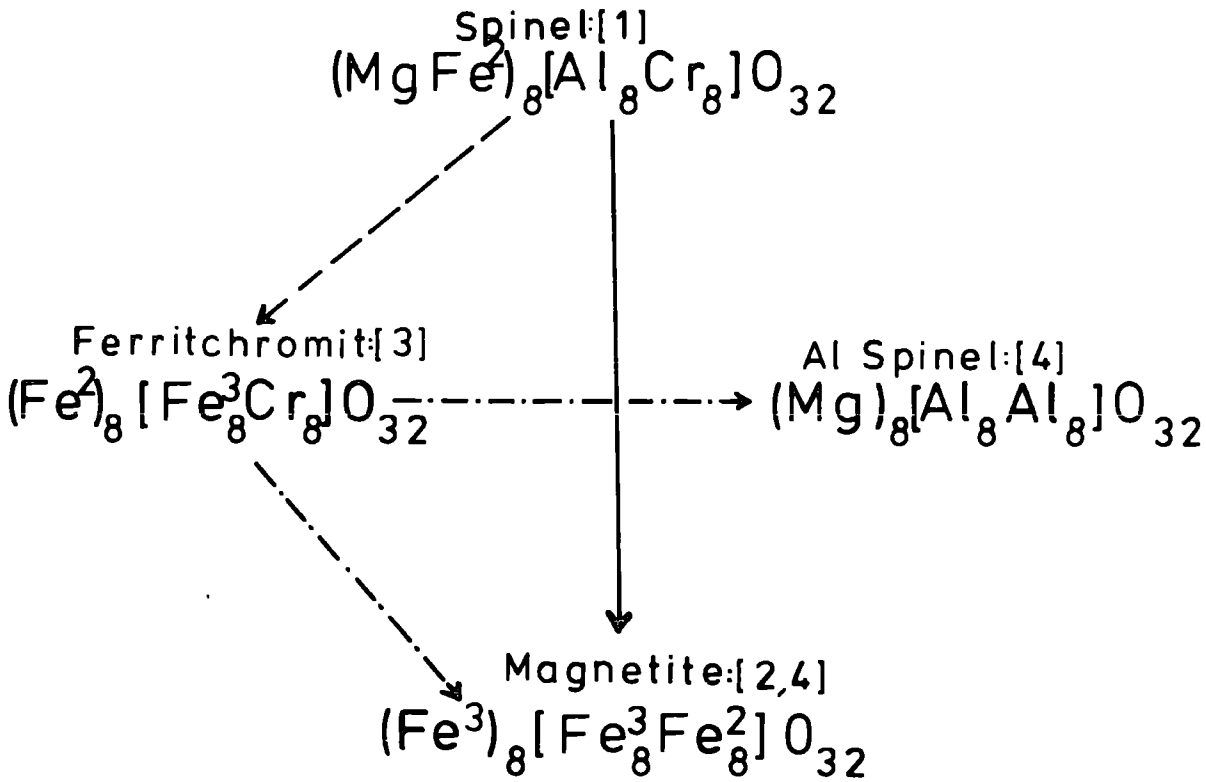

Figure 7.6 A schematic representation of the development of spinel between Stage I and Stage IV.

Carbonatization thus probably post-dates reserpentinization, at least in part, and it probably results from one or both of the following reactions

$$4 \text{ olivine} + 1H_2O + 5CO_2 = 1 \text{ talc} + 5 \text{ magnesite}$$

$$2 \text{ serpentine} + 3CO_2 = 1 \text{ talc} + 3 \text{ magnesite} + 3H_2O$$

These experimentally determined reactions depend largely on the mol % CO_2 in the fluid phase. According to Johannes (1969), serpentine is only stable so long as there is less than 3.0% CO_2, and more than 0.5% CO_2 in the fluid phase, at around 2 Kbars pressure. Below the lower figure serpentine alone is stable. The talc formed is well below the talc isograd, indicating formation by the carbonate producing reaction.

These two samples, 60159 and 60241 represent a localized occurrence of carbonatization, other samples display carbonate traces, Samples 60069 and 60907, but these are sporadic, and close to fault contacts, Figure 7.7

The pseudomorphous nature of the carbonate illustrates great SiO_2 mobility, although no SiO_2 veins were observed.

7.5 Rodingitization

The areal distribution of rodingite, and of partially rodingitized gabbro, correlates well with the distribution of present day serpentinite, Figure 2.1. Rodingite is found through Unit (2), where it is associated with

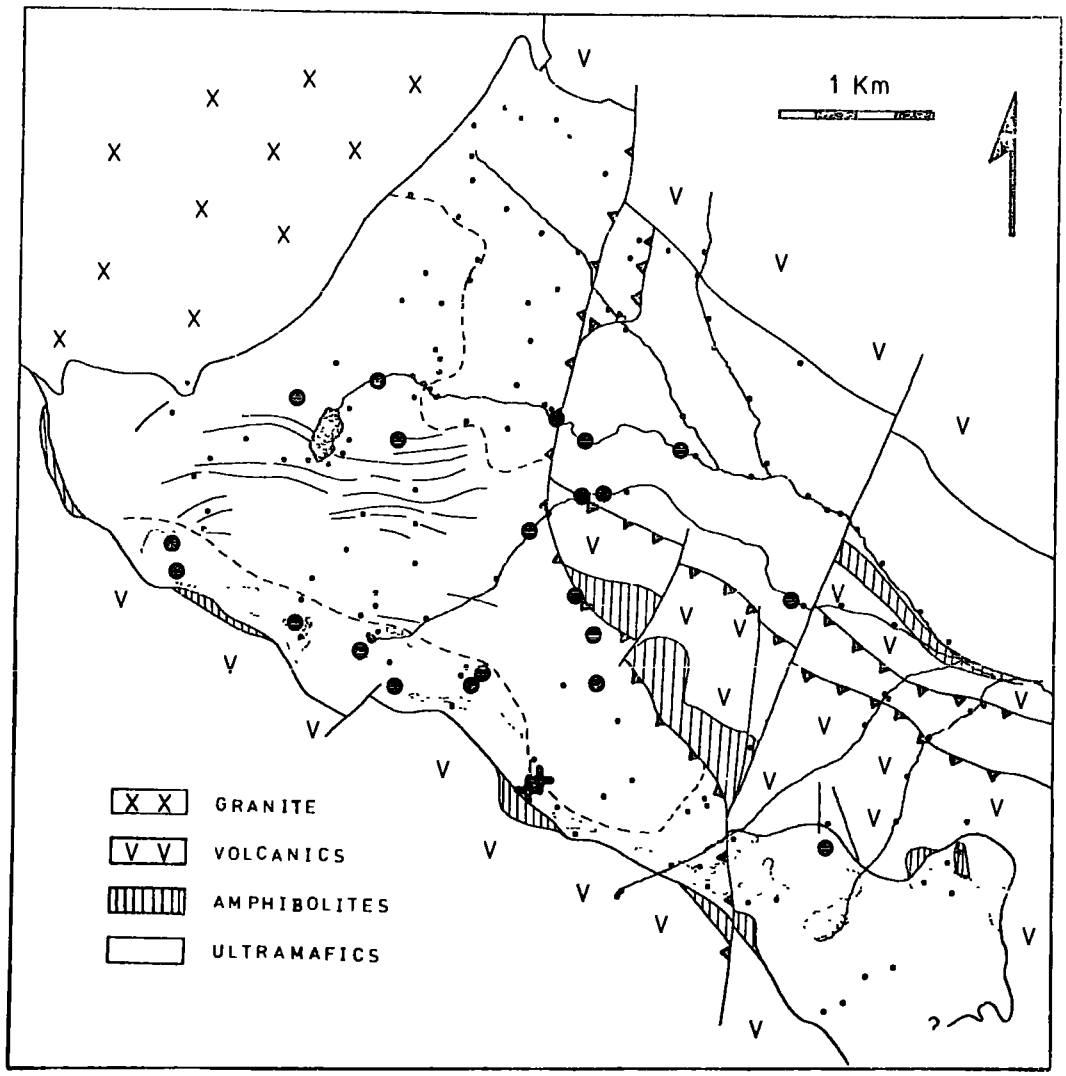

Figure 7.7 Distribution of samples containing a significant trace of carbonate, (closed circles). Completely carbonatized samples are shown as crosses.

serpentinized peridotite. It is also found along Spudusob, and Heazlewood Creeks, in Unit (3a). In this situation it is associated with serpentinized regenerated dunite. Along the western contact, in Unit (3a), gabbro is plentiful, but rodingite is minor. It occurs as an envelope around the gabbro, and it appears to be pervading, and veining, inward.

The rodingitization porcess is known to correlate with serpentinization, although the actual mechanisms and reaction relations are poorly known. The source of the Ca is also a matter of debate. The process could have taken place during Stage II or Stage IV. The western gabbros survived pervasive serpentinization, possibly because they lie in a Ca poor dunite host. The diopside lamellae in primary enstatite appear to have survived serpentinization during Stage II, which mitigates against one potential Ca source.

Most of the rodingite is assigned to Stage IV, because the mineralogy appears primary, and unaffected by metamorphism. The main mineral phases identified were hydrogrossular garnet, epidote, zoisite, vesuvianite, and diopside. In addition, veins of diopside, preh nite, pumpellyite and albite have been identified cutting gabbro, amphibolite and volcanic rock. The mineralogy was not studied in detail.

Diopside lozenges in serpentinites in Unit (2), are secondary in origin, Plate 4.3, and diopside was found to vein serpentine (4); which replaces metamorphic, olivine (3),

above Claim Jumper Creek. In addition, primary enstatites in Unit (1), and in Unit (2), Sample 60094, are corroded and partially replaced by a new generation of diopside. Relicts of enstatite (1), remain in a pseudomorph of diopside (Plate 3.13). Analyses are shown in Table 7.6, and displayed in Figure 3.11. This alteration process accounts for the slight excess of Ca in enstatites from Sample 60094.

Rodingite preferentially replaces feldspar, and relict pyroxene may remain as a stable phase. When carried to completion, the whole rock is converted into a hydro-grossular-vesuvianite assemblage.

The rodingitization process is thought to alter gabbro within serpentinite, and also amphibolite bordering serpentinite.

CHAPTER 8. VOLCANICS AND RELATED ROCKS

8.1 Introduction

In common with most "alpine" ultramafic bodies, the Blue River intrusion is spatially associated with basalt volcanic material. Like many others it is also associated with gabbro. The intrusion evidently metamorphoses pre-existing basalt, and there is nothing to suggest a direct genetic link between these two rock-types.

Bodies of gabbro appear to intrude the ultramafic body, and they are spatially restricted to the ultramafic intrusive. The relationships suggest that the gabbro is quite distinct from the volcanic material, and that it equilibrated with the primary ultramafic intrusive after emplacement. Ultramafic spinel (1) data, in Chapter 3, suggests equilibration between mafic and ultramafic rock-types, if not a genetic link between the two. The chemical similarities and differences between the two mafic rock types, might be expected to reflect this equilibration.

8.2 Sylvester Volcanics

Volcanic rocks, which crop out in the hanging wall of Heazlewood thrust, consist of massive, aphanitic, structureless, grey-green lava flows. Individual flows are rarely discernable, except where they are interbedded

with finely laminated tuff, argillite, or chert. Where the thickness is discernable, it ranges from 1-5m.

Most volcanic rocks show some sign of alteration, and many appear to be turbid and sheared. Original rock textures are preserved, although most samples have been altered to a greenschist facies mineralogy. The rocks are "spilites", as described by Cann (1969).

Gabrielse (1963) subdivided the "greenstones" into three categories, based on the degree of alteration or "saussuritization". The various forms are gradational, and they display only a crude pattern in regional distribution. Least altered samples appear to be found away from the batholith contact.

Type (1) "greenstones", as defined by Gabrielse (1963), consist of a crystalloblastic rock containing the following assemblage:

"tremolite/actinolite-zoisite-clinozoisite-albite-chlorite-carbonate".

Type (2) "greenstones" are less altered. They consist of relict pyroxene, sodic plagioclase, chlorite and zoisite. Pyroxene phenocrysts are often rimmed by fibrous amphibole.

Type (3) "greenstones", as defined by Gabrielse (1963), are not found in the map area, (except in so far as they resemble contact amphibolite). They consist of medium grained metamorphic rocks with a diorite mineralogy, and

they include pegmatitic segregations of "diorite". The rock consists of turbid albite, quartz, chlorite, zoisite, and a porphyroblastic amphibole.

The three categories represent differing degrees of hydrothermal alteration and metamorphism. The differences may represent variations in water availability, grain-size pressure or temperature. Gabrielse (1963) suggests that there might be a positive correlation between the occurrence of the ultramafic intrusives, and the degree of alteration. The mineralogic similarities between basal content amphibolite at the Blue River intrusive, and Type (3) "greenstone" overlying the Zus Mt. intrusive, Figure 5.1, supports this view.

8.3 Gabbroic Intrusions

Sills, lenses, and dykes of fine to medium grained gabbro crop out along the western contact of the ultramafic body. Rodingite is found southeast of claim Jumper Creek, in Unit (2), and along Spudusob Creek, in Unit (3a).

Very little gabbro was found within the "core" region of the intrusive. One major dyke was found, Figure 2.1. This forms the lip of Ice Lake, and it runs discordant to the primary ultramafic foliation for a distance of around 1,700m. The dyke has been largely amphibolitized, and chilled contacts were not observed.

Gabbroic bodies along the western contact are similarly amphibolitized, at least as far south as Heazlewood Creek. These bodies also display an outer skin of rodingite, and they are veined by rodingite material. The amphibolite consists of altered plagioclase, fibrous green-brown pleochroic amphibole, (hornblende), and minor secondary quartz. No free chlorite was observed, and epidote and zoisite are restricted to the outer rodingite envelope.

This mineralogy suggests that hornblende hornfels facies conditions, discussed in Chapter 5, extended out as far as location point 61565, above Heazlewood Creek, Figure 2.3. This position is about equal to the level of the tremolite isograd in ultramafic rocks, Figure 5.4.

Below Heazlewood Creek, altered gabbro retains its original texture, and as in ultramafic rock, diopsidic pyroxene remains stable. Rodingite is again peripheral, and there is a suggestion of grain size increase from margin to core, within a gabbro body.

Relatively unaltered gabbro at the head of Claim Jumper Creek consists of a sub-ophitic to gabbroic textured assemblage, with a 1.5-2.0mm grain-size. The assemblage consists of a fresh but variable diopsidic-augite, albite, replacing plagioclase, granular epidote, and chlorite. Some samples show a minor amount of fibrous amphibole replacing

the pyroxene, but this is not extensive. This assemblage, excepting the relict pyroxene, suggests albite-epidote facies conditions in the outer aureole of the batholith, as discussed in Chapter 5.

The pyroxene appears to be a variable diopsidic-augite. It is locally twinned, and it is very often zoned. It has an extremely variable 2V ranging from around 30 to 65. Chemical analyses are given in Table 8.1, and are illustrated on a pyroxene quadrilateral, Figure 3.11. The pyroxene is low in Fe, and it converges on a composition not dissimilar to that of the ultramafic diopside (1). The chemical trend, as far as it is discernable, is towards Fe enrichment, and Ca depletion. The pyroxene stability contrasts with pyroxene instability, and alteration, in the volcanic suite.

The gabbro also contains what appears to be altered skeletal ilmenite, in addition to albite and chlorite. Probe data indicates that the albite is pure, around (An_5). Chlorite occurs as fibrous interstitial patches, possibly pseudomorphing an earlier phase. The chlorite appears to be "diabantite", Deer, Howie, and Zussman (1962), analyses are shown in Table 8.2. In composition the chemistry is quite distinct from that found in the ultramafic rock, the chlorite is Fe-rich and oxidized. It has an Mgx100/Mg+Fe ratio of 46.

8.4 Magma Chemistry

Samples of volcanic and gabbroic rock were analysed using an X-ray fluorescence technique. Major element oxides, minor element concentrations, and "CIPW" norms are shown in Table 8.3, 8.4. These refer to volcanic and gabbroic rocks respectively. The FeO content was determined using a wet chemical metavanadate method, Wilson (1955). The total Fe content, determined by X-ray fluorescence, has been redistributed accordingly. Oxides have been recalculated to 100%, to negate the influence of a variable and unknown volatile content.

The analyses should be treated with caution, as all rocks show some hydrothermal alteration. The volcanics are "spilites", and as shown by Cann (1969), they are liable to be depleted in Al_2O_3 and CaO. Similarly gabbros are susceptible to alteration, and the presence of rodingite is an illustration of their susceptibility to Ca metasomatism.

The major element analyses, shown in Tables 8.3 and 8.4, indicate that both magma types fall within a restricted range of basalt composition. The volcanic suite is slightly more variable than the gabbro. The volcanic analyses are similar to a single Type (2) basalt analysis quoted by Gabrielse (1963). The analyses show a large degree of scatter, and differentiation trends are not convincing.

The combined alkali plot, Figure 8.1, shows that both

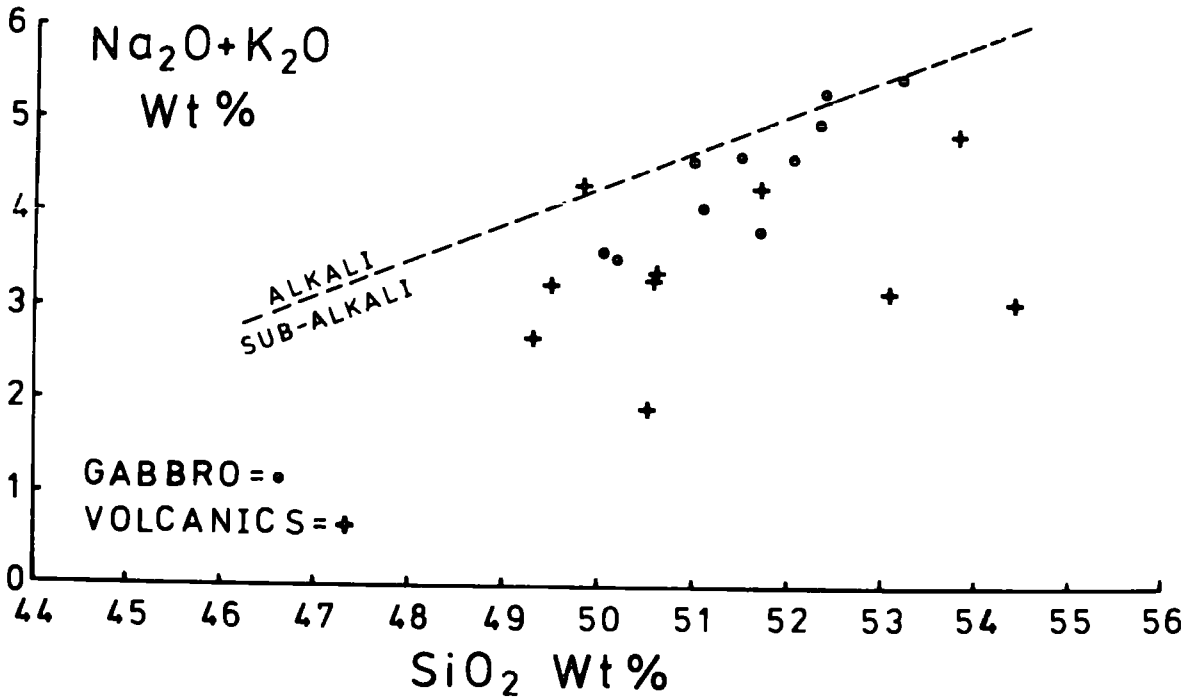

Figure 8.1 Total alkali v SiO_2 plot, showing the alkali-subalkali basalt divide proposed by MacDonald (1968).

populations lie below the alkali-sub alkali divide proposed by MacDonald (1968). The alkalis and in particular the K content, are low.

Engel (1965, 1971), and Cann (1971) describe a number of chemical characteristics which differentiate between present day "ocean floor basalt" and continental basalt. These include enrichment in CaO, Al_2O_3 and Na/K ratio, and a reduction in the K_2O and TiO_2 content. The two magma types are both compatible with an ocean-floor origin.

Cann (1971) notes that superficial oxidation will distort the normative mineralogy. He suggests that norms should be calculated with all Fe considered as FeO. This is a slight overcorrection.

Figure 8.2 shows the normative mineralogy plotted after converting Fe to FeO. The gabbros are all olivine normative, as are many of the volcanics. Olivine was not noted in either rock-type, but it is susceptible to alteration. The two populations contain roughly the same proportions of pyroxene, olivine and feldspar. The proportions of normative hypersthene and diopside are extremely erratic, Tables 8.3, 8.4.

The trace element data is also erratic. Some samples appear to be enriched in Ba and Sr, and as such they display "alkali" affinities. These elements are relatively mobile, and this may just reflect redistribution during hydrothermal alteration.

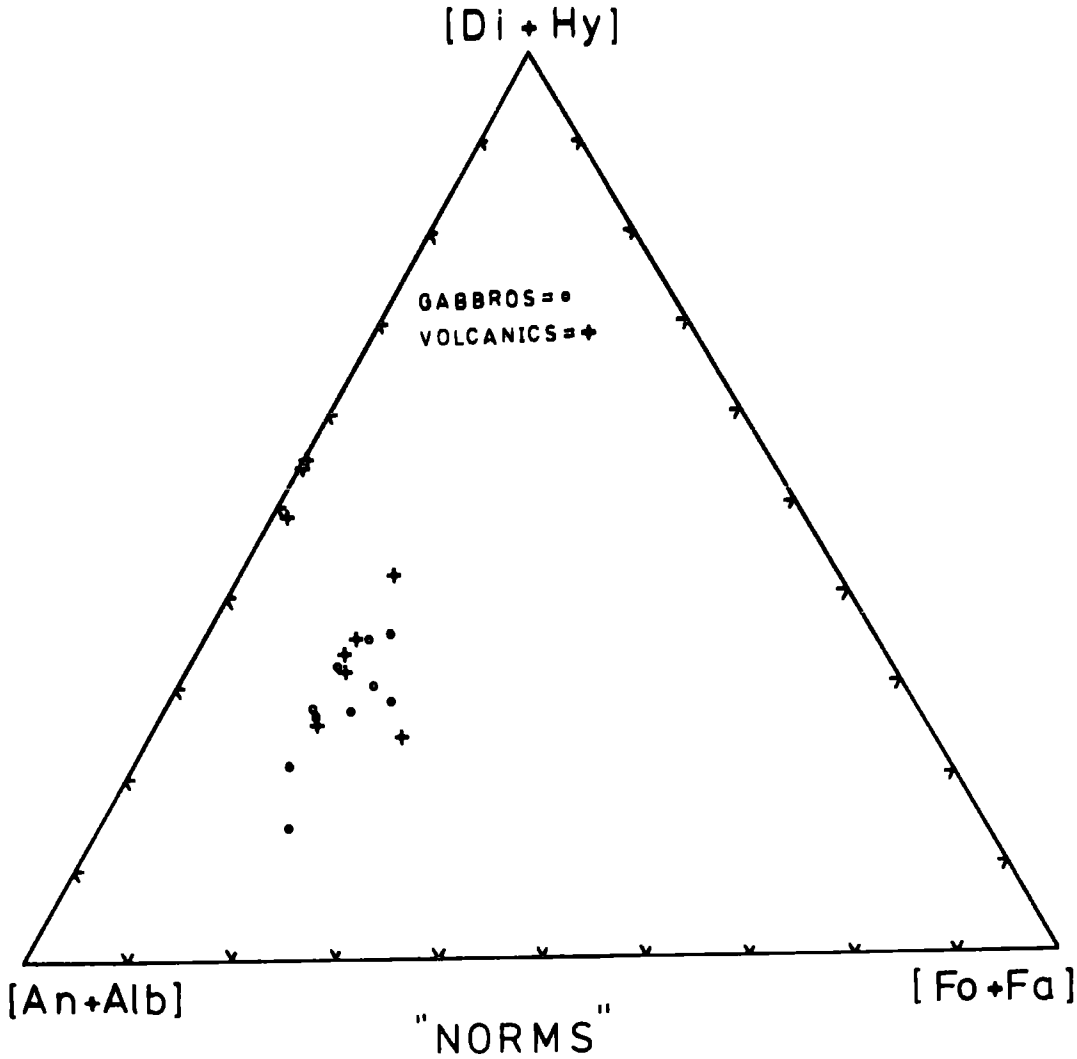

Figure 8.2 Normative proportions plot, showing the proportions of pyroxene, feldspar, and olivine, in volcanic rocks and gabbros. All the Fe is taken as FeO.

Pearce and Cann (1971, 1973) have developed an empirical discrimination technique, based on the comparatively immobile elements Ti, Zr, and Y. They present three plots which discriminate between suites of rocks from known geotectonic environments. Using these plots it is possible to compare data, and infer a likely geotectonic environment for an unknown. They subdivide basalt populations in the following manner:

1. Within Plate Basalts (Continental and Ocean Island).
2. Ocean Floor Basalts (Tholeiitic and Alkali).
3. Low K Tholeiites (Volcanic Arc Basalts).
4. Calc-Alkali Basalts (High K Basalts).

Figure 8.3 discriminates against "Within Plate Basalt" on the basis of Y content. Both suites lie within the field of "Ocean Floor Basalt", but as there is some overlap from the other two fields, this is not distinctive. Figure 8.4 shows that the Ti and Zr content discriminates against "Calc-Alkali Basalts", but it does not preclude a "Low K Tholeiite" origin. The remaining plot, Figure 8.5, uses Sr, which is probably remobilized. It is thus unable to discriminate between the two remaining fields. Sr appears to concentrate in the gabbro.

The data suggests that there are no major differences between Sylvester Volcanic Magma, and the magma that

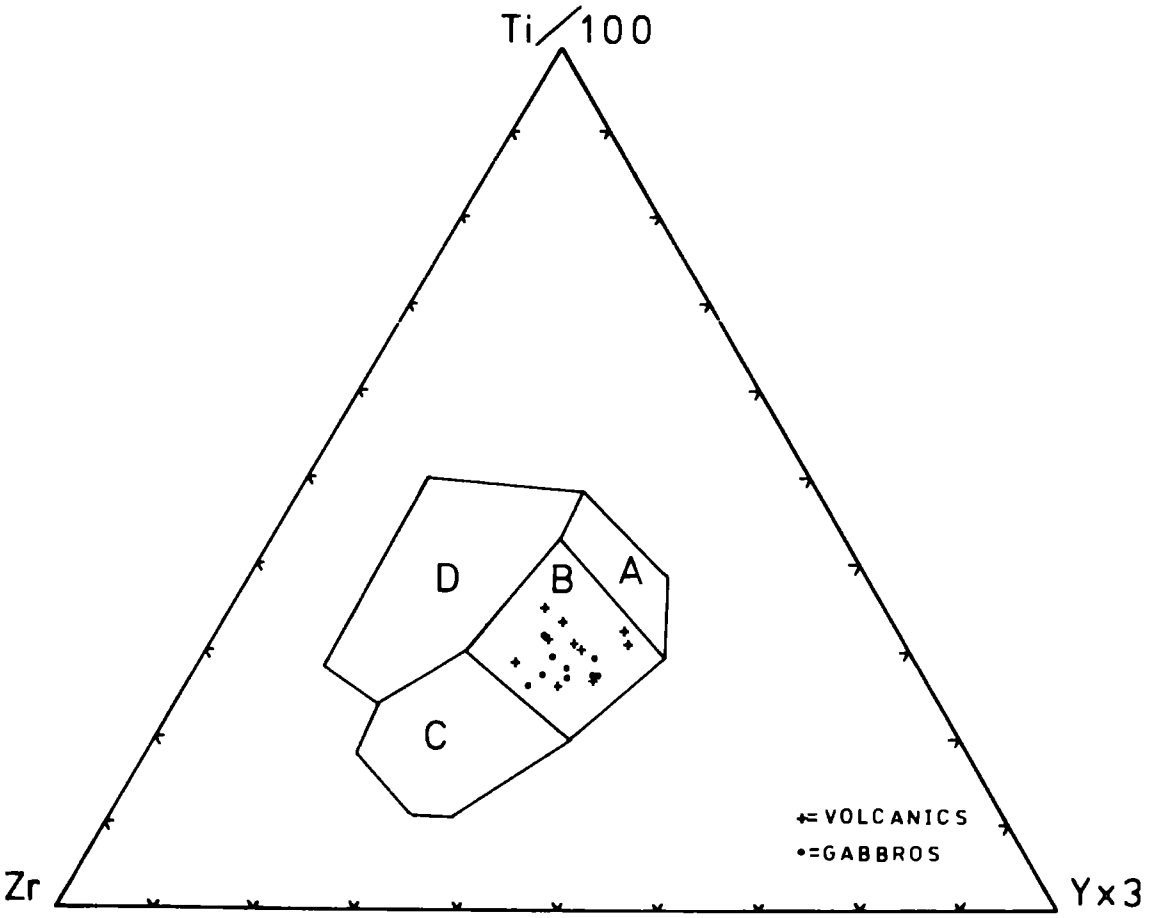

Figure 8.3 Trace element discrimination plot, from Pearce and Cann (1973), within Plate Basalts=D, Low K Tholeiites=A+B, Calc-alkali Basalts=C+B, and Ocean Floor Basalts=B.

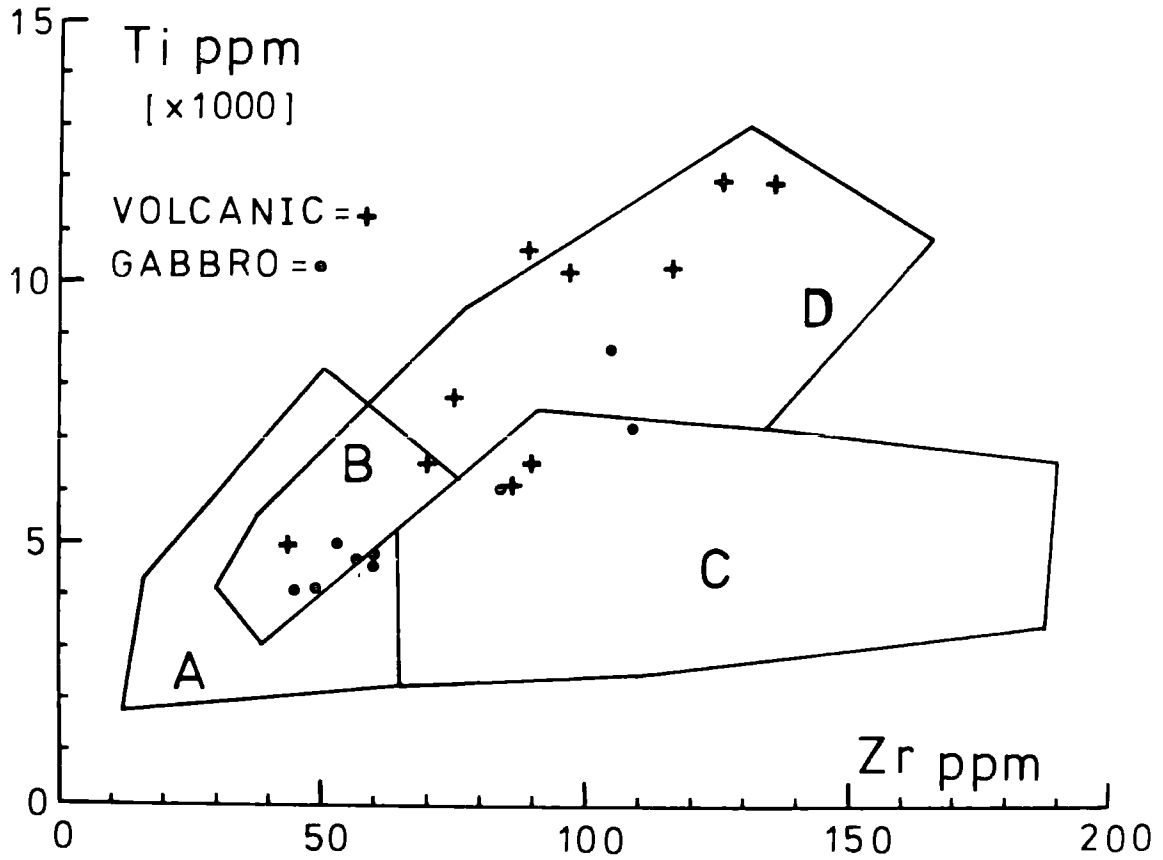

Figure 8.4 Trace element discrimination plot, from Pearce and Cann (1973). Ocean Floor Basalts=D+B, Low K Tholeiites=A+B, Calc-alkali Basalts=C+B.

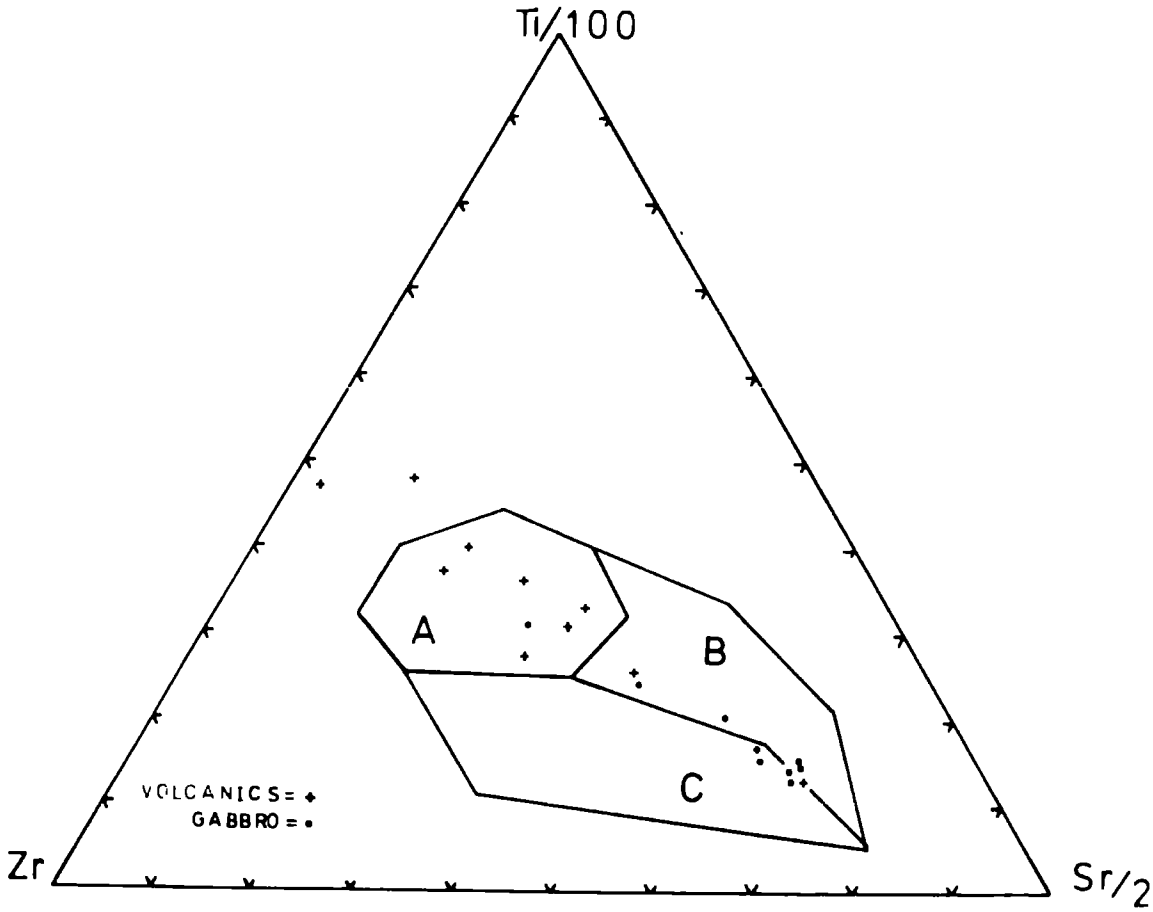

Figure 8.5 Trace element discrimination plot, from Pearce and Cann (1973). Ocean Floor Basalts =C, Low K Tholeiites=A, and Calc-alkali Basalts=B.

segregated out of the peridotite assemblage. They appear, on balance, to resemble tholeiitic olivine basalts, with "Ocean Floor Basalt" affinities.

8.5 Contact Amphibolite

The contact metamorphic aureole noted by Gabrielse (1963), was described in a fair amount of detail by Wolfe (1965, 1967). He presents data on a section across the aureole; as it is exposed along Claim Jumper Creek. This section was re-examined, and the data given by Wolfe appears to be essentially correct. The section is summarized in Table 8.5, from Wolfe (1967).

In common with other aureoles; and amphibolites described from the borders of ultramafic bodies, Green (1964b), Smith and MacGregor (1960), Pamic et al. (1973); the amphibolites are crystalloblastic to nematoblastic, with a pronounced foliation parallel to both the ultramafic contact, (Plate 2.1), and volcanic bedding.

There are two parts to the aureole, an inner zone in which feldspar is reduced, and the amphibole is colourless, and an outer zone, which starts approximately 17m from the contact. This consists of a brown-green pleochroic hornblende, with interfoliated albite, and sphene. The "gneissic-textured" outer amphibolite passes outward into unaltered Type (1) basalt, as defined by Gabrielse (1963).

Table 8.5

Contact Amphibolite

Claim Jumper Creek Section*

Distance	Assemblage	Metamorphic facies
0'(0m)	Hornblende	Lower Amphibolite
2'(0.6m)	Hornblende-Grossular	" "
5'(1.5m)	Hornblende-Grossular-Zoisite	" "
50'(15m)	Hornblende-Zoisite-Albite(An_8) Sphene-Magnetite	Albite-Epidote-Amphibolite
150'(46m)	Hornblende-Albite(An_{10}) Epidote Sphene, Magnetite/pyrite.Quartz	Albite-Epidote-Amphibolite
400'(123m)	Hornblende-Albite(An_{12}) Chlorite-Epidote. Calcite-Sphene-Ilmenite.	Greenschist.

*Data from Wolfe (1967).

In the "inner aureole", the feldspathic component of the gneiss has been replaced by grossular, or hydrogrossular garnet, and the colourless amphibole is set in a matrix of garnet, chlorite and zoisite. This mineralogy is not dissimilar to the rodingite mineralogy, found where gabbros have been altered in serpentinite. It is thought, from the present study, that the "inner aureole" has been metasomatized; and that like gabbro, it has acted as a "sink" for Ca and Mg. It is thus not strictly metamorphic, and the contact P-T environment, on emplacement of the ultramafic body, is difficult to evaluate. Rodingitization is thought to proceed during serpentinization, and it may be significant that Mg mobility has been shown for the Stage IV reserpentinization process, (see Chapter 7).

Table 8.6, and Figure 8.6, show that the dark outer amphibolite is similar in composition to spilitic Sylvester Volcanic rock in Table 8.3. It also shows that the white inner amphibolite is appreciably enriched in MgO and CaO, and depleted in SiO_2 and FeO.

In spite of the metasomatism, the aureole is still attributed to dynamothermal intrusion of the ultramafic body.

The outer aureole contains a mineralogy suggestive of albite-epidote amphibolite facies metamorphism, Wolfe (1967). The inner aureole is albite free, and pre-existing feldspar

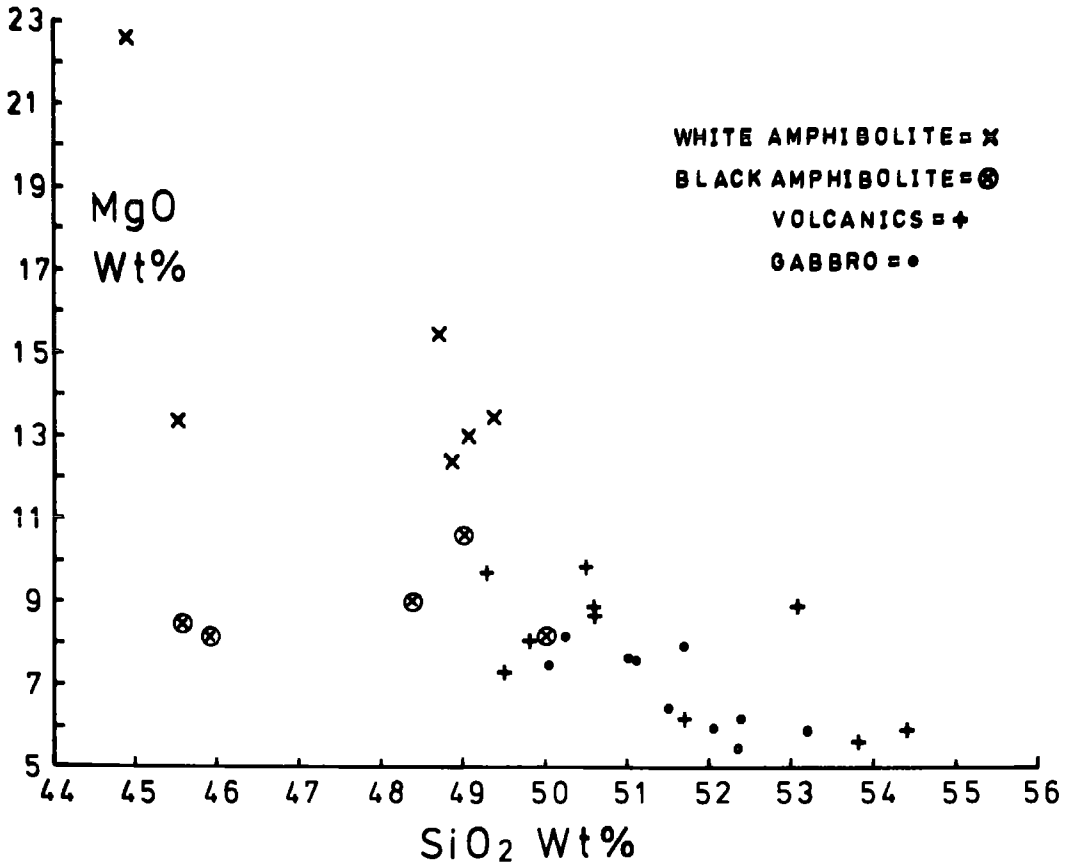

Figure 8.6 Oxide variation plot, showing an increase in MgO in the inner, "white" amphibolite.

has been rodingitized. It is inferred that the feldspar was plagioclase, and it is on this basis, and not the presence of hydrogarnet, that the metamorphism is assigned to the Lower Almandine Amphibolite facies. The contact temperature must therefore have been in excess of 550°C, and a figure of 600-650°C is more realistic for the actual contact.

Wolfe considered that metasomatism occurred during initial metamorphism, but later rodingitization is favoured in this study.

CHAPTER 9. CONCLUSIONS

9.1 Conclusions

The results of the present study confirm many of the observations made by Gabrielse (1955, 1963), and Wolfe (1965, 1967). The study goes further, and it attempts to integrate the various peculiarities of the Blue River Ultramafic body.

The data indicates that the body is a high temperature "alpine" peridotite. Field relationships suggest that hot peridotite was intruded into relatively cold basalt, with the consequential development of a dynamo-thermal metamorphic aureole. The relationships also suggest that only minor structural reorganization has occurred subsequently; and the body retains many of its "primative" structural relationships, dating to the time of emplacement. This is inspite of the fact that the whole greenstone assemblage now overlies an enormous thickness of miogeosynclinal sediment and carbonate.

Bodies of relatively undeformed gabbro are found along what is inferred to be an original contact. The gabbro is restricted to the ultramafic body, and it is concluded that it was intruded into the basalt assemblage with the peridotite. It probably segregated into pods along the cooler margins of the body, at some stage after emplacement. The mafic-ultramafic assemblage probably equilibrated together, in

isolation, in the basalt sequence.

The peridotite is flow banded into dunite and harzburgite layers. These display a slight compositional difference. Excess Al is a feature of harzburgite. Mineral analyses indicate that the enstatite Al content is fixed, and the variable Al excess above that required for enstatite, is found in the spinel phase. Dunites have Al poor spinels, which are compatible with a derivation from a basalt magma. The spinels display a continuous Al depletion trend from harzburgite to dunite, and it is thought that this represents incomplete segregation of Al out of an original Al rich enstatite phase, in the primary peridotite. Enstatite attained a fixed, P-T controlled composition, by partitioning Al into magma, or into spinel.

Chemical analyses indicate that the host basalt composition is similar to that of the segregated gabbro. Both have a composition compatible with their being tholeiitic "Ocean Floor Basalts".

Temperature estimates, based on thermodynamic data on coexisting mineral pairs, suggest an intrusion temperature of around 1200°C, and a basalt segregation temperature of around 1000°C. The olivine deformational fabric, suggests that the ultramafic body was largely consolidated, and subject to stress at temperatures in excess of 1000°C.

The ultramafic body evidently underwent a period of marginal serpentinization, as metamorphic olivine has been identified as being formed at a later stage. The serpentinite formed, is inferred to have contained a brucite component, as this was evidently involved in the metamorphic reaction.

The Cassiar batholith truncates the Blue River Ultramafic body, and isograds representing the incoming of metamorphic olivine, tremolite, olivine with talc, and enstatite, have been established parallel to the batholith contact. The olivine and enstatite reactions conform to the experimentally determined reactions proposed by Bowen and Tuttle (1949). Experimental work suggests that the batholith contact reached a temperature of 580-600°C. This is based on the presence of enstatite, and of hornblende and anthophyllite, and on the composition of metamorphic chlorite. The outer olivine isograd is thought to represent a temperature of 325-340°C, based on experimental work on the brucite based, "olivine regeneration" reaction, and also on experimental serpentine dehydration work.

Olivine regenerated by the low temperature reaction evidently formed point nucleated porphyroblasts, in serpentinite. Early olivine is FeMn rich, and later olivine is MgNi rich. Porphyroblasts are zoned, and the matrix serpentine is modified by reaction. Brucite plays an important part in the process, perhaps because it is relatively mobile, and not silicate structured.

Metamorphism involves massive dehydration, and consequent volume decrease. It also marks a change from a ductile to a brittle state. This may aid tectonism, and a major fault appears to have truncated the body, in the waning stages of metamorphism.

The metamorphism was accompanied by oxidation, and the effect of increased fO_2 on primary spinel has profoundly altered the distribution of the trace elements Ni and Mn. On oxidation the spinel releases Al, which enters serpentine to become "chlorite", and Fe, (with minor Ni and Mn), enters the spinel structure to form "ferritchromit" and chromium magnetite. Above the talc-olivine isograd appreciable Fe is soaked up by the spinel, and the olivine ceases to be zoned. Olivine reaches a maximum forsterite content of Fo_{95}.

The oxidation process is not restricted to areas of metamorphosed serpentinite, similar reactions occur in primary peridotite. Harzburgite Al rich spinels appear to be more susceptible to oxidation than dunite, Al poor spinels.

During the waning stages of metamorphism the body was faulted, and antigorite serpentine was formed. The distribution of antigorite is related to the Cassiar batholith contact, and it is defined by a retrogressive isograd.

Pervasive serpentinization to lizardite and chrysotile occurred at a later stage. It bears no relation to the

batholith. Euhedral, zoned, metamorphic olivines are entirely replaced by serpentine and brucite. Volume for volume replacement seems irrefutable. Reserpentinized rocks show a marked concentration of brucite, particularly surrounding the replaced olivines. This is evidence for cation mobility. Some euhedral serpentine pseudomorphs after olivine are replaced by carbonate. The carbonate replaces both the serpentine pseudomorph, and the brucite envelope. This again reflects cation mobility.

Reserpentinization involves a drop in fO_2, and a return to the oxidation state operative prior to oxidation. Ferritchromit, with a composition approaching magnetite, appears to be unstable, and it reacts with chlorite to form a green spinel rich in Al. This is not dissimilar to the original primary spinel.

In general terms, the primary assemblage, which makes up the Blue River Ultramafic body, has a bearing on the composition of the Upper Mantle, from which it was almost certainly derived. It has a bearing on the ultimate origin of "alpine" peridotite, and on the equilibration processes which occur between Upper Mantle peridotite, and magma, formed by partial melting of some unspecified parent.

The metamorphic study has established the existence of all three of the metamorphic reactions proposed by Bowen and Tuttle (1949). It illustrates the importance of brucite

as a mobile component during both metamorphism, and also serpentinization. The "serpentinization-regeneration" process is particularly significant in relation to geotectonics, as serpentine has been postulated as a significant phase in the lower crust and Upper Mantle, Hess (1955, 1965). If this is the case, then regeneration will be important during subduction, as a source of water, density change, and change in structural state, from ductile to brittle.

The influence of oxygen is important, particularly with respect to the distribution of Ni, an economically significant element. This is not readily taken back into the olivine structure, in the presence of free sulphur.

Plate 3.4 Photomicrograph: Primary olivine showing fractures parallel to original strain lamellae. Antigorite "feathers" are overprinted onto both olivine and intergranular serpentine, Sample 61615. Cross Nicols. Field width 1.7mm.

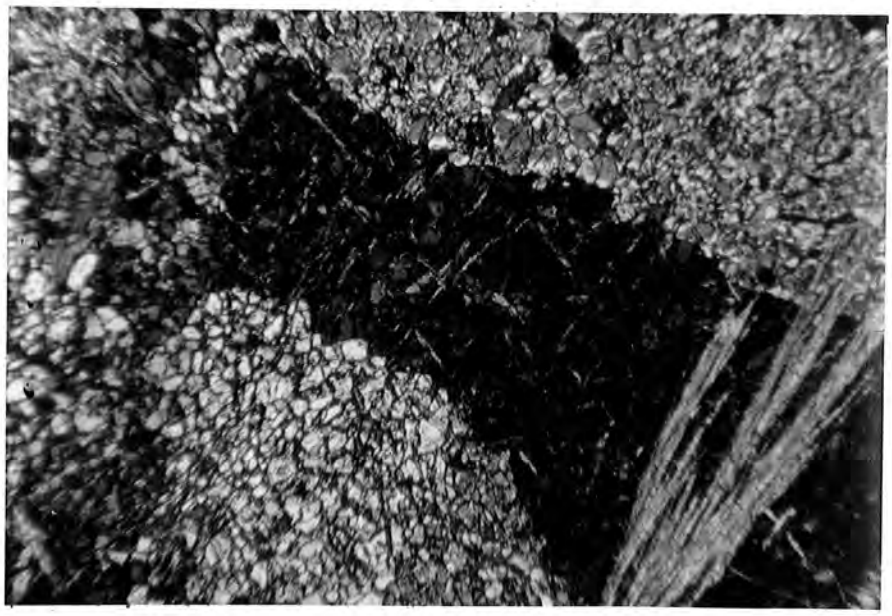

Plate 3.6 Photomicrograph: shattered primary olivine, showing intergranular Al serpentine, and anthophyllite blades, Sample 60196. Crossed Nicols. Field width 1.7mm.

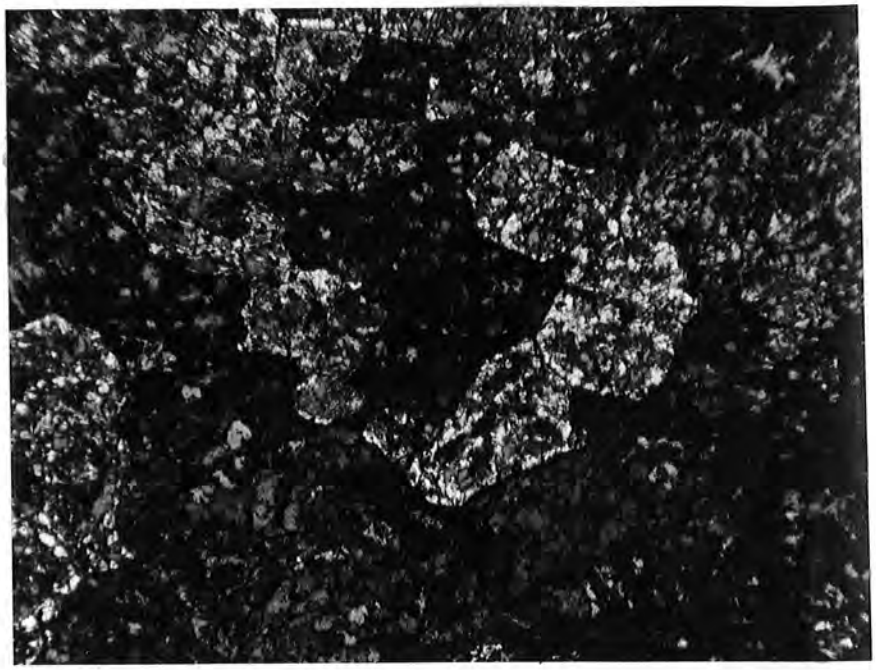

Plate 3.7 Photomicrograph: Primary olivine, granules coated with metamorphic olivine, Sample 60186. Much of the original olivine has been replaced by antigorite. Crossed Nicols. Field width 1.7mm.

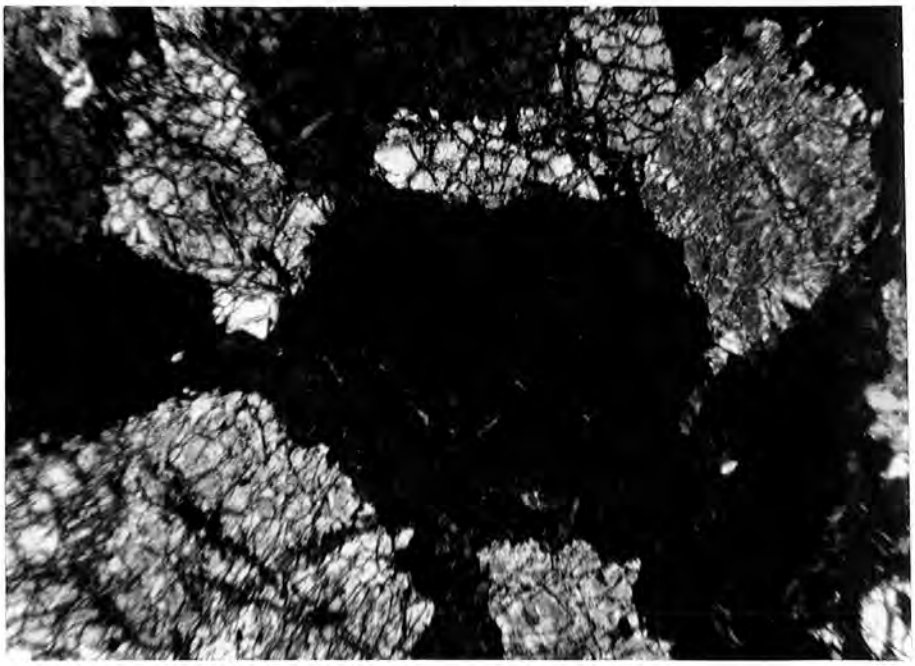

Plate 3.8 Photomicrograph: Metamorphic olivines with a granular texture, Sample 61623. Crossed Nicols. Field width 1.7mm.

Plate 3.9 Photomicrograph: Strained, deformed, and shattered enstatite in primary peridotite, Sample 60163. Crossed Nicols. Field width 1.7mm.

Plate 3.10 Photomicrograph: Relict diopside exsolution blebs in a bastite pseudomorph in Sample 60067. Crossed Nicols. Field width 1.7mm.

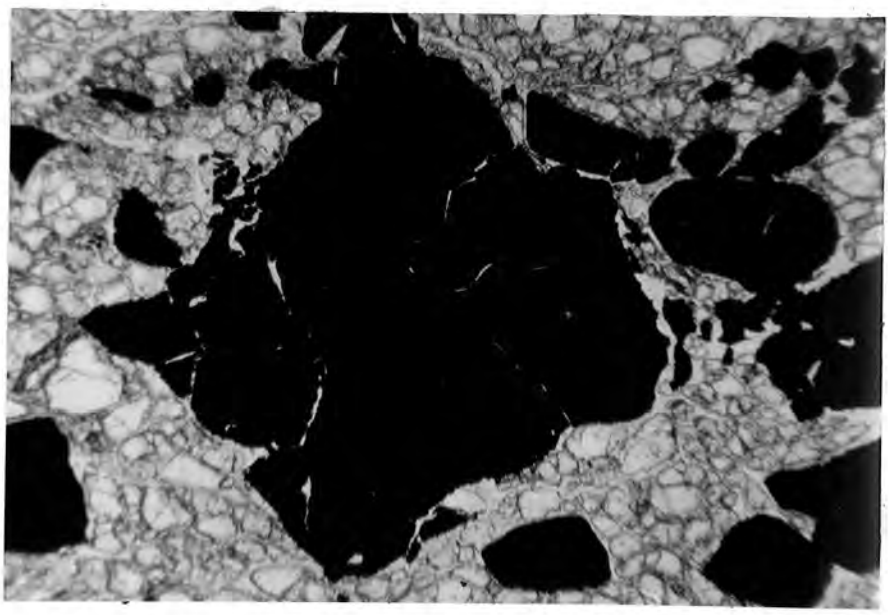

Plate 3.11 Photomicrograph: Irregular, fractured, spinel enclosed by granular primary olivine, and serpentine, Sample 60237. Plane polarised light. Field width 1.7mm.

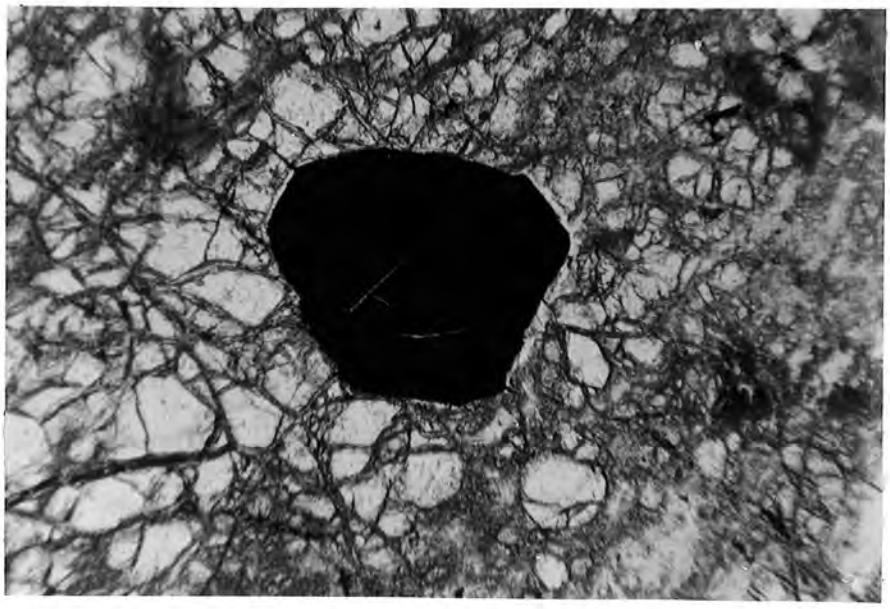

Plate 3.12 Photomicrograph: Euhedral primary spinel enclosed in granular olivine (1), Sample 60186. Plane polarised light. Field width 1.7mm.

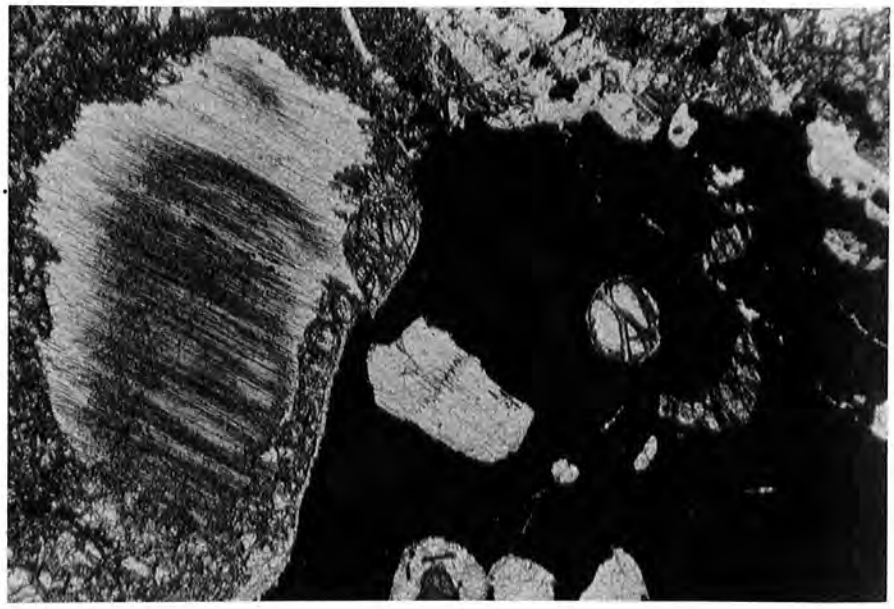

Plate 3.13 Photomicrograph: Irregular, poikilitic, primary spinel in Sample 60094. The spinel encloses round primary enstatite. Plane polarised light. Field width 1.7mm.

Plate 4.2 Photomicrograph: A bastite pseudomorph after enstatite in Sample 60092. Magnetite replaces diopside exsolution lamellae. The enclosing serpentinite is mesh textured. Crossed Nicols. Field width 1.7mm.

Plate 4.3 Photomicrograph: Bastite pseudomorphs after enstatite (1). The enstatite cleavage is retained. The birefringent lozenges are of diopside (4), Sample 60041.

Plate 4.4 Photomicrograph: Chlorite formed at the expense of bastite, in mesh textured serpentinite, in Sample 60084. Crossed Nicols. Field width 1.7mm.

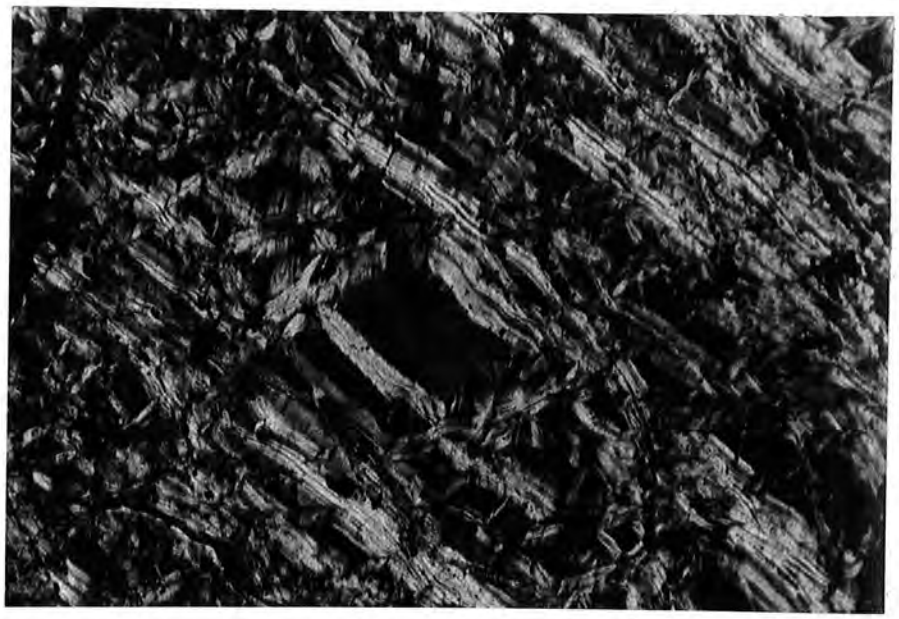

Plate 4.5 Photomicrograph: Mesh textured serpentinite, showing ribbon serpentine, and a serpentine mesh, displaying a weak hour-glass texture, Sample 60041. Crossed Nicols. Field width 1.7mm.

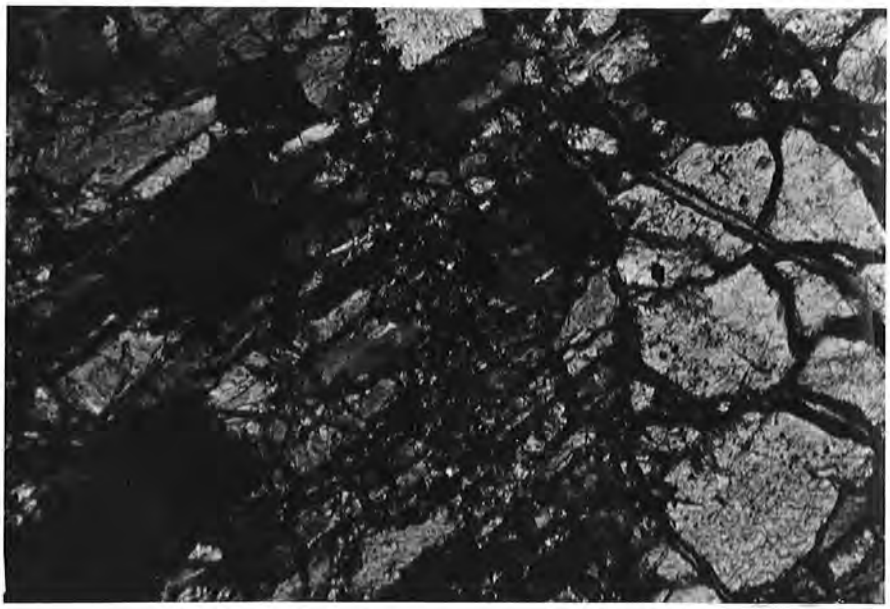

Plate 5.3 Photomicrograph: Olivine (3) pseudomorph after bastite, Sample 60174. Crossed Nicols. Field width 0.8mm.

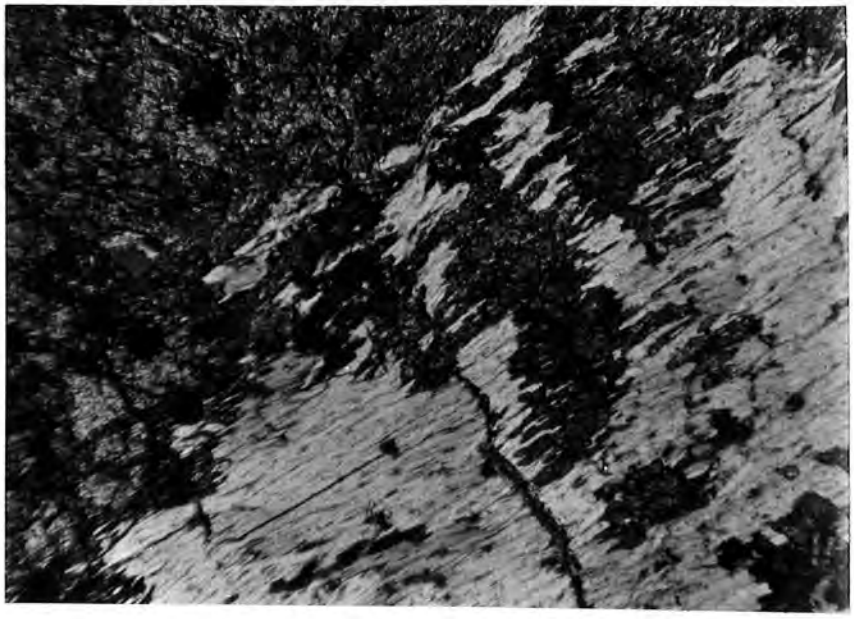

Plate 5.4 Photomicrograph: Lenticular granules of olivine (3), in a chlorite pseudomorph after bastite, Sample 60341. Crossed Nicols. Field width 0.8mm.

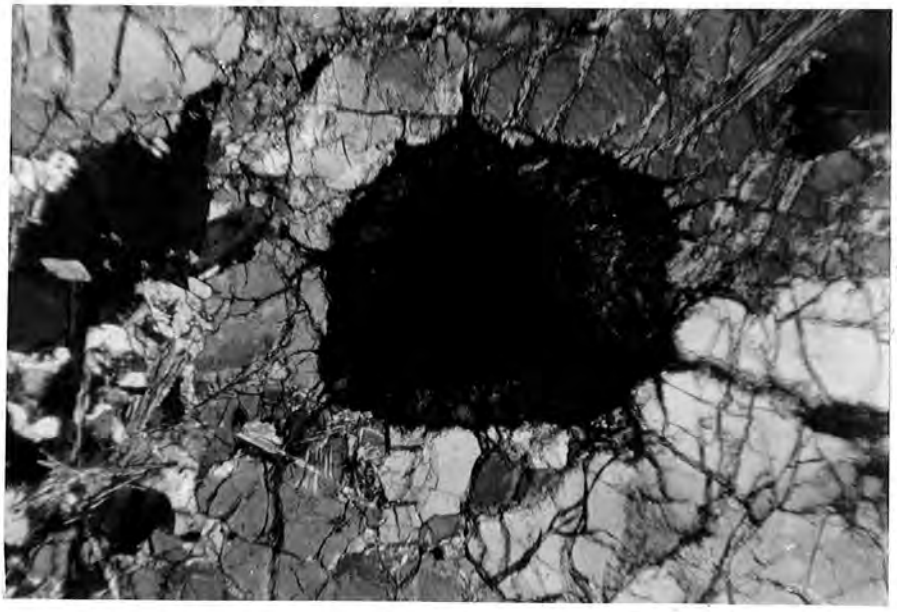

Plate 5.5 Photomicrograph: Primary spinel enveloped by a halo of Al serpentine. The halo is interstitial to granular olivine, from which it is developed, Sample 60185. Crossed Nicols. Field width 1.7mm.

Plate 5.6 Photomicrograph: Altered interstitial primary spinel, enveloped by Al serpentine, in Sample 60226. Crossed Nicols. Field width 1.7mm.

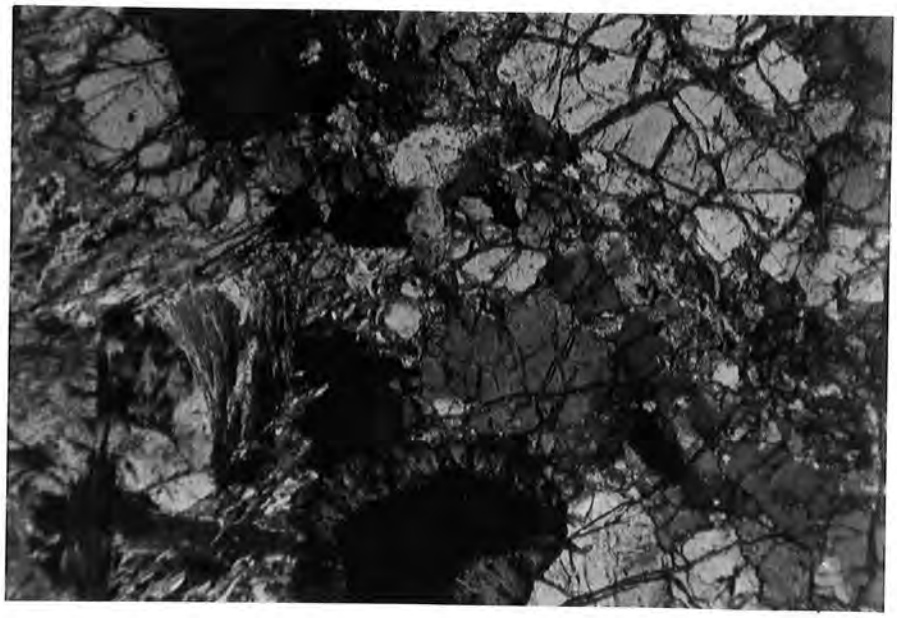

Plate 5.7 Photomicrograph: Altered peridotite in Unit (3c). Note the Al serpentine halo around the spinel, and the sheafs and blades of tremolite, overprinted on olivine (1), Sample 60184. Crossed Nicols. Field width 1.7mm.

Plate 5.10 Photomicrograph: Recrystallized chlorite enveloping an altered poikilic spinel, in Sample 60341. The halo is analogous to the Al-serpentine envelope shown in Plate 5.6. Crossed Nicols. Field width 1.7mm.

Plate 5.11 Photomicrograph: Metamorphic olivine (3) crystals in Sample 60157. Note the euhedral nature of the olivine outlines. Note also the enclosing modified matrix serpentine. Crossed Nicols. Field width 1.7mm.

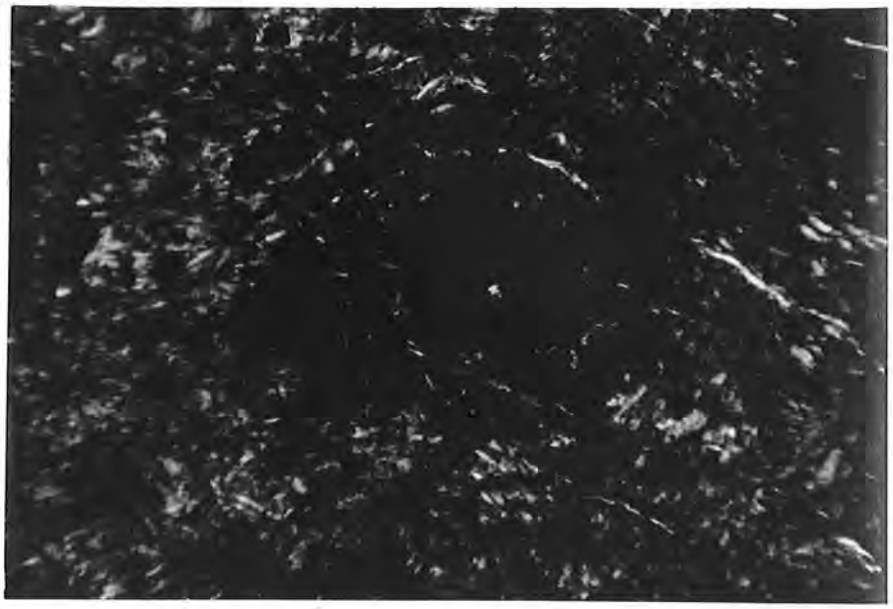

Plate 5.12 Photomicrograph: An irregular brucite enriched serpentine pseudomorph, after metamorphic olivine, Sample 60055. Crossed Nicols. Field width 1.7mm.

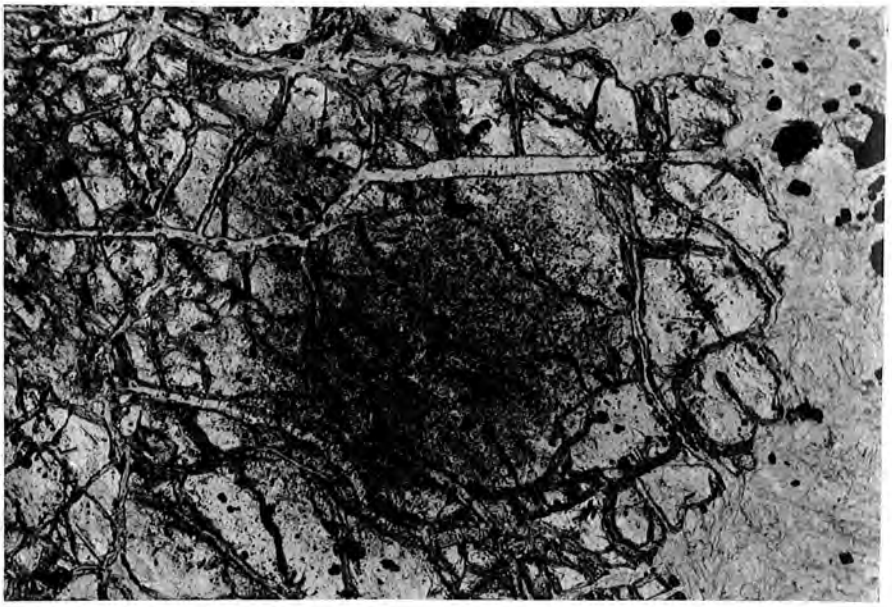

Plate 5.14 Photomicrograph: A single strongly cored crystal of olivine (3). Note the magnetite concentration in the crystal core, and the clear outer margin, Sample 60894. Plane Polarised light. Field width 1.0mm.

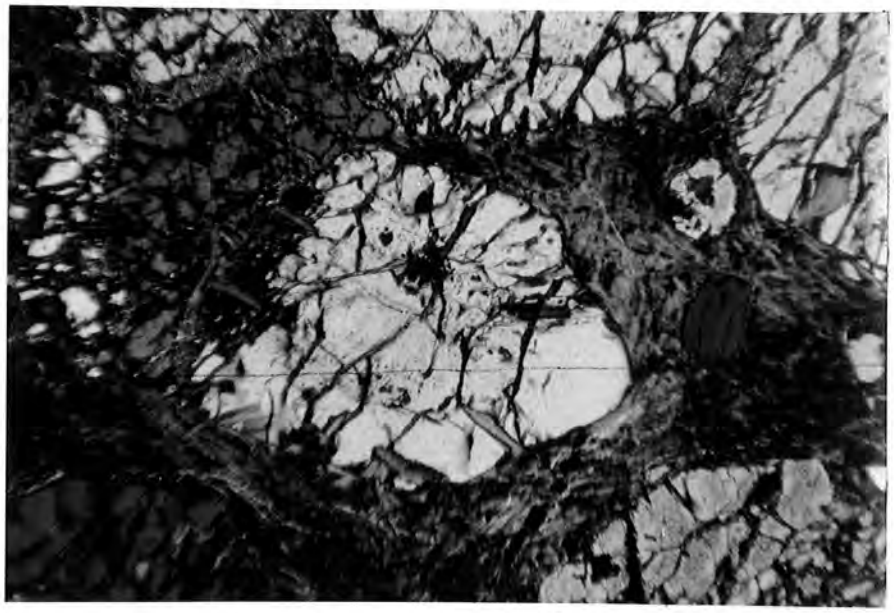

Plate 5.17 Photomicrograph: Metamorphic olivine (3) with a rounded euhedral outline. Note the weak core and the preferential growth into modified matrix serpentine, Sample 61632. Crossed Nicols. Field width 1.7mm.

Plate 5.18 Photomicrograph: Metamorphic olivine (3), as above, with preferential marginal growth into modified matrix serpentine, Sample 61632. Crossed Nicols. Field Width 1.7mm.

Plate 5.19 Slide photograph. Note the strongly cored olivines, and the concentration of cored olivine into trails, representing fractures. Note also the talc matrix serparating grains and clusters, Sample 60894. Plane polarised light. Field width 43.0mm.

Plate 5.20 Photomicrograph. Strongly cored olivine(3) in Sample 60157. Note the turbid core region, and the clear outer margin. Note also the modified matrix serpentine, replacement serpentine (4), and birefringent brucite along the interface between the two. Crossed Nicols, Field Width 1.7mm.

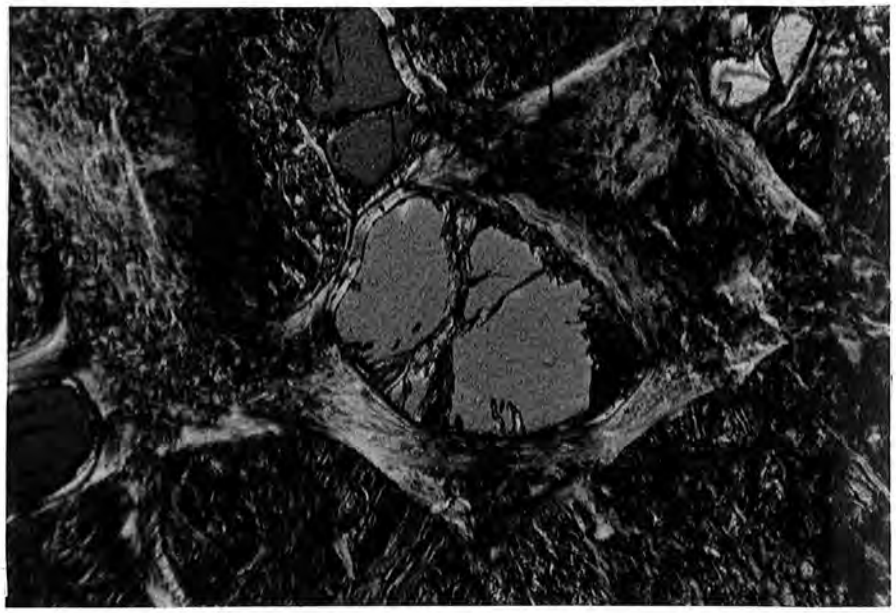

Plate 5.21 Photomicrograph: Fibrous modified matrix serpentine surrounding a marginal type olivine, in Sample 60157. Note the textural contrast with replacement serpentine (4). Crossed Nicols. Field width 1.7mm.

Plate 5.22 Photomicrograph: Recrystallized asbestos in Sample 61525. Note the magnetite partition inherited from asbestos. Crossed Nicols. Field width 1.7mm.

Plate 5.24 Photomicrograph: Tremolite blades imprinted on metamorphic olivine, in Sample 60227. Crossed Nicols. Field width 0.8mm.

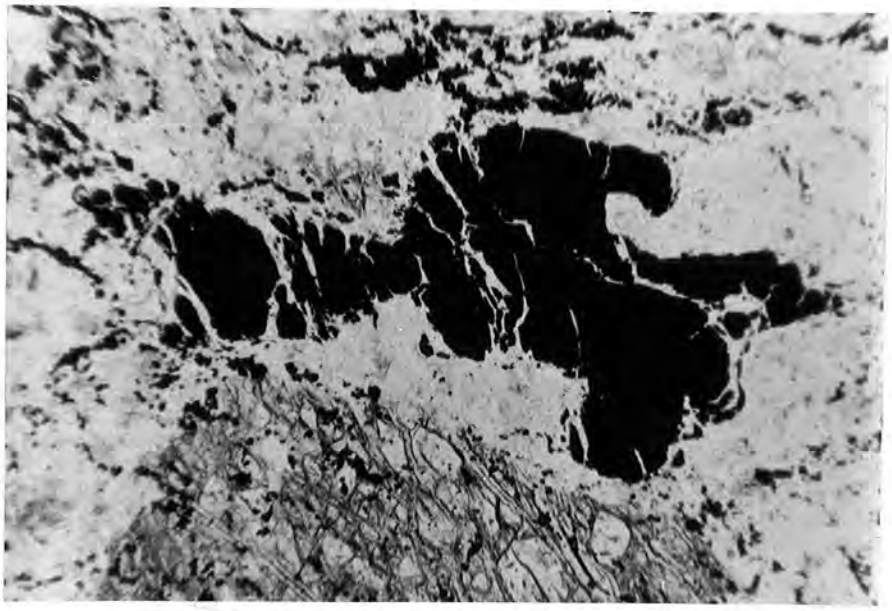

Plate 5.25 Photomicrograph: Fractured and altered spinel, now ferritchromit, surrounded by a matrix of talc, and Al serpentine in Sample 60133. Note that serpentine (4) is restricted to olivine (3). Plane polarised light. Field width 1.7mm.

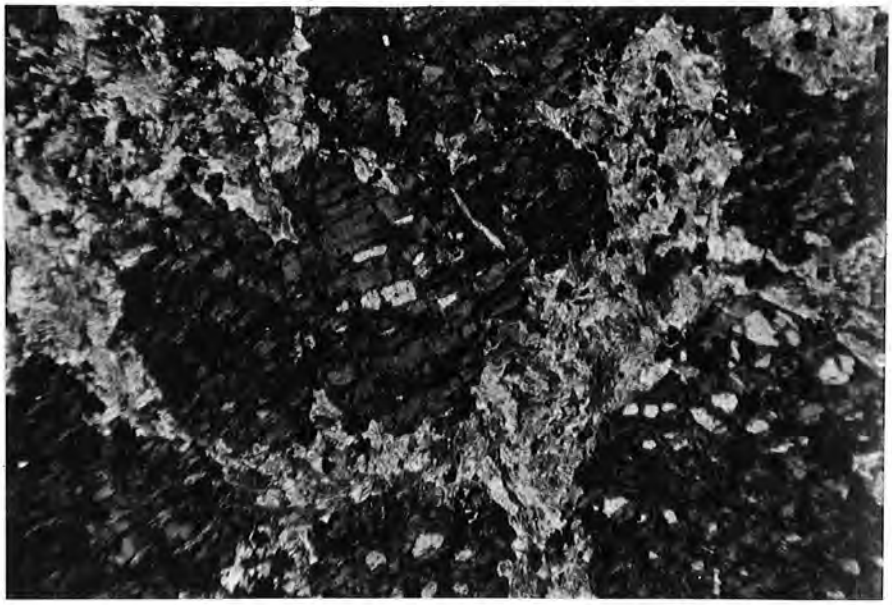

Plate 5.26 Photomicrograph: Serpentine (4) replacing olivine (3) in Sample 61598. Note the metamorphic olivine is enveloped in a matrix of talc and chlorite. Serpentine is restricted to the olivine. Crossed Nicols. Field width 1.7mm.

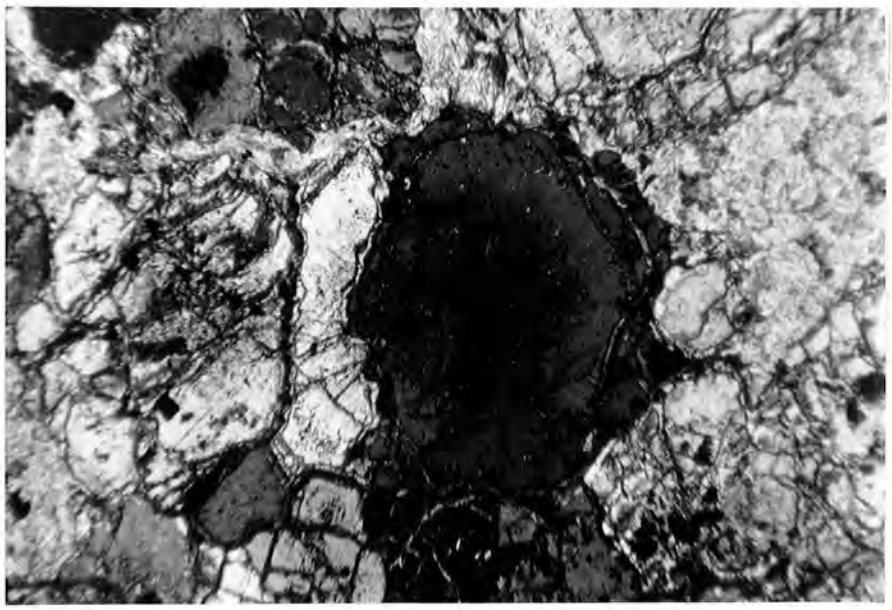

Plate 5.28 Photomicrograph: A single cored olivine in Sample 60894. Note the outer, clear, margin with a crystal defect, which is out of optical continuity. Crossed Nicols. Field width 1.7mm.

Plate 7.1 Photomicrograph: A mosaic of metamorphic olivine in Sample 60907, overprinted by feathers of antigorite serpentine. Crossed Nicols. Field width 1.7mm.

Plate 7.3 Photomicrograph: Feathery, antigorite replacing metamorphic olivine, in Sample 60107. Crossed Nicols. Field width 1.7mm.

Plate 7.4 Photomicrograph: Feathery antigorite and disseminated birefringent talc, in Sample 60180. Crossed Nicols. Field width 1.7mm.

Plate 7.5 Photomicrograph: Euhedral olivine (3), pseudomorphed by serpentine (4), and enveloped by a reaction halo of brucite and magnetite. Crossed Nicols, Field width 1.7mm.

Plate 7.6 Photomicrograph: A serpentine pseudomorph after olivine (3), in Sample 60102. The interface between modified matrix serpentine and retrogressive serpentine is enriched with brucite and magnetite. Crossed Nicols. Field width 1.7mm.

Plate 7.7 Photomicrograph: Granular spinel (4) surrounding a large altered primary spinel, in Sample 60143. Note the laths of chlorite associated with the spinel. Plane polarised light. Field width 1.7mm.

Plate 7.8 Photomicrograph: Granular spinel (4) cubes in recrystallized chlorite, Sample 61603. Crossed Nicols. Field width 1.7mm.

Plate 7.10 Photomicrograph: Recrystallized laths of talc and chlorite, forming a matrix to olivine (3), in Sample 60199. Light grey is talc, darker grey is chlorite. Crossed Nicols. Field width 1.7mm.

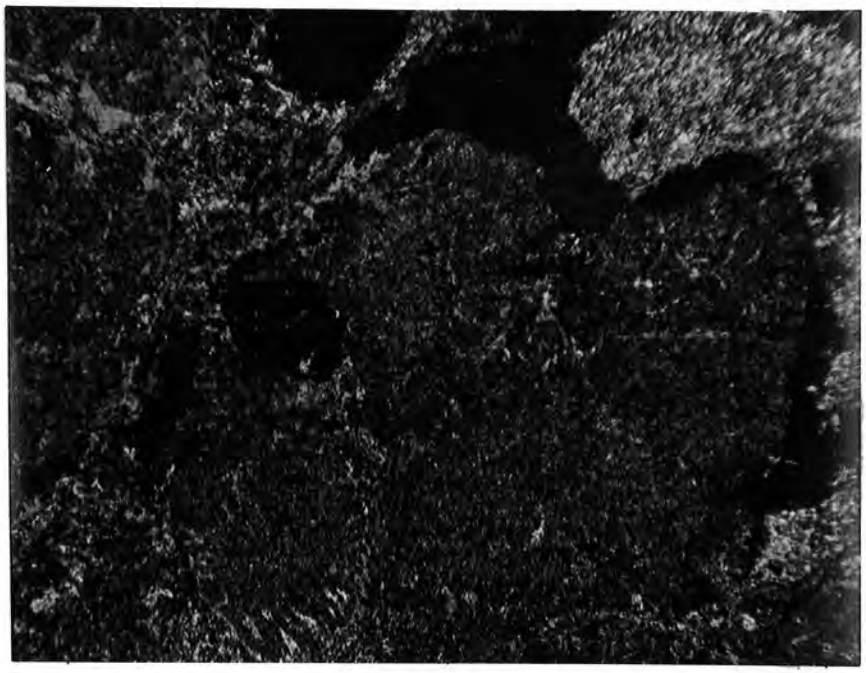

Plate 7.11 Photomicrograph: Carbonate pseudomorphs after metamorphic olivine, in Sample 60159. Note the sharp crystal outlines, and the coating derived from brucite. Crossed Nicols. Field width 1.7mm.

References

Aumento, F., and Loubat, H., (1971). The Mid Atlantic Ridge near 45°N, XVI. Serpentinized Ultramafic intrusions: Canadian Jour. Earth Sci., V.8, p.

Ball, M.C., and Taylor, H.F.W., (1961). The dehydration of brucite: Mineralog. Mag., V.32, p.754-766.

Ball, M.C., and Taylor, H.F.W., (1963). The dehydration of chrysotile in air and under hydrothermal conditions: Mineralog. Mag., V.33, p.467-482.

Bowen, N.L., and Tuttle, O.F., (1949). The System $MgO-SiO_2-H_2O$: Geol. Soc. America Bull., V.60, p.439-480.

Boyd, F.R., (1959). Hydrothermal investigation of amphiboles in Researches in Geochemistry, P.H. Abelson, ed., p.377-396.

Brindley, G.W., and Hayami, P.M.S., (1965). Mechanism of formation of forsterite and enstatite from serpentine: Mineralog. Mag., V.35, p.189-195.

Cann, J.R., (1969). Spilites from the Carlsberg Ridge, Indian Ocean: Jour. Petrology, V.10, p.1-19.

Cann, R.J., (1971). Major element variations in Ocean Floor Basalt: Phil. Trans. Roy. Soc. Lond. A., V.268, p.495-505.

Carmichael, I.S.E., (1967). The Iron-titanium oxides of sialic volcanic rocks, and their associated ferromagnesian silicates. Contr. Mineral. Petrol., V.14, p.36-64.

Challis, G.A., (1965). The origin of the New Zealand ultramafic intrusions: Jour. Petrology, V.6,p.322-364.

Chinner, G.A., (1962). Almandine in thermal Aureoles: Jour. Petrology, V.3, p.316-340.

Choudhuri, A., and Winkler, H.G.F., (1967). Anthophyllit und Hornblende in einigen metamorphen Reaktionen: Contr. Mineral. Petrol. V.14, p.293-315.

Coleman, R.G., and Keith, T.E., (1971). A chemical study of serpentinization - Burro Mountain, California: Jour. Petrology, V.12, p.311-328.

Deer, W.A., Howie, R.A., and Zussman, J., (1962). Rock-forming minerals Volumes 1-5: Longmans, Green and Co. Ltd., London.

Douglas, R.J.W., H. Gabrielse, J.O. Wheeler, D.F.Stott, and Belyea, H.R., (1970). Geology of Western Canada: in Geology and Economic Minerals of Canada, Edit. R.J.W. Douglas.

Duncumb, P., and Reed, S.J.B., (1968). The calculation of stopping power and back-scatter effects in electron microanalysis. In Quantitative electron probe microanalysis: Nat. Bur. Standards, Special Publ. 298, p.133-154.

Engel, A.E.J., (1971). Characteristics, occurrence and origins of basalts of the oceans: Phil. Trans. Roy. Soc. Lond.A., V.268, p.268-493.

Engel, A.E.J., Engel, C.G. and Havens, R.G., (1965). Chemical characteristics of Oceanic basalts, and the Upper Mantle: Bull. Geol. Soc. Am., V.76, p.719-734.

Engin, T., and Aucott, J.W., (1971). A microprobe study of chromites from the Andizlik-Zimparalik area, southwest Turkey: Mineralog. Mag., V.38, p.76-82.

Engin, T., and Hirst, D.M., (1970). The Alpine chrome ores of the Andizlik-Zimparalik area, Fethiye (southwest Turkey). Trans. Inst. Mining Met., Sect.B, 79: B.16-27.

Engin, T., and Hirst, D.M., (1970). Serpentinization of harzburgites from the alpine peridotite belt of southwest Turkey: Chemical Geology, V.6, p.281-295.

England, R.N., and Davies, H.L., (1973). Mineralogy of ultramafic cumulates and tectonites from Eastern Papua: Earth and Planetary Sci. Letters, V.17, p.416-425.

Evans, B.W., and Trommsdorff, V., (1970). Regional metamorphism of ultramafic rocks in the central Alps: parageneses in the system $CaO-MgO-SiO_2-H_2O$. Schweiz. Miner. Petrogr. Mitt., V.50, p.481-492.

Fawcett, J.J., and Yoder, H.S. Jnr., (1966). Phase relationships in the chlorites in the system $MgO-Al_2O_3-SiO_2-H_2O$: Am. Miner., V.51, p.353-380.

Fitton, J.G., and Gill, R.C.O., (1970). The oxidation of ferrous iron in rocks during mechanical grinding: Geochim. et Cosmochim. Acta, V.34, p.518-524.

Flanagan, F.J., (1969). U.S. Geological Survey Standards-II. First compilation of data for the new U.S.G.S. rocks: Geochim. et Cosmochim. Acta, V.33, p.81-120.

Flanagan, F.J., (1973). 1972 values for international reference samples: Geochim. et Cosmochim. Acta, V.37, p.1189-1200.

Francis, G.H., (1956). The serpentinite mass in Glen Urquhart, Invernesshire, Scotland: Am. Jour. Sci., V.254, p.201-226.

Frost, B.R., (1973). Contact metamorphism of the Ingalls ultramafic complex, at Paddy-go-easy Pass, Central Cascades, Washington: Unpublished Ph.D. thesis, University of Washington, Seattle.

Fyfe, W.S., (1958). A further attempt to determine the vapour pressure of brucite: Am. Jour. Sci., V.256, p.729.

Gabrielse, H., (1955). Petrology and structure of the McDame Ultramafic belt, British Columbia, Unpublished Ph.D. thesis, Columbia University.

Gabrielse, H., (1963). McDame Map Area, Cassiar District, British Columbia: Geol. Survey Canada. Mem.319, 130p.

Gabrielse, H., (1967). Tectonic evolution of the Northern Canadian Cordillera: Canadian Jour. Earth Sci., V.4, p.271.

Gabrielse, H., (1969). Geology of the Jennings River Map Area, British Columbia. (104-O): Geol. Surv. Canada. Paper 68-55.

Gabrielse, H., and Wheeler, J.O., (1961). Tectonic framework of southern Yukon and northwestern British Columbia: Geol. Surv. Canada. Paper 60-24.

Gillery, F.H., (1959). X-ray studies of synthetic Mg-Al serpentines and chlorites. Am. Miner.,V.44, p.143.

Green, D.H., (1964a). The petrogenesis of the high temperature peridotite in the Lizard area, Cornwall: Jour. Petrology, V.5, p.134-188.

Green, D.H., (1964b). The metamorphic aureole of the peridotite at the Lizard, Cornwall: Jour. Geology, V.72, p.543-563.

Greenwood, H.J., (1963). The synthesis and stability of anthophyllite: Jour. Petrology, V.4, p.317-351.

Hancock, W.G., (1964). The Mount Tawai Peridotite, North Borneo: Unpublished Ph.D. thesis, University of Durham.

Heinrich, K.F.J., (1966). The absorbtion correction model for microprobe analysis: Trans. 2nd. Nat. Conf. Electron Microprobe Analysis, Boston, paper 7, 2p.

Hess, H.H., (1955). Serpentines, orogeny and epeirogeny: Geol. Soc. Amer. Spec. Paper 62, p.391-408.

Hess, H.H., (1965). Mid-ocean ridges and tectonics of the sea floor, in Submarine geology and geophysics: Proc. 17th Symposium Colston Research Soc., p.317-334.

Hess, H., Smith, R.J., and Dengo, G., (1952). Antigorite from the vicinity of Caracas, Venezuela: Am. Miner., V.37, p.68.

Himmelberg, G.R., and Loney, R.A., (1973). Petrology of the Vulcan Peak Alpine-Type Peridotite, Southwestern Oregon: Bull. Geol. Soc. Am., V.84, p.1585-1600.

Holland, J.G., and Brindle, D.W., (1966). A self consistent mass absorbtion correction for silicate analysis by X-ray fluorescence: Spectrochim. Acta, V.22, p.2083-2093.

Hostetler, P.G., Coleman, R.G., Mumpton, F.A., and Evans, B.W., (1966). Brucite in Alpine serpentinites: Am. Miner. V.51, p.75-98.

Iishi, K., Saito, M., (1973). Synthesis of Antigorite: Am. Miner., V.58, p.915-919.

Irvine, T.N., (1965). Chromium spinel as a petrogenetic indicator; Part 1. Theory: Canadian Jour. Earth Sci., V.2, p.648-672.

Irvine, T.N., (1967). Chromium spinel as a petrogenetic indicator; Part 2. Petrologic applications: Canadian Jour. Earth Sci., V.4, p.71-103.

Irvine, T.N., and Smith, C.H., (1967). The ultramafic rocks of the Muskox Intrusion, Northwest Territories, Canada: p.38-49. In Wyllie, P.J., ed., Ultramafic and Related Rocks: John Wiley, New York.

Jahns, R.H., (1967). Serpentinites of the Roxbury district, Vermont: p.137-160, in Wyllie, P.J., ed., Ultramafic and Related Rocks: John Wiley, New York.

Jackson, E.D., (1961). Primary textures and mineral associations in the ultramafic zone of the Stillwater Complex, Montana: U.S. Geol. Survey, Prof. Paper, V.358, p.358-464.

Jackson, E.D., (1969). Chemical variation in coexisting chromite and olivine in chromitite zones of the Stillwater Complex: Econ. Geol. Monograph, V.4, p.41-71.

Johannes, W., (1968). Experimental investigation of the reaction forsterite + H_2O = Serpentine + brucite: Contr. Mineral. Petrol. V.19, p.309-315.

Johannes, W., (1969). An experimental investigation of the system $MgO-SiO_2-H_2O-CO_2$: Am. Jour. Sci., V.267, p.1083-1104.

King, E.G., Barany, R., Weller, W.W., and Pankratz, L.B., (1967). Thermodynamic properties of forsterite and serpentine: U.S. Dept. Interior, Bureau of Mines R.I. p.6962.

Kitahara, S., Takenouch, S., and Kennedy, G.L. (1966). Phase relations in the system $MgO-SiO_2-H_2O$ at high temperatures and pressures: Am. Jour. Sci., V.264, p.223-233.

Kitahara, S., and Kennedy, G.C., (1967). The calculated equilibrium curves for some reactions in the system $MgP-SiO_2-H_2O$, at pressures of up to 30 Kbars: Am. Jour. Sci., V.265, p.211-217.

Kornprobst, J., (1969). Le massif ultra-basique des Beni Bouchera, (Rif interne, Maroc): Contr. Mineral. Petrol., V.28, p.283-322.

Loney, R.A., Himmelberg, G.R., and R.G. Coleman, (1971). Structure and petrology of the Alpine-type peridotite at Burro Mountain, California, U.S.A: Jour. Petrology, V.12, p.245-309.

MacDonald, G.A., (1968). Composition and origin of Hawaiian lavas: Geol. Soc. Amer. Mem. 116, p.477-522.

MacGregor, I.D., (1967). Mineralogy of model mantle compositions. p.382-393. In Wyllie, P.J., ed., Ultramafic and related rocks. John Wiley, New York.

MacGregor, I.D., and Smith, C.H., (1963). The use of chrome spinels in petrographic studies of ultramafic intrusions: Canadian Mineral. V.7, p.403-412.

Mamet, B.L., and Gabrielse, H., (1969). Foraminiferal zonation and stratigraphy of the Type section of the Nizi Formation, (Carboniferous System, Chesteran Stage), British Columbia: Geol. Surv. Canada, Paper 69-16.

Medaris, L.G., (1972). High pressure peridotites in southwest Oregon: Bull. Geol. Soc. Amer. V.83, p.41-57.

Metz, P., (1967). Experimentelle Bildung von Forsterit und Calcit uas Tremolit und Dolomit. (German with English abstract): Geochimica et Cosmochimica Acta, V.31, p.1517-1532.

Monger, J.W.H., and Ross, C.A., (1971). Distribution of fusulinaceans in the western Canadian Cordillera: Canadian Jour. Earth. Sci., V.8, p.259-278.

Monger, J.W.H., Souther, J.G., and H. Gabrielse, (1972). Evolution of the Canadian Cordillera: A plate tectonic model: Am. Jour. Sci., V.272, p.577-602.

Muir, J.E., and Naldrett, A.J., (1973). A natural occurrence of two-phase chromium-bearing spinels: Can. Miner., V.11, p.930-939.

Nelson, B.W., and Roy, R., (1958). Synthesis of the chlorites and their structural and chemical constitution. Am. Miner. V.43, p.707.

O'Hara, M.J., (1963). Distribution of iron between coexisting olivines and calcium poor pyroxenes in peridotites, gabbros, and other magnesian environments: Am. Jour. Sci., V.261, p.33-46.

Oliver, R.L. and Nesbitt, R.W., (1972). Metamorphic olivine in ultramafic rocks from Western Australia: Contr. Mineral. Petrol. V.36, p.335-342.

Onyeagochi, A.C., (1974). Alteration of chromite from the Twin Sisters Dunite, Washington: Am. Mineral. V.59, p.608-612.

Page, N.J., (1967). Serpentinization at Burro Mountain, California: Contr. Miner. Petrol., V.14, p.321-342.

Page, N.J., (1968). Chemical differences among the serpentine 'polymorphs'. Am. Miner. V.53, p.201-215.

Pamic, J., Scavnicar, S., and Medjimorec, S., (1973). Mineral assemblages of amphibolites associated with alpine type ultramafics in the Dinaride Ophiolite zone, Yugoslavia: Jour. Petrology, V.14, p.133-157.

Pearce, J.A., and Cann, J.R., (1971). Ophiolite origin investigated by discriminant analysis, using Ti, Zr and Y: Earth Planetary Science Letters, V.12, p.339.

Pearce, J.A., and Cann, J.R., (1973). Tectonic setting of basic volcanic rocks determined using trace element analyses: Earth and Planetary Science Letters, V.19, p.290-300.

Peters, T., (1968). Distribution of Mg, Fe, Al, Ca, and Na, in coexisting olivine, orthopyroxene and clinopyroxene in the Totalp Serpentinite, (Davos, Switzerland) and in the alpine metamorphosed Malenco Serpentinite (N.Italy): Contr. Mineral. Petrol. V.18, p.65-75.

Pitcher, W.S., and Read, H.H., (1960). The aureole of the main Donegal granite: Quart. Jour. Geol. Soc. London, V.116, p.1-36.

Powell, B.M., and Powell, R. (in press). Al olivine-clinopyroxene geothermometer: Contr. Mineral. Petrol.

Ragan, D.M., (1963). Emplacement of the Twin Sisters Dunite, Washington: Am. Jour. Sci., V.261, p.549-565.

Ragan, D.M., (1969). Olivine recrystallization textures: Mineralog. Mag., V.37, p.238-240.

Raleigh, C.B., (1965). The Structure and Petrology of an alpine-peridotite on Cypress Island, Washington, U.S.A: Beitr. Mineral. Petrog. V.11, p.719-741.

Raleigh, C.B., (1967). Experimental deformation of ultramafic rocks and minerals: p.191-199. In Wyllie, P.J., ed., Ultramafic and Related Rocks: John Wiley, New York.

Raleigh, C.B., Paterson, M.S., (1965). Experimental deformation of serpentinite and its tectonic implications: Jour. Geophys. Res., V.70, p.3965-3985.

Reed, S.J.B., (1965). Characteristic fluorescence corrections in electron-microprobe microanalysis: British Jour. Appl. Phys., V.16, p.913-926.

Reeves, M.J., (1971). Geochemistry and mineralogy of British Carboniferous seatearths from northern coalfields: Unpublished Ph.D. thesis, University of Durham.

Rodgers, K.A., (1973). Chrome-spinels from the Massif du Sud, southern New Caledonia: Mineralog. Mag., V.39, p.326-339.

Ross, C.A., (1969). Upper Paleozoic Fusulinacea: Contribution to Canadian Paleontology. Geol. Surv. Canada. Bull., 182, p.129-134.

Scarfe, C.M., and Wyllie, P.J., (1967). Serpentine Dehydration curves, and their bearing on serpentinite deformation in orogenesis: Nature V.215, p.945-946.

Seki, Y., (1951). Metamorphism of ultrabasic rocks caused by intrusion of granodiorite in the Miyamori District, Iwate Prefecture - Metamorphism of serpentine rock: (in Japanese with English abstract): Jour. Geol. Soc. Japan, V.57, p.35-43.

Simpkin, A., and Smith, J.V., (1970). Minor element distribution in olivine: Jour. Geology, V.78, p.304-325.

Simpson, E.S., (1920). A graphic method for the comparison of minerals with four variable components forming two isomorphous pairs: Mineralog. Mag., V.19, p.99-106.

Smith, C.H., and MacGregor, I.D., (1960). Ultramafic intrusive conditions illustrated by the Mount Albert Ultramafic pluton, Gaspe, Quebec: Geol. Soc. America Bull., V.71, p.178.

Springer, R.K., (1971). Geology of the Pine Hill Intrusive Complex, El Dorado County, California. Unpublished Ph.D. thesis, University of California, Davis, California.

Springer, R.K., (1974). Contact metamorphosed ultramafic rocks in the Western Sierra Nevada Foothills, California: Jour. Petrology, V.15, p.160-195.

Stevens, R.E., (1944). Composition of some chromites of the western hemisphere: Am. Miner. V.29, p.1-34.

Stoll, W.C., (1958). Geology and Petrology of the Masinloc chromite deposit, Zambales, Luzon, Philippine Islands: Bull. Geol. Soc. Am., V.69, p.419.

Sweatman, T.R., and Long, J.V.P., (1969). Quantitative electron-probe microanalysis of rock forming minerals. Jour. Petrology, V.10, p.332-379.

Thayer, T.P., (1963). The Canyon Mountain Complex, Oregon, and the alpine mafic magma stem: U.S. Geol. Surv., Profess. Paper, 475-C, C82-C85.

Thayer, T.P., (1966). Serpentinization considered as a constant volume process: Am. Miner. V.51, p.685-710.

Trommsdorff, V., and Evans, B.W., (1972). Progressive metamorphism of antigorite schist in the Bergell tonalite aureole, (Italy): Am. Jour. Sci., V.272, p.423-437.

Velde, B., (1973). Phase equilibria in the system MgO-Al_2O_3-SiO_2-H_2O: Chlorites and associated minerals: Mineralog. Mag., V.39, p.297-312.

Wager, L.R., and Mitchell, R.L., (1951). The distribution of trace elements during strong fractionation of basic magma - a further study of the Skaergaard Intrusion; East Greenland, Geochim. Cosmochim. Acta, V.1, p.129-208.

Wenner, D.B., and Taylor, H.P., (1971). Temperatures of serpentinization of ultramafic rocks, based on O^{18}/O^{16} fractionation between coexisting serpentine and magnetite: Contr. Mineral. Petrol., V.32, p.165-185.

Whittaker, E.J.W., and Wicks, P.J., (1970). Chemical differences among the serpentine "polymorphs": a discussion. Am. Miner., V.55, p.1025-1047.

Wilkinson, J.F.G., (1953). Some aspects of the alpine-type serpentinites of Queensland: Geol. Mag., V.90, p.305-321.

Wilson, A.D., (1955). A new method for the determination of ferrous iron in rocks and minerals: Bull. Geol. Surv. Great Britain, V.9, p.56-58.

Winkler, H.G.F., (1967). Petrogenesis of metamorphic rocks: Springer Verlag, New York.

Wolfe, W.J., (1965). The Blue River Ultramafic intrusion, Cassiar District, British Columbia. Geol. Survey. Canada, Paper 64-48.

Wolfe, W.J., (1967). Petrology, mineralogy, and geochemistry of the Blue River ultramafic intrusion, Cassiar District, British Columbia, Unpublished Ph.D. thesis, Yale University.

Yamaguchi, M., (1964). Petrogenetic significance of ultrabasic inclusions in basaltic rocks from southwest Japan: Mem. Faculty Sci., Kyushu Univ., Ser.D, Geology, V.15, No.1, p.163-219.

Yoder, H.S., (1952). The $MgO-Al_2O_3-SiO_2-H_2O$ system and the related metamorphic facies: Amer. Jour. Sci., Bowen Vol., p.569.

Appendix I. Sample Data

Occurrence and Location

Table 1.1 summarizes some of the more important outcrop and rock data. Hand specimens were collected at most, but not all the listed location points. The location number, given in Table 1.1, is assigned to the relevant sample, and to any additional data relating to that sample. Mineral and chemical data can thus be correlated directly with sample location, shown in Figure 2.3. Sectioned samples used in this study are represented as dots in those text figures concerned with mineral distribution. These sample numbers are shown on a subsidiary sample location map, Figure 1.3.

Samples numbered in the 60000 series were collected in the summer of 1970, and those in the 61000 series were collected on a revisit to the area in 1972.

The sample location map, Figure 2.3, is a copy of Map 17-1964, published by the Geological Survey of Canada. The geology shown is that proposed by Wolfe (1965). Minor amendments to this map, which result from the present study, are shown in Figure 2.1. All three maps are located in the map pocket.

The sample location points, shown in Figures 1.3 and 2.3, have been allocated Universal Transverse Mercator, (U.T.M.), coordinates, and these are listed in Table 1.1. The points

are extrapolated from the four assigned locations shown on Figure 1.3. These have the following coordinates

U.T.M. (NW) 442100-6602600 09
U.T.M. (NE) 445500-6605500 09
U.T.M. (SE) 447400-6600500 09
U.T.M. (SW) 445000-6590500 09

Table 1.1 also lists the rock-type, and a qualifier, and in some cases the most important foliation, (F), or joint set, (J). Samples powdered for X-ray fluorescence wholerock analysis are listed as (XRF); although the data has not been included in this study. Sectioned samples are shown as (TS), and specimens which have been analysed using the electron microprobe are listed as (P.T.S.).

Some samples also show an estimate of serpentine percentage, based on a crude determination of the rock density. Specimens were weighed in both air and water, and the specific gravity was calculated. In a simple system consisting of olivine (S.G. = 3.25), enstatite (S.G. = 3.15) and serpentine (S.G. = 2.50); it should be possible to determine the serpentine percentage by means of the following relationship, Wolfe (1965).

$$\% \text{ serpentine} = 471.029 - 147.058 \times \text{S.G.(rock)}$$

As noted by Wolfe, this relationship is not strictly applicable in a system containing additional phases, such as talc, tremolite, and chlorite.

Ultramafic Mineralogy

Table 1.2 summarizes the phase content of each of the sectioned ultramafic samples shown in Figure 1.3. The specimens are listed by unit, so as to bring out the textural and mineralogical characteristics of each unit. The units are defined in the text, (Chapter 3), and the unit distribution is shown in Figure 3.1, in the text.

Minerals have been identified, and assigned to a development stage on the basis of rock texture, and mineral chemistry. The development stages are discussed in Chapter 2.

The original rock consisted of dunite (D), and peridotite (P). Where there is sufficient evidence to determine the original lithology, this data is also given.

'TABLE 1.1 OUTCROP AND SAMPLE DATA FROM THE BLUE RIVER ULTRAMAFIC BODY'

60001	CHERT	LAYERED						446900	6600510	09
60002	SERPENTINE	FRACTURED		F178	20W			446830	6600530	09
60003	AMPHIBOLITE	BANDED						446720	6600460	09
60004	SERPENTINE	SHEARED	85					446650	6600420	09
60005	AMPHIBOLITE	SHEARED	95	F140	38S	XRF	TS	446690	6600390	09
60006	RODINGITE	APHANITIC						446630	6600390	09
60007	SERPENTINE	SHEARED						446670	6600400	09
60008	VOLCANIC	BANDED		F104	32S			446100	6599900	09
60009	QUARTZITE	SEDIMENT						446030	6599850	09
60010	RODINGITE	APHANITIC						445500	6599390	09
60011	SERPENTINE	MASSIVE						445470	6599380	09
60012	SERPENTINE	SHEARED	100			XRF	TS	445450	6599380	09
60013	GABBRO	FINE					PTS	445450	6599380	09
60014	GABBRO	MASSIVE					PTS	445470	6599280	09
60015	GABBRO	FINE						445630	6599440	09
60016	VOLCANIC	MASSIVE		F124	23S			446180	6599630	09
60017	VOLCANIC	SHEARED					TS	446260	6599600	09
60018	SERPENTINE	SHEARED	85				PTS	446220	6599480	09
60019	SERPENTINE	MASSIVE						446110	6599440	09
60020	GABBRO	MASSIVE					TS	445290	6599490	09
60021	DUNITE	REGENERATED	100			XRF	PTS	445400	6599770	09
60022	GABBRO	MASSIVE						445460	6599780	09
60023	SERPENTINE	SHEARED				XRF	TS	445500	6599810	09
60024	RODINGITE	MASSIVE						446000	6602020	09
60025	DUNITE	REGENERATED						446000	6602140	09
60026	CHROMITE	VEIN						446020	6602140	09
60027	DUNITE	REGENERATED						446000	6602200	09
60028	SERPENTINE	SHEARED						445990	6602110	09
60029	DUNITE	REGENERATED					TS	446020	6601870	09
60030	DUNITE	REGENERATED	100	F128	61W		TS	446000	6601800	09

'TABLE 1.1 OUTCROP AND SAMPLE DATA FROM THE BLUE RIVER ULTRAMAFIC BODY'

60031	SEDIMENT	STREAM						445720	6601930	09
60032	DUNITE	REGENERATED	100					445610	6602120	09
60033	DUNITE	REGENERATED	90	F096	42N		TS	445530	6602230	09
60034	DUNITE	REGENERATED	90	F115	49S	XRF	TS	445500	6602020	09
60035	DUNITE	REGENERATED	95			XRF	PTS	445580	6602000	09
60036	DUNITE	REGENERATED		F171	54W			446080	6601800	09
60037	RODINGITE	MASSIVE						446220	6601730	09
60038	DUNITE	REGENERATED	85				PTS	446260	6601690	09
60039	SERPENTINE	BASTITE	100					446380	6601650	09
60040	SERPENTINE	BASTITE	85			XRF	TS	447300	6600300	09
60041	SERPENTINE	BASTITE	85				TS	447250	6600280	09
60042	SERPENTINE	BASTITE	85					447000	6600160	09
60043	SERPENTINE	SHEARED	80			XRF	TS	446940	6600120	09
60044	VOLCANIC	MASSIVE		F124	42S			446870	6600050	09
60045	VOLCANIC	MASSIVE					TS	446780	6599890	09
60046	VOLCANIC	BRECCIATED				XRF		446760	6599830	09
60047	VOLCANIC	SHEARED						446600	6599700	09
60048	VOLCANIC	MASSIVE					TS	446650	6599670	09
60049	RODINGITE	DIABAISIC		J168	75W			446580	6599520	09
60050	AMPHIBOLITE	BANDED						446500	6599370	09
60051	RODINGITE	MASSIVE	85			XRF		446320	6599190	09
60052	VOLCANIC	MASSIVE						446350	6599310	09
60053	GABBRO	FINE						445920	6599230	09
60054	GABBRO	MASSIVE						445850	6599250	09
60055	DUNITE	REGENERATED	100			XRF	PTS	445700	6599170	09
60056	SERPENTINE	SHEARED	85			XRF	TS	445910	6599160	09
60057	VOLCANIC	MASSIVE		F120	44S	XRF		446680	6600880	09
60058	ARGILLITE	BEDDED		F127	45S	XRF	TS	446770	6600830	09
60059	AMPHIBOLITE	LAYERED						446980	6600710	09
60060	SEDIMENT	STREAM						447120	6600640	09

'TABLE 1.1 OUTCROP AND SAMPLE DATA FROM THE BLUE RIVER ULTRAMAFIC BODY'

60061	SEDIMENT	STREAM					447090	6600630	09
60062	SERPENTINE	SHEARED	80		XRF	TS	447100	6600700	09
60063	SERPENTINE	SHEARED	85		XRF		447050	6600730	09
60064	RODINGITE	MASSIVE	80		XRF		447020	6600790	09
60065	SERPENTINE	BASTITE	85			TS	446930	6600950	09
60066	SERPENTINE	SHEARED		J162 79E			445200	6601800	09
60067	DUNITE	REGENERATED	80	F150 49S	XRF	PTS	445160	6601780	09
60068	DUNITE	REGENERATED		F092 29S			445110	6601790	09
60069	SERPENTINE	MASSIVE	80			PTS	445000	6601770	09
60070	DUNITE	PRIMARY	30		XRF		444200	6601830	09
60071	PERIDOTITE	BANDED		F104 47S	XRF	TS	443870	6601040	09
60072	DUNITE	MASSIVE	5	F093 68S	XRF	TS	443940	6601080	09
60073	PERIDOTITE	BANDED	25		XRF		444080	6601120	09
60074	PERIDOTITE	BANDED		F113 69S			444220	6601200	09
60075	DUNITE	MASSIVE	30		XRF	PTS	444300	6601280	09
60076	PERIDOTITE	BANDED			XRF		444350	6601250	09
60077	DUNITE	MASSIVE					444350	6601380	09
60078	SERPENTINE	SHEARED	85			TS	444530	6601550	09
60079	SERPENTINE	SHEARED	85			PTS	444900	6601780	09
60080	VOLCANIC	BANDED				TS	447120	6599580	09
60081	VOLCANIC	BANDED		F115 32S			447110	6599510	09
60082	VOLCANIC	BRECCIATED			XRF		447100	6599470	09
60083	AMPHIBOLITE	BANDED		F087 31S		TS	447050	6599390	09
60084	SERPENTINE	BASTITE	75		XRF	TS	447000	6599320	09
60085	AMPHIBOLITE	BANDED		F040 48S			446820	6599380	09
60086	RODINGITE	MASSIVE				TS	446820	6599210	09
60087	RODINGITE	MASSIVE					447100	6599130	09
60088	SERPENTINE	SHEARED	75			TS	446990	6599150	09
60089	RODINGITE	MASSIVE					446860	6599120	09
60090	SERPENTINE	BASTITE					446650	6598840	09

'TABLE 1.1 OUTCROP AND SAMPLE DATA FROM THE BLUE RIVER ULTRAMAFIC BODY'

60091	SERPENTINE	BASTITE			XRF	TS	446610	6598700	09
60092	SERPENTINE	BASTITE	80		XRF	TS	446430	6598630	09
60093	SERPENTINE	BASTITE	90		XRF		446320	6598530	09
60094	PERIDOTITE	SHEARED	50	F099 55N	XRF	PTS	446270	6598490	09
60095	SERPENTINE	MASSIVE	85		XRF		446200	6598470	09
60096	SERPENTINE	SHEARED			XRF	TS	446110	6598450	09
60097	SERPENTINE	BASTITE					446520	6598880	09
60098	SERPENTINE	BASTITE	90				446380	6598880	09
60099	RODINGITE	APHANITIC					446220	6598950	09
60100	SERPENTINE	SHEARED	90				445800	6598900	09
60101	SERPENTINE	SHEARED	60		XRF		446120	6599030	09
60102	DUNITE	REGENERATED	90		XRF	PTS	445950	6602320	09
60103	SERPENTINE	SHEARED	95	F039 88W			446200	6602350	09
60104	SERPENTINE	MASSIVE	80		XRF		446250	6602450	09
60105	SERPENTINE	MASSIVE	85		XRF	TS	446300	6602520	09
60106	DUNITE	REGENERATED					445930	6602370	09
60107	DUNITE	REGENERATED	90			TS	445750	6602630	09
60108	DUNITE	REGENERATED	80				445730	6602790	09
60109	DUNITE	REGENERATED	100	F032 72E	XRF	PTS	445690	6602870	09
60110	SERPENTINE	BANDED	80	F050 64E	XRF		447780	6602970	09
60111	SERPENTINE	BRECCIATED					445780	6602880	09
60112	SERPENTINE	SHEARED	90		XRF		445690	6602940	09
60113	SERPENTINE	SHEARED	95	F144 51N			445700	6603150	09
60114	SERPENTINE	SHEARED		F092 33N		TS	445730	6603210	09
60115	SILTSTONE	SEDIMENT			XRF		445750	6603230	09
60116	SERPENTINE	MASSIVE	70		XRF		445600	6603270	09
60117	SERPENTINE	MASSIVE	70			TS	445540	6603280	09
60118	SERPENTINE	MASSIVE			XRF		445470	6603260	09
60119	VOLCANIC	MASSIVE		J063 80N			446560	6600920	09
60120	VOLCANIC	BANDED		F156 28W		TS	446450	6600970	09

'TABLE 1.1 OUTCROP AND SAMPLE DATA FROM THE BLUE RIVER ULTRAMAFIC BODY'

60121	RODINGITE	APHANITIC	80			XRF		446340	6600980	09
60122	SERPENTINE	BASTITE	90				TS	446210	6601000	09
60123	SERPENTINE	SHEARED					PTS	446140	6601070	09
60124	AMPHIBOLITE	BANDED		F139	61S			446000	6601160	09
60125	SERPENTINE	SHEARED						446090	6601080	09
60126	GABBRO	MASSIVE						445700	6601900	09
60127	DUNITE	REGENERATED		F045	65W			445310	6602700	09
60128	SERPENTINE	MASSIVE	70			XRF	PTS	445230	6602780	09
60129	SILTSTONE			F122	42S		TS	445150	6602900	09
60130	DUNITE	REGENERATED		F095	55E			445020	6603100	09
60131	DUNITE	REGENERATED	65	F112	55N	XRF		445020	6603130	09
60132	DUNITE	REGENERATED		F049	89W			445020	6603210	09
60133	DUNITE	REGENERATED	50				PTS	445380	6603370	09
60134	DUNITE	REGENERATED		F072	50W			445250	6603290	09
60135	DUNITE	REGENERATED						445140	6603270	09
60136	SERPENTINE	SHEARED	80			XRF		445250	6604010	09
60137	DUNITE	REGENERATED	80	F067	67E	XRF	PTS	445150	6603770	09
60138	DUNITE	REGENERATED		F039	44W			445030	6603910	09
60139	RODINGITE	BANDED						446580	6601190	09
60140	SERPENTINE	BASTITE	90				TS	446560	6601440	09
60141	SERPENTINE	SHEARED	85			XRF		446600	6601400	09
60142	SERPENTINE	BASTITE				XRF		446630	6601340	09
60143	SERPENTINE	BASTITE	85			XRF	PTS	446720	6601220	09
60144	AMPHIBOLITE	BANDED						446800	6601100	09
60145	SERPENTINE	SHEARED						446870	6601000	09
60146	VOLCANIC	MASSIVE		F118	51S			445780	6599720	09
60147	SERPENTINE	SHEARED						445690	6599810	09
60148	AMPHIBOLITE	BANDED		F078	80W			445690	6599810	09
60149	VOLCANIC	MASSIVE						445860	6600280	09
60150	PERIDOTITE	MASSIVE	30					445210	6599900	09

'TABLE 1.1 OUTCROP AND SAMPLE DATA FROM THE BLUE RIVER ULTRAMAFIC BODY'

60151	DUNITE	SUGARY	25		XRF		445210	6599900	09
60152	DUNITE	SUGARY	30	F1C2 47W	XRF	TS	445100	6599980	09
60153	PERIDOTITE	MASSIVE	30		XRF	PTS	444850	6599850	09
60154	GABBRO	DIABAISIC					444690	6599680	09
60155	SERPENTINE	SHEARED	85		XRF	TS	444660	6599620	09
60156	SEDIMENT	SILTSTONE					444630	6599560	09
60157	DUNITE	REGENERATED	90			PTS	444590	6599800	09
60158	DUNITE	REGENERATED	90		XRF		444400	6599900	09
60159	DUNITE	CARBONATIZED	70	F032 44E	XRF	PTS	444410	6599980	09
60160	PERIDOTITE	BANDED	10		XRF	PTS	444480	6600120	09
60161	PERIDOTITE	MASSIVE			XRF		444700	6600330	09
60162	DUNITE	SUGARY	25		XRF		444700	6600330	09
60163	PERIDOTITE	MASSIVE	20		XRF	PTS	444920	6600360	09
60164	DUNITE	SUGARY			XRF		444920	6600360	09
60165	PERIDOTITE	MASSIVE					445100	6600520	09
60166	AMPHIBOLITE	SHEARED					445120	6600670	09
60167	DUNITE	SUGARY	75		XRF		444990	6600700	09
60168	PERIDOTITE	MASSIVE	40		XRF	PTS	444880	6600620	09
60169	DUNITE	SUGARY	30		XRF		444660	6600580	09
60170	SERPENTINE	SHEARED	80		XRF		444990	6600970	09
60171	DUNITE	REGENERATED	50			PTS	444660	6602320	09
60172	DUNITE	REGENERATED	30		XRF	PTS	444020	6602430	09
60173	PERIDOTITE	MASSIVE	20		XRF	TS	443860	6602550	09
60174	DUNITE	SUGARY	30	F120 35S	XRF	PTS	442500	6602000	09
60175	PERIDOTITE	MASSIVE	15		XRF		442500	6602000	09
60176	PERIDOTITE	BANDED		F032 89E	XRF		442430	6601940	09
60177	PERIDOTITE	MASSIVE			XRF		442400	6601800	09
60178	GABBRO	DIABAISIC				TS	442360	6601690	09
60179	PERIDOTITE	ALTERED	50		XRF	PTS	442300	6601600	09
60180	PERIDOTITE	ALTERED	65		XRF	PTS	442280	6601420	09

'TABLE 1.1 OUTCROP AND SAMPLE DATA FROM THE BLUE RIVER ULTRAMAFIC BODY'

60181	RODINGITE	DIABAISIC					442280	6601420	09
60182	PERIDOTITE	ALTERED			XRF		442380	6601390	09
60183	PERIDOTITE	ALTERED	55				442140	6601500	09
60184	PERIDOTITE	ALTERED	15			PTS	442480	6601690	09
60185	PERIDOTITE	BANDED	15		XRF	PTS	442500	6601800	09
60186	PERIDOTITE	SUGARY	20		XRF	PTS	442550	6602130	09
60187	CHROMITE	MASSIVE					442680	6602200	09
60188	DUNITE	SUGARY	10		XRF	PTS	442790	6602260	09
60189	PERIDOTITE	BANDED	10	F083 78S	XRF		442980	6602400	09
60190	PERIDOTITE	BANDED	25			TS	443150	6602500	09
60191	PERIDOTITE	SHEARED			XRF	TS	443400	6602690	09
60192	PERIDOTITE	BANDED	45		XRF		443550	6602800	09
60193	DUNITE	ALTERED	55		XRF		443620	6602860	09
60194	PERIDOTITE	ALTERED	25		XRF		443700	6602920	09
60195	PERIDOTITE	ALTERED	60			TS	443830	6603040	09
60196	DUNITE	SUGARY	45		XRF	PTS	444020	6603220	09
60197	PERIDOTITE	MASSIVE	50		XRF		444020	6603220	09
60198	PERIDOTITE	ALTERED	45		XRF		444070	6603460	09
60199	DUNITE	REGENERATED	60		XRF	PTS	443970	6603680	09
60200	PERIDOTITE	TALCOSE	70		XRF		443910	6603760	09
60201	GRANITE	COARSE					443900	6603790	09
60202	PERIDOTITE	BANDED	45	F017 75E		TS	444210	6603560	09
60203	DUNITE	SUGARY	60			TS	444200	6603330	09
60204	PERIDOTITE	MASSIVE	30				444100	6603000	09
60205	PERIDOTITE	MASSIVE	25		XRF	TS	444100	6602810	09
60206	DUNITE	REGENERATED	45			PTS	444680	6603000	09
60207	DUNITE	REGENERATED					444600	6603020	09
60208	DUNITE	REGENERATED	45				444550	6603040	09
60209	DUNITE	REGENERATED	50	F086 77S	XRF	PTS	444790	6603070	09
60210	DUNITE	REGENERATED		F078 56N			444810	6603130	09

'TABLE 1.1 OUTCROP AND SAMPLE DATA FROM THE BLUE RIVER ULTRAMAFIC BODY'

60211	DUNITE	REGENERATED	60					444750	6604090	09
60212	DUNITE	REGENERATED	55				TS	444650	6604120	09
60213	DUNITE	REGENERATED	60	F033	87W		PTS	444550	6604210	09
60214	DUNITE	REGENERATED						444460	6604250	09
60215	DUNITE	REGENERATED	80				TS	444350	6604110	09
60216	DUNITE	REGENERATED	70			XRF		444380	6603990	09
60217	DUNITE	REGENERATED						444300	6603900	09
60218	DUNITE	REGENERATED	55				PTS	444320	6603780	09
60219	DUNITE	REGENERATED	60	F171	46E			444450	6603520	09
60220	PERIDOTITE	BANDED	60	F076	51E		TS	444320	6603300	09
60221	GABBRO	ALTERED					TS	444270	6603180	09
60222	PERIDOTITE	MASSIVE						444060	6602630	09
60223	PERIDOTITE	MASSIVE	40					443610	6602510	09
60224	DUNITE	MASSIVE	45	J148	41N		TS	443620	6602580	09
60225	DUNITE	SUGARY						443800	6602580	09
60226	PERIDOTITE	BANDED		F102	87S		TS	443940	6602520	09
60227	DUNITE	REGENERATED		F109	85N		TS	443970	6602480	09
60228	PERIDOTITE	MASSIVE	45					443970	6602480	09
60229	DUNITE	REGENERATED						444550	6602370	09
60230	DUNITE	REGENERATED						444570	6602330	09
60231	DUNITE	REGENERATED	80				TS	444680	6602300	09
60232	PERIDOTITE	MASSIVE						443850	6602230	09
60233	PERIDOTITE	MASSIVE					TS	443770	6602140	09
60234	PERIDOTITE	MASSIVE						443750	6602090	09
60235	PERIDOTITE	MASSIVE						443580	6602050	09
60236	PERIDOTITE	BANDED		F121	54S			443670	6601900	09
60237	DUNITE	SUGARY					PTS	443800	6601840	09
60238	DUNITE	BANDED						443990	6601820	09
60239	PERIDOTITE	MASSIVE						443880	6601440	09
60240	VOLCANIC	MASSIVE						445280	6599280	09

'TABLE 1.1 OUTCROP AND SAMPLE DATA FROM THE BLUE RIVER ULTRAMAFIC BODY'

60241	DUNITE	CARBONATIZED				TS	444430	6600000	09
60242	VOLCANIC	GABBROIC					446620	6600460	09
60243	MINERALS	PANNED					446900	6600060	09
60244	RODINGITE	APHANITIC					447230	6598350	09
60245	SERPENTINE	SHEARED					447230	6598350	09
60246	SERPENTINE	SHEARED					447200	6598560	09
60247	MINERALS	PANNED					446580	6600810	09
60248	MINERALS	PANNED					446890	6600970	09
60249	PERIDOTITE	MASSIVE		F060 80S			444600	6604560	09
60250	GRANITE	COARSE				TS	444620	6604580	09
60251	VOLCANIC	MASSIVE					445620	6603660	09
60252	VOLCANIC	MASSIVE					445780	6603450	09
60253	LIMESTONE						445670	6603080	09
60694	SERPENTINE	MASSIVE	90		XRF	TS	444630	6602250	09
60822	SERPENTINE	MASSIVE	60			TS	444510	6602170	09
60860	SERPENTINE	ALTERED	90			TS	444120	6600580	09
60862	DUNITE	REGENERATED	60			TS	443980	6600550	09
60867	SERPENTINE	MASSIVE	75			PTS	444010	6600480	09
60871	PERIDOTITE	ALTERED	90		XRF	TS	444880	6601010	09
60872	DUNITE	MASSIVE	45		XRF	PTS	443730	6601410	09
60874	PERIDOTITE	MASSIVE	15			PTS	443750	6601340	09
60876	PERIDOTITE	MASSIVE	30			PTS	444030	6601530	09
60886	DUNITE	PRIMARY	0		XRF	TS	444260	6601770	09
60893	DUNITE	SHATTERED	60			TS	444180	6602630	09
60894	DUNITE	REGENERATED	45			PTS	444160	6602530	09
60902	DUNITE	PRIMARY	45			PTS	443470	6602870	09
60907	SERPENTINE	ANTIGORITE	90			PTS	444100	6601230	09

'TABLE 1.1 OUTCROP AND SAMPLE DATA FROM THE BLUE RIVER ULTRAMAFIC BODY'

61521	RODINGITE	SHEARED				446700	6600880	09
61522	CHERT	BEDDED	F110	38S		446600	6600950	09
61523	SERPENTINE	SHEARED	F110	90		446100	6600100	09
61524	DUNITE	REGENERATED	F108	80S		444700	6602300	09
61525	DUNITE	REGENERATED			TS	444150	6602250	09
61526	DUNITE	BANDED	F145	80E	XRF	444000	6602000	09
61527	DUNITE	REGENERATED	F136	85N		446050	6601850	09
61528	SERPENTINE	SHEARED				446000	6602180	09
61529	DUNITE	REGENERATED			XRF	445950	6602350	09
61530	DUNITE	REGENERATED	F070	75E		445600	6602200	09
61531	DUNITE	REGENERATED	J125	64S	XRF	445500	6602000	09
61532	DUNITE	REGENERATED	J125	41S		444600	6602700	09
61533	DUNITE	REGENERATED	F050	45N	XRF	444840	6603000	09
61534	DUNITE	REGENERATED	F065	90		445000	6603150	09
61535	DUNITE	REGENERATED	J155	75S	TS	445280	6603200	09
61536	DUNITE	REGENERATED				445480	6603320	09
61537	SERPENTINE	SHEARED				445700	6603000	09
61538	DUNITE	REGENERATED	F145	60W		445200	6601840	09
61539	VOLCANIC	SHEARED				444800	6601800	09
61540	VOLCANIC	SHEARED				444680	6601700	09
61541	VOLCANIC	SHEARED			TS	444680	6601700	09
61542	VOLCANIC	SHEARED				444680	6601700	09
61543	SERPENTINE	SHEARED				444680	6601700	09
61544	SERPENTINE	SHEARED			XRF	444680	6601700	09
61545	SERPENTINE	SHEARED			XRF	444680	6601700	09
61546	SERPENTINE	SHEARED			XRF	444680	6601700	09
61547	GABBRO					444680	6601700	09
61548	PERIDOTITE	BANDED	F111	68N		443880	6601440	09
61549	DUNITE	MASSIVE			XRF	444000	6601850	09
61550	PERIDOTITE	ALTERED	F035	90	XRF	443940	6601780	09

'TABLE 1.1 OUTCROP AND SAMPLE DATA FROM THE BLUE RIVER ULTRAMAFIC BODY'

61551	DUNITE	MASSIVE				TS	443850	6601680	09
61552	PERIDOTITE	SHEARED	J030	68E	XRF	TS	443500	6601750	09
61553	PERIDOTITE	SHEARED	J170	65E	XRF		443500	6601600	09
61554	PERIDOTITE				XRF		443450	6601550	09
61555	GABBRO	ALTERED					443450	6601550	09
61556	PERIDOTITE				XRF	TS	443350	6601520	09
61557	PERIDOTITE						443280	6601420	09
61558	DUNITE				XRF	PTS	443100	6601350	09
61559	PERIDOTITE				XRF		443050	6601280	09
61560	DUNITE	FRESH			XRF	PTS	443050	6601200	09
61561	RODINGITE	SHEARED					443000	6601200	09
61562	GABBRO	ALTERED			XRF		443000	6601200	09
61563	SERPENTINE	SHEARED				TS	443000	6601080	09
61564	RODINGITE	BRECCIATED				TS	443000	6601080	09
61565	GABBRO	MASSIVE				TS	443000	6601080	09
61566	VOLCANIC				XRF		443000	6601000	09
61567	VOLCANIC		J026	90		TS	443000	6600980	09
61568	RODINGITE	ALTERED				TS	445700	6599550	09
61569	RODINGITE	CARBONACEOUS				TS	445700	6599550	09
61570	RODINGITE	COARSE				TS	445700	6599550	09
61571	SERPENTINE				XRF		445650	6600000	09
61572	SERPENTINE	BANDED			XRF	TS	445800	6600100	09
61573	AMPHIBOLITE	BANDED			XRF	TS	445800	6600100	09
61574	AMPHIBOLITE	BANDED			XRF	TS	445800	6600100	09
61575	AMPHIBOLITE	BANDED				TS	445800	6600100	09
61576	AMPHIBOLITE	BANDED				TS	445800	6600100	09
61577	DUNITE	REGENERATED				PTS	445550	6599800	09
61578	SERPENTINE	SHEARED			XRF	TS	445550	6599800	09
61579	GABBRO	FRESH				TS	445550	6599800	09
61580	SERPENTINE	SHEARED			XRF		446250	6599550	09

'TABLE 1.1 OUTCROP AND SAMPLE DATA FROM THE BLUE RIVER ULTRAMAFIC BODY'

61581	RODINGITE	SHEARED				446000	6599650	09
61582	CHERT	BEDDED	F104 25S		TS	446500	6600200	09
61583	VOLCANIC			XRF		446500	6600200	09
61584	SERPENTINE				TS	446700	6600400	09
61585	RODINGITE	BANDED	F150 70N			446700	6600400	09
61586	AMPHIBOLITE	BANDED			TS	446700	6600400	09
61587	AMPHIBOLITE	BANDED		XRF		446700	6600400	09
61588	GABBRO	ALTERED				446800	6600470	09
61589	SERPENTINE	BASTITE		XRF		447300	6600250	09
61590	SERPENTINE	BASTITE		XRF		447000	6600100	09
61591	SERPENTINE	BASTITE		XRF		446000	6601500	09
61592	RODINGITE	MASSIVE		XRF	TS	446500	6601550	09
61593	RODINGITE	MASSIVE		XRF	TS	446400	6601600	09
61594	SERPENTINE	SHEARED	F140 35S	XRF		446380	6601650	09
61595	DUNITE	REGENERATED				445250	6603050	09
61596	SERPENTINE	SHEARED	F120 52E			445220	6603150	09
61597	DUNITE	REGENERATED	F035 65W	XRF		445020	6603980	09
61598	DUNITE	REGENERATED		XRF	PTS	445000	6604000	09
61599	DUNITE	REGENERATED		XRF		444920	6604080	09
61600	DUNITE	REGENERATED		XRF	PTS	444900	6604100	09
61601	DUNITE	REGENERATED		XRF		444400	6604100	09
61602	DUNITE	REGENERATED		XRF		444400	6604100	09
61603	SERPENTINE	TALCOSE	J180 90	XRF	PTS	444300	6603950	09
61604	SERPENTINE	TALCOSE	J176 86N	XRF		444350	6603900	09
61605	DUNITE	REGENERATED		XRF		444350	6603800	09
61606	DUNITE	REGENERATED		XRF		444420	6603700	09
61607	DUNITE	REGENERATED		XRF	PTS	444500	6603600	09
61608	DUNITE	REGENERATED		XRF		444650	6603450	09
61609	DUNITE	REGENERATED		XRF	TS	444750	6603400	09
61610	DUNITE	REGENERATED		XRF		444850	6603300	09

'TABLE 1.1 OUTCROP AND SAMPLE DATA FROM THE BLUE RIVER ULTRAMAFIC BODY.'

61611	DUNITE	REGENERATED	F045 9C	XRF	TS	445000	6603280	09
61612	PERIDOTITE	ALTERED		XRF	PTS	443450	6602400	09
61613	PERIDOTITE	ALTERED		XRF		443500	6602300	09
61614	PERIDOTITE	ALTEPED			TS	443420	6602200	09
61615	DUNITE	ALTERED			TS	443380	6602120	09
61616	PERIDOTITE	ALTERED		XRF	TS	443280	6602050	09
61617	PERIDOTITE	ALTERED		XRF		443200	6602040	09
61618	PERIDOTITE	ALTERED		XRF	TS	443140	6602100	09
61619	DUNITE	ALTERED			PTS	443000	6602180	09
61620	PERIDOTITE	ALTERED		XRF		443120	6602180	09
61621	DUNITE	REGENERATED		XRF		443700	6602400	09
61622	PERIDOTITE	ALTERED			TS	443900	6602450	09
61623	DUNITE	REGENERATED			PTS	444500	6602480	09
61624	DUNITE	REGENERATED		XRF		444500	6602650	09
61625	DUNITE	REGENERATED			PTS	444650	6602800	09
61626	DUNITE	REGENERATED		XRF		444700	6602920	09
61627	SERPENTINITE	SHEARED		XRF	TS	444900	6601100	09
61628	SERPENTINITE	SHEARED			TS	444900	6601100	09
61629	SERPENTINITE	BASTITE			TS	444800	6601150	09
61630	PERIDOTITE	MASSIVE		XRF		444780	6601050	09
61631	PERIDOTITE	MASSIVE		XRF		444520	6600640	09
61632	DUNITE	REGENERATED		XRF	PTS	444150	6600700	09
61633	DUNITE	REGENERATED		XRF	PTS	443950	6600480	09
61634	DUNITE	REGENERATED		XRF	TS	443620	6600630	09
61635	DUNITE	REGENERATED		XRF	PTS	443600	6600800	09
61636	DUNITE	REGENERATED			TS	443400	6600900	09
61637	DUNITE	REGENERATED		XRF	PTS	443500	6600980	09

'TABLE 1.2 MINERALOGY OF SECTIONED ULTRAMAFIC SAMPLES'
'SYMBOLS USED TO DENOTE MINERAL TYPE'

OLV	(1)	PRIMARY OLIVINE FROM THE BLUE RIVER ULTRAMAFIC BODY
OPX	(1/3)	PRIMARY AND METAMORPHIC ORTHOPYROXENE
CPX	(1)	PRIMARY AND ALTERED PRIMARY CLINOPYROXENE
SPL RED	(1)	PRIMARY SPINELS FROM THE BLUE RIVER COMPLEX
SRP	(2)	SERPENTINE DERIVED FROM PRIMARY OLIVINE (1)
MAG	(2)	MAGNETITE FROM PRIMARY OLIVINE (1) AND PYROXENE (1)
OLV	(3)	REGENERATED OLIVINE
TLC DSM	(3)	DISSEMINATED TALC FROM REACTION (8)
SRP ALM	(3)	ALUMINIUM RICH SERPENTINE FROM SRP (1) AND SPL (1)
SPL BLK	(3)	OXIDIZED SPINEL DERIVED FROM SPINEL (1)
TRM	(3)	TREMOLITE AND/OR ANTHOPHYLLITE BLADES
CHL	(3/4)	CHLORITE FORMED FROM AL SERPENTINE
SRP	(4)	SERPENTINE DERIVED FROM REGENERATED OLIVINE (3)
TLC XTL	(4)	RECRYSTALLIZED TALC FROM TLC (3) BY REACTION
BRC	(4)	BRUCITE FORMED BY REACTION (6)
SPL GRN	(4)	GREEN SPINEL FORMED DURING RESERPENTINIZATION
SRP ANT	(4)	ANTIGORITE FORMED FROM SRP(2) AND OLV (1/3)

'UNIT (1) BELOW THE TALC ISOGRAD'

	OLV (1) #	OPX (1) #	CPX (1) #	SPL RFD (1) #	SRP (2) +	MAG (2) +	OLV (3) X	TLC DSM (3) X	SRP ALM (3) X	SPL BLK (3) X	TRM (3) X	CHL (4) *	SRP (4) *	TLC XTL (4) *	BRC (4) *	SPL GRN (4) *	SRP ANT (4) *	
60071	#	#	#	#	+	+		X	X	X							*	P
60075	#			#	+	+				X							*	D
60078																		
60152	#	#		#	+	+												P
60153	#			#	+	+	X										*	P
60160	#	#	#	#	+	+	X		X									P
60163	#	#		#	+	+												P
60168	#	#	#	#	+	+						*					*	P
60169	#			#	+	+												D
60237	#			#		+			X	X							*	D
60871				#		+		X									*	D
60872	#			#	+	+											*	D
60874	#			#	+	+	X											P
60876	#	#		#	+	+	X		X	X							*	P
60902	#			#	+	+				X							*	D
61551	#			#	+	+											*	D
61552	#			#		+	X		X	X	X						*	P
61556	#			#		+	X		X	X	X						*	P
61558	#			#		+							*				*	D
61560	#			#	+	+	X										*	D

'TABLE 1.2 MINERALOGY OF SECTIONED ULTRAMAFIC SAMPLES'
'UNIT (2) BELOW THE OLIVINE ISOGRAD'

	OLV (1) #	OPX (1) #	CPX (1) #	SPL RED (1) #	SRP (2) +	MAG (2) +	OLV (3) X	TLC DSM (3) X	SRP ALM (3) X	SPL BLK (3) X	TRM (3) X	CHL (4) *	SRP (4) *	TLC XTL (4) *	BRC (4) *	SPL GRN (4) *	SRP ANT (4) *	
60018				#	+	+												P
60040					+	+				X		*	*					P
60041			#	#	+	+							*					P
60043					+	+							*					
60062					+	+				X		*	*					
60084					+	+				X		*						
60088					+	+				X		*						P
60092			#	#	+	+				X		*						P
60094	#	#	#	#	+	+												P
60096			#		+	+				X		*						P
60143				#	+	+						*	*			*		P

'TABLE 1.2 MINERALOGY OF SECTIONED ULTRAMAFIC SAMPLES'
'UNIT (3A) BELOW THE ANTIGORITE ISOGRAD'

	OLV (1) #	OPX (1) #	CPX (1) #	SPL RED (1) #	SRP (2) +	MAG (2) +	OLV (3) X	TLC DSM (3) X	SRP ALM (3) X	SPL BLK (3) X	TRM (3) X	CHL (4) *	SRP (4) *	TLC XTL (4) *	BRC (4) *	SPL GRN (4) *	SRP ANT (4) *	
60021				#	+	+	X						*		*			D
60023					+	+			X	X								
60155				#	+	+												
60157				#	+	+	X						*		*			D
60159				#	+	+							*					D
60241				#	+	+												D
61577				#	+	+	X						*		*			D
61632				#	+	+	X											D
60029			#		+	+	X						*		*			P
60030					+	+							*		*			P
60033			#	#	+	+							*		*			P
60034					+	+	X			X			*		*			
60035				#	+	+	X						*		*			D
60038				#	+	+							*					P
60102				#	+	+	X			X			*		*			D
60105				#	+	+			X				*					
60122					+	+				X			*					
60123				#		+	X	X		X							*	
60140					+	+				X		*	*			*		
61592			#		+	+							*		*			
61593				#	+	+							*					P

'TABLE 1.2 MINERALOGY OF SECTIONED ULTRAMAFIC SAMPLES'
'UNIT (3A) ABOVE THE ANTIGORITE ISOGRAD'

	OLV (1) #	OPX (1) #	CPX (1) #	SPL RED (1) #	SRP (2) +	MAG (2) +	OLV (3) X	TLC DSM (3) X	SRP ALM (3) X	SPL BLK (3) X	TRM (3) X	CHL (4) *	SRP (4) *	TLC XTL (4) *	BRC (4) *	SPL GRN (4) *	SRP ANT (4) *	
60860					+	+				X							*	D
60862				#		+	X			X							*	D
60867				#		+	X			X							*	D
61633				#		+	X			X							*	P
61634				#		+	X			X							*	P
61635						+	X			X							*	D
61636						+	X			X							*	D
61637				#		+	X			X							*	P
60067			#			+	X			X							*	P
60079						+				X							*	D
60107						+				X							*	D
60109						+	X			X			*				*	
60117				#		+	X			X	X		*				*	P
60128				#		+	X			X			*	*				P
60171					+	+	X			X							*	D
60172						+	X	X	X	X	X							P
60227						+	X	X	X	X	X							P
60694						+	X			X							*	D
60822						+	X			X							*	D
60907			#	#		+	X			X							*	P
61525					+	+	X			X							*	D
61623					+	+	X			X	X						*	D
61625					+	+	X	X		X	X							P

'TABLE 1.2 MINERALOGY OF SECTIONED ULTRAMAFIC SAMPLES'
'UNIT (3B) WEST AND EAST'

	OLV (1) #	OPX (3) #	CPX (1) #	SPL RED (1) #	SRP (2) +	MAG (2) +	OLV (3) X	TLC DSM (3) X	SRP ALM (3) X	SPL BLK (3) X	TRM (3) X	CHL (4) *	SRP (4) *	TLC XTL (4) *	BRC (4) *	SPL GRN (4) *	SRP ANT (4) *	
60179						+	X	X		X							*	P
60180						+	X			X		*		*			*	P
60133							X	X	X	X							*	P
60137							X			X	X	*	*	*				P
60199							X	X		X		*	*	*		*		P
60202							X			X	X	*	*					P
60206					+	+	X	X		X	X						*	P
60209				#			X	X	X	X	X	*		*				P
60212		#					X			X	X	*	*			*		P
60213		#					X	X		X	X	*	*			*		P
60215		#					X			X	X	*	*	*		*		D
60218							X			X		*	*	*		*		D
60221						+	X			X							*	D
60894				#		+	X	X	X	X			*					D
61535							X	X	X	X			*				*	D
61598							X	X	X	X	X		*					P
61600							X	X	X	X	X							P
61603		#					X	X		X	X	*	*			*		P
61607							X	X	X	X	X							P
61609							X	X	X	X	X					*		D
61611							X	X	X	X	X		*					P

'TABLE 1.2 MINERALOGY OF SECTIONED ULTRAMAFIC SAMPLES'
'UNIT (3C) ABOVE THE TALC ISOGRAD'

	OLV (1) #	CPX (1) #	CPX (1) #	SPL RED (1) #	SRP (2) +	MAG (2) +	OLV (3) X	TLC DSM (3) X	SRP ALM (3) X	SPL BLK (3) X	TRM (3) X	CHL (4) *	SRP (4) *	TLC XTL (4) *	BRC (4) *	SPL GRN (4) *	SRP ANT (4) *	
60173	#					+		X	X	X	X							
60174	#			#		+	X	X				*		*			*	P
60184	#					+			X	X	X						*	P
60185	#					+			X	X	X							P
60186	#			#		+	X	X		X		*					*	P
60188	#			#	+	+	X	X	X									P
60190	#					+	X	X	X	X							*	P
60191	#					+			X	X	X							P
60195	#					+	X		X	X	X							P
60196	#			#		+			X	X	X							D
60204	#					+	X		X	X	X						*	P
60224	#			#		+		X	X	X							*	D
60226	#	#		#		+		X	X	X	X						*	P
60233	#					+		X		X	X						*	P
60341	#					+	X	X		X	X	*						P
61622	#					+			X	X	X							P
60886	#			#	+	+			X									D
60893	#					+		X	X	X							*	P
61612	#					+			X	X	X							P
61614	#			#	+	+		X	X	X	X						*	P
61615	#			#		+			X								*	D
61616	#			#		+		X	X		X						*	P
61618	#			#		+	X	X	X	X	X						*	P
61619	#			#	+	+		X										D

Appendix II. Mineral Data

Electron Microprobe Micro-analysis

The mineral analyses listed in this appendix were obtained by electron microprobe micro-analysis, using the Durham University, Cambridge Instrument Company, "Geoscan Mark II" electron microprobe.

The petrological data given in Table 1.2 was obtained from a study of a large number of polished thin sections, and a few ordinary thin sections. The polished thin sections were prepared by Vancouver Petrographics Ltd., on behalf of Rio Tinto Canadian Exploration Ltd. The analysed samples were chosen from among the polished thin sections; on the basis of mineralogy and texture. Where possible all the main coexisting phases were analysed.

Efforts were made to standardize operating conditions, in order to avoid undue bias and all the coexisting phases were analysed for the same elements, under the same conditions. The one exception is found in Table 8.1, which lists gabbro pyroxenes that have been analysed for Na and K. The general methods employed are those described by Sweatman and Long (1969).

The Durham University "Geoscan" was operated under a high vacuum, at an accelerating voltage of 15 kV, and a specimen current of 0.04 μA. The electron beam was kept focussed throughout, giving a spot analysis of diameter 2-5 μM.

Appendix Table 2.1

Optimum analysing conditions and standards used for electron microprobe analysis

Atomic Number	Element	Line	Analysing Crystal	Counter	Peak 2θ	Background Location	Standard
12	Mg	$K\alpha_1$	K.A.P.	Flow	$43^\circ 42'$	$+/-2^\circ$	MgO
13	Al	"	"	"	$36^\circ 32'$	$+/-2^\circ$	Al_2O_3
14	Si	"	"	"	$31^\circ 02'$	$+1^\circ 30$	Wollastonite (Wo-2)
20	Ca	"	LiF	"	$113^\circ 02'$	$+/-2^\circ$	Wollastonite (Wo-2)
22	Ti	"	"	"	$86^\circ 05'$	$+/-2^\circ$	TiO_2
24	Cr	"	"	"	$69^\circ 16'$	$+/-2^\circ$	Cr_2O_3
25	Mn	"	"	"	$62^\circ 48'$	$+/-2^\circ$	Mn
26	Fe	"	"	"	$57^\circ 20'$	$+/-2^\circ$	Fe
28	Ni	"	"	"	$48^\circ 34'$	$+/-2^\circ$	Ni
11	Na	"	K.A.P.	"	$53^\circ 14'$	$+1^\circ 30$	Jadeite (JD-1)
19	K	"	Quartz	"	$67^\circ 58'$	-2°	Orthoclase (AF-15)

Note: Names in brackets refer to University of Durham Standard names.

Secondary X-rays were analysed using a wavelength dispersive system. The "Geoscan" has two spectrometers, set at a take-off angle of 75°. These allow two elements to be analysed simultaneously. One spectrometer was used with a LiF crystal, and the other with a K.A.P. crystal. Appendix Table 2.1 shows the optimum analysing conditions for the nine main elements, and also conditions for the alkalis, Na and K.

The wavelength dispersive system is based on a comparative technique, and the standards used for each element are also given in Appendix Table 2.1. These are metals, simple oxides, and simple silicates of known composition. The standards and the polished thin sections were carbon coated simultaneously prior to use, and they were both stored in a dessicator when not in use.

Data from the "Geoscan" was corrected for the effects of atomic number, Duncumb and Reed (1968), mass absorption, Heinrich (1966), and fluorescence, Reed (1965). Corrections were made using an on-line Varian 620-100 computer. The correction procedure was applied using the computer program "Tim 3", written by Dr. A. Peckett.

The on-line computer was able to produce a corrected analysis in a matter of seconds, and machine drift was readily detected. The following procedure was adopted in setting up the "Geoscan" at the start of a probe session.

1. Standard peaks were located, and analysed, (5-10 x 10 second counts).
2. Standard backgrounds were analysed, above and below the peak, (4-5 x 10 second counts each).
3. Unknown backgrounds were taken, above and below the peak, (4-5 x 10 second counts each).
4. Unknown peaks were analysed, (6-10 x 10 second counts).
5. Results were calculated.
6. If the results were satisfactory, further unknown peaks were recorded, and the process was continued. If the results were not satisfactory, standard peaks were relocated, and reanalysed.

Background values obtained for each phase were used throughout a session, and they were not reanalysed for each individual crystal. Background values were checked by taking peak position values on minerals which contain the same average atomic number as the unknown, but do not contain the element in question. The two methods gave reasonably consistent results, and where a descrepancy was found, the lower value was taken. The Si background was determined in this way. Data from Al_2O_3 is applicable to olivine.

Detection limits are calculated from the formula:

$$\sqrt{\frac{3}{M}} = Rb/Tb$$

where M = mean peak counts/sec/%
Rb = mean background counts per second
Tb = counting time on the background.

Calculation detection limits are in the range 200-500 ppm, (0.02-0.05%). The overall accuracy taking into account counting precision and uncertainties in the correction procedure, is probably in the order of $\pm$ 2% of the amount of the major constituents present. Trace elements probably have a somewhat lower accuracy.

The probe analyses given in the succeeding tables are all spot analyses made at one point, at one time. Brucite was the only phase which readily deteriorated under the electron beam, and in all other cases it was possible to complete an analysis before this occurred.

Corrected analyses, with Fe (total) taken as Fe^{++}, were tabulated and recast into their atomic proportions, using the computer program "Tablit" developed by Mr. E.B. Curran. This program was also used to calculate end member compositions, and the distribution of Fe^{2} and Fe^{3} in spinel, according to the method proposed by Carmichael (1967).

Hydrated minerals are presented on a water free basis, and the apparent percentage deficiency is taken to be the water content.

'TABLE 3.1 PRIMARY OLIVINE (1) FROM THE BLUE RIVER ULTRAMAFIC BODY'

	1	2	3	4	5	6	7	8	9	10
	60094A1	60094B1	60094C1	60094D1	60153B1	60153C1	60153H1	60153D1	60160A1	60160B1
OXIDE WEIGHT PERCENTAGE										
SIO2	40.81	41.34	41.10	41.21	40.94	41.64	41.92	41.66	41.01	40.87
TIO2	0.01	-	0.02	0.02	0.05	0.06	0.02	0.04	0.03	0.04
AL2O3	0.03	0.07	0.06	0.04	0.11	0.09	0.07	0.10	0.04	0.03
CR2O3	0.01	0.01	0.03	0.02	0.05	0.05	0.03	0.23	0.01	0.04
FEO	9.25	9.24	9.31	9.17	8.60	8.60	8.55	6.61	9.28	9.70
MNO	0.12	0.12	0.13	0.14	0.12	0.16	0.16	0.13	0.18	0.13
MGO	49.72	49.28	49.68	49.31	49.62	49.49	49.45	51.39	49.56	49.17
CAO	-	-	0.02	-	0.02	0.01	0.02	0.02	-	0.01
NIO	0.25	0.30	0.30	0.28	0.24	0.23	0.32	0.44	0.32	0.32
TOTAL	100.20	100.36	100.65	100.19	99.75	100.33	100.54	100.62	100.43	100.31
ATOMIC PROPORTIONS ON THE BASIS OF 4 OXYGENS										
SI	0.996	1.006	0.999	1.005	1.000	1.010	1.014	1.001	0.999	0.999
TI	0.000	0.000	0.000	0.000	0.001	0.001	0.000	0.001	0.001	0.001
AL	0.001	0.002	0.002	0.001	0.003	0.003	0.002	0.003	0.001	0.001
CR	0.000	0.000	0.001	0.000	0.001	0.001	0.001	0.004	0.000	0.001
FE2	0.189	0.188	0.189	0.187	0.176	0.174	0.173	0.133	0.189	0.198
MN	0.002	0.002	0.003	0.003	0.002	0.003	0.003	0.003	0.004	0.003
MG	1.809	1.737	1.799	1.791	1.807	1.789	1.783	1.840	1.799	1.790
CA	0.000	0.000	0.001	0.000	0.001	0.000	0.001	0.001	0.000	0.000
NI	0.005	0.006	0.006	0.005	0.005	0.004	0.006	0.009	0.006	0.006
END MEMBER COMPOSITIONS										
MG	90.43	90.37	90.36	90.42	91.02	90.96	91.00	93.14	90.32	89.91
FE	9.57	9.63	9.64	9.58	8.98	9.04	9.00	6.86	9.68	10.09

'TABLE 3.1 PRIMARY OLIVINE (1) FROM THE BLUE RIVER ULTRAMAFIC BODY'

	11	12	13	14	15	16	17	18	19	20
	60163A1	60163B1	60163C1	60163D1	60163E1	60163F1	60075A1	60075B1	60075C1	60075D1
OXIDE WEIGHT PERCENTAGE										
SIO2	40.99	41.21	41.16	41.28	40.75	41.23	41.34	41.25	41.62	40.92
TIO2	0.04	0.02	0.04	0.03	0.04	0.06	-	-	0.03	-
AL2O3	0.14	0.14	0.22	0.13	0.15	0.11	0.15	0.14	0.17	0.27
CR2O3	0.05	0.05	0.03	0.04	0.05	0.05	0.07	0.05	0.06	0.06
FEO	8.57	8.84	8.87	9.02	8.83	8.96	7.37	8.04	7.78	7.61
MNO	0.13	0.15	0.12	0.15	0.14	0.10	0.14	0.11	0.12	0.12
MGO	49.87	50.05	49.65	49.40	49.57	49.81	50.76	51.09	50.81	50.74
CAO	0.01	0.01	0.01	-	0.01	-	-	-	0.01	0.02
NIO	0.32	0.27	0.29	0.37	0.30	0.31	0.22	0.22	0.35	0.35
TOTAL	100.12	100.74	100.39	100.42	99.84	100.63	100.05	100.90	100.95	100.09
ATOMIC PROPORTIONS ON THE BASIS OF 4 OXYGENS										
SI	0.998	0.998	1.000	1.004	0.997	1.000	1.001	0.994	1.001	0.993
TI	0.001	0.000	0.001	0.001	0.001	0.001	0.000	0.000	0.001	0.000
AL	0.004	0.004	0.006	0.004	0.004	0.003	0.004	0.004	0.005	0.008
CR	0.001	0.001	0.001	0.001	0.001	0.001	0.001	0.001	0.001	0.001
FE2	0.175	0.179	0.180	0.183	0.181	0.182	0.149	0.162	0.156	0.154
MN	0.003	0.003	0.002	0.003	0.003	0.002	0.003	0.002	0.002	0.002
MG	1.810	1.807	1.798	1.790	1.807	1.801	1.832	1.835	1.821	1.835
CA	0.000	0.000	0.000	0.000	0.000	0.000	0.000	0.000	0.000	0.001
NI	0.006	0.005	0.006	0.007	0.006	0.006	0.004	0.004	0.007	0.007
END MEMBER COMPOSITIONS										
MG	91.08	90.84	90.77	90.56	90.78	90.74	92.33	91.78	91.97	92.12
FE	8.92	9.16	9.23	9.44	9.22	9.26	7.67	8.22	8.03	7.88

'TABLE 3.1 PRIMARY OLIVINE (1) FROM THE BLUE RIVER ULTRAMAFIC BODY'

	21	22	23	24	25	26	27	28	29	30
	60902A1	60902B1	60902C1	60237A1	60237B1	60237C1	60237D1	60872A1	60872B1	60872C1
OXIDE WEIGHT PERCENTAGE										
SIO2	41.56	41.19	41.36	41.69	41.82	41.55	41.62	41.69	41.26	41.20
TIO2	0.03	0.06	0.04	-	0.04	0.07	0.03	-	-	-
AL2O3	0.10	0.21	0.22	0.07	0.02	0.09	0.05	0.09	0.07	0.05
CR2O3	0.02	0.03	0.01	-	0.05	0.05	0.03	-	-	-
FEO	7.52	7.76	7.45	5.20	5.36	5.70	5.34	8.24	8.32	8.38
MNO	0.12	0.15	0.12	0.08	0.08	0.11	0.10	0.11	0.16	0.11
MGO	50.59	50.17	50.96	52.27	52.74	52.57	52.60	49.91	49.91	49.90
CAO	0.02	0.03	0.01	0.02	0.02	-	0.02	0.02	0.02	0.04
NIO	0.31	0.31	0.34	0.38	0.52	0.42	0.47	0.47	0.49	0.44
TOTAL	100.27	99.91	100.51	99.71	100.65	100.56	100.26	100.53	100.23	100.12
ATOMIC PROPORTIONS ON THE BASIS OF 4 OXYGENS .										
SI	1.005	1.001	0.998	1.003	0.999	0.995	0.998	1.008	1.003	1.002
TI	0.001	0.001	0.001	0.000	0.001	0.001	0.001	0.000	0.000	0.000
AL	0.003	0.006	0.006	0.002	0.001	0.003	0.001	0.003	0.002	0.001
CR	0.000	0.001	0.000	0.000	0.001	0.001	0.001	0.000	0.000	0.000
FE2	0.152	0.158	0.150	0.105	0.107	0.114	0.107	0.167	0.169	0.171
MN	0.002	0.003	0.002	0.002	0.002	0.002	0.002	0.002	0.003	0.002
MG	1.823	1.817	1.832	1.875	1.878	1.876	1.880	1.799	1.808	1.809
CA	0.001	0.001	0.000	0.001	0.001	0.000	0.001	0.001	0.001	0.001
NI	0.006	0.006	0.007	0.007	0.010	0.008	0.009	0.009	0.010	0.009
END MEMBER COMPOSITIONS										
MG	92.19	91.87	92.30	94.63	94.53	94.16	94.51	91.42	91.29	91.28
FE	7.81	8.13	7.70	5.37	5.47	5.84	5.49	8.58	8.71	8.72

'TABLE 3.1 PRIMARY OLIVINE (1) FROM THE BLUE RIVER ULTRAMAFIC BODY'

	31	32	33	34	35	36	37	38	39	40
	60876A1	60876B1	60876C1	60876D1	60876E1	60876F1	60876G1	60876H1	61558A1	61558B1
OXIDE WEIGHT PERCENTAGE										
SIO2	41.30	41.37	41.22	40.92	41.33	40.78	40.46	41.29	41.21	41.09
TIO2	0.06	0.04	0.05	0.02	0.05	0.03	0.04	0.06	0.07	0.02
AL2O3	0.06	0.09	0.07	0.04	0.10	0.06	0.42	0.08	0.09	0.08
CR2O3	0.07	0.03	0.05	0.05	0.07	0.06	0.05	0.05	0.05	0.04
FEO	8.98	8.78	9.10	10.16	9.16	8.82	8.83	9.28	8.82	8.67
MNO	0.12	0.11	0.14	0.12	0.12	0.17	0.13	0.14	0.12	0.14
MGO	49.22	49.84	49.38	49.01	49.33	50.18	49.40	49.64	49.99	49.77
CAO	0.03	0.01	0.01	0.01	0.01	-	-	0.02	0.01	0.03
NIO	0.27	0.32	0.35	0.30	0.35	0.36	0.24	0.23	0.22	0.27
TOTAL	100.11	100.59	100.37	100.63	100.52	100.46	99.57	100.79	100.58	100.11
ATOMIC PROPORTIONS ON THE BASIS OF 4 OXYGENS										
SI	1.006	1.003	1.003	0.998	1.004	0.992	0.992	1.001	0.999	1.001
TI	0.001	0.001	0.001	0.000	0.001	0.001	0.001	0.001	0.001	0.000
AL	0.002	0.003	0.002	0.001	0.003	0.002	0.012	0.002	0.003	0.002
CR	0.001	0.001	0.001	0.001	0.001	0.001	0.001	0.001	0.001	0.001
FE2	0.183	0.178	0.185	0.207	0.186	0.179	0.181	0.188	0.179	0.177
MN	0.002	0.002	0.003	0.002	0.002	0.004	0.003	0.003	0.002	0.003
MG	1.788	1.800	1.791	1.782	1.786	1.819	1.805	1.794	1.807	1.806
CA	0.001	0.000	0.000	0.000	0.000	0.000	0.000	0.001	0.000	0.001
NI	0.005	0.006	0.007	0.006	0.007	0.007	0.005	0.004	0.004	0.005
END MEMBER COMPOSITIONS										
MG	90.60	90.90	90.49	89.47	90.45	90.86	90.76	90.37	90.88	90.96
FE	9.40	9.10	9.51	10.53	9.55	9.14	9.24	9.63	9.12	9.04

'TABLE 3.1 PRIMARY OLIVINE (1) FROM THE BLUE RIVER ULTRAMAFIC BODY'

	41	42	43	44	45	46	47	48	49	50
	61558C1	60174A1	60174B1	60174D1	60174E1	60184A1	60185A1	60185B1	60185C1	60185D1
OXIDE WEIGHT PERCENTAGE										
SIO2	41.16	41.32	40.84	41.19	41.38	41.21	41.21	40.49	40.82	40.74
TIO2	0.02	0.02	-	0.04	0.02	0.01	0.03	0.03	0.05	0.05
AL2O3	0.05	0.09	0.09	0.12	0.14	0.10	0.37	0.11	0.11	0.10
CR2O3	0.08	0.03	0.05	0.02	0.04	0.03	0.05	0.05	0.02	0.01
FEO	8.82	8.33	8.66	8.51	8.49	9.59	9.21	9.68	9.08	9.03
MNO	0.09	0.17	0.16	0.14	0.14	0.16	0.16	0.14	0.23	0.13
MGO	49.64	49.69	49.91	49.88	49.34	48.49	48.93	49.36	49.93	50.06
CAO	0.03	0.01	-	-	0.01	0.01	0.02	0.05	0.01	0.02
NIO	0.28	0.25	0.17	0.23	0.24	0.30	0.26	0.23	0.27	0.27
TOTAL	100.17	99.91	99.88	100.13	99.80	99.90	100.24	100.14	100.52	100.41
ATOMIC PROPORTIONS ON THE BASIS OF 4 OXYGENS										
SI	1.002	1.006	0.997	1.002	1.009	1.009	1.004	0.992	0.993	0.992
TI	0.000	0.000	0.000	0.001	0.000	0.000	0.001	0.001	0.001	0.001
AL	0.001	0.003	0.003	0.003	0.004	0.003	0.011	0.003	0.003	0.003
CR	0.002	0.001	0.001	0.000	0.001	0.001	0.001	0.001	0.000	0.000
FE2	0.180	0.170	0.177	0.173	0.173	0.196	0.188	0.198	0.185	0.184
MN	0.002	0.004	0.003	0.003	0.003	0.003	0.003	0.003	0.005	0.003
MG	1.801	1.803	1.816	1.808	1.792	1.769	1.776	1.801	1.810	1.816
CA	0.001	0.000	0.000	0.000	0.000	0.000	0.001	0.001	0.000	0.001
NI	0.005	0.005	0.003	0.004	0.005	0.006	0.005	0.005	0.005	0.005
END MEMBER COMPOSITIONS										
MG	90.85	91.24	90.98	91.13	91.06	89.86	90.29	89.95	90.52	90.69
FE	9.15	8.76	9.02	8.87	8.94	10.14	9.71	10.05	9.48	9.31

'TABLE 3.1 PRIMARY OLIVINE (1) FROM THE BLUE RIVER ULTRAMAFIC BODY'

	51	52	53	54	55	56	57	58	59	60
	60186D1	60186E1	60186G1	60186J1	61619A1	61619B1	61619C1	61619D1	61612A1	61612B1
OXIDE WEIGHT PERCENTAGE										
SIO2	41.25	40.99	41.24	41.22	41.63	41.15	41.60	41.11	41.29	41.75
TIO2	0.05	0.07	0.02	0.01	0.02	-	0.01	0.01	0.02	-
AL2O3	0.06	0.07	0.11	0.06	0.15	0.16	0.15	0.15	0.04	0.10
CR2O3	0.04	0.06	0.06	0.02	-	0.07	0.03	0.02	0.02	0.04
FEO	8.70	8.54	8.54	8.57	7.96	8.17	8.23	7.96	7.36	7.19
MNO	0.14	0.12	0.16	0.12	0.09	0.13	0.10	0.11	0.17	0.17
MGO	49.75	50.18	49.23	50.06	50.25	50.77	49.97	50.77	51.55	50.49
CAO	-	0.01	-	0.02	0.02	-	-	-	-	-
NIO	0.24	0.25	0.27	0.29	0.28	0.19	0.21	0.33	0.26	0.29
TOTAL	100.23	100.29	99.63	100.37	100.40	100.64	100.30	100.46	100.71	100.03
ATOMIC PROPORTIONS ON THE BASIS OF 4 OXYGENS										
SI	1.003	0.996	1.008	1.001	1.006	0.995	1.007	0.995	0.994	1.010
TI	0.001	0.001	0.000	0.000	0.000	0.000	0.000	0.000	0.000	0.000
AL	0.002	0.002	0.003	0.002	0.004	0.005	0.004	0.004	0.001	0.003
CR	0.001	0.001	0.001	0.000	0.000	0.001	0.001	0.000	0.000	0.001
FE2	0.177	0.174	0.175	0.174	0.161	0.165	0.167	0.161	0.148	0.145
MN	0.003	0.002	0.003	0.002	0.002	0.003	0.002	0.002	0.003	0.003
MG	1.803	1.818	1.793	1.811	1.810	1.829	1.803	1.831	1.850	1.820
CA	0.000	0.000	0.000	0.001	0.001	0.000	0.000	0.000	0.000	0.000
NI	0.005	0.005	0.005	0.006	0.005	0.004	0.004	0.006	0.005	0.006
END MEMBER COMPOSITIONS										
MG	90.93	91.17	90.97	91.12	91.75	91.59	91.44	91.81	92.42	92.44
FE	9.07	8.83	9.03	8.88	8.25	8.41	8.56	8.19	7.58	7.56

'TABLE 3.1 PRIMARY OLIVINE (1) FROM THE BLUE RIVER ULTRAMAFIC BODY'

	61	62	63	64	65	66	67	68	69
	61612C1	60196A1	60196B1	60196C1	60196D1	60196E1	60196F1	60196G1	60196H1
OXIDE WEIGHT PERCENTAGE									
SIO2	41.61	41.35	41.04	40.77	41.15	41.11	40.91	41.00	41.26
TIO2	-	0.02	0.02	0.02	0.03	0.06	0.02	0.04	0.01
AL2O3	0.05	0.17	0.10	0.10	0.10	0.11	0.13	0.13	0.15
CR2O3	0.03	0.03	0.06	0.09	0.05	0.04	0.05	0.03	0.04
FEO	7.54	8.79	8.81	9.15	8.85	8.86	9.01	9.25	8.94
MNO	0.20	0.15	0.15	0.13	0.10	0.16	0.11	0.13	0.15
MGO	50.59	49.79	50.14	49.48	49.69	49.92	49.66	49.25	49.35
CAO	0.02	-	0.01	-	0.03	-	-	-	0.02
NIO	0.29	0.29	0.35	0.27	0.28	0.22	0.31	0.27	0.19
TOTAL	100.33	100.59	100.68	100.01	100.28	100.48	100.20	100.10	100.11
ATOMIC PROPORTIONS ON THE BASIS OF 4 OXYGENS									
SI	1.006	1.002	0.995	0.997	1.001	0.998	0.997	1.001	1.005
TI	0.000	0.000	0.000	0.000	0.001	0.001	0.000	0.001	0.000
AL	0.001	0.005	0.003	0.003	0.003	0.003	0.004	0.004	0.004
CR	0.001	0.001	0.001	0.002	0.001	0.001	0.001	0.001	0.001
FE2	0.152	0.178	0.179	0.187	0.180	0.180	0.184	0.189	0.182
MN	0.004	0.003	0.003	0.003	0.002	0.003	0.002	0.003	0.003
MG	1.822	1.799	1.812	1.803	1.801	1.807	1.804	1.792	1.791
CA	0.001	0.000	0.000	0.000	0.001	0.000	0.000	0.000	0.001
NI	0.006	0.006	0.007	0.005	0.005	0.004	0.006	0.005	0.004
END MEMBER COMPOSITIONS									
MG	92.09	90.84	90.88	90.48	90.82	90.79	90.65	90.34	90.63
FE	7.91	9.16	9.12	9.53	9.18	9.21	9.35	9.66	9.37

'TABLE 3.4 ORTHOPYROXENE (1) FROM THE BLUE RIVER ULTRAMAFIC BODY'

	1	2	3	4	5	6	7	8	9	10
	60160A1	60160B1	60163A1	60163B1	60163C1	60163D1	60876A1	60876B1	60876C1	60094A1
OXIDE WEIGHT PERCENTAGE										
SIO2	55.82	55.54	56.10	56.20	56.39	56.23	56.41	56.22	56.19	56.69
TIO2	0.08	0.06	0.09	0.09	0.07	0.09	0.06	0.09	0.04	0.03
AL2O3	3.06	3.27	3.10	2.25	2.85	2.82	2.75	2.75	2.69	3.01
CR2O3	0.61	0.65	0.68	0.42	0.70	0.62	0.68	0.67	0.72	1.01
FEO	5.96	6.17	5.88	5.82	5.96	5.92	5.69	5.67	5.73	6.09
MNO	0.14	0.14	0.14	0.13	0.17	0.13	0.11	0.15	0.16	0.14
MGO	33.23	33.73	33.96	34.57	33.88	33.40	33.44	32.14	34.25	32.13
CAO	0.62	0.64	0.79	0.41	0.56	0.79	0.84	2.32	0.72	0.98
NIO	-	-	0.03	-	-	0.01	-	-	-	-
TOTAL	99.52	100.20	100.77	99.89	100.58	100.01	99.98	100.01	100.50	100.08
ATOMIC PROPORTIONS ON THE BASIS OF 6 OXYGENS										
SI	1.933	1.915	1.921	1.938	1.933	1.938	1.943	1.944	1.928	1.953
TI	0.002	0.002	0.002	0.002	0.002	0.002	0.002	0.002	0.001	0.001
AL	0.125	0.133	0.125	0.091	0.115	0.115	0.112	0.112	0.109	0.122
CR	0.017	0.018	0.018	0.011	0.019	0.017	0.019	0.018	0.020	0.028
FE2	0.173	0.178	0.168	0.168	0.171	0.171	0.164	0.164	0.164	0.176
MN	0.004	0.004	0.004	0.004	0.005	0.004	0.003	0.004	0.005	0.004
MG	1.715	1.733	1.733	1.777	1.731	1.716	1.716	1.656	1.752	1.650
CA	0.023	0.024	0.029	0.015	0.021	0.029	0.031	0.086	0.026	0.036
NI	0.000	0.000	0.001	0.000	0.000	0.000	0.000	0.000	0.000	0.000
END MEMBER COMPOSITIONS										
CA	1.20	1.22	1.50	0.77	1.07	1.52	1.62	4.50	1.36	1.94
MG	89.57	89.39	89.59	90.49	89.81	89.39	89.65	86.69	89.96	88.43
FE	9.23	9.39	8.92	8.74	9.12	9.09	8.73	8.81	8.69	9.63

'TABLE 3.4 ORTHOPYROXENE (1) FROM THE BLUE RIVER ULTRAMAFIC BODY'

	11	12	13	14	15
	60094B1	60094C1	60094D1	60094E1	60094F1
OXIDE WEIGHT PERCENTAGE					
SIO2	55.89	55.50	55.06	54.56	55.35
TIO2	0.03	-	0.03	0.01	0.03
AL2O3	2.52	2.74	2.85	2.97	2.84
CR2O3	0.73	0.74	1.08	1.00	0.82
FEO	5.81	5.72	5.97	5.69	5.84
MNO	0.11	0.15	0.13	0.12	0.19
MGO	32.64	32.81	32.51	32.53	32.96
CAO	1.79	1.68	2.21	2.52	2.19
NIO	-	-	0.02	0.07	-
TOTAL	99.52	99.34	99.86	99.47	100.22
ATOMIC PROPORTIONS ON THE BASIS OF 6 OXYGENS					
SI	1.942	1.932	1.915	1.906	1.916
TI	0.001	0.000	0.001	0.000	0.001
AL	0.103	0.112	0.117	0.122	0.116
CR	0.020	0.020	0.030	0.028	0.022
FE2	0.169	0.167	0.174	0.166	0.169
MN	0.003	0.004	0.004	0.004	0.006
MG	1.690	1.702	1.686	1.694	1.701
CA	0.067	0.063	0.082	0.094	0.081
NI	0.000	0.000	0.001	0.002	0.000
END MEMBER COMPOSITIONS					
CA	3.46	3.24	4.24	4.82	4.15
MG	87.62	87.93	86.64	86.51	86.92
FE	8.92	8.83	9.13	8.67	8.93

'TABLE 3.6 CLINCPYROXENE (1) FROM THE BLUE RIVER ULTRAMAFIC BODY'

	1	2	3	4	5	6	7	8	9	10
	60067A1	60067B1	60067C1	60067D1	60067E1	60067F1	60067G1	60876A1	60094A1	60094B1
OXIDE WEIGHT PERCENTAGE										
SIO2	53.09	53.89	53.33	53.72	53.81	53.95	52.16	52.62	53.85	51.76
TIO2	0.13	0.10	0.15	0.08	0.08	0.11	0.14	0.13	0.05	0.02
AL2O3	2.21	2.13	2.47	1.92	1.59	1.98	3.41	2.80	2.23	3.00
CR2O3	0.56	0.39	0.55	0.40	0.31	0.40	0.99	0.92	1.17	1.31
FEO	2.00	2.15	2.12	1.96	1.85	2.15	2.11	1.99	1.79	2.38
MNO	0.09	0.10	0.08	0.06	0.10	0.10	0.09	0.09	0.07	0.13
MGO	17.28	17.01	16.79	17.07	17.26	17.22	16.35	17.07	17.38	18.02
CAO	24.10	24.38	24.22	24.46	24.63	24.50	24.40	23.63	23.56	24.04
NIO	-	-	-	-	-	-	-	-	-	-
TOTAL	99.46	100.15	99.71	99.67	99.63	100.41	99.65	99.25	100.10	100.66
ATOMIC PROPORTIONS ON THE BASIS OF 6 OXYGENS										
SI	1.939	1.953	1.942	1.956	1.960	1.951	1.907	1.925	1.948	1.880
TI	0.004	0.003	0.004	0.002	0.002	0.003	0.004	0.004	0.001	0.001
AL	0.095	0.091	0.106	0.082	0.068	0.084	0.147	0.121	0.095	0.128
CR	0.016	0.011	0.016	0.012	0.009	0.011	0.029	0.027	0.033	0.038
FE2	0.061	0.065	0.065	0.060	0.056	0.065	0.065	0.061	0.054	0.072
MN	0.003	0.003	0.002	0.002	0.003	0.003	0.003	0.003	0.002	0.004
MG	0.940	0.919	0.911	0.926	0.937	0.928	0.891	0.931	0.937	0.976
CA	0.943	0.947	0.945	0.954	0.962	0.950	0.956	0.926	0.913	0.936
NI	0.000	0.000	0.000	0.000	0.000	0.000	0.000	0.000	0.000	0.000
END MEMBER COMPOSITIONS										
CA	48.43	48.96	49.14	49.14	49.11	48.80	49.94	48.23	47.90	47.08
MG	48.29	47.51	47.37	47.69	47.86	47.70	46.54	48.45	49.14	49.08
FE	3.28	3.53	3.49	3.17	3.04	3.50	3.52	3.32	2.95	3.84

'TABLE 3.6 CLINOPYROXENE (1) FROM THE BLUE RIVER ULTRAMAFIC BODY'

	11	12	13
	60160A1	60160B1	60160C1
OXIDE WEIGHT PERCENTAGE			
SIO2	51.75	51.70	51.66
TIO2	0.15	0.13	0.15
AL2O3	3.44	3.65	3.50
CR2O3	1.10	1.16	1.03
FEO	2.19	2.10	2.13
MNO	0.07	0.07	0.10
MGO	15.96	16.02	16.69
CAO	23.64	23.59	23.36
NIO	-	-	-
TOTAL	98.30	98.42	98.62
ATOMIC PROPORTIONS ON THE BASIS OF 6 OXYGENS			
SI	1.915	1.910	1.904
TI	0.004	0.004	0.004
AL	0.150	0.159	0.152
CR	0.032	0.034	0.030
FE2	0.068	0.065	0.066
MN	0.002	0.002	0.003
MG	0.880	0.882	0.917
CA	0.937	0.934	0.923
NI	0.000	0.000	0.000
END MEMBER COMPOSITIONS			
CA	49.66	49.60	48.35
MG	46.63	46.84	48.04
FE	3.71	3.56	3.60

'TABLE 3.8 PRIMARY SPINEL (I) FROM THE BLUE RIVER ULTRAMAFIC BODY'

	1	2	3	4	5	6	7	8	9	10
	60094A1	60094B1	60094C1	60055A1	60055B1	60055C1	61577A1	60153A1	60153B1	60153C1
OXIDE WEIGHT PERCENTAGE										
SIO2	-	-	-	-	-	-	-	-	-	0.23
TIO2	-	-	0.02	0.19	0.21	0.18	0.20	0.08	0.08	0.10
AL2O3	31.23	30.64	30.60	10.53	9.77	10.55	12.51	26.08	26.91	25.83
CR2O3	36.61	36.99	37.39	59.32	58.93	59.19	54.58	40.18	40.53	35.52
FE2O3	1.96	1.81	2.51	1.56	2.43	1.36	4.50	3.35	2.99	7.30
FEO	15.51	15.51	15.61	16.97	17.44	18.20	15.40	15.53	16.00	16.86
MNO	0.26	0.21	0.25	0.44	0.40	0.46	0.18	0.27	0.13	0.39
MGO	13.70	13.56	13.77	10.60	10.20	9.83	12.02	13.03	13.18	12.21
CAO	0.01	-	-	0.02	-	-	-	-	-	-
NIO	-	-	-	-	-	-	-	-	-	-
TOTAL	99.28	98.72	100.15	99.63	99.38	99.77	99.39	98.52	99.82	98.44
ATOMIC PROPORTIONS ON THE BASIS OF 32 OXYGENS										
SI	0.000	0.000	0.000	0.000	0.000	0.000	0.000	0.000	0.000	0.057
TI	0.000	0.000	0.004	0.038	0.042	0.036	0.039	0.015	0.015	0.019
AL	8.761	8.661	8.544	3.272	3.062	3.291	3.831	7.550	7.674	7.537
CR	6.687	7.012	7.001	12.359	12.386	12.382	11.208	7.800	7.751	6.950
FE3	0.351	0.327	0.447	0.309	0.486	0.271	0.880	0.619	0.544	1.360
FE2	3.087	3.110	3.092	3.741	3.878	4.028	3.346	3.190	3.237	3.490
MN	0.052	0.043	0.050	0.098	0.090	0.103	0.040	0.056	0.027	0.082
MG	4.858	4.845	4.860	4.163	4.041	3.876	4.653	4.768	4.751	4.504
CA	0.003	0.000	0.000	0.006	0.000	0.000	0.000	0.000	0.000	0.000
NI	0.000	0.000	0.000	0.000	0.000	0.000	0.000	0.000	0.000	0.000

'TABLE 3.8 PRIMARY SPINEL (1) FROM THE BLUE RIVER ULTRAMAFIC BODY'

	11	12	13	14	15	16	17	18	19	20
	60157A1	60157B1	60157C1	60159A1	60159B1	60159C1	60160A1	60160B1	60160C1	60163A1
OXIDE WEIGHT PERCENTAGE										
SIO2	-	-	-	-	-	-	-	-	-	-
TIO2	0.29	0.28	0.27	0.30	0.34	0.36	0.01	-	-	0.08
AL2O3	11.42	12.89	10.95	16.46	16.22	15.70	40.01	39.79	39.95	35.43
CR2O3	55.57	53.93	56.07	49.07	50.29	49.82	27.50	27.45	28.07	31.65
FE2O3	4.17	3.41	4.20	4.78	3.74	4.67	2.44	2.34	2.30	2.97
FEO	16.56	16.36	16.20	16.86	16.73	17.13	13.21	13.12	12.67	13.35
MNO	0.40	0.42	0.40	0.16	0.17	0.14	-	-	-	0.17
MGO	11.08	11.11	11.22	11.46	11.54	11.25	16.33	16.22	16.72	15.65
CAO	-	0.02	-	0.03	0.02	0.03	-	0.04	-	-
NIO	-	-	-	-	-	-	-	-	-	-
TOTAL	99.49	98.42	99.31	99.12	99.05	99.10	99.50	98.96	99.71	99.30
ATOMIC PROPORTIONS ON THE BASIS OF 32 OXYGENS										
SI	0.000	0.000	0.000	0.000	0.000	0.000	0.000	0.000	0.000	0.000
TI	0.057	0.055	0.053	0.058	0.066	0.070	0.002	0.000	0.000	0.014
AL	3.533	3.997	3.396	4.987	4.918	4.780	10.666	10.665	10.610	9.665
CR	11.527	11.215	11.662	9.970	10.225	10.171	4.916	4.934	4.999	5.790
FE3	0.823	0.675	0.832	0.925	0.724	0.908	0.415	0.400	0.390	0.517
FE2	3.634	3.599	3.565	3.624	3.599	3.700	2.498	2.495	2.387	2.584
MN	0.089	0.094	0.089	0.035	0.037	0.031	0.000	0.000	0.000	0.033
MG	4.333	4.355	4.399	4.389	4.423	4.329	5.503	5.496	5.613	5.397
CA	0.000	0.006	0.000	0.008	0.006	0.008	0.000	0.010	0.000	0.000
NI	0.000	0.000	0.000	0.000	0.000	0.000	0.000	0.000	0.000	0.000

'TABLE 3.8 PRIMARY SPINEL (1) FROM THE BLUE RIVER ULTRAMAFIC BODY'

	21	22	23	24	25	26	27	28	29	30
	60163B1	60168A1	60168B1	60168C1	60075A1	60237A1	60237B1	60237C1	60874A1	60874B1
OXIDE WEIGHT PERCENTAGE										
SIO2	-	-	-	-	-	-	-	-	-	-
TIO2	0.12	0.07	0.05	0.05	0.16	0.29	0.23	0.21	0.10	0.09
AL2O3	36.19	26.21	24.28	26.42	13.48	9.02	8.61	9.05	24.47	24.66
CR2O3	31.64	40.81	41.28	41.16	53.25	60.40	58.88	59.39	43.96	43.30
FE2O3	2.32	2.88	4.64	2.27	4.38	2.82	3.19	2.40	1.76	1.97
FEO	13.42	16.19	16.04	16.08	18.49	14.61	18.67	19.27	15.01	15.53
MNO	0.21	0.26	0.27	0.19	0.36	0.21	0.35	0.31	-	0.29
MGO	15.76	12.74	12.62	12.86	10.14	12.26	9.36	9.16	13.41	12.90
CAO	-	0.02	-	-	-	0.02	0.03	-	-	-
NIO	-	-	-	-	-	-	-	-	-	-
TOTAL	99.66	99.18	99.18	99.03	100.26	99.63	99.32	99.79	98.71	98.74
ATOMIC PROPORTIONS ON THE BASIS OF 32 OXYGENS										
SI	0.000	0.000	0.000	0.000	0.000	0.000	0.000	0.000	0.000	0.000
TI	0.021	0.013	0.009	0.009	0.031	0.057	0.047	0.042	0.019	0.017
AL	9.808	7.555	7.064	7.611	4.132	2.791	2.732	2.857	7.096	7.168
CR	5.750	7.888	8.054	7.951	10.946	12.534	12.526	12.572	8.549	8.440
FE3	0.401	0.530	0.862	0.417	0.857	0.557	0.646	0.484	0.326	0.366
FE2	2.580	3.311	3.311	3.286	4.021	3.208	4.202	4.316	3.088	3.203
MN	0.041	0.054	0.056	0.039	0.079	0.047	0.080	0.070	0.000	0.061
MG	5.399	4.642	4.641	4.683	3.929	4.796	3.754	3.655	4.916	4.740
CA	0.000	0.005	0.000	0.000	0.000	0.006	0.009	0.000	0.000	0.000
NI	0.000	0.000	0.000	0.000	0.000	0.000	0.000	0.000	0.000	0.000

'TABLE 3.8 PRIMARY SPINEL (1) FROM THE BLUE RIVER ULTRAMAFIC BODY'

	31	32	33	34	35	36	37	38	39	40
	60876A1	60876B1	60876C1	60174A1	60186A1	60186B1	60188A1	60188B1	61615A1	61615B1
OXIDE WEIGHT PERCENTAGE										
SIO2	-	-	-	0.10	-	-	-	-	-	-
TIO2	0.09	0.03	0.07	0.11	0.20	0.15	0.11	0.04	0.19	0.19
AL2O3	33.26	32.04	32.34	22.82	20.06	20.57	25.76	28.34	16.95	17.10
CR2O3	34.88	35.37	35.83	43.96	44.77	44.08	41.94	39.18	47.20	47.10
FE2O3	1.88	2.45	2.14	2.07	3.74	3.65	2.45	1.69	4.63	5.02
FEO	14.61	14.20	14.70	17.72	18.30	18.94	15.82	16.80	20.70	21.23
MNO	0.15	0.20	0.19	0.33	0.40	0.39	0.10	0.07	0.48	0.50
MGO	14.69	14.62	14.55	11.32	10.46	10.05	13.10	12.60	8.60	8.42
CAO	-	-	-	-	-	-	0.01	-	-	-
NIO	-	-	-	-	-	-	-	-	-	-
TOTAL	99.56	98.91	99.82	98.43	97.93	97.83	99.29	98.72	98.75	99.56
ATOMIC PROPORTIONS ON THE BASIS OF 32 OXYGENS										
SI	0.000	0.000	0.000	0.025	0.000	0.000	0.000	0.000	0.000	0.000
TI	0.016	0.005	0.012	0.021	0.039	0.029	0.020	0.007	0.037	0.037
AL	9.180	8.937	8.948	6.770	6.087	6.250	7.414	8.134	5.241	5.254
CR	6.456	6.616	6.648	8.745	9.109	8.982	8.094	7.541	9.787	9.704
FE3	0.331	0.436	0.378	0.392	0.724	0.708	0.450	0.310	0.914	0.985
FE2	2.861	2.810	2.886	3.729	3.939	4.083	3.230	3.421	4.541	4.627
MN	0.030	0.040	0.038	0.070	0.087	0.085	0.021	0.014	0.107	0.110
MG	5.125	5.155	5.089	4.245	4.012	3.860	4.766	4.571	3.361	3.270
CA	0.000	0.000	0.000	0.000	0.000	0.000	0.003	0.000	0.000	0.000
NI	0.000	0.000	0.000	0.000	0.000	0.000	0.000	0.000	0.000	0.000

'TABLE 3.8 PRIMARY SPINEL (1) FROM THE BLUE RIVER ULTRAMAFIC BODY'

	41	42	43	44	45	46	47	48	49	50
	61615C1	61616A1	61616B1	61616C1	61619A1	60196A1	60196B1	60196C1	60196D1	60902A1
OXIDE WEIGHT PERCENTAGE										
SIO2	-	-	-	-	-	0.10	-	0.19	-	-
TIO2	0.20	0.23	0.15	0.18	0.17	0.13	0.29	0.12	0.14	0.20
AL2O3	16.78	26.28	29.36	30.13	13.81	22.03	20.86	21.73	21.71	10.53
CR2O3	47.37	38.13	37.00	35.98	49.95	40.24	41.07	41.74	42.12	53.79
FE2O3	4.63	4.74	3.02	2.98	5.45	4.86	5.95	5.21	4.59	6.10
FEO	21.15	17.28	17.79	16.62	21.15	20.93	22.03	21.73	21.54	19.24
MNO	0.48	0.32	0.33	0.16	0.49	0.38	0.20	0.28	0.20	0.53
MGO	8.33	12.05	12.17	12.97	8.11	8.91	8.46	8.99	8.86	9.06
CAO	-	-	-	0.01	-	0.01	-	0.02	-	0.02
NIO	-	0.01	-	-	-	-	-	-	-	-
TOTAL	98.94	99.04	99.82	99.03	99.13	97.59	98.86	100.01	99.16	99.47
ATOMIC PROPORTIONS ON THE BASIS OF 32 OXYGENS										
SI	0.000	0.000	0.000	0.000	0.000	0.026	0.000	0.048	0.000	0.000
TI	0.039	0.043	0.027	0.033	0.034	0.025	0.056	0.023	0.027	0.040
AL	5.193	7.622	8.345	8.549	4.332	6.720	6.349	6.496	6.545	3.319
CR	9.831	7.415	7.052	6.845	10.507	8.230	8.382	8.367	8.515	11.370
FE3	0.915	0.877	0.548	0.540	1.091	0.946	1.156	0.994	0.883	1.227
FE2	4.644	3.555	3.587	3.345	4.707	4.529	4.757	4.608	4.607	4.303
MN	0.107	0.067	0.067	0.033	0.110	0.083	0.044	0.060	0.043	0.120
MG	3.259	4.417	4.372	4.652	3.216	3.435	3.255	3.397	3.377	3.610
CA	0.000	0.000	0.000	0.003	0.000	0.003	0.000	0.005	0.000	0.006
NI	0.000	0.002	0.000	0.000	0.000	0.000	0.000	0.000	0.000	0.000

'TABLE 3.8 PRIMARY SPINEL (1) FROM THE BLUE RIVER ULTRAMAFIC BODY'

	51	52	53	54	55	56	57	58	59	60
	60902B1	61560A1	61560B1	61560C1	61551A1	61556A1	61556B1	61632A1	61632B1	61632C1
OXIDE WEIGHT PERCENTAGE										
SIO2	-	-	-	-	-	-	-	-	-	-
TIO2	0.18	0.18	0.19	0.17	0.25	0.06	0.06	0.23	0.22	0.20
AL2O3	10.21	14.02	15.25	13.10	19.55	32.35	32.21	11.60	11.85	11.80
CR2O3	54.32	52.29	49.91	51.43	46.01	34.63	34.39	55.61	53.29	55.69
FE2O3	5.95	4.71	5.09	5.72	3.92	2.86	3.32	4.75	4.83	4.21
FEO	18.97	18.81	18.41	18.58	16.76	16.64	16.31	16.43	18.24	17.61
MNO	0.48	0.37	0.43	0.41	0.21	0.13	0.13	0.40	0.40	0.49
MGO	9.21	10.02	10.17	9.69	11.65	13.35	13.53	11.32	9.80	10.54
CAO	-	-	-	-	-	-	-	-	-	-
NIO	-	-	-	-	-	-	-	-	-	-
TOTAL	99.32	100.40	99.45	99.10	98.35	100.02	99.95	100.34	98.63	100.54
ATOMIC PROPORTIONS ON THE BASIS OF 32 OXYGENS										
SI	0.000	0.000	0.000	0.000	0.000	0.000	0.000	0.000	0.000	0.000
TI	0.036	0.035	0.037	0.034	0.048	0.011	0.011	0.045	0.044	0.039
AL	3.224	4.287	4.673	4.077	5.877	9.006	8.968	3.554	3.721	3.624
CR	11.502	10.721	10.255	10.734	9.274	6.464	6.421	11.425	11.220	11.470
FE3	1.199	0.919	0.996	1.136	0.752	0.508	0.590	0.929	0.968	0.825
FE2	4.249	4.080	4.002	4.102	3.574	3.286	3.222	3.571	4.063	3.837
MN	0.109	0.081	0.095	0.092	0.045	0.026	0.026	0.088	0.090	0.108
MG	3.676	3.873	3.939	3.812	4.427	4.698	4.762	4.384	3.890	4.092
CA	0.000	0.000	0.000	0.000	0.000	0.000	0.000	0.000	0.000	0.000
NI	0.000	0.000	0.000	0.000	0.000	0.000	0.000	0.000	0.000	0.000

'TABLE 3.8 PRIMARY SPINEL (1) FROM THE BLUE RIVER ULTRAMAFIC BODY'

	61	62	63	64	65	66	67	68	69	70
	61633A1	61634A1	61637A1	61637B1	61637C1	60143A1	60143B1	61593A1	60907A1	60907B1
OXIDE WEIGHT PERCENTAGE										
SIO2	-	-	-	-	-	0.28	-	-	-	-
TIO2	-	0.01	0.02	-	0.02	0.08	0.09	-	0.15	0.04
AL2O3	27.83	22.39	23.50	22.24	23.77	25.10	27.93	31.18	34.46	36.81
CR2O3	35.68	45.40	40.52	40.34	40.62	39.42	37.46	34.72	30.36	28.06
FE2O3	4.89	1.81	5.55	6.53	5.92	4.45	3.91	2.56	4.95	4.28
FEO	18.10	17.68	17.76	17.79	18.34	17.99	18.34	17.55	13.03	14.81
MNO	0.35	0.16	0.35	0.35	0.38	0.64	0.31	0.21	0.16	0.16
MGO	11.35	11.35	11.30	10.96	11.18	11.26	11.59	12.22	15.68	14.72
CAO	-	-	-	-	-	0.02	-	-	-	-
NIO	-	-	-	-	-	-	-	-	-	-
TOTAL	98.20	98.80	99.00	98.21	100.23	99.24	99.63	98.44	98.79	98.88
ATOMIC PROPORTIONS ON THE BASIS OF 32 OXYGENS										
SI	0.000	0.000	0.000	0.000	0.000	0.069	0.000	0.000	0.000	0.000
TI	0.000	0.002	0.004	0.000	0.004	0.015	0.017	0.000	0.026	0.007
AL	8.114	6.633	6.931	6.656	6.938	7.327	8.028	8.893	9.478	10.083
CR	6.975	9.019	8.014	8.096	7.950	7.716	7.220	6.640	5.600	5.154
FE3	0.910	0.342	1.045	1.247	1.103	0.829	0.717	0.466	0.869	0.748
FE2	3.744	3.716	3.716	3.777	3.798	3.726	3.740	3.551	2.543	2.878
MN	0.073	0.034	0.074	0.075	0.080	0.134	0.064	0.043	0.032	0.031
MG	4.183	4.251	4.213	4.146	4.125	4.155	4.211	4.406	5.452	5.097
CA	0.000	0.000	0.000	0.000	0.000	0.005	0.000	0.000	0.000	0.000
NI	0.000	0.000	0.000	0.000	0.000	0.000	0.000	0.000	0.000	0.000

'TABLE 3.8 PRIMARY SPINEL (1) FROM THE BLUE RIVER ULTRAMAFIC BODY'

	71	72	73	74	75	76	77	78	79	80
	60035A1	60035B1	60035C1	60038A1	60038B1	60038C1	60102A1	60102B1	60209A1	60209B1
OXIDE WEIGHT PERCENTAGE										
SIO2	0.06	0.08	0.17	0.18	-	-	-	-	0.04	0.25
TIO2	0.17	0.12	0.13	0.01	-	-	-	0.08	0.08	0.04
AL2O3	11.81	12.53	11.77	21.35	25.71	28.80	21.52	22.50	23.86	25.25
CR2O3	56.14	55.55	54.78	41.13	37.48	35.88	44.49	43.98	40.34	39.36
FE2O3	4.19	4.00	5.53	7.21	6.68	6.10	4.91	4.28	4.39	5.72
FEO	17.21	16.99	16.66	19.44	16.48	16.64	14.79	15.08	18.07	14.74
MNO	0.39	0.39	0.40	0.31	0.19	0.23	0.34	0.30	0.69	0.46
MGO	10.99	11.17	11.27	10.34	12.41	12.98	13.03	13.09	10.85	13.82
CAO	-	-	0.13	-	0.04	-	0.04	-	-	0.01
NIO	-	-	-	-	-	-	-	-	-	-
TOTAL	100.96	100.83	100.84	99.97	98.99	100.63	99.12	99.31	98.32	99.65
ATOMIC PROPORTIONS ON THE BASIS OF 32 OXYGENS										
SI	0.016	0.021	0.044	0.045	0.000	0.000	0.000	0.000	0.010	0.061
TI	0.033	0.023	0.025	0.002	0.000	0.000	0.000	0.015	0.015	0.007
AL	3.602	3.809	3.587	6.343	7.464	8.119	6.319	6.566	7.084	7.234
CR	11.482	11.324	11.196	8.194	7.297	6.782	8.759	8.606	8.031	7.562
FE3	0.816	0.776	1.076	1.367	1.238	1.098	0.920	0.797	0.832	1.046
FE2	3.724	3.664	3.602	4.097	3.394	3.328	3.081	3.122	3.806	2.996
MN	0.085	0.085	0.088	0.066	0.040	0.047	0.072	0.063	0.147	0.095
MG	4.237	4.293	4.342	3.883	4.554	4.625	4.836	4.829	4.072	5.005
CA	0.000	0.000	0.036	0.000	0.011	0.000	0.011	0.000	0.000	0.003
NI	0.000	0.000	0.000	0.000	0.000	0.000	0.000	0.000	0.000	0.000

'TABLE 4.1 SERPENTINE (2) DERIVED FROM OLIVINE (1)'

	1	2	3	4	5	6	7	8	9	10
	60153D2	60153A2	60153B2	60153C2	60153E2	60153F2	60163A2	60094A2	60094B2	60094C2
OXIDE WEIGHT PERCENTAGE										
SIO2	40.38	41.98	42.01	41.37	40.62	43.76	40.47	40.46	39.67	40.27
TIO2	0.04	0.04	0.04	0.06	0.02	0.04	0.04	-	-	-
AL2O3	0.87	0.61	0.80	0.57	0.85	0.42	2.25	0.83	1.10	0.99
FEO	3.05	2.34	2.57	2.11	2.17	2.61	2.69	2.60	2.72	2.37
MNO	0.11	-	-	-	0.05	-	0.02	0.04	0.03	0.02
MGO	38.69	39.65	39.27	39.91	39.61	39.52	37.86	41.06	40.28	40.13
CAO	0.03	0.03	0.03	0.03	0.06	0.03	0.07	0.09	-	0.15
CR2O3	0.69	0.07	0.05	0.03	0.74	0.02	0.10	0.02	0.01	0.03
NIO	0.14	0.16	0.09	0.11	0.06	0.22	0.17	0.10	1.11	0.46
TOTAL	84.00	84.88	84.86	84.19	84.18	86.62	83.67	85.19	84.92	84.42
ATOMIC PROPORTIONS ON THE BASIS OF 28 OXYGENS										
SI	7.870	8.027	8.036	7.973	7.860	8.186	7.867	7.758	7.683	7.792
TI	0.006	0.006	0.006	0.009	0.003	0.006	0.006	0.000	0.000	0.000
AL	0.200	0.138	0.180	0.130	0.194	0.093	0.516	0.188	0.251	0.226
FE2	0.497	0.374	0.411	0.340	0.351	0.408	0.437	0.417	0.441	0.384
MN	0.018	0.000	0.000	0.000	0.008	0.000	0.003	0.006	0.005	0.003
MG	11.238	11.299	11.195	11.463	11.423	11.018	10.968	11.734	11.627	11.572
CA	0.006	0.006	0.006	0.006	0.012	0.006	0.015	0.016	0.000	0.031
CR	0.106	0.011	0.008	0.005	0.113	0.003	0.015	0.003	0.002	0.005
NI	0.022	0.025	0.014	0.017	0.009	0.033	0.027	0.015	0.173	0.072

'TABLE 4.1 SERPENTINE (2) DERIVED FROM OLIVINE (1)'

	11	12	13	14	15	16	17	18	19	20
	60094C2	60018A2	60C18B2	60C18C2	60C18D2	60018E2	60C38A2	60C38B2	60038C2	60C38D2
OXIDE WEIGHT PERCENTAGE										
SIO2	39.04	41.43	41.85	39.68	40.91	41.41	40.54	40.74	40.48	39.48
TIO2	-	-	0.02	0.03	C.02	-	-	0.02	-	-
AL2O3	1.26	0.39	C.54	0.68	C.47	C.52	C.93	1.05	1.39	1.87
FEO	2.35	1.97	2.11	2.35	2.05	1.84	3.08	3.19	2.67	2.89
MNO	0.10	0.05	0.07	0.01	C.06	-	0.01	-	0.07	0.06
MGO	39.39	39.82	40.45	40.57	40.16	40.89	39.63	39.83	39.01	39.31
CAO	0.56	-	0.03	0.01	0.02	0.01	0.05	C.05	0.06	0.06
CR2O3	0.88	0.14	0.18	0.50	0.20	0.16	0.11	0.10	0.29	0.62
NIO	0.17	C.22	0.31	0.22	0.37	C.18	0.12	C.12	0.16	0.08
TOTAL	83.75	84.02	85.56	84.05	84.26	85.01	84.47	85.10	84.13	84.37
ATOMIC PROPORTIONS ON THE BASIS OF 28 OXYGENS										
SI	7.650	8.002	7.953	7.722	7.905	7.909	7.845	7.829	7.848	7.664
TI	0.000	0.000	0.003	0.004	0.003	0.000	0.000	0.003	0.000	0.000
AL	0.291	0.089	0.121	0.156	0.107	0.117	0.212	0.238	0.318	0.428
FE2	C.385	0.318	0.335	0.383	C.331	0.294	0.499	0.513	0.433	0.469
MN	0.017	0.008	0.011	0.002	0.010	0.000	0.002	0.000	0.011	0.010
MG	11.504	11.462	11.457	11.767	11.566	11.639	11.429	11.407	11.271	11.374
CA	C.118	0.000	0.006	0.002	0.004	0.002	0.010	0.010	0.012	0.012
CR	0.136	0.021	0.027	0.077	0.031	0.024	0.017	0.015	0.044	0.095
NI	0.027	C.034	C.047	C.034	C.058	C.028	0.019	0.019	0.025	0.012

'TABLE 4.1 SERPENTINE (2) DERIVED FROM OLIVINE (1)'

21

60038E2

OXIDE WEIGHT PERCENTAGE

SIO2	37.36
TIO2	-
AL2O3	5.08
FEO	3.96
MNO	0.01
MGO	37.32
CAO	0.01
CR2O3	0.77
NIO	0.05
TOTAL	84.56

ATOMIC PROPORTIONS ON THE BASIS OF 28 OXYGENS

SI	7.282
TI	0.000
AL	1.167
FE2	0.646
MN	0.002
MG	10.841
CA	0.002
CR	0.119
NI	0.008

'TABLE 6.1 OLIVINE (3) FROM UNIT (3A) BELOW THE TALC ISOGRAD'

	1	2	3	4	5	6	7	8	9	10
	61577A3	61577B3	61577C3	61577D3	60021A3	60021B3	60021C3	60021D3	60021E3	60021F3
OXIDE WEIGHT PERCENTAGE										
SIO2	40.46	41.60	41.32	40.83	40.46	40.28	40.22	40.58	40.58	40.48
TIO2	0.04	0.02	–	0.02	0.05	0.03	0.02	0.03	0.04	0.04
AL2O3	0.10	0.03	0.07	0.05	0.06	0.05	0.06	0.07	0.06	0.05
CR2O3	0.06	0.02	0.03	0.03	0.03	0.09	0.06	0.04	0.08	0.06
FEO	9.77	6.02	8.13	8.81	9.72	10.14	9.87	9.34	9.79	9.80
MNO	1.37	0.19	0.78	0.94	1.40	1.50	1.38	1.32	1.31	1.28
MGO	48.79	52.84	50.24	49.95	48.39	47.49	48.00	48.37	48.27	48.44
CAO	0.09	0.03	0.03	0.07	0.03	0.06	0.05	0.03	–	0.01
NIO	–	0.03	–	–	–	–	–	–	–	–
TOTAL	100.68	100.78	100.60	100.70	100.14	99.64	99.66	99.78	100.13	100.16
ATOMIC PROPORTIONS ON THE BASIS OF 4 OXYGENS										
SI	0.990	0.994	1.000	0.993	0.995	0.998	0.995	0.999	0.998	0.995
TI	0.001	0.000	0.000	0.000	0.001	0.001	0.000	0.001	0.001	0.001
AL	0.003	0.001	0.002	0.001	0.002	0.001	0.002	0.002	0.002	0.001
CR	0.001	0.000	0.001	0.001	0.001	0.002	0.001	0.001	0.002	0.001
FE2	0.200	0.120	0.165	0.179	0.200	0.210	0.204	0.192	0.201	0.202
MN	0.028	0.004	0.016	0.019	0.029	0.031	0.029	0.028	0.027	0.027
MG	1.780	1.882	1.813	1.810	1.774	1.754	1.769	1.775	1.769	1.775
CA	0.002	0.001	0.001	0.002	0.001	0.002	0.001	0.001	0.000	0.000
NI	0.000	0.001	0.000	0.000	0.000	0.000	0.000	0.000	0.000	0.000
END MEMBER COMPOSITIONS										
MG	88.63	93.81	90.94	90.12	88.56	87.89	88.36	88.98	88.55	88.61
FE	11.37	6.19	9.06	9.88	11.44	12.11	11.64	11.02	11.45	11.39

'TABLE 6.1 OLIVINE (3) FROM UNIT (3A) BELOW THE TALC ISOGRAD'

	11	12	13	14	15	16	17	18	19	20
	60157A3	60157B3	60157C3	60157D3	60157E3	60157F3	60157G3	60157H3	60157I3	60157J3
OXIDE WEIGHT PERCENTAGE										
SIO2	41.29	40.30	41.72	41.87	39.98	40.89	41.61	40.34	41.26	41.72
TIO2	0.07	0.04	0.02	0.02	0.02	0.04	0.02	0.04	0.06	0.02
AL2O3	0.07	0.10	0.05	0.07	0.07	0.07	0.03	0.05	0.07	0.12
CR2O3	0.08	0.06	0.08	0.08	0.06	0.08	0.12	0.06	0.06	0.05
FEO	4.13	10.47	4.01	3.85	12.23	7.81	3.00	11.71	8.87	6.49
MNO	0.02	0.72	0.02	-	1.16	0.22	-	1.30	0.42	0.10
MGO	53.53	48.06	53.66	54.03	46.76	51.15	54.59	46.62	49.06	51.12
CAO	0.01	0.06	-	-	0.06	0.03	0.01	0.09	0.07	0.04
NIO	0.42	-	0.31	0.34	-	-	0.56	-	-	0.03
TOTAL	99.62	99.81	99.87	100.26	100.34	100.29	99.94	100.21	99.87	99.69
ATOMIC PROPORTIONS ON THE BASIS OF 4 OXYGENS										
SI	0.992	0.995	0.997	0.997	0.992	0.991	0.992	1.000	1.007	1.008
TI	0.001	0.001	0.000	0.000	0.000	0.001	0.000	0.001	0.001	0.000
AL	0.002	0.003	0.001	0.002	0.002	0.002	0.001	0.001	0.002	0.003
CR	0.002	0.001	0.002	0.002	0.001	0.002	0.002	0.001	0.001	0.001
FE2	0.083	0.216	0.080	0.077	0.254	0.158	0.060	0.243	0.181	0.131
MN	0.000	0.015	0.000	0.000	0.024	0.005	0.000	0.027	0.009	0.002
MG	1.916	1.768	1.912	1.917	1.729	1.847	1.939	1.722	1.785	1.841
CA	0.000	0.002	0.000	0.000	0.002	0.001	0.000	0.002	0.002	0.001
NI	0.008	0.000	0.006	0.007	0.000	0.000	0.011	0.000	0.000	0.001
END MEMBER COMPOSITIONS										
MG	95.83	88.43	95.96	96.15	86.14	91.90	97.01	86.44	90.39	93.25
FE	4.17	11.57	4.04	3.85	13.86	8.10	2.99	13.56	9.61	6.75

'TABLE 6.1 OLIVINE (3) FROM UNIT (3A) BELOW THE TALC ISOGRAD'

	21	22	23	24	25	26	27	28	29	30
	60157K3	60157L3	60157M3	60123A3	60123B3	60123C3	60123D3	60123E3	60067A3	60067B3
OXIDE WEIGHT PERCENTAGE										
SIO2	40.57	42.42	40.89	42.36	41.77	41.79	41.11	40.97	40.12	40.46
TIO2	0.02	0.07	0.07	0.04	0.07	0.04	0.04	0.04	0.05	0.02
AL2O3	0.07	0.07	0.07	0.07	0.05	0.10	0.05	0.05	0.08	0.07
CR2O3	0.09	0.08	0.11	0.10	0.15	0.08	0.06	0.14	0.19	0.12
FEO	12.73	4.11	9.85	7.67	8.04	8.21	7.58	8.58	10.85	11.75
MNO	1.36	0.06	0.64	0.29	0.50	0.58	0.18	0.89	1.53	1.52
MGO	45.53	52.98	48.63	49.97	50.04	49.87	50.86	49.39	47.34	46.62
CAO	0.07	0.01	0.07	-	-	-	0.01	0.01	0.10	0.07
NIO	0.05	0.67	-	-	-	-	0.12	-	-	-
TOTAL	100.49	100.47	100.33	100.50	100.62	100.67	100.01	100.07	100.26	100.63
ATOMIC PROPORTIONS ON THE BASIS OF 4 OXYGENS										
SI	1.007	1.009	1.000	1.019	1.008	1.009	0.997	1.000	0.992	0.999
TI	0.000	0.001	0.001	0.001	0.001	0.001	0.001	0.001	0.001	0.000
AL	0.002	0.002	0.002	0.002	0.001	0.003	0.001	0.001	0.002	0.002
CR	0.002	0.002	0.002	0.002	0.003	0.002	0.001	0.003	0.004	0.002
FE2	0.264	0.082	0.202	0.154	0.162	0.166	0.154	0.175	0.224	0.243
MN	0.029	0.001	0.013	0.006	0.010	0.012	0.004	0.018	0.032	0.032
MG	1.684	1.878	1.773	1.792	1.800	1.795	1.839	1.797	1.745	1.716
CA	0.002	0.000	0.002	0.000	0.000	0.000	0.000	0.000	0.003	0.002
NI	0.001	0.013	0.000	0.000	0.000	0.000	0.002	0.000	0.000	0.000
END MEMBER COMPOSITIONS										
MG	85.19	95.77	89.19	91.79	91.25	90.99	92.11	90.27	87.18	86.21
FE	14.81	4.23	10.81	8.21	8.75	9.01	7.89	9.73	12.82	13.79

'TABLE 6.1 OLIVINE (3) FROM UNIT (3A) BELOW THE TALC ISOGRAD'

	31	32	33	34	35	36	37	38	39	40
	60067C3	60067D3	60067E3	60067F3	60067G3	60907A3	60907B3	60907C3	60907D3	60907E3
OXIDE WEIGHT PERCENTAGE										
SIO2	40.09	40.19	40.22	40.24	40.24	41.22	41.19	40.93	41.01	41.22
TIO2	0.06	0.05	0.07	0.05	0.08	0.03	-	-	0.08	0.02
AL2O3	0.05	0.05	0.07	0.07	0.08	0.08	0.11	0.09	0.08	0.07
CR2O3	0.10	0.06	0.11	0.14	0.13	0.06	0.06	0.05	0.02	0.04
FEO	10.61	11.14	10.84	11.39	11.48	8.29	7.70	8.05	9.52	9.34
MNO	0.60	1.50	1.28	1.32	1.50	0.53	0.27	0.33	0.20	0.10
MGO	48.81	46.60	47.07	46.63	46.81	50.41	50.90	50.46	49.10	49.11
CAO	0.04	0.08	0.09	0.07	0.11	0.02	0.06	0.05	0.01	-
NIO	-	-	-	-	-	-	-	0.02	0.35	0.32
TOTAL	100.36	99.66	99.75	99.91	100.43	100.64	100.29	99.98	100.37	100.22
ATOMIC PROPORTIONS ON THE BASIS OF 4 OXYGENS										
SI	0.986	1.000	0.998	0.999	0.995	0.998	0.997	0.996	1.001	1.005
TI	0.001	0.001	0.001	0.001	0.001	0.001	0.000	0.000	0.001	0.000
AL	0.001	0.001	0.002	0.002	0.002	0.002	0.003	0.003	0.002	0.002
CR	0.002	0.001	0.002	0.003	0.003	0.001	0.001	0.001	0.000	0.001
FE2	0.218	0.232	0.225	0.237	0.238	0.168	0.156	0.164	0.194	0.190
MN	0.012	0.032	0.027	0.028	0.031	0.011	0.006	0.007	0.004	0.002
MG	1.788	1.728	1.740	1.725	1.726	1.818	1.836	1.830	1.785	1.785
CA	0.001	0.002	0.002	0.002	0.003	0.001	0.002	0.001	0.000	0.000
NI	0.000	0.000	0.000	0.000	0.000	0.000	0.000	0.000	0.007	0.006
END MEMBER COMPOSITIONS										
MG	88.58	86.77	87.36	86.72	86.52	91.05	91.92	91.47	90.00	90.26
FE	11.42	13.23	12.64	13.28	13.48	8.95	8.08	8.53	10.00	9.74

'TABLE 6.1 OLIVINE (3) FROM UNIT (3A) BELOW THE TALC ISOGRAD'

	41	42	43	44	45	46	47	48	49	50
	60035A3	60035B3	60035C3	60035D3	60035E3	60035F3	60035G3	60035H3	60035I3	60102A3
OXIDE WEIGHT PERCENTAGE										
SIO2	41.10	40.02	41.62	41.36	40.90	40.03	42.02	41.98	42.18	40.81
TIO2	0.04	0.03	0.03	0.05	0.03	-	-	0.02	0.06	0.05
AL2O3	0.61	0.64	0.71	0.71	0.97	0.08	0.09	0.17	0.12	0.05
CR2O3	0.09	0.07	0.12	0.02	0.06	0.08	0.09	0.05	0.05	0.04
FEO	6.97	8.65	3.86	4.75	7.52	10.52	3.76	5.13	4.25	7.93
MNO	0.33	0.82	0.03	0.06	0.55	1.34	-	0.02	-	1.59
MGO	51.31	49.21	53.59	52.18	50.35	48.86	54.51	52.29	53.95	49.93
CAO	0.08	0.12	0.05	0.02	0.06	0.08	-	0.07	0.03	0.06
NIO	0.25	0.04	0.15	0.16	-	-	0.13	0.14	0.16	0.02
TOTAL	100.78	99.60	100.16	99.31	100.44	100.99	100.60	99.87	100.80	100.48
ATOMIC PROPORTIONS ON THE BASIS OF 4 OXYGENS										
SI	0.988	0.983	0.991	0.996	0.988	0.981	0.995	1.007	0.999	0.993
TI	0.001	0.001	0.001	0.001	0.001	0.000	0.000	0.000	0.001	0.001
AL	0.017	0.019	0.020	0.020	0.028	0.002	0.003	0.005	0.003	0.001
CR	0.002	0.001	0.002	0.000	0.001	0.002	0.002	0.001	0.001	0.001
FE2	0.140	0.178	0.077	0.096	0.152	0.216	0.075	0.103	0.084	0.161
MN	0.007	0.017	0.001	0.001	0.011	0.028	0.000	0.000	0.000	0.033
MG	1.839	1.802	1.901	1.873	1.813	1.785	1.925	1.869	1.904	1.811
CA	0.002	0.003	0.001	0.001	0.002	0.002	0.000	0.002	0.001	0.002
NI	0.005	0.001	0.003	0.003	0.000	0.000	0.002	0.003	0.003	0.000
END MEMBER COMPOSITIONS										
MG	92.60	90.24	96.09	95.08	91.74	88.00	96.27	94.76	95.77	90.31
FE	7.40	9.76	3.91	4.92	8.26	12.00	3.73	5.24	4.23	9.69

'TABLE 6.1 OLIVINE (3) FROM UNIT (3A) BELOW THE TALC ISOGRAD'

	51	52	53	54	55	56	57	58	59	60
	60102B3	60102C3	60102D3	60109A3	60109B3	60109C3	60109D3	60109E3	60109F3	61623A3
OXIDE WEIGHT PERCENTAGE										
SIO2	40.79	40.71	41.42	41.27	41.90	41.92	41.87	41.44	41.05	41.93
TIO2	0.04	0.09	0.02	0.03	0.01	0.04	0.04	0.03	0.03	0.05
AL2O3	0.07	0.06	0.44	0.21	0.21	0.20	0.24	0.27	0.21	0.08
CR2O3	0.08	0.09	0.03	0.10	0.10	0.04	0.04	0.10	0.06	0.04
FEO	7.93	6.99	6.72	6.10	5.31	5.30	5.70	6.04	7.17	5.35
MNO	1.60	1.26	1.17	0.13	0.14	0.09	0.13	0.22	0.26	0.06
MGO	49.16	50.46	50.30	52.29	52.28	52.53	52.22	51.35	51.42	52.70
CAO	0.04	0.06	0.06	0.02	0.01	0.01	0.01	0.10	0.06	0.11
NIO	-	0.09	-	0.35	0.35	0.47	0.36	0.14	0.06	0.36
TOTAL	99.71	99.81	100.16	100.50	100.31	100.60	100.61	99.69	100.32	100.68
ATOMIC PROPORTIONS ON THE BASIS OF 4 OXYGENS										
SI	1.000	0.992	1.002	0.991	1.003	1.001	1.001	1.001	0.992	1.000
TI	0.001	0.002	0.000	0.001	0.000	0.001	0.001	0.001	0.001	0.001
AL	0.002	0.002	0.013	0.006	0.006	0.006	0.007	0.008	0.006	0.002
CR	0.002	0.002	0.001	0.002	0.002	0.001	0.001	0.002	0.001	0.001
FE2	0.163	0.143	0.136	0.123	0.106	0.106	0.114	0.122	0.145	0.107
MN	0.033	0.026	0.024	0.003	0.003	0.002	0.003	0.005	0.005	0.001
MG	1.796	1.833	1.813	1.871	1.865	1.869	1.860	1.849	1.851	1.874
CA	0.001	0.002	0.002	0.001	0.000	0.000	0.000	0.003	0.002	0.003
NI	0.000	0.002	0.000	0.007	0.007	0.009	0.007	0.003	0.001	0.007
END MEMBER COMPOSITIONS										
MG	90.17	91.58	91.89	93.73	94.47	94.55	94.10	93.59	92.50	94.55
FE	9.83	8.42	8.11	6.27	5.53	5.45	5.90	6.41	7.50	5.45

'TABLE 6.1 OLIVINE (3) FROM UNIT (3A) BELOW THE TALC ISOGRAD'

	61	62	63	64	65	66	67	68	69	70
	61623B3	61623C3	61623D3	61623E3	61625A3	61625B3	61625C3	61625D3	61625E3	61625F3
OXIDE WEIGHT PERCENTAGE										
SIO2	40.76	41.43	41.50	41.43	41.61	41.24	41.70	41.78	41.24	41.40
TIO2	0.08	0.06	0.02	0.04	0.03	0.05	0.03	0.03	0.07	0.03
AL2O3	0.13	0.16	0.17	0.23	0.06	0.04	0.05	0.06	0.06	0.08
CR2O3	0.03	0.08	0.05	0.05	0.02	0.08	0.09	0.05	0.02	0.05
FEO	9.22	8.35	8.46	6.53	5.44	7.14	6.68	5.24	7.56	7.59
MNO	1.08	0.18	0.27	0.07	0.13	0.43	0.41	0.10	0.21	0.47
MGO	48.91	49.80	50.01	50.80	52.52	51.12	51.09	52.72	50.30	50.24
CAO	0.09	-	0.04	0.03	0.01	0.07	0.06	0.02	0.08	0.07
NIO	0.17	0.34	0.13	0.30	0.24	0.09	0.13	0.23	0.19	0.09
TOTAL	100.47	100.40	100.65	99.48	100.06	100.26	100.24	100.23	99.73	100.42
ATOMIC PROPORTIONS ON THE BASIS OF 4 OXYGENS										
SI	0.996	1.004	1.003	1.005	0.999	0.997	1.005	1.000	1.003	1.002
TI	0.001	0.001	0.000	0.001	0.001	0.001	0.001	0.001	0.001	0.001
AL	0.004	0.005	0.005	0.007	0.002	0.001	0.001	0.002	0.002	0.002
CR	0.001	0.002	0.001	0.001	0.000	0.002	0.002	0.001	0.000	0.001
FE2	0.188	0.169	0.171	0.132	0.109	0.144	0.135	0.105	0.154	0.162
MN	0.022	0.004	0.006	0.001	0.003	0.009	0.008	0.002	0.004	0.010
MG	1.781	1.799	1.802	1.836	1.879	1.842	1.835	1.881	1.823	1.813
CA	0.002	0.000	0.001	0.001	0.000	0.002	0.002	0.001	0.002	0.002
NI	0.003	0.007	0.003	0.006	0.005	0.002	0.003	0.004	0.004	0.002
END MEMBER COMPOSITIONS										
MG	89.42	91.23	91.07	93.20	94.38	92.32	92.77	94.62	92.02	91.36
FE	10.58	8.77	8.93	6.80	5.62	7.68	7.23	5.38	7.98	8.64

'TABLE 6.1 OLIVINE (3) FROM UNIT (3A) BELOW THE TALC ISOGRAD'

	71	72	73	74	75	76	77	78	79	80
	61625G3	61625H3	61625I3	61625J3	60171A3	60171B3	60171C3	60171D3	60171E3	60171F3
OXIDE WEIGHT PERCENTAGE										
SIO2	41.27	41.49	41.46	41.45	41.83	40.58	42.70	42.42	41.94	41.71
TIO2	0.03	0.06	0.06	0.04	0.04	0.02	0.03	0.02	0.05	0.05
AL2O3	0.05	0.08	0.07	0.06	0.04	0.13	0.05	0.08	0.07	0.06
CR2O3	0.04	0.02	0.04	0.03	0.06	0.03	0.05	0.03	0.05	0.04
FEO	7.26	6.96	7.81	6.23	4.12	9.31	4.33	4.24	4.01	5.58
MNO	0.06	0.36	0.65	0.07	0.03	1.16	0.03	0.01	0.03	0.10
MGO	50.74	50.53	50.04	51.64	53.22	48.44	53.11	53.13	53.42	52.89
CAO	0.03	0.02	0.03	-	0.01	0.15	0.03	0.01	0.01	0.05
NIO	0.49	0.12	-	0.31	0.37	0.41	0.39	0.31	0.28	0.09
TOTAL	99.97	99.64	100.16	99.83	99.72	100.23	100.72	100.25	99.86	100.57
ATOMIC PROPORTIONS ON THE BASIS OF 4 OXYGENS										
SI	1.001	1.007	1.006	1.001	1.002	0.996	1.012	1.009	1.002	0.997
TI	0.001	0.001	0.001	0.001	0.001	0.000	0.001	0.000	0.001	0.001
AL	0.001	0.002	0.002	0.002	0.001	0.004	0.001	0.002	0.002	0.002
CR	0.001	0.000	0.001	0.001	0.001	0.001	0.001	0.001	0.001	0.001
FE2	0.147	0.141	0.158	0.126	0.083	0.191	0.086	0.084	0.080	0.112
MN	0.001	0.007	0.013	0.001	0.001	0.024	0.001	0.000	0.001	0.002
MG	1.834	1.827	1.809	1.859	1.900	1.772	1.876	1.884	1.902	1.883
CA	0.001	0.001	0.001	0.000	0.000	0.004	0.001	0.000	0.000	0.001
NI	0.010	0.002	0.000	0.006	0.007	0.008	0.007	0.006	0.005	0.002
END MEMBER COMPOSITIONS										
MG	92.51	92.48	91.33	93.59	95.81	89.17	95.60	95.70	95.93	94.31
FE	7.49	7.52	8.67	6.41	4.19	10.83	4.40	4.30	4.07	5.69

'TABLE 6.1 OLIVINE (3) FROM UNIT (3A) BELOW THE TALC ISOGRAD'

	81	82	83	84	85	86	87	88	89	90
	60171G3	60171H3	60171I3	60171J3	61632A3	61632B3	61632C3	61632D3	61632E3	61632F3
OXIDE WEIGHT PERCENTAGE										
SIO2	40.75	40.85	40.18	40.15	40.53	41.69	40.81	40.86	41.64	41.41
TIO2	0.03	0.02	0.01	0.01	0.02	0.04	0.02	0.05	0.01	0.01
AL2O3	0.09	0.05	0.08	0.08	0.11	0.07	0.14	0.07	0.09	0.03
CR2O3	0.05	0.06	0.10	0.02	0.03	0.04	0.09	0.05	0.05	0.05
FEO	8.35	7.06	8.69	7.78	9.40	4.61	9.35	10.01	4.94	8.93
MNO	0.99	1.07	1.23	0.74	0.34	0.02	0.31	0.43	0.02	0.21
MGO	49.47	50.53	49.22	50.79	49.15	53.25	48.59	48.31	53.46	50.21
CAO	0.12	0.09	0.07	0.10	-	-	0.01	0.03	-	0.01
NIO	-	-	0.15	0.08	-	0.23	-	-	0.57	-
TOTAL	99.85	99.73	99.73	99.75	99.58	99.95	99.32	99.81	100.78	100.86
ATOMIC PROPORTIONS ON THE BASIS OF 4 OXYGENS										
SI	0.997	0.995	0.989	0.982	0.996	0.998	1.004	1.004	0.992	1.001
TI	0.001	0.000	0.000	0.000	0.000	0.001	0.000	0.001	0.000	0.000
AL	0.003	0.001	0.002	0.002	0.003	0.002	0.004	0.002	0.003	0.001
CR	0.001	0.001	0.002	0.000	0.001	0.001	0.002	0.001	0.001	0.001
FE2	0.171	0.144	0.179	0.159	0.193	0.092	0.192	0.206	0.098	0.181
MN	0.021	0.022	0.026	0.015	0.007	0.000	0.006	0.009	0.000	0.004
MG	1.804	1.835	1.805	1.851	1.800	1.900	1.782	1.769	1.899	1.809
CA	0.003	0.002	0.002	0.003	0.000	0.000	0.000	0.001	0.000	0.000
NI	0.000	0.000	0.003	0.002	0.000	0.004	0.000	0.000	0.011	0.000
END MEMBER COMPOSITIONS										
MG	90.41	91.71	89.82	91.39	89.99	95.35	89.96	89.18	95.05	90.73
FE	9.59	8.29	10.18	8.61	10.01	4.65	10.04	10.82	4.95	9.27

'TABLE 6.1 OLIVINE (3) FROM UNIT (3A) BELOW THE TALC ISOGRAD'

	91	92	93	94	95	96	97	98	99	100
	61633A3	61633B3	61633C3	61633D3	61635A3	61635B3	61635C3	61635D3	61635E3	61635F3
OXIDE WEIGHT PERCENTAGE										
SIO2	39.89	40.31	40.27	40.28	41.09	41.17	41.18	41.99	40.99	41.35
TIO2	0.01	0.02	0.02	-	0.07	0.04	0.02	0.02	0.06	0.04
AL2O3	0.29	0.07	0.07	0.08	0.05	0.06	0.03	0.03	0.03	0.05
CR2O3	0.10	0.06	0.07	0.09	0.06	0.05	0.04	0.06	0.04	0.03
FEO	11.85	11.67	11.79	12.04	6.58	6.85	6.91	6.65	8.33	8.28
MNO	1.43	1.62	1.14	1.82	0.45	0.48	0.54	0.36	1.35	1.23
MGO	45.74	46.70	46.48	45.86	51.99	51.63	51.26	51.11	49.34	49.28
CAO	-	0.02	-	0.04	0.03	0.06	0.05	0.05	0.12	0.06
NIO	-	-	-	-	0.01	0.01	-	0.07	-	-
TOTAL	99.31	100.47	99.84	100.21	100.33	100.35	100.03	100.34	100.26	100.32
ATOMIC PROPORTIONS ON THE BASIS OF 4 OXYGENS										
SI	0.999	0.997	1.001	1.002	0.991	0.993	0.997	1.010	1.000	1.006
TI	0.000	0.000	0.000	0.000	0.001	0.001	0.000	0.000	0.001	0.001
AL	0.009	0.002	0.002	0.002	0.001	0.002	0.001	0.001	0.001	0.001
CR	0.002	0.001	0.001	0.002	0.001	0.001	0.001	0.001	0.001	0.001
FE2	0.248	0.242	0.245	0.250	0.133	0.138	0.140	0.134	0.170	0.168
MN	0.030	0.034	0.024	0.038	0.009	0.010	0.011	0.007	0.028	0.025
MG	1.707	1.722	1.722	1.700	1.868	1.857	1.849	1.832	1.794	1.787
CA	0.000	0.001	0.000	0.001	0.001	0.002	0.001	0.001	0.003	0.002
NI	0.000	0.000	0.000	0.000	0.000	0.000	0.000	0.001	0.000	0.000
END MEMBER COMPOSITIONS										
MG	85.97	86.21	86.48	85.48	92.94	92.61	92.45	92.85	90.07	90.21
FE	14.03	13.79	13.52	14.52	7.06	7.39	7.55	7.15	9.93	9.79

'TABLE 6.1 OLIVINE (3) FROM UNIT (3A) BELOW THE TALC ISOGRAD'

	101	102	103	104	105	106	107	108	109	110
	61635G3	61637A3	61637B3	61637C3	61637D3	61637E3	60867A3	60867B3	60867C3	60867D3
OXIDE WEIGHT PERCENTAGE										
SIO2	41.74	40.22	40.88	40.88	40.02	40.77	41.55	40.86	41.43	42.10
TIO2	0.05	0.04	0.03	0.01	0.04	0.02	0.06	0.08	0.06	0.02
AL2O3	0.04	0.08	0.07	0.06	0.08	0.09	0.04	0.07	0.08	0.06
CR2O3	0.04	0.04	0.05	0.04	0.03	0.02	0.09	0.07	0.03	0.10
FEO	7.05	10.51	9.71	9.73	11.56	9.47	6.74	7.29	7.72	5.79
MNO	0.61	0.97	0.86	0.79	1.87	1.52	0.21	0.39	0.76	0.07
MGO	50.53	47.62	48.55	48.87	46.28	47.72	50.99	50.31	50.43	52.00
CAO	0.05	-	0.04	0.03	0.04	0.08	-	0.01	0.08	-
NIO	-	0.13	0.04	-	-	-	-	-	-	-
TOTAL	100.11	99.61	100.23	100.41	99.92	99.69	99.68	99.08	100.59	100.14
ATOMIC PROPORTIONS ON THE BASIS OF 4 OXYGENS										
SI	1.009	0.997	1.001	0.999	0.997	1.005	1.006	1.000	1.001	1.009
TI	0.001	0.001	0.001	0.000	0.001	0.000	0.001	0.001	0.001	0.000
AL	0.001	0.002	0.002	0.002	0.002	0.003	0.001	0.002	0.002	0.002
CR	0.001	0.001	0.001	0.001	0.001	0.000	0.002	0.001	0.001	0.002
FE2	0.143	0.218	0.199	0.199	0.241	0.195	0.136	0.149	0.156	0.116
MN	0.012	0.020	0.018	0.016	0.039	0.032	0.004	0.008	0.016	0.001
MG	1.820	1.759	1.772	1.780	1.718	1.754	1.840	1.834	1.816	1.857
CA	0.001	0.000	0.001	0.001	0.001	0.002	0.000	0.000	0.002	0.000
NI	0.000	0.003	0.001	0.000	0.000	0.000	0.000	0.000	0.000	0.000
END MEMBER COMPOSITIONS										
MG	92.15	88.07	89.10	89.21	85.97	88.54	92.89	92.10	91.37	94.05
FE	7.85	11.93	10.90	10.79	14.03	11.46	7.11	7.90	8.63	5.95

'TABLE 6.1 OLIVINE (3) FROM UNIT (3A) BELOW THE TALC ISOGRAD'

	111	112	113
	60867E3	60867F3	60867G3
OXIDE WEIGHT PERCENTAGE			
SIO2	40.84	41.93	41.40
TIO2	0.05	0.03	0.02
AL2O3	0.10	0.07	0.07
CR2O3	0.04	0.04	0.05
FEO	9.05	5.46	8.18
MNO	0.99	0.05	0.67
MGO	49.03	53.11	50.36
CAO	-	-	0.02
NIO	-	-	-
TOTAL	100.10	100.69	100.77
ATOMIC PROPORTIONS ON THE BASIS OF 4 OXYGENS			
SI	0.999	0.999	1.000
TI	0.001	0.001	0.000
AL	0.003	0.002	0.002
CR	0.001	0.001	0.001
FE2	0.185	0.109	0.165
MN	0.021	0.001	0.014
MG	1.788	1.886	1.813
CA	0.000	0.000	0.001
NI	0.000	0.000	0.000
END MEMBER COMPOSITIONS			
MG	89.68	94.50	91.01
FE	10.32	5.50	8.99

'TABLE 6.2 OLIVINE (3) PSEUDOMORPHS AFTER BASTITE SERPENTINE'

	1	2	3	4	5	6	7	8	9	10
	60153A3	60153E3	60153F3	60186A3	60186B3	60186C3	60186F3	60186H3	60186I3	60174C3
OXIDE WEIGHT PERCENTAGE										
SIO2	38.92	39.33	39.75	41.42	40.68	40.95	41.01	41.08	41.27	40.46
TIO2	0.08	0.11	0.08	0.03	0.06	0.04	0.06	0.04	0.05	0.04
AL2O3	0.08	0.12	0.15	0.04	0.08	0.05	0.07	0.06	0.08	0.12
CR2O3	0.10	0.10	0.10	0.03	0.02	0.09	0.06	0.05	0.07	0.06
FEO	16.50	15.58	15.15	7.11	8.34	8.17	8.91	8.72	9.41	10.13
MNO	0.57	0.51	0.54	0.11	0.16	0.17	0.16	0.20	0.14	0.30
MGO	44.11	44.91	44.89	51.65	50.22	51.06	50.11	49.80	48.97	48.73
CAO	0.06	0.02	0.03	0.02	0.01	0.03	-	0.02	0.11	-
NIO	0.15	0.01	-	0.01	0.32	0.10	0.08	-	0.05	0.08
TOTAL	100.57	100.69	100.69	100.42	99.89	100.66	100.46	99.97	100.15	99.92
ATOMIC PROPORTIONS ON THE BASIS OF 4 OXYGENS										
SI	0.982	0.986	0.993	0.998	0.993	0.990	0.996	1.001	1.006	0.995
TI	0.002	0.002	0.002	0.001	0.001	0.001	0.001	0.001	0.001	0.001
AL	0.002	0.004	0.004	0.001	0.002	0.001	0.002	0.002	0.002	0.003
CR	0.002	0.002	0.002	0.001	0.000	0.002	0.001	0.001	0.001	0.001
FE2	0.348	0.327	0.317	0.143	0.170	0.165	0.181	0.178	0.192	0.208
MN	0.012	0.011	0.011	0.002	0.003	0.003	0.003	0.004	0.003	0.006
MG	1.659	1.677	1.671	1.854	1.827	1.840	1.814	1.809	1.780	1.785
CA	0.002	0.001	0.001	0.001	0.000	0.001	0.000	0.001	0.003	0.000
NI	0.003	0.000	0.000	0.000	0.006	0.002	0.002	0.000	0.001	0.002
END MEMBER COMPOSITIONS										
MG	82.15	83.25	83.59	92.72	91.32	91.60	90.78	90.86	90.13	89.27
FE	17.85	16.75	16.41	7.28	8.68	8.40	9.22	9.14	9.87	10.73

'TABLE 6.2 OLIVINE (3) PSEUDOMORPHS AFTER BASTITE SERPENTINE'

	11	12	13	14	15	16	17	18
	60174F3	60180A3	60180B3	60180C3	60179B3	60179E3	60179F3	61633E3
OXIDE WEIGHT PERCENTAGE								
SIO2	41.31	40.87	41.09	40.72	41.37	41.30	41.50	41.04
TIO2	0.05	0.06	0.04	0.06	0.04	0.05	0.05	0.01
AL2O3	0.15	0.07	0.09	0.08	0.07	0.19	0.06	0.10
CR2O3	0.07	0.22	0.11	0.05	0.12	0.10	0.09	0.03
FEO	8.94	7.84	8.96	8.53	8.82	7.97	7.43	8.14
MNO	0.23	0.23	0.86	0.26	0.56	0.23	0.26	0.47
MGO	49.70	50.21	47.96	49.44	48.93	50.22	50.37	49.89
CAO	-	0.02	-	-	0.03	0.03	0.03	-
NIO	-	0.12	-	0.22	-	0.11	0.07	0.19
TOTAL	100.45	99.64	99.11	99.36	99.94	100.20	99.86	99.87
ATOMIC PROPORTIONS ON THE BASIS OF 4 OXYGENS								
SI	1.002	0.997	1.013	0.999	1.009	1.001	1.006	1.001
TI	0.001	0.001	0.001	0.001	0.001	0.001	0.001	0.000
AL	0.004	0.002	0.003	0.002	0.002	0.005	0.002	0.003
CR	0.001	0.004	0.002	0.001	0.002	0.002	0.002	0.001
FE2	0.181	0.160	0.185	0.175	0.180	0.162	0.151	0.166
MN	0.005	0.005	0.018	0.005	0.012	0.005	0.005	0.010
MG	1.797	1.825	1.762	1.808	1.779	1.814	1.821	1.813
CA	0.000	0.001	0.000	0.000	0.001	0.001	0.001	0.000
NI	0.000	0.002	0.000	0.004	0.000	0.002	0.001	0.004
END MEMBER COMPOSITIONS								
MG	90.61	91.72	89.68	90.92	90.28	91.60	92.10	91.16
FE	9.39	8.28	10.32	9.08	9.72	8.40	7.90	8.84

'TABLE 6.3 OLIVINE (3) FROM UNIT (3B) ABOVE THE TALC ISOGRAD'

	1	2	3	4	5	6	7	8	9	10
	60179A3	60179C3	60179D3	60179G3	60179H3	60180D3	60180E3	60180F3	60128A3	60128B3
OXIDE WEIGHT PERCENTAGE										
SIO2	41.33	41.35	41.65	41.41	41.51	41.12	41.27	41.19	41.49	41.19
TIO2	0.06	0.05	0.06	0.07	0.04	0.07	0.03	0.07	0.02	0.06
AL2O3	0.20	0.11	0.08	0.11	0.05	0.06	0.23	0.16	0.06	0.06
CR2O3	0.15	0.04	0.07	0.07	0.04	0.14	0.11	0.04	0.04	0.03
FEO	7.70	7.76	7.29	7.62	7.25	8.69	8.60	8.65	5.49	6.37
MNO	0.17	0.25	0.23	0.22	0.15	0.91	0.22	0.30	0.12	0.48
MGO	49.65	50.61	50.96	50.55	51.10	49.72	49.00	49.47	52.37	51.50
CAO	0.02	0.02	0.04	0.02	-	0.03	0.08	0.02	-	0.02
NIO	0.15	0.05	0.19	-	0.36	-	0.03	0.01	0.33	0.37
TOTAL	99.43	100.24	100.57	100.07	100.50	100.74	99.57	99.91	99.92	100.08
ATOMIC PROPORTIONS ON THE BASIS OF 4 OXYGENS										
SI	1.008	1.001	1.003	1.003	1.001	0.998	1.008	1.004	0.998	0.996
TI	0.001	0.001	0.001	0.001	0.001	0.001	0.001	0.001	0.000	0.001
AL	0.006	0.003	0.002	0.003	0.001	0.002	0.007	0.005	0.002	0.002
CR	0.003	0.001	0.001	0.001	0.001	0.003	0.002	0.001	0.001	0.001
FE2	0.157	0.157	0.147	0.154	0.146	0.176	0.176	0.176	0.111	0.129
MN	0.004	0.005	0.005	0.005	0.003	0.019	0.005	0.006	0.002	0.010
MG	1.804	1.826	1.829	1.824	1.836	1.798	1.785	1.797	1.878	1.855
CA	0.001	0.001	0.001	0.001	0.000	0.001	0.002	0.001	0.000	0.001
NI	0.003	0.001	0.004	0.000	0.007	0.000	0.001	0.000	0.006	0.007
END MEMBER COMPOSITIONS										
MG	91.83	91.84	92.35	91.99	92.48	90.21	90.82	90.78	94.33	93.05
FE	8.17	8.16	7.65	8.01	7.52	9.79	9.18	9.22	5.67	6.95

'TABLE 6.3 OLIVINE (3) FROM UNIT (3B) ABOVE THE TALC ISOGRAD'

	11	12	13	14	15	16	17	18	19	20
	60128C3	60128D3	60133A3	60133B3	60133C3	60133D3	60133E3	60206A3	60206B3	60206C3
OXIDE WEIGHT PERCENTAGE										
SIO2	40.67	41.08	41.20	41.12	41.28	41.02	41.26	41.79	41.81	41.51
TIO2	0.02	0.08	0.02	0.04	0.03	0.04	0.03	-	0.04	0.02
AL2O3	0.07	0.06	0.04	0.05	0.05	0.07	0.05	0.11	0.17	0.13
CR2O3	0.05	0.05	0.05	0.03	0.04	0.07	0.09	0.06	0.01	0.03
FEO	7.61	6.67	5.72	5.91	5.94	6.14	6.10	5.32	5.12	6.88
MNO	1.46	0.61	0.11	0.20	0.60	0.42	1.11	0.14	0.05	0.11
MGO	49.96	51.61	52.82	52.59	51.99	52.21	51.80	52.51	52.42	51.33
CAO	0.11	0.04	-	-	0.01	-	-	-	0.02	0.02
NIO	-	0.05	0.27	0.13	0.09	0.09	-	0.21	0.25	0.45
TOTAL	99.95	100.25	100.23	100.07	100.03	100.06	100.44	100.14	99.89	100.48
ATOMIC PROPORTIONS ON THE BASIS OF 4 OXYGENS										
SI	0.993	0.992	0.990	0.990	0.996	0.990	0.994	1.002	1.003	1.000
TI	0.000	0.001	0.000	0.001	0.001	0.001	0.001	0.000	0.001	0.000
AL	0.002	0.002	0.001	0.001	0.001	0.002	0.001	0.003	0.005	0.004
CR	0.001	0.001	0.001	0.001	0.001	0.001	0.002	0.001	0.000	0.001
FE2	0.155	0.135	0.115	0.119	0.120	0.124	0.123	0.107	0.103	0.139
MN	0.030	0.012	0.002	0.004	0.012	0.009	0.023	0.003	0.001	0.002
MG	1.818	1.858	1.892	1.888	1.869	1.878	1.860	1.876	1.874	1.842
CA	0.003	0.001	0.000	0.000	0.000	0.000	0.000	0.000	0.001	0.001
NI	0.000	0.001	0.005	0.003	0.002	0.002	0.000	0.004	0.005	0.009
END MEMBER COMPOSITIONS										
MG	90.74	92.66	94.17	93.88	93.40	93.41	92.74	94.48	94.75	92.90
FE	9.26	7.34	5.83	6.12	6.60	6.59	7.26	5.52	5.25	7.10

'TABLE 6.3 OLIVINE (3) FROM UNIT (3B) ABOVE THE TALC ISOGRAD'

	21	22	23	24	25	26	27	28	29	30
	60206D3	60206E3	60206F3	60206G3	60206H3	60206I3	60894A3	60894B3	60894C3	60894D3
OXIDE WEIGHT PERCENTAGE										
SIO2	40.85	41.16	41.91	41.13	41.54	41.46	41.91	41.43	41.84	42.27
TIO2	0.02	0.01	0.01	0.02	0.03	0.02	0.06	0.07	0.08	0.06
AL2O3	0.11	0.17	0.15	0.23	0.11	0.17	0.07	0.07	0.05	0.07
CR2O3	0.06	0.06	0.05	0.04	0.01	0.07	0.02	0.02	0.05	0.04
FEO	7.11	7.12	6.94	7.97	5.48	6.88	4.70	5.85	5.03	4.52
MNO	0.21	0.35	0.23	0.08	0.05	0.62	0.04	0.64	0.14	0.10
MGO	51.77	50.43	50.30	49.47	52.34	51.18	53.19	51.72	53.09	53.28
CAO	0.03	0.13	0.02	0.02	-	0.02	0.01	0.03	0.04	0.01
NIO	0.03	0.16	0.04	0.45	0.35	0.04	0.29	-	0.21	0.22
TOTAL	100.19	99.59	99.65	99.41	99.91	100.46	100.29	99.83	100.53	100.57
ATOMIC PROPORTIONS ON THE BASIS OF 4 OXYGENS										
SI	0.988	1.001	1.015	1.005	0.999	0.999	1.000	1.000	0.998	1.005
TI	0.000	0.000	0.000	0.000	0.001	0.000	0.001	0.001	0.001	0.001
AL	0.003	0.005	0.004	0.007	0.003	0.005	0.002	0.002	0.001	0.002
CR	0.001	0.001	0.001	0.001	0.000	0.001	0.000	0.000	0.001	0.001
FE2	0.144	0.145	0.141	0.163	0.110	0.139	0.094	0.118	0.100	0.090
MN	0.004	0.007	0.005	0.002	0.001	0.013	0.001	0.013	0.003	0.002
MG	1.866	1.828	1.815	1.802	1.876	1.838	1.892	1.861	1.888	1.887
CA	0.001	0.003	0.001	0.001	0.000	0.001	0.000	0.001	0.001	0.000
NI	0.001	0.003	0.001	0.009	0.007	0.001	0.006	0.000	0.004	0.004
END MEMBER COMPOSITIONS										
MG	92.65	92.32	92.59	91.63	94.40	92.39	95.24	93.41	94.82	95.36
FE	7.35	7.68	7.41	8.37	5.60	7.61	4.76	6.59	5.18	4.64

'TABLE 6.3 OLIVINE (3) FROM UNIT (3B) ABOVE THE TALC ISOGRAD'

	31	32	33	34	35	36	37	38	39	40
	60894E3	60894F3	60199A3	60199B3	60199C3	60199D3	60199E3	60199F3	61218A3	61218B3
OXIDE WEIGHT PERCENTAGE										
SIO2	41.55	42.13	41.02	41.50	41.19	41.16	40.99	41.22	41.26	41.39
TIO2	0.07	0.10	-	0.05	0.04	0.01	0.01	0.04	0.06	-
AL2O3	0.07	0.12	0.08	0.12	0.13	0.10	0.08	0.11	0.14	0.09
CR2O3	-	0.07	0.03	0.04	0.11	0.10	-	0.04	0.07	0.08
FEO	5.48	5.37	7.79	7.05	8.69	8.41	7.50	8.00	7.87	7.63
MNO	0.24	0.21	0.05	0.11	0.08	0.10	0.10	0.12	0.29	0.24
MGO	52.94	52.36	51.52	51.91	49.45	49.75	50.97	50.70	50.42	49.71
CAO	0.04	0.06	-	-	-	-	0.02	0.02	0.05	-
NIO	0.17	0.10	0.26	0.16	0.40	0.34	0.28	0.24	0.23	0.29
TOTAL	100.56	100.52	100.75	100.94	100.09	99.97	99.95	100.49	100.39	99.43
ATOMIC PROPORTIONS ON THE BASIS OF 4 OXYGENS										
SI	0.994	1.005	0.990	0.995	1.003	1.003	0.995	0.997	0.999	1.010
TI	0.001	0.002	0.000	0.001	0.001	0.000	0.000	0.001	0.001	0.000
AL	0.002	0.003	0.002	0.003	0.004	0.003	0.002	0.003	0.004	0.003
CR	0.000	0.001	0.001	0.001	0.002	0.002	0.000	0.001	0.001	0.002
FE2	0.110	0.107	0.157	0.141	0.177	0.171	0.152	0.162	0.159	0.156
MN	0.005	0.004	0.001	0.002	0.002	0.002	0.002	0.002	0.006	0.005
MG	1.887	1.862	1.852	1.854	1.795	1.806	1.844	1.828	1.819	1.807
CA	0.001	0.002	0.000	0.000	0.000	0.000	0.001	0.001	0.001	0.000
NI	0.003	0.002	0.005	0.003	0.008	0.007	0.005	0.005	0.004	0.006
END MEMBER COMPOSITIONS										
MG	94.28	94.35	92.13	92.81	90.95	91.24	92.28	91.75	91.67	91.84
FE	5.72	5.65	7.87	7.19	9.05	8.76	7.72	8.25	8.33	8.16

'TABLE 6.3 OLIVINE (3) FROM UNIT (3B) ABOVE THE TALC 'ISOGRAD'

	41	42	43	44	45	46	47	48	49	50
	61218C3	61218D3	61218E3	60218F3	61607A3	61607B3	61607C3	61607D3	61607E3	60209A3
OXIDE WEIGHT PERCENTAGE										
SIO2	41.13	41.35	41.12	41.25	41.30	41.64	41.92	41.46	41.19	41.84
TIO2	-	0.01	-	0.01	0.02	0.02	0.01	0.05	-	0.05
AL2O3	0.11	0.11	0.07	0.07	0.11	0.11	0.36	0.14	0.26	0.17
CR2O3	0.07	0.07	0.04	0.07	0.03	0.03	0.05	0.03	0.02	0.04
FEO	6.82	7.51	8.23	8.75	7.50	7.34	7.06	7.29	7.23	7.04
MNO	0.22	0.31	0.17	0.41	0.16	0.13	0.19	0.16	0.13	0.24
MGO	50.96	50.67	50.43	50.06	50.60	50.77	50.58	50.52	50.94	49.84
CAO	0.02	-	-	0.11	-	-	0.02	0.02	0.02	0.05
NIO	0.36	0.53	0.36	0.22	0.21	0.26	0.22	0.19	0.25	0.05
TOTAL	99.69	100.56	100.42	100.95	99.93	100.30	100.41	99.86	100.04	99.32
ATOMIC PROPORTIONS ON THE BASIS OF 4 OXYGENS										
SI	0.999	0.999	0.997	0.998	1.002	1.005	1.009	1.005	0.997	1.017
TI	0.000	0.000	0.000	0.000	0.000	0.000	0.000	0.001	0.000	0.001
AL	0.003	0.003	0.002	0.002	0.003	0.003	0.010	0.004	0.007	0.005
CR	0.001	0.001	0.001	0.001	0.001	0.001	0.001	0.001	0.000	0.001
FE2	0.139	0.152	0.167	0.177	0.152	0.148	0.142	0.148	0.146	0.143
MN	0.005	0.006	0.003	0.008	0.003	0.003	0.004	0.003	0.003	0.005
MG	1.844	1.825	1.823	1.805	1.829	1.826	1.814	1.825	1.838	1.805
CA	0.001	0.000	0.000	0.003	0.000	0.000	0.001	0.001	0.001	0.001
NI	0.007	0.010	0.007	0.004	0.004	0.005	0.004	0.004	0.005	0.001
END MEMBER COMPOSITIONS										
MG	92.80	92.03	91.45	90.68	92.17	92.37	92.55	92.35	92.50	92.42
FE	7.20	7.97	8.55	9.32	7.83	7.63	7.45	7.65	7.50	7.58

'TABLE 6.3 OLIVINE (3) FROM UNIT (3B) ABOVE THE TALC ISOGRAD'

	51	52	53	54	55	56	57	58	59	60
	60209B3	60209C3	60209D3	60209E3	60209F3	60209G3	60172A3	60172B3	60172C3	60172D3
OXIDE WEIGHT PERCENTAGE										
SIO2	41.91	41.52	41.38	41.79	41.63	41.71	41.51	41.45	41.63	41.77
TIO2	0.02	0.03	-	0.01	0.02	0.07	0.03	0.05	0.06	0.03
AL2O3	0.32	0.31	0.20	0.18	0.19	0.24	0.20	0.27	0.14	0.13
CR2O3	0.06	0.03	0.04	0.09	0.03	0.04	0.02	0.06	0.04	0.06
FEO	5.03	5.89	5.96	6.36	5.17	5.74	6.02	5.78	5.69	5.64
MNO	0.13	0.14	0.27	0.04	0.15	0.12	0.13	0.18	0.13	0.13
MGO	52.43	52.93	52.31	51.40	52.61	52.52	51.66	51.76	52.00	52.38
CAO	-	-	0.04	0.02	-	-	0.02	0.03	-	-
NIO	0.21	-	0.13	0.50	0.23	0.28	0.32	0.30	0.25	0.22
TOTAL	100.11	100.85	100.33	100.39	100.03	100.72	99.91	99.88	99.94	100.36
ATOMIC PROPORTIONS ON THE BASIS OF 4 OXYGENS										
SI	1.003	0.991	0.994	1.004	0.999	0.996	1.001	0.999	1.002	1.000
TI	0.000	0.001	0.000	0.000	0.000	0.001	0.001	0.001	0.001	0.001
AL	0.009	0.009	0.006	0.005	0.005	0.007	0.006	0.008	0.004	0.004
CR	0.001	0.001	0.001	0.002	0.001	0.001	0.000	0.001	0.001	0.001
FE2	0.101	0.118	0.120	0.128	0.104	0.115	0.121	0.117	0.114	0.113
MN	0.003	0.003	0.005	0.001	0.003	0.002	0.003	0.004	0.003	0.003
MG	1.870	1.882	1.873	1.841	1.881	1.870	1.856	1.859	1.864	1.870
CA	0.000	0.000	0.001	0.001	0.000	0.000	0.001	0.001	0.000	0.000
NI	0.004	0.000	0.003	0.010	0.004	0.005	0.006	0.006	0.005	0.004
END MEMBER COMPOSITIONS										
MG	94.76	93.99	93.73	93.47	94.63	94.11	93.74	93.93	94.09	94.18
FE	5.24	6.01	6.27	6.53	5.37	5.89	6.26	6.07	5.91	5.82

'TABLE 6.3 OLIVINE (3) FROM UNIT (3B) ABOVE THE TALC ISOGRAD'

	61	62	63	64	65	66	67	68	69	70
	60172E3	60172F3	61603A3	61603B3	60213A3	60213B3	60213C3	60213D3	60213E3	60213F3
OXIDE WEIGHT PERCENTAGE										
SIO2	41.45	41.62	41.62	41.79	41.95	42.01	41.72	41.83	41.92	41.80
TIO2	0.06	0.03	-	0.01	0.04	0.09	0.04	0.04	0.04	0.04
AL2O3	0.26	0.42	0.15	0.17	0.24	0.27	0.22	0.20	0.24	0.20
CR2O3	0.05	0.06	0.04	0.04	0.12	0.08	0.04	-	0.03	0.02
FEO	5.48	5.70	5.64	5.69	5.38	4.84	4.86	4.99	4.96	4.79
MNO	0.16	0.17	0.14	0.11	0.13	0.10	0.14	0.11	0.10	0.11
MGO	51.88	52.05	52.58	52.42	52.57	52.97	52.67	52.76	52.98	52.70
CAO	0.03	0.03	-	-	0.04	0.01	0.03	0.01	0.02	0.04
NIO	0.22	0.26	0.15	0.31	0.25	0.31	0.20	0.21	0.33	0.19
TOTAL	99.59	100.29	100.32	100.54	100.72	100.68	99.92	100.15	100.62	99.89
ATOMIC PROPORTIONS ON THE BASIS OF 4 OXYGENS										
SI	1.000	0.998	0.997	1.000	1.000	1.000	1.000	1.001	0.999	1.002
TI	0.001	0.001	0.000	0.000	0.001	0.002	0.001	0.001	0.001	0.001
AL	0.007	0.012	0.004	0.005	0.007	0.008	0.006	0.006	0.007	0.006
CR	0.001	0.001	0.001	0.001	0.002	0.002	0.001	0.000	0.001	0.000
FE2	0.111	0.114	0.113	0.114	0.107	0.096	0.097	0.100	0.099	0.096
MN	0.003	0.002	0.003	0.002	0.003	0.002	0.003	0.002	0.002	0.002
MG	1.865	1.860	1.878	1.869	1.868	1.878	1.882	1.881	1.881	1.882
CA	0.001	0.001	0.000	0.000	0.001	0.000	0.001	0.000	0.001	0.001
NI	0.004	0.005	0.003	0.006	0.005	0.006	0.004	0.004	0.006	0.004
END MEMBER COMPOSITIONS										
MG	94.25	94.09	94.19	94.15	94.44	95.03	94.94	94.85	94.91	95.04
FE	5.75	5.91	5.81	5.85	5.56	4.97	5.06	5.15	5.09	4.96

'TABLE 6.3 OLIVINE (3) FROM UNIT (3B) ABOVE THE TALC 'ISOGRAD'

	71	72	73	74	75	76	77	78	79	80
	60213G3	61600A3	61600B3	61600C3	61600D3	61600E3	61600F3	61600G3	61598A3	61598B3
OXIDE WEIGHT PERCENTAGE										
SIO2	41.98	41.44	41.65	41.08	41.14	41.62	41.54	41.73	41.22	41.56
TIO2	0.01	0.08	0.04	0.06	0.03	0.04	0.05	0.05	0.02	0.02
AL2O3	0.25	0.15	0.15	0.11	0.13	0.17	0.15	0.13	0.17	0.22
CR2O3	0.06	0.10	0.05	0.05	0.04	0.23	0.03	0.09	0.05	0.03
FEO	4.86	7.83	7.87	8.11	8.10	7.54	7.79	8.08	4.32	4.51
MNO	0.15	0.16	0.09	0.15	0.14	0.18	0.14	0.20	0.13	0.16
MGO	53.00	50.78	50.81	49.62	50.24	50.18	50.48	49.46	53.52	53.66
CAO	0.04	0.05	–	0.03	–	–	–	–	0.01	–
NIO	0.23	0.19	0.29	0.31	0.36	0.29	0.39	0.32	0.25	0.28
TOTAL	100.58	100.78	100.95	99.52	100.18	100.25	100.57	100.06	99.69	100.44
ATOMIC PROPORTIONS ON THE BASIS OF 4 OXYGENS										
SI	1.000	0.999	1.001	1.004	0.999	1.007	1.003	1.013	0.990	0.991
TI	0.000	0.001	0.001	0.001	0.001	0.001	0.001	0.001	0.000	0.000
AL	0.007	0.004	0.004	0.003	0.004	0.005	0.004	0.004	0.005	0.006
CR	0.001	0.002	0.001	0.001	0.001	0.004	0.001	0.002	0.001	0.001
FE2	0.097	0.158	0.158	0.166	0.165	0.153	0.157	0.164	0.087	0.090
MN	0.003	0.003	0.002	0.003	0.003	0.004	0.003	0.004	0.003	0.003
MG	1.881	1.824	1.821	1.807	1.818	1.809	1.816	1.789	1.915	1.907
CA	0.001	0.001	0.000	0.001	0.000	0.000	0.000	0.000	0.000	0.000
NI	0.004	0.004	0.006	0.006	0.007	0.006	0.008	0.006	0.005	0.005
END MEMBER COMPOSITIONS										
MG	94.96	91.88	91.92	91.45	91.57	92.05	91.90	91.41	95.54	95.34
FE	5.04	8.12	8.08	8.55	8.43	7.95	8.10	8.59	4.46	4.66

'TABLE 6.3 OLIVINE (3) FROM UNIT (3B) ABOVE THE TALC ISOGRAD'

	81	82	83	84	85	86	87
	61598C3	61598D3	60137A3	60137B3	60137C3	60137D3	60137F3
OXIDE WEIGHT PERCENTAGE							
SIO2	41.42	41.85	42.41	41.82	42.28	41.92	41.39
TIO2	-	0.02	-	0.03	0.02	0.04	0.05
AL2O3	0.22	0.15	0.07	0.09	0.07	0.04	0.03
CR2O3	0.03	0.06	0.07	0.07	0.07	0.03	0.07
FEO	4.36	4.56	4.34	4.78	4.78	4.74	5.02
MNO	0.13	0.16	0.08	0.12	0.12	0.12	0.12
MGO	53.71	53.44	53.07	52.75	52.38	53.55	52.84
CAO	-	-	-	0.01	0.01	-	0.02
NIO	0.30	0.20	0.09	0.28	0.09	0.17	0.27
TOTAL	100.17	100.44	100.13	99.95	99.82	100.61	99.81
ATOMIC PROPORTIONS ON THE BASIS OF 4 OXYGENS							
SI	0.990	0.997	1.010	1.002	1.012	0.998	0.995
TI	0.000	0.000	0.000	0.001	0.000	0.001	0.001
AL	0.006	0.004	0.002	0.003	0.002	0.001	0.001
CR	0.001	0.001	0.001	0.001	0.001	0.001	0.001
FE2	0.087	0.091	0.086	0.096	0.096	0.094	0.101
MN	0.003	0.003	0.002	0.002	0.002	0.002	0.002
MG	1.913	1.898	1.884	1.884	1.869	1.899	1.894
CA	0.000	0.000	0.000	0.000	0.000	0.000	0.001
NI	0.006	0.004	0.002	0.005	0.002	0.003	0.005
END MEMBER COMPOSITIONS							
MG	95.52	95.28	95.53	95.04	95.01	95.15	94.82
FE	4.48	4.72	4.47	4.96	4.99	4.85	5.18

'TABLE 6.4 ENSTATITE(3) ANALYSES'

	1	2	3	4	5	6
	61603A3	61603B3	6C213A3	60213B3	6C213C3	60213D3
OXIDE WEIGHT PERCENTAGE						
SIO2	57.27	57.29	58.03	57.90	57.71	57.97
TIO2	0.01	0.03	0.04	0.06	0.07	0.05
AL2O3	1.45	1.80	1.15	1.28	1.49	1.61
CR2O3	0.22	0.12	0.21	0.06	0.09	0.09
FEO	4.49	4.28	3.91	3.94	4.49	3.53
MNO	0.21	0.17	0.22	0.12	0.21	0.12
MGO	36.16	35.97	36.65	36.46	36.46	36.78
CAO	0.15	0.08	0.09	0.13	0.08	0.10
NIO	-	-	0.12	-	-	-
TOTAL	99.96	99.74	100.42	99.95	100.60	100.25
ATOMIC PROPORTIONS ON THE BASIS OF 6 OXYGENS						
SI	1.959	1.960	1.970	1.972	1.960	1.965
TI	0.000	0.001	0.001	0.002	0.002	0.001
AL	0.058	0.073	0.046	0.051	0.060	0.064
CR	0.006	0.003	0.006	0.002	0.002	0.002
FE2	0.128	0.122	0.111	0.112	0.128	0.100
MN	0.006	0.005	0.006	0.003	0.006	0.003
MG	1.843	1.834	1.854	1.851	1.845	1.858
CA	0.005	0.003	0.003	0.005	0.003	0.004
NI	0.000	0.000	0.003	0.000	0.000	0.000
END MEMBER COMPOSITIONS						
CA	0.28	0.15	0.17	0.24	0.15	0.18
MG	92.94	93.37	93.89	93.89	93.11	94.55
FE	6.78	6.49	5.94	5.87	6.74	5.27

'TABLE 6.5 MODIFIED MATRIX SERPENTINE (1) IN UNIT (3A)'

	1	2	3	4	5	6	7	8	9	10
	60021A3	60021B3	60021C3	60157B3	61593A3	60102A3	60102B3	60102D3	60035B3	60035C3
OXIDE WEIGHT PERCENTAGE										
SIO2	40.70	40.37	41.17	40.56	40.85	41.63	41.51	40.76	41.18	40.15
TIO2	0.10	0.02	0.01	0.03	0.02	-	0.06	0.04	0.01	-
AL2O3	0.16	0.23	0.07	0.12	0.68	0.09	0.07	0.56	0.77	0.90
FEO	1.43	1.56	1.21	1.29	1.88	1.11	1.25	1.60	2.08	1.67
MNO	0.03	0.06	0.05	-	0.06	0.03	0.06	0.18	-	-
MGO	40.16	40.62	41.39	41.48	37.75	41.45	41.30	39.47	40.31	40.47
CAO	0.04	0.01	0.03	0.10	0.03	0.06	0.07	0.01	0.02	0.03
CR2O3	0.32	0.31	0.07	0.09	0.29	0.08	0.17	0.88	0.40	0.61
NIO	0.04	0.10	0.02	0.13	0.05	0.06	0.16	0.08	0.17	0.11
TOTAL	82.98	83.28	84.02	83.80	81.61	84.51	84.65	83.58	84.94	83.94
ATOMIC PROPORTIONS ON THE BASIS OF 28 OXYGENS										
SI	7.947	7.873	7.928	7.852	8.096	7.962	7.943	7.923	7.885	7.780
TI	0.015	0.003	0.001	0.004	0.003	0.000	0.009	0.006	0.001	0.000
AL	0.037	0.053	0.016	0.027	0.159	0.020	0.016	0.128	0.174	0.206
FE2	0.234	0.254	0.195	0.209	0.312	0.178	0.200	0.260	0.333	0.271
MN	0.005	0.010	0.008	0.000	0.010	0.005	0.010	0.030	0.000	0.000
MG	11.686	11.806	11.879	11.967	11.150	11.815	11.777	11.434	11.503	11.688
CA	0.008	0.002	0.006	0.021	0.006	0.012	0.014	0.002	0.004	0.006
CR	0.049	0.048	0.011	0.014	0.045	0.012	0.026	0.135	0.061	0.093
NI	0.006	0.016	0.003	0.020	0.008	0.009	0.025	0.013	0.026	0.017

'TABLE 6.5 MODIFIED MATRIX SERPENTINE (1) IN UNIT (3A)'

	11	12	13	14	15	16
	60035D3	61632A3	61632B3	61632C3	61632D3	61632E3
OXIDE WEIGHT PERCENTAGE						
SIO2	40.44	36.51	41.42	40.99	41.77	41.33
TIO2	0.01	0.02	0.02	0.01	0.02	0.03
AL2O3	0.76	0.24	0.18	0.22	0.12	0.15
FEO	1.81	1.81	1.65	1.65	1.35	1.45
MNO	-	-	0.04	-	0.02	-
MGO	39.90	39.96	41.00	40.19	40.36	40.22
CAO	0.01	-	0.04	0.06	0.03	0.05
CR2O3	0.53	0.30	0.40	0.27	0.34	0.30
NIO	0.11	0.22	0.18	0.31	0.21	0.19
TOTAL	83.57	79.06	84.93	83.70	84.22	83.72
ATOMIC PROPORTIONS ON THE BASIS OF 28 OXYGENS						
SI	7.864	7.566	7.921	7.951	8.026	7.996
TI	0.001	0.003	0.003	0.001	0.003	0.004
AL	0.174	0.059	0.041	0.050	0.027	0.034
FE2	0.294	0.314	0.264	0.268	0.217	0.235
MN	0.000	0.000	0.006	0.000	0.003	0.000
MG	11.563	12.341	11.685	11.619	11.557	11.596
CA	0.002	0.000	0.008	0.012	0.006	0.010
CR	0.081	0.049	0.060	0.041	0.052	0.046
NI	0.017	0.037	0.028	0.048	0.032	0.030

'TABLE 6.7 AL RICH MATRIX SERPENTINE BELOW THE TALC ISOGRAD'

	1	2	3	4	5	6	7	8	9	10
	61623A3	61625A3	61625B3	61625C3	61625D3	61625E3	60109E3	60206A3	60206B4	60206C3
OXIDE WEIGHT PERCENTAGE										
SIO2	32.90	38.82	39.69	38.36	39.10	38.70	42.68	38.83	42.48	38.71
TIO2	0.03	0.09	0.07	0.08	0.05	0.06	0.03	0.04	–	0.02
AL2O3	4.86	4.16	3.16	4.41	3.99	3.37	1.07	3.02	1.55	3.13
FEO	3.27	3.83	3.74	3.73	3.19	3.51	2.76	3.62	2.93	3.70
MNO	0.09	0.02	0.01	0.03	0.05	–	0.04	0.04	0.04	0.04
MGO	37.96	37.14	37.22	37.22	36.96	37.35	40.01	37.92	37.91	37.52
CAO	0.12	0.05	0.07	0.06	0.08	0.07	0.03	0.02	0.05	0.04
CR2O3	0.56	0.65	0.38	0.46	0.69	0.39	0.01	0.46	0.18	0.53
NIO	0.11	0.22	0.21	0.24	0.22	0.21	0.17	0.22	0.23	0.22
TOTAL	79.90	84.98	84.55	84.59	84.33	83.66	86.80	84.17	85.37	83.91
ATOMIC PROPORTIONS ON THE BASIS OF 28 OXYGENS										
SI	6.837	7.509	7.695	7.454	7.590	7.588	7.994	7.581	8.081	7.584
TI	0.005	0.013	0.010	0.012	0.007	0.009	0.004	0.006	0.000	0.003
AL	1.191	0.949	0.722	1.010	0.913	0.779	0.236	0.695	0.348	0.723
FE2	0.568	0.620	0.607	0.606	0.518	0.576	0.432	0.591	0.466	0.606
MN	0.016	0.003	0.002	0.005	0.008	0.000	0.006	0.007	0.006	0.007
MG	11.756	10.707	10.755	10.779	10.692	10.915	11.168	11.033	10.748	10.955
CA	0.027	0.010	0.015	0.012	0.017	0.015	0.006	0.004	0.010	0.008
CR	0.092	0.099	0.058	0.071	0.106	0.060	0.001	0.071	0.027	0.082
NI	0.018	0.034	0.033	0.038	0.034	0.033	0.026	0.035	0.035	0.035

'TABLE 6.7 AL RICH MATRIX SERPENTINE BELOW THE TALC ISOGRAD'

	11	12	13
	60206D4	60206F3	60206F4
OXIDE WEIGHT PERCENTAGE			
SIO2	41.23	38.17	41.07
TIO2	0.02	-	0.02
AL2O3	1.52	3.03	1.77
FEO	2.95	3.36	3.22
MNO	-	0.04	0.01
MGO	38.92	38.36	38.81
CAO	0.01	0.05	0.01
CR2O3	-	0.06	0.02
NIO	0.22	0.16	0.21
TOTAL	84.87	83.53	85.14
ATOMIC PROPORTIONS ON THE BASIS OF 28 OXYGENS			
SI	7.913	7.507	7.872
TI	0.003	0.000	0.003
AL	0.344	0.703	0.400
FE2	0.474	0.553	0.516
MN	0.000	0.007	0.002
MG	11.133	11.244	11.086
CA	0.002	0.011	0.002
CR	0.000	0.056	0.003
NI	0.034	0.025	0.032

'TABLE 6.8 AL-SERPENTINE (3) AND CHLORITE (3) ABOVE THE TALC ISOGRAD'

	1	2	3	4	5	6	7	8	9	10
	60174A3	60174B3	60184B3	60184C3	60184D3	60184E3	60185A3	60185B3	60186A3	61612A3
OXIDE WEIGHT PERCENTAGE										
SIO2	33.57	32.65	35.54	31.13	31.58	33.21	33.81	37.58	30.43	31.83
TIO2	0.03	0.02	0.09	0.05	0.06	0.06	0.02	0.06	0.08	0.04
AL2O3	11.81	12.21	10.49	16.56	15.57	14.68	11.65	9.47	15.95	13.65
FEO	2.40	2.48	3.04	4.00	3.91	2.74	2.87	2.61	2.61	3.69
MNO	0.03	-	0.01	-	-	-	-	-	-	-
MGO	34.85	33.64	34.96	33.76	33.89	35.30	35.15	31.70	33.17	33.43
CAO	0.04	0.05	0.09	0.02	0.04	0.05	0.01	1.11	0.03	0.06
CR2O3	2.53	3.27	0.96	0.21	0.12	0.31	0.87	1.07	1.85	0.38
NIO	0.18	0.12	0.22	0.20	0.26	0.21	0.19	0.19	0.20	0.14
TOTAL	85.44	84.44	85.40	85.93	85.43	86.56	84.57	83.79	84.32	83.22
ATOMIC PROPORTIONS ON THE BASIS OF 28 OXYGENS										
SI	6.471	6.384	6.822	5.981	6.099	6.283	6.562	7.304	5.949	6.302
TI	0.004	0.003	0.013	0.007	0.009	0.009	0.003	0.009	0.012	0.006
AL	2.684	2.815	2.374	3.751	3.545	3.275	2.666	2.170	3.676	3.186
FE2	0.387	0.406	0.488	0.643	0.632	0.434	0.466	0.424	0.427	0.611
MN	0.005	0.000	0.002	0.000	0.000	0.000	0.000	0.000	0.000	0.000
MG	10.011	9.803	10.001	9.666	9.754	9.953	10.167	9.182	9.665	9.864
CA	0.008	0.010	0.019	0.004	0.008	0.010	0.002	0.231	0.006	0.013
CR	0.386	0.506	0.146	0.032	0.018	0.046	0.133	0.164	0.286	0.059
NI	0.028	0.019	0.034	0.031	0.040	0.032	0.030	0.030	0.031	0.022

'TABLE 6.8 AL-SERPENTINE (3) AND CHLORITE (3) ABOVE THE TALC ISOGRAD'

	11	12	13	14	15	16	17	18	19	20
	61612B3	60196A3	60196B3	61607A3	61607B3	61607C3	60218A3	60218B3	60218C3	60218D3
OXIDE WEIGHT PERCENTAGE										
SIO2	30.61	29.71	30.95	32.08	31.49	31.24	30.00	34.34	28.94	32.78
TIO2	0.03	0.06	0.04	0.02	0.05	0.04	0.06	0.08	0.06	0.09
AL2O3	13.23	16.66	15.53	13.42	14.35	13.99	17.31	12.77	17.61	16.48
FEO	3.56	3.36	3.29	3.26	3.09	3.26	3.38	3.59	3.28	3.57
MNO	-	-	-	-	-	-	-	0.03	0.02	0.01
MGO	33.77	32.32	33.04	34.25	34.27	34.15	33.02	33.66	32.00	32.69
CAO	0.02	0.03	0.06	0.03	0.04	0.01	-	0.03	0.02	0.02
CR2O3	0.52	1.45	1.53	0.98	1.22	1.09	0.55	0.91	0.83	0.89
NIO	-	0.22	0.24	0.11	0.26	0.18	0.27	0.19	0.27	0.23
TOTAL	81.74	83.81	84.68	84.15	84.77	83.96	84.59	85.59	83.03	86.76
ATOMIC PROPORTIONS ON THE BASIS OF 28 OXYGENS										
SI	6.182	5.862	6.038	6.281	6.131	6.143	5.848	6.592	5.754	6.208
TI	0.005	0.009	0.006	0.003	0.007	0.006	0.009	0.012	0.009	0.013
AL	3.150	3.876	3.572	3.098	3.294	3.244	3.978	2.890	4.128	3.680
FE2	0.601	0.555	0.537	0.534	0.503	0.536	0.551	0.575	0.546	0.566
MN	0.000	0.000	0.000	0.000	0.000	0.000	0.000	0.005	0.003	0.002
MG	10.165	9.504	9.607	9.994	9.943	10.009	9.593	9.630	9.483	9.227
CA	0.004	0.006	0.013	0.006	0.008	0.002	0.000	0.006	0.004	0.004
CR	0.083	0.226	0.236	0.152	0.188	0.169	0.085	0.138	0.130	0.133
NI	0.000	0.035	0.038	0.017	0.041	0.028	0.042	0.029	0.043	0.035

'TABLE 6.8 AL-SERPENTINE (3) AND CHLORITE (3) ABOVE THE TALC ISOGRAD'

	21	22	23	24	25	26	27	28	29	30
	61598C3	61598D3	61598E3	61598F3	61600A3	61600B3	61600C3	60209A3	60209B3	60209C3
OXIDE WEIGHT PERCENTAGE										
SIO2	32.06	33.45	32.90	32.87	31.85	31.82	30.61	33.96	34.00	34.96
TIO2	0.06	0.05	0.04	0.05	0.08	0.09	0.04	0.03	0.03	0.02
AL2O3	13.92	12.82	13.77	13.44	17.44	18.33	18.15	11.25	11.43	10.87
FEO	2.85	2.61	2.70	2.67	3.17	3.33	3.48	3.36	3.27	3.24
MNO	-	0.03	-	-	-	-	-	-	-	-
MGO	34.55	35.93	35.46	35.56	31.93	32.85	32.42	35.86	36.14	35.80
CAO	0.03	0.03	0.02	0.02	0.06	0.02	0.04	0.02	-	0.03
CR2O3	0.53	0.57	0.52	0.44	0.39	0.56	0.38	0.67	0.81	0.81
NIO	0.18	0.20	0.17	0.14	0.27	0.29	0.19	0.19	0.19	0.13
TOTAL	84.18	85.69	85.58	85.19	85.19	87.29	85.31	85.34	85.87	85.86
ATOMIC PROPORTIONS ON THE BASIS OF 28 OXYGENS										
SI	6.254	6.402	6.304	6.325	6.122	5.984	5.899	6.552	6.520	6.688
TI	0.009	0.007	0.006	0.007	0.012	0.013	0.006	0.004	0.004	0.003
AL	3.201	2.893	3.111	3.049	3.952	4.064	4.124	2.559	2.584	2.452
FE2	0.465	0.418	0.433	0.430	0.510	0.524	0.561	0.542	0.525	0.518
MN	0.000	0.005	0.000	0.000	0.000	0.000	0.000	0.000	0.000	0.000
MG	10.044	10.248	10.126	10.198	9.147	9.207	9.312	10.312	10.329	10.206
CA	0.006	0.006	0.004	0.004	0.012	0.004	0.008	0.004	0.000	0.006
CR	0.082	0.086	0.079	0.067	0.059	0.083	0.058	0.102	0.123	0.123
NI	0.028	0.031	0.026	0.022	0.042	0.044	0.029	0.029	0.029	0.020

'TABLE 6.8 AL-SERPENTINE (3) AND CHLORITE (3) ABOVE THE TALC ISOGRAD'

	31	32	33	34	35	36
	60133A3	60133B3	60133C3	61603C3	61603D3	61603E3
OXIDE WEIGHT PERCENTAGE						
SIO2	33.61	33.42	33.52	30.96	30.30	30.61
TIO2	0.02	0.06	0.02	-	-	-
AL2O3	9.89	10.11	9.89	18.56	17.78	17.93
FEO	2.84	2.01	2.75	2.73	3.03	2.48
MNO	-	-	-	0.01	0.06	-
MGO	35.47	35.05	35.38	33.47	33.22	33.55
CAO	0.02	-	-	-	-	0.02
CR2O3	1.03	1.22	1.05	0.49	0.46	0.69
NIO	0.27	0.17	0.06	0.23	0.22	0.19
TOTAL	83.15	82.04	82.67	86.45	85.07	85.47
ATOMIC PROPORTIONS ON THE BASIS OF 28 OXYGENS						
SI	6.652	6.668	6.660	5.869	5.855	5.869
TI	0.003	0.009	0.003	0.000	0.000	0.000
AL	2.308	2.378	2.317	4.148	4.051	4.053
FE2	0.470	0.335	0.457	0.433	0.490	0.398
MN	0.000	0.000	0.000	0.002	0.010	0.000
MG	10.462	10.422	10.477	9.456	9.568	9.588
CA	0.004	0.000	0.000	0.000	0.000	0.004
CR	0.161	0.192	0.165	0.073	0.070	0.105
NI	0.043	0.027	0.010	0.035	0.034	0.029

'TABLE 6.9 FERRITCHROMIT (3) AND MAGNETITE FROM THE BLUE RIVER BODY'

	1	2	3	4	5	6	7	8	9	10
	60153A3	60237A3	61552A3	61552B3	61612A3	60196A3	60196B3	60196C3	61593A3	60035A3
OXIDE WEIGHT PERCENTAGE										
SIO2	0.29	-	2.06	2.90	0.43	-	-	0.25	0.01	0.52
TIO2	0.03	0.22	0.40	0.25	0.70	0.44	0.12	0.42	0.05	0.01
AL2O3	0.02	8.78	0.48	1.44	0.19	5.28	12.82	3.36	0.01	0.10
CR2O3	2.36	58.06	26.49	25.80	9.35	36.37	42.74	35.38	0.25	0.73
FE2O3	64.94	3.08	37.20	36.03	56.86	25.48	12.21	27.29	67.49	68.26
FEO	29.81	22.09	29.65	25.88	28.36	26.80	23.90	27.38	30.26	29.87
MNO	0.13	0.42	0.64	0.51	0.33	0.49	0.29	0.64	0.18	0.07
MGO	0.38	7.23	2.51	5.60	1.73	3.14	6.03	2.52	0.07	1.33
CAO	0.04	0.01	0.01	-	0.01	0.02	-	-	0.03	-
NIO	0.44	-	0.47	0.44	0.65	0.26	-	0.21	-	0.08
TOTAL	98.44	99.89	99.91	98.85	98.61	98.28	98.11	97.45	98.35	100.97
ATOMIC PROPORTIONS ON THE BASIS OF 32 OXYGENS										
SI	0.090	0.000	0.608	0.838	0.131	0.000	0.000	0.075	0.003	0.157
TI	0.007	0.045	0.089	0.054	0.161	0.097	0.025	0.094	0.012	0.002
AL	0.007	2.811	0.167	0.490	0.068	1.817	4.150	1.182	0.004	0.036
CR	0.581	12.466	6.178	5.891	2.260	8.391	9.276	8.348	0.062	0.174
FE3	15.214	0.630	8.259	7.832	13.084	5.596	2.523	6.129	15.901	15.470
FE2	7.762	5.018	7.316	6.252	7.253	6.541	5.488	6.834	7.924	7.523
MN	0.034	0.097	0.160	0.125	0.085	0.121	0.067	0.162	0.048	0.018
MG	0.176	2.926	1.104	2.410	0.788	1.366	2.467	1.121	0.033	0.557
CA	0.013	0.003	0.003	0.000	0.003	0.006	0.000	0.000	0.010	0.000
NI	0.110	0.000	0.112	0.102	0.160	0.061	0.000	0.050	0.000	0.019

'TABLE 6.9 FERRITCHROMIT (3) AND MAGNETITE FROM THE BLUE RIVER BODY'

	11	12	13	14	15	16	17	18	19	20
	60038A3	60038B3	60102A3	60109A3	60109B3	60109C3	60133A3	60067A3	60067B3	60069A3
OXIDE WEIGHT PERCENTAGE										
SIO2	2.08	0.62	0.26	1.61	2.90	1.72	0.64	0.80	0.90	0.14
TIO2	-	-	0.07	0.26	0.21	0.12	0.20	0.21	0.29	0.12
AL2O3	7.46	0.29	-	0.45	0.90	0.53	0.01	0.50	0.38	-
CR2O3	15.56	1.62	0.62	21.44	15.60	16.48	13.78	19.57	19.36	0.63
FE2O3	42.37	65.71	68.52	42.42	46.09	47.94	53.12	47.50	46.02	68.06
FEO	21.51	29.91	30.59	25.61	25.91	25.84	26.59	25.57	26.57	29.37
MNO	0.22	0.07	0.01	1.01	1.01	0.89	0.78	1.25	1.17	0.12
MGO	8.37	1.14	0.69	3.71	4.77	3.71	2.39	3.27	2.44	0.88
CAO	-	-	0.03	-	-	-	-	0.01	-	0.01
NIO	-	-	-	0.63	0.65	0.73	0.70	0.61	0.72	0.42
TOTAL	97.57	99.36	100.79	97.14	98.04	97.96	98.21	99.29	97.85	99.75
ATOMIC PROPORTIONS ON THE BASIS OF 32 OXYGENS										
SI	0.582	0.190	0.079	0.486	0.856	0.516	0.195	0.238	0.274	0.043
TI	0.000	0.000	0.016	0.059	0.047	0.027	0.046	0.047	0.066	0.028
AL	2.462	0.105	0.000	0.160	0.313	0.187	0.004	0.176	0.136	0.000
CR	3.444	0.392	0.149	5.114	3.640	3.907	3.322	4.607	4.653	0.153
FE3	8.927	15.122	15.658	9.633	10.238	10.818	12.189	10.644	10.528	15.702
FE2	5.037	7.650	7.769	6.463	6.396	6.480	6.781	6.368	6.756	7.531
MN	0.052	0.018	0.003	0.258	0.253	0.226	0.201	0.315	0.301	0.031
MG	3.497	0.520	0.312	1.668	2.098	1.658	1.086	1.451	1.105	0.402
CA	0.000	0.000	0.010	0.000	0.000	0.000	0.000	0.003	0.000	0.003
NI	0.000	0.000	0.000	0.153	0.154	0.176	0.172	0.146	0.176	0.104

'TABLE 6.9 FERRITCHROMIT (3) AND MAGNETITE FROM THE BLUE RIVER BODY'

	21	22	23	24	25	26	27	28	29	30
	60069B3	60907A3	60907B3	60907C3	60907D3	60174A3	60174B3	60184A3	60184B3	60186A3
OXIDE WEIGHT PERCENTAGE										
SIO2	0.11	0.54	2.52	2.01	0.54	6.02	2.47	3.68	8.85	0.50
TIO2	0.32	0.04	0.16	0.17	0.04	1.02	0.61	0.45	0.18	0.32
AL2O3	0.72	0.06	0.88	0.40	0.30	3.56	2.07	1.98	5.66	0.24
CR2O3	29.09	1.92	23.30	20.98	1.25	44.04	44.84	22.45	22.65	28.40
FE2O3	37.17	68.72	38.38	42.69	65.62	6.80	19.67	35.48	26.32	39.17
FEO	25.64	25.13	25.02	25.40	28.38	26.52	17.55	26.72	20.17	27.93
MNO	1.85	0.20	2.12	1.80	1.19	0.63	0.58	0.63	0.44	0.57
MGO	2.22	4.11	4.28	3.88	1.50	8.67	11.43	5.56	15.33	2.28
CAO	-	0.03	-	0.01	0.03	-	-	0.01	0.02	0.01
NIO	0.35	0.55	0.43	0.38	0.50	-	-	0.31	0.07	0.42
TOTAL	97.47	101.30	97.09	97.72	99.35	97.26	99.22	97.27	99.69	99.84
ATOMIC PROPORTIONS ON THE BASIS OF 32 OXYGENS										
SI	0.034	0.159	0.752	0.601	0.165	1.669	0.675	1.074	2.270	0.149
TI	0.073	0.009	0.036	0.038	0.009	0.213	0.125	0.099	0.035	0.072
AL	0.259	0.021	0.310	0.141	0.108	1.164	0.667	0.681	1.712	0.084
CR	7.005	0.446	5.495	4.963	0.302	9.652	9.685	5.179	4.593	6.689
FE3	8.521	15.196	8.617	9.613	15.099	1.419	4.044	7.791	5.081	8.782
FE2	6.532	6.176	6.243	6.357	7.257	6.149	4.010	6.521	4.328	6.959
MN	0.477	0.050	0.536	0.456	0.308	0.148	0.134	0.156	0.096	0.144
MG	1.008	1.800	1.903	1.730	0.683	3.582	4.654	2.418	5.861	1.012
CA	0.000	0.009	0.000	0.003	0.010	0.000	0.000	0.003	0.005	0.003
NI	0.086	0.130	0.103	0.091	0.123	0.000	0.000	0.073	0.014	0.101

'TABLE 6.9 FERRITCHROMIT (3) AND MAGNETITE FROM THE BLUE RIVER BODY'

	31	32	33	34	35	36	37	38	39	40
	60186B3	60867A3	60867B3	60867C3	61633A3	61633B3	61633C3	61635A3	61635B3	61635C3
OXIDE WEIGHT PERCENTAGE										
SIO2	0.59	0.52	0.42	0.59	0.58	0.92	1.20	3.42	1.93	2.62
TIO2	0.29	0.06	0.06	0.05	-	-	-	0.08	0.19	0.15
AL2O3	0.27	0.36	0.02	-	-	11.53	4.65	1.47	0.77	1.15
CR2O3	27.74	25.13	23.14	16.64	0.06	35.49	30.63	23.66	24.52	24.05
FE2O3	39.37	43.19	44.72	51.04	67.31	19.32	31.80	37.74	39.68	37.37
FEO	27.94	25.93	26.25	27.05	29.38	23.91	25.39	25.80	27.04	27.48
MNO	0.54	1.06	0.99	0.72	0.19	1.39	1.98	0.95	0.91	0.92
MGO	2.29	2.97	2.49	2.18	1.19	5.85	4.10	5.78	3.61	3.82
CAO	0.02	0.02	0.02	0.02	-	-	-	-	0.02	-
NIO	0.36	0.61	0.48	0.66	-	0.05	0.24	0.48	0.54	0.31
TOTAL	99.41	99.85	98.59	98.95	98.71	98.46	99.99	99.38	99.21	97.87
ATOMIC PROPORTIONS ON THE BASIS OF 32 OXYGENS										
SI	0.176	0.154	0.127	0.179	0.179	0.254	0.343	0.980	0.569	0.777
TI	0.065	0.013	0.014	0.011	0.000	0.000	0.000	0.017	0.042	0.033
AL	0.095	0.126	0.007	0.000	0.000	3.747	1.565	0.497	0.267	0.402
CR	6.558	5.894	5.532	3.984	0.015	7.735	6.914	5.362	5.711	5.637
FE3	8.860	9.642	10.177	11.633	15.625	4.008	6.833	8.142	8.797	8.338
FE2	6.938	6.434	6.639	6.852	7.580	5.513	6.063	6.186	6.663	6.814
MN	0.137	0.266	0.254	0.185	0.050	0.325	0.479	0.231	0.227	0.231
MG	1.021	1.313	1.122	0.984	0.547	2.403	1.745	2.469	1.585	1.688
CA	0.006	0.006	0.006	0.006	0.000	0.000	0.000	0.000	0.006	0.000
NI	0.087	0.146	0.117	0.161	0.000	0.011	0.055	0.111	0.128	0.074

'TABLE 6.9 FERRITCHROMIT (3) AND MAGNETITE FROM THE BLUE RIVER BODY'

	41	42	43	44	45	46	47	48	49	50
	61635D3	61637A3	61637B3	61637C3	61623A3	61625A3	61625B3	61625C3	60206A3	60206B3
OXIDE WEIGHT PERCENTAGE										
SIO2	0.10	0.49	1.01	1.04	4.29	2.45	3.09	1.73	0.65	0.52
TIO2	0.06	-	-	-	0.51	0.40	0.39	0.17	0.20	0.16
AL2O3	0.01	0.07	0.06	0.03	1.97	0.51	0.85	0.07	0.23	0.21
CR2O3	0.49	0.47	0.50	0.26	22.28	23.71	24.79	8.45	26.91	27.77
FE2O3	69.17	67.81	67.35	65.79	36.14	38.97	36.80	56.80	39.59	39.02
FEO	29.71	28.48	28.24	26.82	25.66	27.10	26.34	27.78	28.35	27.35
MNO	0.26	0.15	0.20	0.18	0.69	0.88	0.89	0.38	1.02	0.99
MGO	0.77	1.86	2.21	2.70	7.08	4.02	5.19	2.85	1.50	1.99
CAO	0.01	-	-	-	0.01	-	0.01	0.05	-	-
NIO	0.36	-	0.64	0.43	0.38	0.54	0.48	0.76	0.57	0.48
TOTAL	100.94	99.33	100.21	97.25	99.01	98.58	98.83	99.04	99.02	98.49
ATOMIC PROPORTIONS ON THE BASIS OF 32 OXYGENS										
SI	0.030	0.149	0.304	0.321	1.215	0.723	0.898	0.520	0.196	0.157
TI	0.014	0.000	0.000	0.000	0.109	0.089	0.085	0.038	0.045	0.036
AL	0.004	0.025	0.021	0.011	0.658	0.178	0.291	0.025	0.082	0.075
CR	0.117	0.113	0.119	0.063	4.989	5.535	5.694	2.008	6.428	6.645
FE3	15.788	15.560	15.249	15.281	7.703	8.660	8.046	12.848	9.003	8.889
FE2	7.537	7.263	7.106	6.923	6.078	6.693	6.400	6.983	7.165	6.924
MN	0.067	0.039	0.051	0.047	0.166	0.220	0.219	0.097	0.261	0.254
MG	0.348	0.845	0.991	1.242	2.988	1.769	2.247	1.277	0.675	0.898
CA	0.003	0.000	0.000	0.000	0.003	0.000	0.003	0.016	0.000	0.000
NI	0.088	0.000	0.155	0.107	0.087	0.128	0.112	0.184	0.139	0.117

'TABLE 6.9 FERRITCHROMIT (3) AND MAGNETITE FROM THE BLUE RIVER BODY'

	51	52	53	54	55	56	57	58	59	60
	60206C3	60209A3	60209B3	60209C3	60137A3	61598A3	61598B3	61598C3	61598D3	61607A3
OXIDE WEIGHT PERCENTAGE										
SIO2	0.65	0.37	0.17	0.28	2.39	0.97	5.60	2.93	0.18	2.61
TIO2	0.11	0.23	0.21	0.22	0.18	0.32	0.28	0.08	0.12	0.26
AL2O3	0.24	0.49	0.31	0.31	0.12	0.29	0.22	0.13	0.20	0.05
CR2O3	25.91	30.20	26.71	27.29	22.47	12.23	10.04	2.90	4.74	12.79
FE2O3	40.78	37.79	41.41	40.03	42.20	54.97	46.92	60.61	63.96	49.78
FEO	28.19	26.04	26.65	25.45	26.73	24.79	29.14	27.85	26.76	29.46
MNO	0.89	1.04	0.92	1.19	1.05	0.69	0.62	0.22	0.23	0.55
MGO	1.59	2.97	2.31	2.86	4.17	4.13	5.27	3.95	2.20	2.70
CAO	–	–	0.01	–	–	0.01	–	0.01	0.04	–
NIO	0.61	0.55	0.57	0.46	0.52	0.78	0.77	0.79	0.87	0.37
TOTAL	98.97	99.68	99.27	98.09	99.83	99.18	98.86	99.47	99.30	98.57
ATOMIC PROPORTIONS ON THE BASIS OF 32 OXYGENS										
SI	0.196	0.110	0.051	0.085	0.699	0.288	1.625	0.867	0.055	0.784
TI	0.025	0.051	0.047	0.050	0.040	0.072	0.061	0.018	0.027	0.059
AL	0.086	0.171	0.110	0.110	0.041	0.102	0.075	0.045	0.072	0.018
CR	6.192	7.076	6.337	6.517	5.194	2.875	2.303	0.679	1.138	3.038
FE3	9.277	8.428	9.353	9.100	9.285	12.300	10.246	13.502	14.623	11.255
FE2	7.127	6.455	6.689	6.430	6.537	6.165	7.072	6.895	6.799	7.403
MN	0.228	0.261	0.234	0.305	0.260	0.174	0.152	0.055	0.059	0.140
MG	0.716	1.312	1.033	1.287	1.817	1.830	2.279	1.743	0.996	1.209
CA	0.000	0.000	0.003	0.000	0.000	0.003	0.000	0.003	0.013	0.000
NI	0.148	0.131	0.138	0.112	0.122	0.187	0.180	0.188	0.213	0.089

'TABLE 6.9 FERRITCHROMIT (3) AND MAGNETITE FROM THE BLUE RIVER BODY'

	61	62	63	64	65	66	67	68
	61607B3	61607C3	61603A3	61603B3	60218A3	6160CA3	6160CB3	6160CC3
OXIDE WEIGHT PERCENTAGE								
SIO2	1.54	1.02	-	1.87	0.11	0.34	0.40	0.12
TIO2	0.67	0.42	0.04	0.10	0.50	0.41	0.35	0.15
AL2O3	0.14	0.07	3.45	2.44	3.33	0.18	0.16	0.11
CR2O3	18.46	13.04	14.50	14.72	25.47	16.68	11.34	3.24
FE2O3	46.39	51.96	52.38	48.75	37.55	52.49	57.24	66.75
FEO	26.45	28.51	24.51	26.89	27.72	27.09	28.44	28.82
MNO	0.78	0.61	0.50	0.47	0.89	1.06	0.66	0.25
MGO	3.98	1.77	4.00	3.87	2.06	2.62	1.88	1.66
CAO	-	0.04	-	0.12	-	-	-	0.01
NIO	0.42	0.47	0.81	0.88	0.15	0.35	0.36	0.16
TOTAL	98.73	97.91	100.19	100.11	97.78	101.22	100.83	101.27
ATOMIC PROPORTIONS ON THE BASIS OF 32 OXYGENS								
SI	0.458	0.313	0.000	0.543	0.033	0.100	0.119	0.036
TI	0.150	0.097	0.009	0.022	0.113	0.091	0.079	0.034
AL	0.049	0.025	1.183	0.835	1.179	0.063	0.056	0.039
CR	4.343	3.161	3.333	3.379	6.044	3.892	2.678	0.767
FE3	10.390	11.991	11.463	10.653	8.483	11.660	12.867	15.051
FE2	6.584	7.312	5.961	6.530	6.960	6.688	7.105	7.222
MN	0.197	0.158	0.123	0.116	0.226	0.265	0.167	0.063
MG	1.721	0.809	1.733	1.675	0.922	1.152	0.837	0.741
CA	0.000	0.013	0.000	0.037	0.000	0.000	0.000	0.003
NI	0.101	0.116	0.189	0.206	0.036	0.083	0.086	0.039

'TABLE 6.10 AMPHIBOLES FROM THE BLUE RIVER ULTRAMAFIC BODY'

	1	2	3	4	5	6	7	8	9	10
	60206A3	60209A3	60209B3	61598A3	61598B3	61600A3	60179A3	60179B3	60184A3	60184B3
OXIDE WEIGHT PERCENTAGE										
SIO2	58.60	57.66	58.24	57.88	57.39	57.97	58.37	58.19	57.10	57.31
TIO2	0.04	0.01	0.04	0.02	0.08	-	0.05	0.05	0.05	0.04
AL2O3	0.22	0.28	0.30	0.38	0.47	0.22	0.12	0.16	0.26	0.59
CR2O3	0.06	0.06	0.09	0.01	0.13	0.08	0.11	0.14	0.12	0.39
FEO	0.87	0.82	0.84	0.80	1.09	0.89	1.16	1.26	1.63	1.64
MNO	0.01	0.03	0.07	0.04	0.07	0.02	0.05	0.07	0.03	0.07
MGO	24.49	24.26	24.45	24.24	24.69	23.95	24.26	23.46	24.00	23.66
CAO	13.94	13.52	12.81	13.23	12.75	13.72	13.64	13.72	12.57	12.55
NIO	-	0.05	-	0.19	0.14	-	-	-	0.05	-
TOTAL	98.23	96.69	96.84	96.79	96.81	96.85	97.76	97.05	95.81	96.25
ATOMIC PROPORTIONS ON THE BASIS OF 23 OXYGENS										
SI	7.931	7.925	7.966	7.939	7.881	7.954	7.944	7.979	7.931	7.923
TI	0.004	0.001	0.004	0.002	0.008	0.000	0.005	0.005	0.005	0.004
AL	0.035	0.045	0.048	0.061	0.076	0.036	0.019	0.026	0.043	0.096
CR	0.006	0.007	0.010	0.001	0.014	0.009	0.012	0.015	0.013	0.043
FE2	0.098	0.094	0.096	0.092	0.125	0.102	0.132	0.145	0.189	0.190
MN	0.001	0.003	0.008	0.005	0.008	0.002	0.006	0.008	0.004	0.008
MG	4.940	4.969	4.984	4.955	5.053	4.897	4.921	4.794	4.968	4.875
CA	2.022	1.991	1.878	1.945	1.876	2.017	1.989	2.016	1.871	1.859
NI	0.000	0.006	0.000	0.021	0.015	0.000	0.000	0.000	0.006	0.000

'TABLE 6.10 AMPHIBOLES FROM THE BLUE RIVER ULTRAMAFIC BODY'

	11	12	13	14	15	16	17	18	19	20
	60184C3	60184D3	60213A3	60213B3	61625A3	61625B3	61607A3	61607B3	60185A3	60185B3
OXIDE WEIGHT PERCENTAGE										
SIO2	56.01	55.02	56.42	57.16	55.55	57.35	57.69	57.92	57.82	57.44
TIO2	0.08	0.07	0.05	0.05	0.05	0.08	0.07	0.07	0.07	0.08
AL2O3	1.94	1.96	2.18	1.53	0.22	0.18	0.29	0.31	0.30	0.51
CR2O3	0.49	0.46	0.20	0.13	0.05	0.06	0.11	0.06	0.03	0.32
FEO	1.55	1.70	1.97	1.68	1.03	1.00	1.02	1.15	1.43	1.44
MNO	0.01	0.03	0.04	0.06	-	0.02	0.01	0.05	0.04	0.03
MGO	23.86	23.91	23.67	23.83	23.92	23.63	23.83	24.74	23.79	22.73
CAO	12.30	12.09	12.08	12.60	13.71	13.66	13.59	12.40	12.87	13.35
NIO	-	-	-	-	0.15	0.16	-	-	0.05	-
TOTAL	96.24	95.24	96.61	97.04	94.68	96.14	96.61	96.70	96.40	95.90
ATOMIC PROPORTIONS ON THE BASIS OF 23 OXYGENS										
SI	7.749	7.705	7.772	7.836	7.839	7.942	7.940	7.940	7.969	7.971
TI	0.008	0.007	0.005	0.005	0.005	0.008	0.007	0.007	0.007	0.008
AL	0.316	0.324	0.354	0.247	0.037	0.029	0.047	0.050	0.049	0.083
CR	0.054	0.051	0.022	0.014	0.006	0.007	0.012	0.007	0.003	0.035
FE2	0.179	0.199	0.227	0.193	0.122	0.116	0.117	0.132	0.165	0.167
MN	0.001	0.004	0.005	0.007	0.000	0.002	0.001	0.006	0.005	0.004
MG	4.920	4.990	4.860	4.869	5.030	4.877	4.888	5.055	4.887	4.701
CA	1.824	1.814	1.783	1.851	2.073	2.027	2.004	1.822	1.901	1.985
NI	0.000	0.000	0.000	0.000	0.017	0.018	0.000	0.000	0.006	0.000

'TABLE 6.10 AMPHIBOLES FROM THE BLUE RIVER ULTRAMAFIC BODY'

	21	22	23
	61612A3	60196A3	60196B3
OXIDE WEIGHT PERCENTAGE			
SIO2	59.48	57.99	57.91
TIO2	0.09	0.05	0.05
AL2O3	0.32	0.67	0.68
CR2O3	0.05	0.09	0.11
FEO	1.25	6.50	6.42
MNO	0.03	0.19	0.19
MGO	23.18	31.37	31.28
CAO	13.90	0.19	0.17
NIO	0.03	0.18	-
TOTAL	98.33	97.23	96.81
ATOMIC PROPORTIONS ON THE BASIS OF 23 OXYGENS			
SI	8.033	7.841	7.853
TI	0.009	0.005	0.005
AL	0.051	0.107	0.109
CR	0.005	0.010	0.012
FE2	0.141	0.735	0.728
MN	0.003	0.022	0.022
MG	4.666	6.322	6.322
CA	2.012	0.028	0.025
NI	0.003	0.020	0.000

'TABLE 6.11 TALC ANALYSES FROM THE BLUE RIVER ULTRAMAFIC BODY'

	1	2	3	4	5	6	7	8	9
	60209A3	61600A3	61600B3	60199A3	60199B3	60180A3	60133A3	60133B3	61607A3
OXIDE WEIGHT PERCENTAGE									
SIO2	59.73	59.25	61.52	60.44	60.36	59.09	60.87	60.99	61.59
TIO2	0.05	0.07	0.04	0.03	0.06	0.05	0.01	0.01	0.07
AL2O3	1.35	0.72	0.62	0.54	0.73	1.41	0.16	0.16	0.15
CR2O3	0.03	0.17	0.10	0.10	0.18	0.16	0.02	0.02	0.04
FEO	0.65	0.84	1.05	1.35	1.26	1.36	0.68	0.71	0.91
MNO	-	-	-	-	-	-	-	-	-
MGO	30.79	30.55	30.92	29.72	29.86	32.68	31.10	30.49	30.34
CAO	0.02	0.05	0.02	0.02	0.01	0.04	-	0.02	-
NIO	0.21	0.22	0.21	0.18	0.22	0.21	-	-	0.26
TOTAL	92.83	91.87	94.48	92.38	92.68	95.00	92.84	92.40	93.36
ATOMIC PROPORTIONS ON THE BASIS OF 22 OXYGENS									
SI	7.792	7.824	7.891	7.932	7.899	7.600	7.922	7.967	7.978
TI	0.005	0.007	0.004	0.003	0.006	0.005	0.001	0.001	0.007
AL	0.208	0.112	0.094	0.084	0.113	0.214	0.025	0.025	0.023
CR	0.003	0.018	0.010	0.010	0.019	0.016	0.002	0.002	0.004
FE2	0.071	0.093	0.113	0.148	0.138	0.146	0.074	0.078	0.099
MN	0.000	0.000	0.000	0.000	0.000	0.000	0.000	0.000	0.000
MG	5.987	6.013	5.911	5.813	5.824	6.264	6.033	5.936	5.857
CA	0.003	0.007	0.003	0.003	0.001	0.006	0.000	0.003	0.000
NI	0.022	0.023	0.022	0.019	0.023	0.022	0.000	0.000	0.027

'TABLE 7.1 ANTIGORITE DERIVED FROM OLIVINE AND SERPENTINE'

	1	2	3	4	5	6	7	8	9	10
	61619A4	60186B4	60186C4	60186D4	60184A4	61558A4	61558B4	61558C4	61558D4	61558E4
OXIDE WEIGHT PERCENTAGE										
SIO2	38.96	38.63	41.73	41.54	43.28	41.66	43.01	41.19	41.75	42.37
TIO2	0.04	0.06	0.04	0.02	0.04	0.03	0.02	0.02	0.01	0.06
AL2O3	0.83	3.83	1.30	1.81	1.29	0.05	0.37	0.03	0.11	0.64
FEO	3.18	2.57	2.86	3.16	2.91	1.29	2.32	1.31	1.44	2.69
MNO	-	0.01	-	-	0.03	0.01	-	-	-	0.01
MGO	40.01	38.04	38.21	38.60	39.83	41.34	39.77	40.95	40.61	38.39
CAO	0.04	0.05	0.02	0.04	0.04	0.02	0.01	0.04	0.01	0.06
CR2O3	0.31	0.68	0.63	0.14	-	-	-	0.01	0.01	0.27
NIO	0.19	0.17	0.19	0.19	0.24	0.22	0.21	0.25	0.23	0.44
TOTAL	83.56	84.04	84.98	85.50	87.66	84.62	85.71	83.80	84.17	84.93
ATOMIC PROPORTIONS ON THE BASIS OF 28 OXYGENS										
SI	7.664	7.511	7.996	7.918	8.025	7.968	8.129	7.960	8.024	8.114
TI	0.006	0.009	0.006	0.003	0.006	0.004	0.003	0.003	0.001	0.009
AL	0.192	0.878	0.294	0.407	0.282	0.011	0.082	0.007	0.025	0.144
FE2	0.523	0.418	0.458	0.504	0.451	0.206	0.367	0.212	0.231	0.431
MN	0.000	0.002	0.000	0.000	0.005	0.002	0.000	0.000	0.000	0.002
MG	11.729	11.023	10.912	10.966	11.007	11.784	11.203	11.794	11.632	10.956
CA	0.008	0.010	0.004	0.008	0.008	0.004	0.002	0.008	0.002	0.012
CR	0.048	0.105	0.095	0.021	0.000	0.000	0.000	0.002	0.002	0.041
NI	0.030	0.027	0.029	0.029	0.036	0.034	0.032	0.039	0.036	0.068

'TABLE 7.1 ANTIGORITE DERIVED FROM OLIVINE AND SERPENTINE'

	11	12	13	14	15	16	17	18	19	20
	60902A4	60902B4	60902C4	60237A4	60237B4	60237C4	60067A4	60067B4	60067C4	60067D4
OXIDE WEIGHT PERCENTAGE										
SIO2	41.22	43.02	42.67	37.59	40.85	40.92	40.20	40.81	36.86	40.66
TIO2	0.03	0.02	-	0.03	-	0.02	0.02	0.01	0.06	0.03
AL2O3	0.11	0.25	0.26	2.98	2.69	1.81	1.79	1.75	5.15	2.10
FEO	1.37	2.35	1.73	1.95	1.74	2.29	2.00	1.98	3.37	2.37
MNO	-	0.01	-	-	-	0.01	0.02	0.08	0.02	0.03
MGO	41.73	39.32	40.45	39.49	39.23	39.41	40.02	40.10	37.44	39.63
CAO	0.02	0.03	0.03	0.03	0.02	0.02	0.05	0.04	0.03	0.13
CR2O3	0.03	0.04	0.07	1.07	0.83	0.90	0.11	0.12	1.91	0.99
NIO	0.10	0.20	0.12	0.18	0.18	0.15	0.15	0.23	0.21	0.20
TOTAL	84.61	85.24	85.33	83.32	85.54	85.53	84.36	85.12	85.05	86.14
ATOMIC PROPORTIONS ON THE BASIS OF 28 OXYGENS										
SI	7.894	8.173	8.084	7.388	7.751	7.795	7.748	7.793	7.164	7.710
TI	0.004	0.003	0.000	0.004	0.000	0.003	0.003	0.001	0.009	0.004
AL	0.025	0.056	0.058	0.691	0.602	0.407	0.407	0.394	1.180	0.469
FE2	0.219	0.373	0.274	0.321	0.276	0.365	0.322	0.316	0.548	0.376
MN	0.000	0.002	0.000	0.000	0.000	0.002	0.003	0.013	0.003	0.005
MG	11.911	11.134	11.421	11.567	11.093	11.189	11.495	11.412	10.845	11.199
CA	0.004	0.006	0.006	0.006	0.004	0.004	0.010	0.008	0.006	0.026
CR	0.005	0.006	0.010	0.166	0.125	0.136	0.017	0.018	0.294	0.148
NI	0.015	0.031	0.018	0.028	0.027	0.023	0.023	0.035	0.033	0.031

'TABLE 7.1 ANTIGORITE DERIVED FROM OLIVINE AND SERPENTINE'

	21	22	23	24	25	26	27	28	29	30
	60067E4	60069A4	60069B4	60079A4	60079B4	60079C4	61633A4	61633B4	61633C4	61633D4
OXIDE WEIGHT PERCENTAGE										
SIO2	39.77	40.33	42.83	43.20	39.92	42.69	41.56	44.20	43.97	43.22
TIO2	0.04	0.02	0.01	0.02	0.05	0.03	0.01	-	-	-
AL2O3	1.34	0.70	0.18	0.54	1.54	0.82	0.59	0.32	0.34	0.36
FEO	1.89	2.27	2.66	2.26	2.18	1.64	1.64	1.72	1.69	1.73
MNO	0.06	-	0.01	0.04	-	-	-	-	0.02	0.01
MGO	39.85	40.03	39.10	39.46	39.52	39.55	40.23	40.27	40.97	40.57
CAO	0.03	-	0.03	0.02	0.01	0.05	-	-	-	-
CR2O3	0.26	0.17	-	0.01	0.18	0.44	0.56	0.15	0.05	0.08
NIO	0.12	0.11	0.20	0.18	0.26	0.10	0.09	0.14	0.19	0.16
TOTAL	83.36	83.63	85.02	85.73	83.66	85.32	84.68	86.80	87.23	86.13
ATOMIC PROPORTIONS ON THE BASIS OF 28 OXYGENS										
SI	7.761	7.852	8.173	8.154	7.771	8.082	7.955	8.209	8.138	8.107
TI	0.006	0.003	0.001	0.003	0.007	0.004	0.001	0.000	0.000	0.000
AL	0.308	0.161	0.040	0.120	0.353	0.183	0.133	0.070	0.074	0.080
FE2	0.309	0.370	0.425	0.357	0.355	0.260	0.263	0.267	0.262	0.271
MN	0.010	0.000	0.002	0.006	0.000	0.000	0.000	0.000	0.003	0.002
MG	11.591	11.615	11.119	11.100	11.465	11.160	11.476	11.147	11.300	11.342
CA	0.006	0.000	0.006	0.004	0.002	0.010	0.000	0.000	0.000	0.000
CR	0.040	0.026	0.000	0.001	0.028	0.066	0.085	0.022	0.007	0.012
NI	0.019	0.017	0.031	0.027	0.041	0.015	0.014	0.021	0.028	0.024

'TABLE 7.1 ANTIGORITE DERIVED FROM OLIVINE AND SERPENTINE'

	31	32	33	34	35	36	37	38	39	40
	61635A4	61635B4	61635C4	61635D4	61635E4	61637A4	61637B4	61637C4	60179A4	60179B4
OXIDE WEIGHT PERCENTAGE										
SIO2	42.49	42.69	42.96	42.73	42.90	44.32	43.27	43.22	43.22	41.91
TIO2	0.03	0.02	0.04	0.02	-	-	-	0.03	0.01	0.03
AL2O3	0.96	0.93	1.06	0.60	0.67	0.57	0.54	0.53	0.52	1.84
FEO	2.62	2.51	2.73	2.36	2.95	2.02	2.15	2.38	2.58	2.89
MNO	0.02	0.01	0.03	-	-	-	-	-	-	-
MGO	38.81	39.34	38.03	39.31	38.79	40.44	39.92	40.43	38.91	38.46
CAO	-	-	0.02	0.02	0.01	-	0.02	-	0.04	0.05
CR2O3	0.32	0.31	0.17	0.13	0.29	0.06	-	0.05	0.22	0.66
NIO	0.17	0.21	0.19	0.22	0.23	0.21	0.19	0.19	0.20	0.25
TOTAL	85.42	86.22	85.23	85.39	85.84	87.62	86.09	86.83	85.70	86.09
ATOMIC PROPORTIONS ON THE BASIS OF 28 OXYGENS										
SI	8.075	8.072	8.168	8.111	8.125	8.170	8.131	8.072	8.175	7.932
TI	0.004	0.003	0.006	0.003	0.000	0.000	0.000	0.004	0.001	0.004
AL	0.215	0.206	0.238	0.134	0.150	0.124	0.120	0.117	0.116	0.411
FE2	0.416	0.395	0.434	0.375	0.467	0.311	0.338	0.372	0.408	0.458
MN	0.003	0.002	0.005	0.000	0.000	0.000	0.000	0.000	0.000	0.000
MG	10.992	11.034	10.777	11.121	10.948	11.110	11.180	11.253	10.969	10.849
CA	0.000	0.000	0.004	0.004	0.002	0.000	0.004	0.000	0.008	0.010
CR	0.048	0.046	0.026	0.020	0.043	0.009	0.000	0.007	0.033	0.099
NI	0.026	0.032	0.029	0.034	0.035	0.031	0.029	0.029	0.030	0.038

'TABLE 7.1 ANTIGORITE DERIVED FROM OLIVINE AND SERPENTINE'

	41	42	43	44	45	46	47	48	49	50
	60179C4	60179D4	60179E4	60180A4	60180B4	60180C4	60907A4	60907B4	60907C4	60907D4
OXIDE WEIGHT PERCENTAGE										
SIO2	42.47	40.55	39.09	42.35	42.20	42.93	43.30	42.37	43.41	41.78
TIO2	0.07	0.05	0.05	0.05	0.01	0.03	-	-	-	-
AL2O3	1.53	4.41	4.17	1.22	1.00	0.94	0.28	1.10	0.38	0.88
FEO	3.00	2.95	3.58	3.34	3.09	3.69	2.47	2.37	2.63	2.86
MNO	-	-	0.02	0.02	0.02	0.02	0.01	-	0.01	-
MGO	38.75	37.47	38.07	38.35	38.51	37.89	39.44	39.56	39.47	39.18
CAO	0.02	-	0.02	0.02	0.02	0.05	0.02	0.02	0.01	0.08
CR2O3	0.68	0.62	0.58	0.26	0.11	0.05	0.03	0.24	-	0.26
NIO	0.22	0.23	0.32	0.15	0.12	0.14	0.17	0.12	0.16	0.17
TOTAL	86.74	86.28	85.90	85.76	85.08	85.74	85.72	85.78	86.07	85.21
ATOMIC PROPORTIONS ON THE BASIS OF 28 OXYGENS										
SI	7.978	7.659	7.477	8.045	8.067	8.154	8.181	8.012	8.173	7.987
TI	0.010	0.007	0.007	0.007	0.001	0.004	0.000	0.000	0.000	0.000
AL	0.339	0.982	0.940	0.273	0.225	0.211	0.062	0.245	0.084	0.198
FE2	0.471	0.466	0.573	0.531	0.494	0.586	0.390	0.375	0.414	0.457
MN	0.000	0.000	0.003	0.003	0.003	0.003	0.002	0.000	0.002	0.000
MG	10.848	10.547	10.852	10.858	10.971	10.726	11.106	11.149	11.076	11.162
CA	0.004	0.000	0.004	0.004	0.004	0.010	0.004	0.004	0.002	0.016
CR	0.101	0.093	0.088	0.039	0.017	0.008	0.004	0.036	0.000	0.039
NI	0.033	0.035	0.049	0.023	0.018	0.021	0.026	0.018	0.024	0.026

'TABLE 7.1 ANTIGORITE DERIVED FROM OLIVINE AND SERPENTINE'

	51	52	53	54	55	56	57	58	59	60
	60907E4	60171A4	60171B4	60171C4	60171D4	60867A4	60867B4	60867C4	60867D4	60109A4
OXIDE WEIGHT PERCENTAGE										
SIO2	42.00	36.18	36.84	40.71	40.43	41.43	42.08	41.18	41.57	43.31
TIO2	-	0.03	0.05	0.05	0.02	0.04	0.05	0.03	0.02	-
AL2O3	1.12	2.52	2.82	1.12	1.29	0.01	0.67	0.64	0.79	0.54
FEO	2.73	2.03	2.33	2.95	2.45	1.77	2.34	2.19	1.57	2.12
MNO	-	-	0.01	-	-	-	-	-	-	0.05
MGO	39.37	39.45	36.94	39.10	39.38	40.13	39.83	40.08	39.82	39.99
CAO	0.02	0.25	0.06	0.02	-	0.02	0.01	-	0.03	0.01
CR2O3	0.16	0.59	0.95	-	0.18	0.23	0.20	0.25	0.23	-
NIO	0.19	0.13	0.06	0.10	0.09	0.07	0.05	0.08	0.07	0.15
TOTAL	85.59	81.18	80.06	84.05	83.84	83.70	85.23	84.45	84.10	86.17
ATOMIC PROPORTIONS ON THE BASIS OF 28 OXYGENS										
SI	7.981	7.316	7.528	7.896	7.848	8.021	8.011	7.924	7.992	8.130
TI	0.000	0.005	0.008	0.007	0.003	0.006	0.007	0.004	0.003	0.000
AL	0.251	0.601	0.679	0.256	0.295	0.002	0.150	0.145	0.179	0.120
FE2	0.434	0.343	0.398	0.479	0.398	0.287	0.373	0.352	0.252	0.333
MN	0.000	0.000	0.002	0.000	0.000	0.000	0.000	0.000	0.000	0.008
MG	11.150	11.889	11.249	11.302	11.393	11.579	11.301	11.494	11.410	11.187
CA	0.004	0.054	0.013	0.004	0.000	0.004	0.002	0.000	0.006	0.002
CR	0.024	0.094	0.153	0.000	0.028	0.035	0.030	0.038	0.035	0.000
NI	0.029	0.021	0.010	0.016	0.014	0.011	0.008	0.012	0.011	0.023

'TABLE 7.1 ANTIGORITE DERIVED FROM OLIVINE AND SERPENTINE'

	61	62	63
	60109B4	60109C4	60109D4
OXIDE WEIGHT PERCENTAGE			
SIO2	38.43	41.25	35.84
TIO2	-	0.03	0.07
AL2O3	2.91	1.47	8.26
FEO	2.54	2.97	3.18
MNO	0.02	0.02	-
MGO	40.23	39.16	36.46
CAO	0.03	0.02	-
CR2O3	0.25	-	0.63
NIO	0.19	0.16	0.25
TOTAL	84.60	85.08	84.69
ATOMIC PROPORTIONS ON THE BASIS OF 28 OXYGENS			
SI	7.440	7.900	6.951
TI	0.000	0.004	0.010
AL	0.664	0.332	1.889
FE2	0.411	0.476	0.516
MN	0.003	0.003	0.000
MG	11.608	11.177	10.538
CA	0.006	0.004	0.000
CR	0.038	0.000	0.097
NI	0.030	0.025	0.039

'TABLE 7.2 SERPENTINE REPLACING OLIVINE (3) IN UNIT (3B)'

	1	2	3	4	5	6	7	8	9	10
	61598A4	61598B4	61598G4	61598H4	60218E4	60218F4	60218G4	60218H4	60199A4	60199B4
OXIDE WEIGHT PERCENTAGE										
SIO2	40.67	38.84	39.18	39.81	35.19	37.92	37.34	40.02	34.23	38.10
TIO2	0.02	0.04	0.04	0.04	0.03	0.01	0.06	0.04	0.04	0.01
AL2O3	0.24	0.26	0.41	0.24	0.08	0.16	0.36	0.97	0.07	0.09
FEO	1.29	3.64	3.19	2.42	7.02	3.93	6.10	3.15	5.88	3.22
MNO	0.11	0.13	0.14	0.03	0.54	0.08	0.01	0.05	0.04	0.05
MGO	40.11	38.98	39.65	40.38	32.25	36.96	40.54	38.73	38.80	39.97
CAO	0.05	0.04	0.01	0.04	0.09	0.20	0.01	0.01	0.04	–
CR2O3	0.27	0.37	0.30	0.50	0.32	0.12	0.16	0.20	0.19	0.15
NIO	0.19	0.27	0.20	0.20	0.59	0.02	0.19	0.16	0.52	0.15
TOTAL	82.95	82.57	83.12	83.66	76.11	79.40	84.77	83.33	79.81	81.74
ATOMIC PROPORTIONS ON THE BASIS OF 28 OXYGENS										
SI	7.946	7.757	7.748	7.785	7.823	7.865	7.398	7.856	7.253	7.674
TI	0.003	0.006	0.006	0.006	0.005	0.002	0.009	0.006	0.006	0.002
AL	0.055	0.061	0.096	0.055	0.021	0.039	0.084	0.225	0.017	0.021
FE2	0.211	0.608	0.528	0.396	1.305	0.682	1.011	0.517	1.042	0.542
MN	0.018	0.022	0.023	0.005	0.102	0.014	0.002	0.008	0.007	0.009
MG	11.679	11.603	11.685	11.769	10.685	11.425	11.970	11.331	12.252	11.998
CA	0.010	0.009	0.002	0.008	0.021	0.044	0.002	0.002	0.009	0.000
CR	0.042	0.058	0.047	0.077	0.056	0.020	0.025	0.031	0.032	0.024
NI	0.030	0.043	0.032	0.031	0.106	0.003	0.030	0.025	0.089	0.024

'TABLE 7.2 SERPENTINE REPLACING OLIVINE (3) IN UNIT (3B)'

	11	12
	61603A4	61603B4
OXIDE WEIGHT PERCENTAGE		
SIO2	41.37	41.48
TIO2	0.02	0.02
AL2O3	0.77	0.31
FEO	1.58	1.97
MNO	0.02	-
MGO	41.19	41.56
CAO	0.03	0.03
CR2O3	-	-
NIO	0.17	0.34
TOTAL	85.15	85.71
ATOMIC PROPORTIONS ON THE BASIS OF 28 OXYGENS		
SI	7.876	7.875
TI	0.003	0.003
AL	0.173	0.069
FE2	0.252	0.313
MN	0.003	0.000
MG	11.687	11.760
CA	0.006	0.006
CR	0.000	0.000
NI	0.026	0.052

'TABLE 7.3. SERPENTINE-BRUCITE PSEUDOMORPHS AFTER OLIVINE (3)'

	1	2	3	4	5	6	7	8
	60035A4	60035E4	60035F4	60035G4	60035H4	60035I4	60102C4	60157A4
OXIDE WEIGHT PERCENTAGE								
SIO2	33.14	41.23	33.12	30.73	34.97	36.38	41.93	37.68
TIO2	-	-	-	-	0.01	-	0.02	0.06
AL2O3	0.06	0.12	0.07	0.13	0.09	0.08	0.07	0.04
FEO	3.65	1.34	4.24	3.61	3.24	2.99	1.16	3.61
MNO	-	-	0.04	-	0.02	-	0.03	0.03
MGO	40.76	41.73	42.54	40.02	42.20	41.04	40.99	42.32
CAO	0.06	0.01	0.05	0.04	0.01	0.02	0.07	0.05
CR2O3	-	0.07	0.04	0.04	0.01	0.03	0.15	0.05
NIO	0.28	0.05	0.27	0.26	0.28	0.25	0.14	0.36
TOTAL	77.95	84.55	80.37	74.83	80.83	80.79	84.56	84.20
ATOMIC PROPORTIONS ON THE BASIS OF 28 OXYGENS								
SI	7.110	7.898	6.936	6.901	7.198	7.442	8.013	7.425
TI	0.000	0.000	0.000	0.000	0.002	0.000	0.003	0.009
AL	0.015	0.027	0.017	0.034	0.022	0.019	0.016	0.009
FE2	0.655	0.215	0.743	0.678	0.558	0.512	0.185	0.595
MN	0.000	0.000	0.007	0.000	0.003	0.000	0.005	0.005
MG	13.032	11.914	13.277	13.393	12.946	12.513	11.675	12.429
CA	0.014	0.002	0.011	0.010	0.002	0.004	0.014	0.011
CR	0.000	0.011	0.007	0.007	0.002	0.005	0.023	0.008
NI	0.048	0.008	0.045	0.047	0.046	0.041	0.022	0.057

'TABLE 7.5 GREEN AL-RICH SPINEL FROM FERRITCHROMIT IN UNIT (3B)'

	1	2	3
	60199A4	61603A4	61603B4
OXIDE WEIGHT PERCENTAGE			
SIO2	-	0.52	0.12
TIO2	-	-	-
AL2O3	44.07	50.40	51.00
CR2O3	19.54	10.42	10.32
FE2O3	3.89	8.22	8.09
FEO	12.94	9.40	8.99
MNO	0.15	0.10	0.07
MGO	16.14	20.07	19.95
CAO	0.15	-	-
NIO	-	-	0.15
TOTAL	96.88	99.13	98.69
ATOMIC PROPORTIONS ON THE BASIS OF 32 OXYGENS			
SI	0.000	0.111	0.026
TI	0.000	0.000	0.000
AL	11.820	12.705	12.894
CR	3.514	1.761	1.750
FE3	0.666	1.323	1.306
FE2	2.462	1.681	1.612
MN	0.029	0.018	0.013
MG	5.472	6.395	6.376
CA	0.037	0.000	0.000
NI	0.000	0.000	0.026

'TABLE 7.6 DIOPSIDE(4) FROM ENSTATITE(1)'

	1	2
	60094A4	60094B4
OXIDE WEIGHT PERCENTAGE		
SIO2	49.80	50.27
TIO2	-	-
AL2O3	2.21	2.30
CR2O3	0.74	0.74
FEO	2.08	1.79
MNO	0.05	0.09
MGO	20.89	21.30
CAO	21.43	20.89
NIO	-	-
TOTAL	97.20	97.38
ATOMIC PROPORTIONS ON THE BASIS OF 6 OXYGENS		
SI	1.864	1.871
TI	0.000	0.000
AL	0.098	0.101
CR	0.022	0.022
FE2	0.065	0.056
MN	0.002	0.003
MG	1.165	1.181
CA	0.860	0.833
NI	0.000	0.000
END MEMBER COMPOSITIONS		
CA	41.10	40.19
MG	55.71	56.99
FE	3.19	2.82

'TABLE 8.1 CLINOPYROXENE ANALYSES FROM GABBROIC BODIES'

	1	2	3	4	5	6	7	8	9	10
	60014A1	60014B1	60014C1	60014D1	60014E1	60014F1	60014G1	60013A1	60013B1	60013C1
OXIDE WEIGHT PERCENTAGE										
SIO2	52.31	51.50	51.24	50.56	50.73	50.45	50.81	51.61	51.58	51.35
TIO2	0.32	0.52	0.47	0.57	0.54	0.44	0.53	0.36	0.32	0.45
AL2O3	4.15	3.25	3.86	3.88	3.86	3.77	4.00	4.28	4.37	5.07
FEO	5.63	9.87	5.17	6.75	6.35	7.18	5.47	5.66	4.84	3.85
MNO	0.16	0.30	0.22	0.22	0.25	0.27	0.21	0.24	0.12	0.10
MGO	16.37	14.76	17.32	17.33	16.64	16.36	17.67	16.50	16.45	16.50
CAO	21.29	20.19	21.72	20.51	20.74	20.97	21.01	21.62	21.86	22.04
NA2O	0.09	0.17	0.21	0.31	0.83	0.56	0.63	-	0.01	0.80
K2O	0.03	0.04	0.01	-	0.03	0.02	0.01	0.03	0.05	0.10
TOTAL	100.35	100.60	100.22	100.13	99.97	100.02	100.34	100.30	99.60	100.26
ATOMIC PROPORTIONS ON THE BASIS OF 6 OXYGENS										
SI	1.906	1.909	1.876	1.863	1.873	1.870	1.862	1.887	1.892	1.870
TI	0.009	0.014	0.013	0.016	0.015	0.012	0.015	0.010	0.009	0.012
AL	0.178	0.142	0.167	0.169	0.168	0.165	0.173	0.185	0.189	0.218
FE2	0.172	0.306	0.158	0.208	0.196	0.223	0.168	0.173	0.149	0.117
MN	0.005	0.009	0.007	0.007	0.008	0.008	0.007	0.007	0.004	0.003
MG	0.889	0.815	0.945	0.952	0.916	0.904	0.965	0.899	0.899	0.896
CA	0.831	0.802	0.852	0.810	0.821	0.833	0.825	0.847	0.859	0.860
NA	0.006	0.012	0.015	0.022	0.059	0.040	0.045	0.000	0.001	0.057
K	0.001	0.002	0.000	0.000	0.001	0.001	0.000	0.001	0.002	0.005
END MEMBER COMPOSITIONS										
CA	43.83	41.49	43.43	40.98	42.30	42.33	42.00	43.97	44.97	45.85
MG	46.87	42.19	48.16	48.15	47.19	45.93	49.13	46.66	47.06	47.74
FE	9.31	16.32	8.42	10.87	10.51	11.74	8.87	9.37	7.97	6.42

'TABLE 8.2 CHLORITE FROM GABBRO'

	1	2
	60014A	60014B
OXIDE WEIGHT PERCENTAGE		
SIO2	28.30	28.60
TIO2	0.07	0.13
AL2O3	13.04	14.06
FEO	28.11	27.59
MNO	0.24	0.32
MGO	13.49	12.61
CAO	0.17	0.28
NA2O	0.09	0.05
K2O	0.29	0.38
TOTAL	83.80	84.02
ATOMIC PROPORTIONS ON THE BASIS OF 28 OXYGENS		
SI	6.387	6.406
TI	0.012	0.022
AL	3.470	3.713
FE2	5.306	5.169
MN	0.046	0.061
MG	4.538	4.209
CA	0.041	0.067
NA	0.039	0.022
K	0.084	0.109

APPENDIX III

X-ray Fluorescence analysis

Sample Preparation

Samples were split into fragments using a Cutrock Engineering hydraulic splitter. Weathered fragments were removed, and the remainder were broken into a coarse aggregate, using a Sturtevant 2" x 6" Roll Jaw Crusher. An aggregate sample, weighing 200-500 grams, was reduced to around 100 grams by the process of quartering. The sample fraction was ground to a fine powder, using a Tema Laboratory Disc Mill, model T-100, with tungsten-carbide Widia grinding barrel. Grinding took 3-4 minutes. A small sample was removed after only 30 seconds, in order to avoid the additional oxidation which may occur during prolonged grinding, Fitton and Gill (1970). The sample removed was used for a wet chemical FeO determination.

A few grams of fine powder were pressed into a briquette, using a hydraulic press operated at 5-6 tons/sq.in. A few drops of the organic binding agent "Mowiol" were added to aid cohesion.

Major Element Analysis

Sample briquettes were analysed on a Philips PW1212 automatic spectrometer, after being loaded by a Torrens Industries TE108 Automatic Sample Loader. This is capable

of handling up to 108 samples in a run. Details of the routine operating conditions used during X-ray fluorescence are given by Reeves (1971).

The elements Si, Al, Fe, Mg, Ca, Na, K, Ti, P and S were determined using a Cr target for primary radiation, and an evacuated tube. Mn was analysed separately using a W target.

A "fixed counts" operating procedure was used, in order to minimize the effect of electronic instability and voltage drift. A monitor was used throughout. The time (T) taken to accumulate a predetermined number of counts, (N), on the monitor, was applied to the next three samples. The same procedure was applied for all elements, and the samples were analysed in groups of three.

The international standards G1, G2, W1, T1, S1, GR, GA, AGV-1, GSR-1, and BCR-1 were used to calibrate the data. The compositions of the International Standards were taken from reviews by Flanagan (1969,1973).

The analytical data were corrected for mass absorption differences between the standards and the unknowns, using the iterative computer procedure described by Holland and Brindle (1966), and Reeves (1971).

Trace Element Analysis

The elements Ba, Nb, Zr, Y, Sr, Rb, Zn, Cu and Ni were determined using a W target, and an evacuated X-ray tube.

Appendix Table 3.1

Trace element calibration data

	Detection Limit ppm	Upper limit of standards ppm
Ba	8	5000
Nb	3	250
Zr	3	5000
Y	3	500
Sr	3	1100
Rb	3	1000
Zn	2	1000
Cu	2	1000
Ni	2	1000

Analytical count data were converted into concentrations, (ppm), using the computer program "Tratio", written by Dr. R.C.O. Gill. This program uses the function (peak intensity/background intensity -1) to compensate for matrix and mass absorption effects, using scattered background radiation as an internal standard. Corrections for blank/contamination and K interference are also included in this program. The nominal detection limits for each element are calculated from the formula $3(\bar{B}^{\frac{1}{2}})$, where $\bar{B}$ is the mean background-under-peak, in counts, averaged over all the determinations processed. Appendix Table 3.1 gives the detection limit, and the upper limit of standardization for each element.

The standards used were synthetic spiked glasses prepared by the Pilkington Research Laboratory, (Latham, England), for use in lunar investigations. The standards are in two sets, in order to avoid inter-element interference, as much as is possible.

TABLE 8.3 VOLCANIC MAJORS TRACES AND NORMS,NORM FE AS FEO

	60017	60045	60052	60057	60080	60240	60242	61539	61540	61583
PERCENT										
SIO2	54.40	49.31	50.62	49.51	53.81	50.49	51.69	49.83	53.06	50.59
AL2O3	11.64	11.25	13.74	13.31	11.29	13.06	14.84	12.30	14.50	14.17
FE2O3	6.18	5.68	3.75	3.94	7.87	3.47	2.57	5.60	4.16	3.34
FEO	4.15	7.70	7.07	8.56	4.83	12.01	7.89	8.50	7.63	7.69
MGO	5.96	9.67	8.63	7.30	5.63	9.84	6.16	8.05	8.91	8.84
CAO	12.70	10.76	10.57	11.12	8.73	5.37	10.57	8.32	6.08	9.73
NA2O	2.69	2.45	3.27	2.78	3.91	1.76	4.23	3.65	2.82	2.89
K2O	0.35	0.20	0.05	0.44	0.88	0.17	0.02	0.64	0.31	0.45
TIO2	1.09	1.72	1.09	1.70	1.99	1.99	0.83	1.77	1.30	1.02
MNO	0.18	0.23	0.24	0.25	0.21	0.33	0.17	0.20	0.20	0.22
S	0.00	0.00	0.00	0.00	0.00	0.00	0.00	0.00	0.00	0.00
P2O5	0.19	0.18	0.19	0.16	0.33	0.19	0.16	0.21	0.20	0.20
PPM										
ZN	61	107	86	112	93	627	69	116	94	79
CU	43	68	76	67	30	117	507	19	69	35
NI	57	129	105	81	37	19	22	60	123	92
BA	792	348	97	836	76	71	100	243	712	986
NB	1	0	0	3	6	3	0	1	3	0
ZR	90	116	70	97	136	126	44	89	75	86
Y	24	37	27	30	63	46	22	44	26	29
SR	681	363	151	159	129	14	108	51	82	148
RB	3	0	1	9	9	4	1	22	4	8
CIPW NORM										
QUTZ	3.80	0.00	0.00	0.00	0.00	2.60	0.00	0.00	1.70	0.00
ORTH	2.10	1.20	0.30	2.60	5.30	1.00	0.10	3.80	1.90	2.70
ALBT	23.00	21.00	28.00	23.80	33.50	15.10	35.00	31.40	24.20	24.70
ANOR	18.90	19.40	22.90	22.80	10.80	25.80	21.70	15.50	26.30	24.70
NEPH	0.00	0.00	0.00	0.00	0.00	0.00	0.70	0.00	0.00	0.00
DIOP	36.20	27.70	23.70	26.60	25.80	0.00	25.20	20.70	2.40	18.80
HPER	13.50	12.60	7.20	6.70	18.50	50.40	0.00	1.90	40.60	13.10
CLIV	0.00	14.30	15.30	13.80	1.50	0.00	15.40	22.70	0.00	13.60
MAGN	0.00	0.00	0.00	0.00	0.00	0.00	0.00	0.00	0.00	0.00
ILMN	2.10	3.30	2.10	3.30	3.80	3.80	1.60	3.40	2.50	2.00
APAT	0.50	0.40	0.50	0.04	0.80	0.50	0.40	0.50	0.50	0.50

TABLE 8.4 GABBRO MAJORS TRACES AND NORMS, NORM FE AS FEO

	60013	60014	60015	60020	60022	60053	60054	60126	61547	61555
PERCENT										
SIO2	52.36	52.06	52.38	53.22	50.23	50.06	51.50	51.00	51.10	51.71
AL2O3	14.47	15.91	14.84	16.10	13.07	13.72	13.18	15.26	13.97	15.12
FE2O3	2.69	4.12	2.31	2.52	0.01	2.63	1.83	2.42	2.71	2.46
FEO	8.15	8.31	8.25	8.40	11.24	7.99	9.83	8.10	8.52	7.82
MGO	5.48	5.97	6.18	5.96	8.18	7.48	6.46	7.66	7.62	7.96
CAO	9.85	6.97	8.75	6.35	10.94	12.66	9.62	8.76	9.42	9.21
NA2O	4.93	4.47	5.23	5.21	3.32	3.49	4.03	4.54	3.12	3.70
K2O	0.03	0.12	0.05	0.23	0.20	0.08	0.58	0.02	0.94	0.12
TIO2	0.80	0.82	0.79	0.76	1.19	0.68	1.45	1.01	1.20	0.69
MNO	0.17	0.18	0.16	0.18	0.18	0.17	0.20	0.16	0.19	0.20
S	0.00	0.00	0.00	0.00	0.00	0.00	0.00	0.00	0.00	0.00
P2O5	0.16	0.16	0.15	0.15	0.21	0.15	0.25	0.18	0.27	0.15
PPM										
ZN	71	82	69	81	0	78	92	88	94	75
CU	101	155	83	96	0	59	56	31	45	132
NI	25	35	25	26	0	35	30	56	53	45
BA	54	214	42	254	0	49	306	322	882	83
NB	1	0	3	3	0	2	5	0	2	2
ZR	60	53	57	60	0	45	105	84	109	49
Y	21	22	23	21	0	14	34	26	31	20
SR	350	277	179	419	0	345	794	494	743	84
RB	0	1	3	4	0	2	7	0	26	3
CIPW NORM										
QUTZ	0.00	0.00	0.00	0.00	0.00	0.00	0.00	0.00	0.00	0.00
ORTH	0.00	0.70	0.30	1.40	1.20	0.50	3.50	0.10	5.60	0.70
ALBT	37.70	38.30	39.30	44.60	28.40	24.10	34.50	36.30	26.70	31.70
ANOR	17.50	23.30	17.10	20.10	20.40	21.80	16.40	21.40	21.60	24.60
NEPH	2.50	0.00	3.00	0.00	0.00	3.10	0.00	1.40	0.00	0.00
DIOP	25.80	8.90	21.50	9.00	27.40	33.70	25.20	17.60	19.80	17.00
HPER	0.00	11.90	0.00	5.10	1.60	0.00	0.10	0.00	10.00	10.20
OLIV	14.40	14.80	17.00	17.90	18.20	15.10	16.90	20.80	13.30	14.20
MAGN	0.00	0.00	0.00	0.00	0.00	0.00	0.00	0.00	0.00	0.00
ILMN	1.50	1.60	1.50	1.50	2.30	1.30	2.80	1.90	2.30	1.30
APAT	0.40	0.40	0.40	0.40	0.50	0.40	0.60	0.40	0.60	0.40

TABLE 8.6 AMPHIBOLITE MAJORS TRACES AND NORMS,FE AS FE2 AND FE3

	60003	60005	60050	60083	60085	60124	60166	61574	61575	61576
PERCENT										
SIO2	50.02	48.99	45.57	48.86	48.69	44.93	45.52	49.37	49.05	48.37
AL2O3	12.71	12.71	9.47	15.90	11.92	13.95	13.96	11.06	11.67	13.06
FE2O3	2.23	3.23	4.76	2.31	2.30	2.68	2.41	3.12	3.02	3.34
FEO	10.49	7.44	11.49	3.12	5.24	3.37	2.16	5.22	5.58	10.69
MGO	8.21	10.67	8.45	12.39	15.44	22.61	13.32	13.40	12.98	8.97
CAO	9.60	12.75	15.26	14.01	13.61	11.13	21.89	15.91	15.38	8.91
NA2O	3.41	1.79	1.10	2.06	1.54	0.54	0.11	0.67	1.10	2.87
K2O	0.18	0.37	0.06	0.54	0.16	0.10	0.00	0.01	0.02	0.13
TIO2	1.56	0.87	1.99	0.25	0.30	0.14	0.18	0.39	0.33	1.95
MNO	0.19	0.19	0.28	0.11	0.13	0.09	0.08	0.15	0.14	0.24
S	0.00	0.00	0.00	0.00	0.00	0.00	0.00	0.00	0.00	0.00
P2O5	0.25	0.16	0.32	0.11	0.11	0.10	0.14	0.12	0.12	0.30
PPM										
ZN	63	66	113	26	36	30	18	42	47	95
CU	67	57	66	0	64	0	32	55	16	55
NI	93	144	72	273	339	570	314	194	267	44
BA	359	1168	35	1102	145	455	25	0	23	122
NB	6	0	1	1	0	0	0	2	1	7
ZR	119	44	111	10	9	18	0	4	0	129
Y	44	19	48	2	6	0	0	5	5	47
SR	215	417	23	257	346	606	172	41	38	146
RB	5	1	2	11	3	1	0	0	0	1
CIPW NORM										
ORTHO	1.10	2.20	0.40	3.20	1.00	0.60	0.00	0.10	0.10	0.80
ALBITE	29.20	15.30	9.40	15.20	13.10	4.60	0.00	5.70	9.40	24.60
ANORTH	19.10	25.80	21.00	32.70	25.30	35.50	37.70	27.30	27.00	22.60
NEPH	0.00	0.00	0.00	1.20	0.00	0.00	0.50	0.00	0.00	0.00
DIOP	22.50	29.70	43.80	28.60	33.20	15.10	40.50	40.70	38.90	16.40
HYPER	11.20	14.60	12.30	0.00	5.40	7.40	0.00	19.90	13.50	19.30
OLVN	10.10	5.70	1.60	15.00	17.80	32.40	11.40	0.80	5.70	7.00
CA-ORTH	0.00	0.00	0.00	0.00	0.00	0.00	5.70	0.00	0.00	0.00
MAGNT	3.30	4.70	7.00	3.40	3.40	3.90	3.50	4.50	4.40	4.90
ILMEN	3.00	1.70	3.80	0.50	0.60	0.30	0.30	0.70	0.60	3.70
APATITE	0.60	0.40	0.80	0.30	0.30	0.20	0.30	0.30	0.30	0.70

APPENDIX IV

4.1 X-ray Diffraction Data

Serpentine

The serpentine "polymorphs" were differentiated using an X-ray diffraction technique. Serpentine smears were subjected to Fe filtered CoKα radiation from a Philips PW1130 X-ray generator. Traces were run at a scan speed of 1/4°Min, and a chart speed of 10mm/sec.

Antigorite was identified on the basis of a reduced (020) reflection, and a diagnostic (910) reflection at 4.27Å. In addition, antigorite gives a pair of weak diffuse reflections at 1.563 and 1.541Å respectively.

Chrysotile and lizardite could not be separated, and mesh textured serpentinites appear to contain an element of each. The (020) reflection is strong and markedly skewed. The peak is very often split, suggesting a mixed assemblage. A characteristic lizardite peak occurs with a 2.148Å spacing, and a pair of peaks occur representing 1.536 and 1.503Å respectively.

X-ray diffraction smears are very often contaminated with olivine, talc, tremolite, magnetite, carbonate, and spinel, and no systematic study was undertaken. Two distinctive patterns were found, and these appear to represent antigorite serpentinite and, mesh textured, lizardite-chrysotile serpentine.

Chlorite

Similar X-ray diffraction data was used to differentiate between the 7Å serpentine structure, and the 14Å chlorite structure. Sample 60196 contains a "chlorite" appreciably enriched in Al_2O_3. The "chlorite" resembles serpentine texturally, and X-ray diffraction data failed to produce basal chlorite reflections. The mineral is considered to be a septechlorite.

Sample 61600 contains recognizable recrystallized chlorite, in addition to traces of retrogressive serpentine. X-ray data indicates that at least some of the "chlorite" is chlorite structured, as the following basal reflections were found, in addition to the reflections observed in Sample 60196.

dÅ	hkl
001	7.20
002	14.45
004	29.20
005	36.20

Brucite

Brucite was observed in thin section, and its presence in mesh textured serpentinite was confirmed by X-ray diffraction. Samples containing appreciable brucite are shown in text Figure 7.2.

Brucite has a layered structure, with Mg atoms separated by layers of (OH) ions. The structure produces three main diffraction peaks, which readily identify the phase.

dÅ	hkl
4.77	(001)
2.365	(101)
1.794	(102)

The layered structure may cause preferred orientation on a smear mount. Orientation effects alone are not enough to account for the difference in apparent brucite content observed in Blue River serpentinite.